ҚАЗАҚСТАН РЕСПУБЛИКАСЫ
ҒЫЛЫМ ЖӘНЕ ЖОҒАРЫ БІЛІМ МИНИСТРЛІГІ

SATBAYEV UNIVERSITY
МЕТАЛЛУРГИЯ ЖӘНЕ КЕН БАЙЫТУ ИНСТИТУТЫ

ISSN 2616-6445 (Online)
ISSN 2224-5243 (Print)
DOI 10.31643/2018/166445

Минералдық шикізаттарды кешенді пайдалану

2(345)

Комплексное Использование Минерального Сырья

Complex Use of Mineral Resources

СӘУІР-МАУСЫМ 2028
APRIL-JUNE 2028
АПРЕЛЬ-ИЮНЬ 2028

ЖЫЛЫНА 4 РЕТ ШЫҒАДЫ
QUARTERLY JOURNAL
ВЫХОДИТ 4 РАЗА В ГОД

ЖУРНАЛ 1978 ЖЫЛДАН БАСТАП ШЫҒАДЫ
JOURNAL HAS BEEN PUBLISHING SINCE 1978
ЖУРНАЛ ИЗДАЕТСЯ С 1978 ГОДА

АЛМАТЫ - 2028

Редакция мекен жайы:
«Металлургия және кен байыту институты» АҚ
050010, Қазақстан Республикасы, Алматы қ., Шевченко к-сі, Уәлиханов к-нің қиылысы, 29/133,
Fax. +7 (727) 298-45-03, Tel. +7-(727) 298-45-02, +7 (727) 298-45-19
E mail: journal@kims-imio.kz, product-service@kims-imio.kz
http://kims-imio.com/index.php/main

«Минералдық шикізаттарды кешенді пайдалану» журналы ғылыми жұмыстардың негізгі нәтижелерін жариялау үшін Қазақстан Республикасы Білім және ғылым министірлігінің Білім және ғылым сапасын қамтамасыз ету комитеті ұсынған ғылыми басылымдар тізіміне енгізілген.
Меншік иесі: «Металлургия және кен байыту институты» АҚ

Журнал Қазақстан Республикасының Ақпарат және коммуникация министрлігінің Байланыс, ақпараттандыру және бұқаралық ақпарат құралдары саласындағы мемлекеттік бақылау комитетінде қайта тіркелген

2016 ж. 18 қазандағы № 16180-Ж Куәлігі

Address:
"Institute of Metallurgy and Ore Beneficiation" JSC
29/133 Shevchenko Street, corner of Ch. Valikhanov Street, Almaty, 050010, Kazakhstan
Fax. +7 (727) 298-45-03, Tel. +7-(727) 298-45-02, +7 (727) 298-45-19
E mail: journal@kims-imio.kz, product-service@kims-imio.kz
http://kims-imio.com/index.php/main

The Journal "Complex Use of Mineral Resources" is included in the List of publications recommended by the Committee for Control in the Sphere of Education and Science of the Ministry of Education and Science of the Republic of Kazakhstan for the publication of the main results of scientific activities.
Owner: "Institute of Metallurgy and Ore Beneficiation" JSC

The Journal was re-registered by the Committee for State Control in the Sphere of Communication, Information and Mass Media of the Ministry of Information and Communication of the Republic of Kazakhstan.

Certificate № 16180-Ж since October 18, 2016

Адрес редакции:
АО «Институт металлургии и обогащения»
050010, Республика Казахстан, г. Алматы, ул. Шевченко, уг. ул. Валиханова, 29/133,
Fax. +7 (727) 298-45-03, Tel. +7 (727) 298-45-02, +7 (727) 298-45-19
E mail: journal@kims-imio.kz, product-service@kims-imio.kz
http://kims-imio.com/index.php/main

Журнал «Комплексное использование минерального сырья» включен в Перечень изданий, рекомендуемых Комитетом по контролю в сфере образования и науки Министерства образования и науки Республики Казахстан для публикации основных результатов научной деятельности.
Собственник: АО «Институт металлургии и обогащения»

Журнал перерегистрирован в Комитете государственного контроля в области связи, информатизации и средств массовой информации
Министерства информации и коммуникации Республики Казахстан
Свидетельство № 16180-Ж от 18 октября 2016 г.

Crossref
DOI: 10.31643/2028/6445.12
Metallurgy and Metallurgical Engineering

Optimization of Aluminum Casting Process Using PLA-Based Casting Patterns and Analysis of their Thermal Behavior

[1]Merkibayev Y.S., [1]Chepushtanova T.A., [1*]Bazarbay B., [1]Burshukova G., [1]Berlibek A.M., [2]Sherstnev P., [2]Sommitsch Christof

[1]Satbayev University, Almaty, Kazakhstan
[2]Graz Tehnology University, Austria

** Corresponding author email: b.bazarbay@satbayev.university*

Received: *March 19, 2026*
Peer-reviewed: *May 20, 2026*
Accepted: *May 29, 2026*

ABSTRACT

This paper presents the results of experimental and numerical studies of the casting process of 99.85% pure aluminum using investment-casting technologies with patterns produced by additive manufacturing. The influence of pouring temperature, mold-filling time, and gating-system design on porosity formation and casting quality was analyzed. It was established that increasing the pouring temperature within the range of 700–800°C leads to increased porosity due to higher gas solubility and intensified turbulence of the melt flow. It was shown that the separating gating system ensures a minimum number of defects compared to top and bottom metal-feeding systems. In addition, thermal analysis of PLA and a glass-fiber-reinforced PLA composite was carried out. Pure PLA was found to burn out almost completely (residue about 2.4%), whereas the composite was characterized by a high residual content (~43.6%), which may negatively affect mold quality. The simulation results obtained using the AutoCAST software package showed good agreement with the experimental data and confirmed the effectiveness of numerical modeling for optimization of casting processes. It was established that the optimal pouring-temperature range for aluminum is 720–760°C. The obtained results confirm the potential of using PLA in investment casting technology and make it possible to improve the quality of aluminum castings under industrial production conditions.

Keywords: 3D printing, investment casting, aluminum alloys, additive manufacturing, industrial manufacturing, innovative manufacturing processes.

Information about authors:

Merkibaev Yerik Serikovich — *Ph.D., Senior Lecturer, Department of Metallurgy and Mineral Processing, O.A. Baikonur Mining and Metallurgical Institute, Satbayev university, Almaty, Kazakhstan. Email: y.merkibayev@satbayev.university; ORCID ID: https://orcid.org/0000-0003-3869-6835*

Chepushtanova Tatyana Alexandrovna — *Doctor Ph.D., Candidate of Technical Sciences, Associate Professor of the Department of Metallurgy and Mineral Processing, O.A. Baikonurov Mining and Metallurgical Institute, Satbayev University, Almaty, Kazakhstan. Email: T.Chepushtanova@satbayev.university; ORCID ID: https://orcid.org/0000-0002-6526-0044*

Bazarbay Bauyrzhan Bakytbekuly — *Ph.D., lecturer, A. Burkitbaev Institute of Power Engineering and Mechanical Engineering, Department of Mechanical Engineering Satbayev University, Almaty, Kazakhstan. Email: b.bazarbay@satbayev.university; ORCID ID: https://orcid.org/0000-0002-7387-1654*

Burshukova Gulzia Adilbekovna — *Ph.D., Associate Professor, Department of Transport and Logistics, Satbayev University, Almaty, Kazakhstan. Email: g.burshukova@satbayev.university; ORCID ID: https://orcid.org/0000-0001-9200-2780*

Berlibek Arailym Muratqyzy — *Doctoral student, Master of Science in the Department of Metallurgy and Mineral Processing, O.A. Baikonurov Mining and Metallurgical Institute, Satbayev University, Almaty, Kazakhstan. Email: berlibek99mail.ru; ORCID ID: https://orcid.org/0009-0001-0163-6911*

Sherstnev Pavel — *Doctor Ph.D., Graz University of Technology, Austria. Email: pavelSh@mail.ru; ORCID ID: https://orcid.org/0009-0007-2351-1910*

Christof Sommitsch — *Ph.D., Professor, Graz University of Technology, Austria, Director of the Institute of Materials Science, Welding and Metallurgy. Email: Sommitsch@mail.ru; ORCID ID: https://orcid.org/0000-0002-6854-4851*

Introduction

Porosity is one of the most critical defects in foundry production, significantly affecting the mechanical properties, tightness and fatigue life of aluminum castings [[1, [2], [3]]. The main mechanisms of pore formation are gas saturation of the melt and shrinkage processes during solidification [[4], [5], [6]]. Aluminum alloys are characterized by high solubility of hydrogen in the liquid state and a sharp decrease in its solubility upon transition to the solid phase, which leads to

intense gas evolution and the formation of gas porosity [[7], [8]]. Additional factors that influence the formation of defects include flow turbulence, air entrainment during pouring, and inefficient operation of the gating system, which can lead to the formation of oxide films and inclusions [[2] [9], [10]]. As noted in the works of Campbell [2] and Stefanescu [10], disruption of flow laminarity promotes the capture of double oxide films (bifilms), which are potential centers for the initiation of pores and cracks. Shrinkage porosity develops due to insufficient compensation for volumetric shrinkage, which is approximately 6% for aluminum, and is directly dependent on the efficiency of feeders and directional solidification [[5], [11]]. According to classic research by Flemings [11], the formation of shrinkage defects is determined by local temperature gradients and casting feeding conditions. Therefore, optimizing the design of gating and feeding systems is a key factor in improving casting quality [[12], [13]]. Modern research confirms that the use of numerical modeling allows for the effective prediction of defect formation zones and optimization of process parameters prior to conducting actual experiments [[6], [12], [14]]. The use of software packages such as Auto-CAST improves the accuracy of casting process design and reduces production costs [[6], [14]]. Modern methods for reducing porosity include optimization of gating systems, melt degassing, and the use of numerical modeling [[9], [10], [11]]. In particular, the use of modified gating system designs (bottom, top, and divider) allows for controlling the nature of the melt flow and minimizing turbulence, which reduces the likelihood of air entrainment and oxide film formation [[2], [9], [15]]. Effective degassing is achieved by using fluorine- and chlorine-containing salt fluxes, as well as inert gas bubbling methods (Ar, N_2), which ensure the removal of dissolved hydrogen through diffusion and coalescence of gas bubbles [[7], [16], [17]]. Additionally, filtration systems (ceramic filters) are used to remove non-metallic inclusions and stabilize the melt flow [[18], [19]]. The use of numerical modeling allows for considering the thermal, hydrodynamic, and phase processes occurring during casting [[12], [13], [14]]. Software packages such as Auto-CAST, ProCAST, and MAGMASoft predict temperature distribution, flow rates, shrinkage zones, and potential porosity regions, enabling optimization of gating system design and pouring modes at the design stage [[6], [12], [20]]. The use of defect formation criteria, such as the Niyama criterion, further improves the accuracy of shrinkage porosity prediction and enables evaluation of casting quality at the early stages of development [[21], [22]]. In recent years, particular attention has been paid to the integration of digital modeling, additive technologies, and intelligent defect prediction methods. Current research shows that the use of integrated thermohydrodynamic modeling and digital analysis methods can significantly improve the accuracy of porosity prediction and reduce the number of production tests [[23], [24], [25]]. In addition, the effect of additively manufactured polymer models on the quality of cast parts is being actively studied, including the thermal degradation characteristics of PLA composites, their gas evolution, and the formation of a residual phase.

Studies demonstrate the effectiveness of integrating modeling methods with experimental data and machine learning approaches, which allows for the consideration of real production factors and increases the reliability of predictions [[23], [24], [25]]. Thus, the integrated use of degassing, rational design of gating systems, and digital modeling is the most effective approach to reducing porosity and improving the quality of aluminum castings. With the development of additive technologies, the use of polymer models for investment casting is of particular interest, allowing for a significant increase in accuracy and a reduction in the cost of manufacturing complex-shaped castings [[15], [16]]. In particular, FDM and SLA technologies provide high-precision prototypes with specified geometry and controlled surface roughness [[23], [24]]. PLA (polylactide) is widely used due to its biodegradability, low processing temperature, and ability to undergo almost complete thermal decomposition without the formation of significant residues [[17], [18], [19]]. Thermal destruction of PLA occurs primarily through the depolymerization mechanism with the rupture of ether bonds and the formation of volatile products, which makes this material promising for casting using burnt models [[18], [25]]. The thermodynamic approach demonstrates that both in sulfurizing roasting of Pb–Zn ores and in aluminum alloy casting, the controlling factor is the regulation of phase transformations through changes in gas atmosphere and temperature, which ultimately governs the formation of material structure and defect development [[26], [27]]. The obtained results indicate that the use of 3D-printed PLA models in aluminum investment casting is associated with a

significant influence of polymer thermal decomposition, the mold–pattern interface, and heat and mass transfer conditions on defect formation, including porosity, which requires consideration of material anisotropy, gas evolution behavior, and thermal processing regimes to improve the accuracy and quality of cast products [28].

However, the introduction of composite materials such as glass fiber-reinforced PLA requires further analysis, since the presence of an inorganic phase significantly alters the mechanism of thermal degradation and heat and mass transfer [[20], [21], [22]]. In particular, glass fiber increases thermal stability and shifts the temperature maxima of decomposition, but simultaneously leads to the formation of a residual phase that can impede the removal of decomposition products, impair the gas permeability of the mold, and contribute to the formation of casting defects [[21], [22]]. Furthermore, the interaction of the polymer matrix with the surface of the reinforcing fibers can lead to multistage decomposition kinetics and changes in gas evolution [20].

Despite numerous studies devoted to reducing the porosity of aluminum castings and the use of PLA patterns in investment casting, the complex relationships between pouring parameters, gating system design, thermal degradation of PLA composites, and defect formation remain poorly understood. Most existing studies examine either the hydrodynamic properties of the mold filling process or the thermal behavior of polymer patterns separately. However, the influence of residual PLA composite mass on the quality of aluminum castings and the mechanisms of defect formation have not been fully explored.

The scientific novelty of this study lies in the comprehensive combination of experimental research and numerical modeling of the aluminum casting process using additively manufactured PLA models of varying compositions. This study, for the first time, combinedly evaluates the influence of pouring temperature, gating system design, and the thermal behavior of PLA/PLA composites on the formation of porosity in aluminum castings. Additionally, a relationship was established between the high residual mass of the PLA composite, the characteristics of outgassing during thermal degradation, and the likelihood of defect formation in the cast structure. The obtained results allow us to expand our understanding of defect formation mechanisms and substantiate the selection of optimal materials and process modes for investment casting.

The aim of this study is to comprehensively investigate the influence of process parameters (pouring temperature, pouring time, and gating system design) on the porosity of aluminum castings, as well as to evaluate the thermal behavior of PLA and PLA composite materials for their applicability in investment casting technologies. Particular attention is paid to the relationship between the mechanisms of thermal degradation of polymer patterns and defect formation in metal castings, which allows for the substantiation of the selection of optimal materials and process conditions.

Materials and Methods

Experiments and Casting Simulation

Experimental and numerical studies of the casting process of high-purity aluminum (99.85%) were carried out to analyze porosity formation and optimize technological parameters. Numerical simulation was performed using the Auto-CAST software package, which makes it possible to predict temperature-field distribution, melt-flow velocity, and zones of probable defect formation.

During the study, the main technological parameters of the process were varied, including pouring time, melt temperature, and the design of the gating-feeding system. The pouring time for different types of gating systems was as follows: 12.5 s for the bottom system, 8.5 s for the separating system, and 5 s for the top system, which ensured different melt-flow patterns—from predominantly laminar to turbulent regimes. The geometric parameters of the sprues included diameters of 14 mm and 10 mm with lengths from 50 to 80 mm, which made it possible to regulate the flow rate and the hydrodynamic conditions of mold filling. The dimensions of the ingates were 10×12×15 mm, and those of the runners were 8×10×65 mm and 8×10×90 mm, respectively, ensuring uniform melt distribution and a reduction in local turbulent zones. The experimental conditions were further refined to ensure the reproducibility of the study. High-purity aluminum (99.85%) was used, and the melt was prepared in an electric resistance furnace. Before pouring, the melt was degassed to reduce the dissolved hydrogen content and decrease the likelihood of gas porosity. A sand-clay mold with controlled gas permeability and moisture content was used as the casting mold, providing stable heat-removal and solidification conditions. Temperature

control was carried out using thermocouples and a digital data-recording system.

Table 1 - Design parameters and their calculated values for the feeding and gating systems.

No.	Parameter	Design value
1	Pouring time for the bottom, separating, and top gating systems	12.5 s, 8.5 s, and 5 s, respectively
2	Top and bottom sprue diameter and sprue length for the separating and top gating systems	14 mm, 10 mm, and 50 mm, respectively
3	Top and bottom sprue diameter and sprue length for the bottom gating system	14 mm, 10 mm, and 80 mm, respectively
4	Sprue: diameter and height	15 mm and 20 mm, respectively
5	Runner dimensions: width, height, and length for the separating gate system	8 mm, 10 mm, and 65 mm, respectively
6	Runner dimensions: width, height, and length for the bottom gate system	8 mm, 10 mm, and 90 mm, respectively
7	Ingate dimensions: width, height, and length for the top, separating, and bottom gating systems	10 mm, 12 mm, and 15 mm, respectively
8	Feeder design based on Caine's method; feeder diameter and height for the bottom and separating gating systems	25 mm and 25 mm, respectively
9	Height and diameter of the feeder neck for the bottom and separating gating systems	10 mm and 20 mm, respectively

In addition, the design of the riser (sprue) with a diameter of 15 mm and a height of 20 mm was optimized to ensure stable melt supply and reduce the likelihood of air entrainment. The feeding system was designed based on Caine's method, taking into account the formation of directional solidification; the feeder dimensions were 25×25 mm and the neck dimensions were 10×20 mm, which ensured effective compensation of shrinkage processes. Particular attention was paid to the placement of the feeder in the zone of maximum thermal concentration (hot spot), which contributed to a reduction in shrinkage porosity.

The choice of these parameters was dictated by the need to ensure an optimal balance between mold-filling rate, reduced flow turbulence, and effective feeding of the casting during solidification, which together are aimed at minimizing gas and shrinkage porosity. This is shown in Table 1.

The feeding system was designed with consideration for compensating the volumetric shrinkage of aluminum, which is about 6% during solidification. The feeder dimensions were 25×25 mm, which provided sufficient volume to feed the casting and prevent shrinkage defects. The system design was optimized using simulation results, including hot-spot analysis and directional solidification.

Analysis of the influence of gating-system type showed that when a bottom gate is used, the molten metal enters the lower part of the mold, ensuring a predominantly laminar flow regime and minimizing air entrainment; however, the mold-filling time increases. It was established that as the pouring temperature increases in the range of 700–800°C, a steady growth in porosity is observed, as clearly shown in Fig. 1. This effect is caused by the increased solubility of gases in the aluminum melt at higher temperatures, as well as by the decrease in viscosity, which leads to intensified turbulence and the entrainment of gaseous inclusions. According to the simulation results, porosity increases approximately from 960 to 1120 mm³, whereas the experimental values change from 1030 to 1250 mm³, indicating a higher level of defect formation under real conditions due to the influence of technological factors such as flow turbulence, air entrainment, mold gas permeability, and the limited efficiency of degassing. At the same time, the trends of the Simulation and Experimental dependencies coincide, which confirms the adequacy of the Auto-CAST model despite the presence of a quantitative discrepancy of about 50–130 mm³ associated with the idealization of the calculation conditions. It was established that in the range of 700–740°C the increase in porosity is moderate, whereas at temperatures above 740–780°C a sharp increase in defect formation is observed, indicating the achievement of a critical temperature interval.

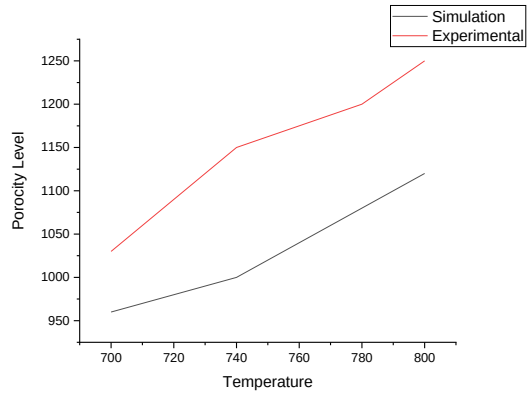

Fig. 1 - Change in porosity as a function of pouring temperature

When a top gating system is used (Fig. 2), the mold is filled in the minimum time; however, due to the free fall of the melt, a turbulent flow regime is formed, which leads to an increase in gas and shrinkage porosity. In this case, porosity increases from 1040 to 1300 mm³ according to simulation results and from 1180 to 1460 mm³ according to experimental data. The increased defect level is caused by intensified turbulence, air entrainment, and the formation of oxide films that serve as pore nucleation sites. A particularly intensive increase in porosity is observed in the range of 780–800°C, which indicates the critical influence of temperature on defect-formation processes.

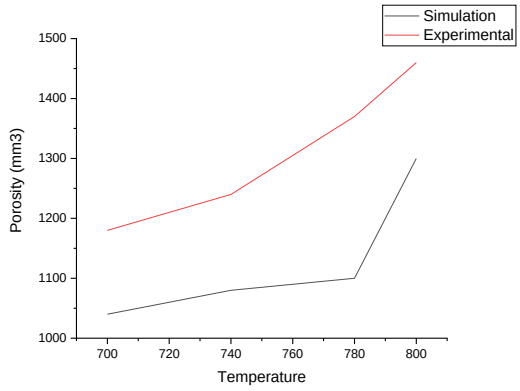

Fig. 2. Change in porosity as a function of pouring temperature

The separating gating system (Fig. 3) proved to be the most effective from the standpoint of minimizing porosity, combining the advantages of bottom and top melt supply. In this system, the sprue and gate are located in the same plane, which ensures an optimal temperature gradient and directional solidification. This promotes the transfer of the shrinkage cavity from the casting volume into the feeder and reduces the probability of defect formation. The analysis showed that porosity increases from 1030 to 1250 mm³ (simulation) and from 1090 to 1420 mm³ (experiment), while the lowest level of defect formation among all considered systems is observed. Similar to the other cases, a sharp increase in porosity is recorded at temperatures above 780°C, which is associated with intensified gas saturation and deterioration of solidification conditions.

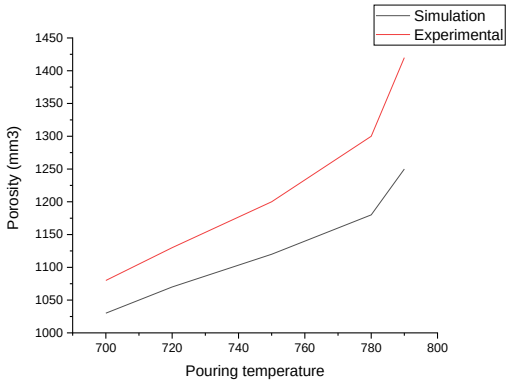

Fig. 3 - Change in porosity as a function of pouring temperature

In addition to the macroscopic analysis of porosity, a microstructural analysis of the samples was carried out using optical metallography methods. The investigations were performed on polished sections prepared by standard methods of mechanical polishing and chemical etching. The microstructural analysis made it possible to reveal the distribution of pores, the nature of the dendritic structure, and the localization of defects depending on the pouring temperature and the type of gating system. The obtained microstructural images further confirmed the results of numerical modeling and experimental porosity analysis. The obtained results demonstrate that the pouring temperature and the type of gating system have a decisive influence on the formation of porosity in aluminum castings. The optimal choice is the use of a separating gating system in combination with a controlled temperature regime (not higher than ~740–760°C), which ensures the minimization of turbulence, effective feeding of the casting, and a reduction in gas and shrinkage defects.

Energy-Dispersive Spectroscopy (EDS) Analysis

The chemical composition of the cast aluminum was determined by energy-dispersive spectroscopy (EDS), the results of which are presented in Fig. 4. It was established that the main phase is aluminum, while impurities of carbon and oxygen are also

detected in the samples, which may be associated with oxidation processes and the interaction of the melt with the surrounding environment.

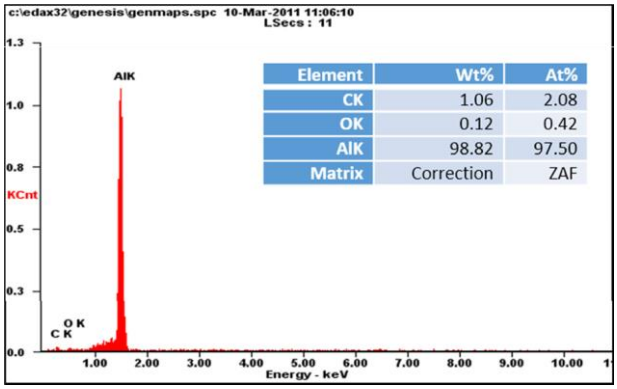

Fig. 4 - EDS analysis of cast aluminum

An increased oxygen content in certain local areas may indicate the formation of Al_2O_3 oxide inclusions, which can act as nucleation centers for gas pores. From a physical point of view, porosity formation is associated with a decrease in gas solubility in the aluminum melt during crystallization and with the local accumulation of gaseous products of thermal degradation of the PLA pattern. During solidification, diffusive release of dissolved hydrogen occurs, as well as restricted removal of gases through the mold, which leads to the formation of closed pores.

The following relationship was used for quantitative evaluation of porosity:

$$P = \left(1 - \frac{V_p}{V_S}\right) 100\%$$

where is the sample volume, is the dense volume, M is the sample mass, and ρ is the material density.

The dense volume was determined by the expression:

$$V_p = \frac{M}{p}$$

The obtained experimental porosity values were compared with the results of numerical simulation. The average discrepancy between the experimental and calculated data was less than 8%, which indicates satisfactory adequacy of the model used. To increase the reliability of the results, measurements were carried out on at least three samples for each casting mode, after which the mean values and standard deviations were calculated. The error in porosity determination did not exceed ±2%.

The combination of macro- and microstructural analysis methods, energy-dispersive spectroscopy, and experimental determination of porosity made it possible to comprehensively assess the influence of technological parameters on defect formation in aluminum castings.

Thermal Analysis of PLA and PLA Composite

Thermogravimetric analysis (TGA), as well as derivative curves (DTG) and differential thermal analysis (DTA), were used to evaluate the thermal behavior of PLA-based materials employed in additive manufacturing. The results for pure PLA and for the PLA composite reinforced with glass fiber are presented in Figures 5 and 6.

As can be seen from Fig. 5, pure PLA demonstrates characteristic single-stage thermal degradation. In the temperature range up to 300 °C, the mass of the sample remains almost unchanged, which indicates the absence of moisture and volatile components. The main decomposition stage occurs in the interval of 320–380 °C, with a maximum degradation rate around 360 °C. In this range, intensive depolymerization is observed with rupture of ether bonds and release of gaseous products. The total mass loss is about 95–98%, and the residual mass does not exceed ~2.4% at 1000 °C (Fig. 5), which indicates almost complete burnout of the material.

From the standpoint of the casting process, the intensive release of volatile products in the range of 320–380 °C is accompanied by the formation of a gaseous environment inside the mold. If the mold has sufficient gas permeability, the degradation products are effectively removed, which reduces the probability of defect formation. The low residual mass of pure PLA indicates almost complete burnout of the pattern and a minimal probability of forming solid residues in the mold cavity. This contributes to obtaining a more homogeneous structure of aluminum castings and reduces the risk of gas porosity formation. In addition, the EDS analysis results show that in castings obtained using pure PLA, the oxygen and carbon contents are minimal, which indicates more complete removal of thermal degradation products and a lower probability of secondary oxidation of the melt during casting.

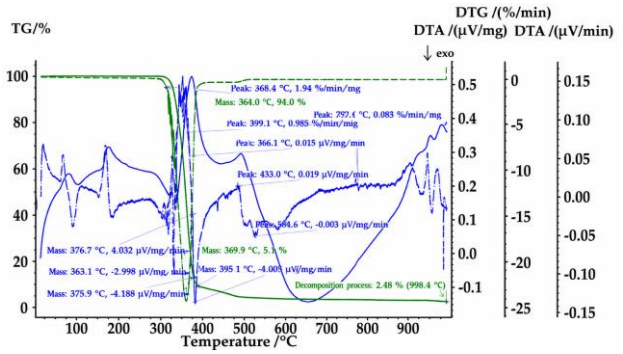

Figure 5 - TGA, DTG, and DTA curves for pure PLA material used in additive manufacturing, demonstrating single-stage thermal degradation and almost complete mass loss

From the standpoint of physicochemical processes, the intensive release of volatile products in the interval of 320–380 °C can lead to a local increase in gas pressure inside the mold. If the molding material has insufficient gas permeability, this contributes to the formation of gas porosity in the casting. Thus, the temperature range of the maximum PLA degradation rate is a critically important parameter when selecting pattern burnout modes.

In contrast, the glass-fiber-reinforced PLA composite (Fig. 6) demonstrates more complex thermal behavior. Up to 300 °C, no significant changes in mass are observed, which indicates system stability. The main decomposition stage is shifted to a higher temperature range of 350–420 °C, with a characteristic maximum around 410 °C, which is associated with the influence of the reinforcing inorganic phase. The presence of several peaks on the DTG and DTA curves (≈367 °C, 431 °C, 490 °C, and 541 °C) indicates a multistage degradation mechanism caused by the interaction of the decomposition products of the polymer matrix with the glass-fiber surface. The key difference is the significant increase in residual mass, which amounts to about 43.61% at 1000 °C, due to the presence of thermally stable glass fiber. This indicates that the material is not subject to complete burnout, unlike pure PLA. The high residual mass of the PLA composite has a direct effect on the quality of aluminum castings. Incomplete burnout of the composite material leads to the accumulation of residual inorganic particles inside the casting mold, which worsens the gas permeability of the molding system and hinders the removal of thermal degradation products. As a result, a local increase in gas pressure occurs in the mold cavity, promoting the formation of gas porosity and surface defects in the castings. Residual glass-fiber particles can become centers of local disturbance of the crystallization of the aluminum melt. This leads to the formation of microdefects, an increase in the number of non-metallic inclusions, and a decrease in the structural homogeneity of the material. The presence of such inclusions worsens surface quality and can reduce the mechanical properties of the finished products.

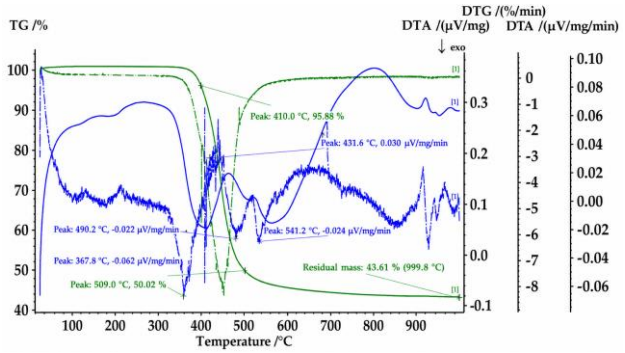

Figure 6 - TGA, DTG, and DTA curves for a PLA-based composite reinforced with glass fiber, demonstrating the multistage nature of thermal decomposition and a high residual mass (~43.6%) caused by the presence of an inorganic phase

A comparison of the thermal curves shows that the addition of glass fiber leads not only to increased thermal resistance but also to a longer duration of gaseous-product release. This may explain the increased probability of defect formation during casting, since more prolonged thermal degradation is accompanied by gas accumulation in the interfacial regions of the mold. In addition, the presence of a residual inorganic phase can worsen the removal of decomposition products and lead to local inclusions in the casting structure. The EDS analysis results confirm this assumption. In samples produced using the PLA composite, an increased content of oxygen and carbon is recorded, which may be associated with residual thermal decomposition products and local oxidation of the melt. This indicates insufficiently complete removal of the burnout products of the composite material and confirms the direct relationship between the high residual mass of the PLA composite and the deterioration in the quality of cast products.

A comparative analysis shows that the addition of glass fiber leads to increased thermal resistance and a shift in the temperature maxima of decomposition; however, it is accompanied by an increase in residual content and a more complex thermal-degradation mechanism. This is important for investment-casting processes: while pure PLA ensures complete material removal without the

formation of significant residues, the composite material can lead to the accumulation of inorganic phases and the formation of defects in the casting mold.

To increase the reliability of the thermal analysis, all tests were performed in triplicate. The temperatures of the maximum decomposition rate were determined as average values, and the variation in the results did not exceed ±5 °C. The obtained data demonstrate good reproducibility of the experimental measurements and agrees with the results of numerical modeling of thermal-degradation processes.

Thus, the results of the thermal analysis (Figs. 5 and 6) confirm that pure PLA is a preferable material for investment-casting technologies, whereas PLA composites require additional optimization of burnout modes, including higher temperature and improved conditions for the removal of decomposition products.

Conclusion

As a result of the experimental and numerical studies of the casting process of aluminum with a purity of 99.85% using investment-casting technology, the following main conclusions were established: the pouring temperature is a key parameter determining the level of porosity of castings. As the temperature increases in the range of 700–800°C, a steady increase in porosity is observed due to the increased solubility of gases in the melt and intensified flow turbulence. It is shown that the experimental porosity values (≈1030–1250 mm³) systematically exceed the simulation results (≈960–1120 mm³) by 50–130 mm³, which is caused by the influence of real production factors such as air entrainment, instability of thermal conditions, and the limited efficiency of degassing. It was established that the type of gating-feeding system has a significant influence on defect formation. The lowest level of porosity is achieved when a separating gating system is used, providing directional solidification and an optimal thermal gradient. When a top gating system is applied, the maximum level of porosity is observed due to the turbulent flow regime and the entrainment of gaseous inclusions, whereas the bottom system provides a more stable (laminar) flow but requires increased mold-filling time.

The modeling results obtained using the Auto-CAST software package showed a high degree of qualitative agreement with the experimental data, which confirms the adequacy of the applied model and its effectiveness for the engineering optimization of casting processes. Thermogravimetric analysis showed that pure PLA completely decomposes in the range of 320–380°C with a residual mass of less than 3%, which makes it a promising material for investment casting. At the same time, the glass-fiber-reinforced PLA composite is characterized by multistage decomposition and a high residual mass (~43.6%), which can lead to deterioration of mold quality. It was established that the optimal pouring-temperature range for aluminum should be within 720–760°C, ensuring a compromise between melt fluidity and minimization of porosity. At temperatures above 780°C, a sharp increase in defect formation is observed, which requires strict control of the technological regime. The combination of numerical modeling methods and experimental studies makes it possible to effectively optimize the technological parameters of the casting process and significantly reduce the level of porosity in aluminum castings.

The practical significance of the results obtained lies in the possibility of implementing them under real foundry-production conditions in order to improve the quality of aluminum castings and reduce the amount of scrap. The established optimal pouring-temperature regimes (720–760°C) can be used in the development of process sheets and regulations for investment casting of aluminum alloys. The use of a separating gating-feeding system makes it possible to reduce the probability of gas porosity formation and increase the structural homogeneity of products without a significant increase in production costs.

The study results can also be used in the design of technological processes employing additively manufactured PLA patterns. The use of pure PLA instead of glass-fiber-reinforced PLA composites provides more complete burnout of the pattern and reduces the risk of residual inclusions in the mold. This is especially important for the production of thin-walled and critical parts used in mechanical engineering, the aerospace industry, and the automotive industry. The use of software modeling in the AutoCAST environment makes it possible, at the design stage, to predict zones of probable defect formation, optimize the design of the gating system, and reduce the number of expensive experimental trials. The implementation of such an approach under production conditions contributes to reduced material costs, lower metal consumption, and increased overall technological efficiency of foundry

production. The obtained results can serve as a basis for further industrial optimization of investment-casting processes, including automation of temperature-regime control, improvement of degassing systems, and development of new materials for additive casting patterns.

CRedit author statement: **Y. Merkibayev, T. Chepushtanova, C. Sommitsch:** Methodology, formal analysis, investigation, Data writing, Original draft preparation, writing–review and editing; **A. Berlibek, B. Bazarbay**: Data curation, Reviewing and Editing; **P. Sherstnev, G. Burshukova:** Investigation.

Conflicts of Interest. On behalf of all authors, the correspondent author declares that there is no conflict of interest.

Gratitude: This research was funded by the Science Committee of the Ministry of Science and Higher Education of the Republic of Kazakhstan (grant No. AP26198529).

Cite this article as: Merkibayev YS, Chepushtanova TA, Bazarbay B, Burshukova G, Berlibek AM, Sherstnev P, Sommitsch Christof. Optimization of Aluminum Casting Process Using PLA-Based Casting Patterns and Analysis of their Thermal Behavior. Kompleksnoe Ispolzovanie Mineralnogo Syra = Complex Use of Mineral Resources. 2028; 345(2):5-15. https://doi.org/10.31643/2028/6445.12

PLA негізіндегі құю үлгілерін пайдалану арқылы алюминий құю процесін оңтайландыру және олардың термиялық әрекеттерін талдау

[1]Меркибаев Е.С., [1]ЧепуштановаТ.А., [1]Базарбай Б.Б., [1]Буршукова,Г.А., [1]Берлібек А.М., [2]Sherstnev P., [2]Sommitsch Christof

[1]Сәтбаев университеті, Алматы ,Қазақстан
[2]Грац техникалық университеті, Австрия

Мақала келді: *19 наурыз 2026*
Сараптамадан өтті: *20 мамыр 2026*
Қабылданды: *29 мамыр 2026*

ТҮЙІНДЕМЕ

Мақалада аддитивті өндіріс әдісімен дайындалған балқымалы үлгілер бойынша құю технологиясын қолдана отырып, тазалығы 99,85% алюминийді құю процесінің эксперименттік және сандық зерттеулерінің нәтижелері ұсынылған. Құю температурасының, қалыпты толтыру уақытының және құю жүйесі конструкциясының кеуектіліктің түзілуіне және алынатын құймалардың сапасына әсері талданды. Құю температурасының 700–800°C аралығында жоғарылауы балқымадағы газдардың ерігіштігінің артуына және ағын турбуленттілігінің күшеюіне байланысты кеуектіліктің ұлғаюына әкелетіні анықталды. Металды берудің жоғарғы және төменгі жүйелерімен салыстырғанда, бөлгіш құю жүйесі ақаулардың ең аз мөлшерін қамтамасыз ететіні көрсетілген. Сонымен қатар, PLA және шыны талшық қосылған PLA-композитінің термиялық талдауы жүргізілді. Таза PLA іс жүзінде толық жанып кететіні (қалдық шамамен 2,4%), ал композит жоғары қалдық құрамымен (~43,6%) сипатталатыны анықталды, бұл құю қалыптарының сапасына кері әсер етуі мүмкін. AutoCAST бағдарламалық кешенін пайдалану арқылы алынған модельдеу нәтижелері эксперименттік деректермен жақсы сәйкестік көрсетті және құю процестерін оңтайландыру үшін сандық модельдеудің тиімділігін растады. Алюминийді құюдың оңтайлы температура диапазоны 720–760°C екені анықталды. Алынған нәтижелер балқымалы үлгілер бойынша құю технологиясында PLA қолданудың перспективалы екенін растайды және өнеркәсіптік өндіріс жағдайында алюминий құймаларының сапасын арттыруға мүмкіндік береді.

Түйін сөздер: 3D-басып шығару, балқытылатын үлгілер бойынша құю, алюминий қорытпалары, аддитивті өндіріс, өнеркәсіптік өндіріс, инновациялық өндірістік процестер.

Авторлар туралы ақпарат:

Меркибаев Ерик Серикович — *Ph.D докторы. О.Ә. Байқоңыров атындағы Тау-кен металлургия институты, Металлургия және пайдалы қазбаларды байыту кафедрасының аға оқытушысы, Сәтбаев университеті, Алматы, Қазақстан. Email: y.merkibayev@satbayev.university; ORCID ID: https://orcid.org/0000-0003-3869-6835*

Чепуштанова Татьяна Александровна — *Ph.D докторы, О.Ә.Байқоңыров атындағы Тау-кен металлургия институты, Металлургия және пайдалы қазбаларды байыту кафедрасының қауымдастырылған профессоры, техника ғылымдарының кандидаты, Сәтбаев университеті, Алматы, Қазақстан. Email: T.Chepushtanova@satbayev.university; ORCID ID: https://orcid.org/0000-0002-6526-0044*

Базарбай Бауыржан Бақытбекұлы — *Ph.D. докторы, А. Бүркітбаев атындағы Энергетика және машина жасау институты, Машина жасау кафедрасының оқытушысы, Сәтбаев университеті, Алматы, Қазақстан. Email: b.bazarbay@satbayev.university; ORCID ID: https://orcid.org/0000-0002-7387-1654*

Буршукова Гулзия Адилбековна — *Ph.D докторы, қауымдастырылған профессор, Көлік және логистика кафедрасы, Сәтбаев университеті, Алматы, Қазақстан. Email: g.burshukova@satbayev.university; ORCID ID: https://orcid.org/0000-0001-9200-2780*

Берлібек Арайлым Мұратқызы	*Докторант, магистр, О.Ә. Байқоңыров атындағы Тау-кен металлургия институты Металлургия және пайдалы қазбаларды байыту кафедрасы, Сәтбаев университеті, Алматы, Қазақстан. Email: berlibek99mail.ru; ORCID ID: https://orcid.org/0009-0001-0163-6911*
Sherstnev Pavel	*Ph.D докторы, Грац технологиялық университеті, Австрия. Email: pavelSh@mail.ru; ORCID ID: https://orcid.org/0009-0007-2351-1910*
Christof Sommitsch	*Ph.D докторы, Материалтану, дәнекерлеу және қалыптау институтының директоры, профессор, Грац технологиялық университеті, Австрия. Email: Sommitsch@mail.ru; ORCID ID: https://orcid.org/0000-0002-6854-4851*

Оптимизация процесса литья алюминия с использованием литьевых схем на основе PLA-материалов и анализа их термического поведения

[1]Меркибаев Е.С., [1]Чепуштанова Т.А., [1]Базарбай Б.Б., [1]Буршукова,Г.А., [1]Берлібек А.М., [2]Sherstnev P., [2]Sommitsch Christof

[1]Satbayev University, Алматы, Казахстан
[2]Грацкий технический университет, Австрия

Поступила: *19 марта 2026*
Рецензирование: *20 мая 2026*
Принята в печать: *29 мая 2026*

АННОТАЦИЯ

В статье представлены результаты экспериментальных и численных исследований процесса литья алюминия чистотой 99,85% с использованием технологий литья по выплавляемым моделям, изготовленным методом аддитивного производства. Проанализировано влияние температуры заливки, времени заполнения формы и конструкции литниковой системы на образование пористости и качество получаемых отливок. Установлено, что повышение температуры заливки в диапазоне 700–800°C приводит к увеличению пористости вследствие роста растворимости газов и усиления турбулентности потока расплава. Показано, что разделительная литниковая система обеспечивает минимальное количество дефектов по сравнению с верхней и нижней системами подачи металла. Также проведён термический анализ PLA и PLA-композита со стекловолокном. Установлено, что чистый PLA практически полностью выгорает (остаток около 2,4%), тогда как композит характеризуется высоким остаточным содержанием (~43,6%), что может отрицательно влиять на качество литейной формы. Результаты моделирования, полученные с использованием программного комплекса AutoCAST, показали хорошее соответствие экспериментальным данным и подтвердили эффективность численного моделирования для оптимизации литейных процессов. Установлено, что оптимальный диапазон температуры заливки алюминия составляет 720–760°C. Полученные результаты подтверждают перспективность использования PLA в технологии литья по выплавляемым моделям и позволяют повысить качество алюминиевых отливок в условиях промышленного производства.

Keywords: 3D-печать, литье по выплавляемым моделям, алюминиевые сплавы, аддитивное производство, промышленное производство, инновационные производственные процессы.

Информация об авторах:

Меркибаев Ерик Серикович	*PhD, старший преподаватель кафедры Металлургии и обогащения полезных ископаемых, Горно-металлургический институт имени О.А. Байконурова, Satbayev university, Almaty, Kazakhstan. Email: y.merkibayev@satbayev.university; ORCID ID: https://orcid.org/0000-0003-3869-6835*
Чепуштанова Татьяна Александровна	*Доктор Ph.D., кандидат технических наук, ассоциированный профессор кафедры Металлургии и обогащения полезных ископаемых, Горно-металлургический институт имени О.А. Байконурова, Satbayev University, Almaty, Kazakhstan. Email: T.Chepushtanova@satbayev.university; ORCID ID: https://orcid.org/0000-0002-6526-0044*
Базарбай Бауыржан Бакытбекұлы	*Доктор Ph.D., преподаватель, Институт энергетики и машиностроения им. А. Буркитбаева, кафедра Машиностроение Satbayev University, Almaty, Kazakhstan. Email: b.bazarbay@satbayev.university; ORCID ID: https://orcid.org/0000-0002-7387-1654*
Буршукова Гулзия Адилбековна	*Доктор Ph.D. ассоц.профессор кафедры транспорта и логистики, Satbayev University, Almaty, Kazakhstan. Email: g.burshukova@satbayev.university; ORCID ID: https://orcid.org/0000-0001-9200-2780*
Берлібек Арайлым Мұратқызы	*Докторант, магистр кафедры Металлургии и обогащения полезных ископаемых, Горно-металлургический институт имени О.А. Байконурова, Satbayev University, Almaty, Kazakhstan. Email: berlibek99mail.ru; ORCID ID: https://orcid.org/0009-0001-0163-6911*
Sherstnev Pavel	*Доктор Ph.D., Грацкий технический университет, Австрия. Email: pavelSh@mail.ru; ORCID ID: https://orcid.org/0009-0007-2351-1910*
Christof Sommitsch	*Доктор Ph.D., директор Института материаловедения, сварки и формовки, профессор Грацского технического университета, Австрия. Email: Sommitsch@mail.ru; ORCID ID: https://orcid.org/0000-0002-6854-4851*

References

[1] Linder J, Axelsson M, Nilsson H. Influence of porosity on fatigue life of aluminium castings. Int. J. Fatigue. 2006; 28:1752–1758. https://doi.org/10.1016/j.ijfatigue.2006.01.001

[2] Campbell J. Complete Casting Handbook; Butterworth-Heinemann: Oxford, UK. 2011. https://www.researchgate.net/publication/259486719_Complete_Casting_Handbook_2011

[3] Ravi B. Casting simulation and optimization: Benefits, bottlenecks and best practices. Indian Foundry J. 2008, 1–12. https://www.researchgate.net/profile/B-Ravi-2/publication/228975218_Casting_Simulation_and_Optimisation_Benefits_Bottlenecks_and_Best_Practices/links/53f0dbac0cf23733e812f5a0/Casting-Simulation-and-Optimisation-Benefits-Bottlenecks-and-Best-Practices.pdf

[4] Flemings MC. Solidification Processing; McGraw-Hill: New York, USA. 1974. https://doi.org/10.1002/9783527603978.mst0173

[5] Choudhari CM, Narkhede BE, Mahajan SK. Casting design and simulation using AutoCAST-X. Procedia Mater. Sci. 2014; 6:786–797. https://doi.org/10.1016/j.mspro.2014.07.095

[6] Barsawade PB, Santhy K, Gholap M, Salot M. Grain refinement of Al-Ti master alloy on as cast and heat treated Al-Si-Mg alloy. 14TH International Conference on Materials Processing And Characterization 2023. 2024. https://doi.org/10.1063/5.0192508

[7] Sigworth GK. Refining of Secondary Aluminum: Important Chemical Factors. Int. J. Minerals, Metals & Materials Society. 2021; 5:7–18. https://doi.org/10.1007/s11837-021-04774-z

[8] Campbell J. Entrainment defects. Mater. Sci. Technol. 2006; 22:127–145. https://doi.org/10.1179/174328406X74248

[9] Stefanescu DM. Science and Engineering of Casting Solidification; Springer: New York, USA. 2009. https://link.springer.com/book/10.1007/978-3-319-15693-4

[10] Kent D Carlson, Beckermann C. Prediction of Shrinkage Pore Volume Fraction Using a Dimensionless Niyama Criterion. Metallurgical and Materials Transactions A. 2009; 7:52–63. https://doi.org/10.1007/s11661-009-0055-3

[11] Dabade UA, Bhedasgaonkar RC. Casting defect analysis using simulation. Procedia CIRP. 2013; 7:616–621. https://doi.org/10.1016/j.procir.2013.06.042

[12] Nimbulkar SL, Dalu RS. Optimization of gating system. Perspect. Sci. 2016; 8:39–42. https://doi.org/10.1016/j.pisc.2016.03.001

[13] Ravi B. Metal Casting: Computer-Aided Design and Analysis; PHI Learning: New Delhi, India. 2015. http://pdfcoffee.com/computer-aided-casting-design-and-simulation-pdf-free.html

[14] Ngo TD, Kashani A, Imbalzano G. Additive manufacturing (3D printing): A review. Compos. Part B. 2018; 143:172–196. https://doi.org/10.1016/j.compositesb.2018.02.012

[15] Gibson I, Rosen D, Stucker B, Khorasani A. Additive Manufacturing Technologies; Springer: New York, USA. 2020. https://doi.org/10.1007/978-3-030-56127-7

[16] Farah S, Anderson DG, Langer R. Physical and mechanical properties of PLA. Adv. Drug Deliv. Rev. 2016; 107:367–392. https://doi.org/10.1016/j.addr.2016.06.012

[17] Tsuji H. Poly (lactic acid): Synthesis and Applications; Wiley: Hoboken, USA. 2010. https://www.researchgate.net/publication/216770320_PolyLactic_Acid_Synthesis_Structures_Properties_Processing_and_Applications

[18] Randall J. Polylactic acid technology. Natural Fibers, Biopolymers, and Biocomposites. 2005; 12:1841–1846. https://doi.org/10.1201/9780203508206.ch16

[19] Pickering KL, Efendy MGA, Le TM. Fiber-reinforced composites. Compos. Part A. 2016; 83:98–112. https://doi.org/10.1016/j.compositesa.2015.08.038

[20] Fu SY, Lauke B. Effects of fiber length and orientation. Compos. Sci. Technol. 1996; 56:1179–1190. https://doi.org/10.1016/S0266-3538(96)00072-3

[21] Thomason JL. Glass fibre sizing and interfacial bonding. Compos. Part A. 2002; 33:1641–1652. https://doi.org/10.1016/j.compositesa.2019.105619

[22] Chacón JM, Caminero MA, García-Plaza E, Nunez PJ. Additive manufacturing of PLA structures using fused deposition modelling: Effect of process parameters on mechanical properties and their optimal selection. 2017; 124:143-157. https://doi.org/10.1016/j.matdes.2017.03.065

[23] Torrado Perez AR, Roberson DA. Failure Analysis and Anisotropy Evaluation of 3D-Printed Tensile Test Specimens of Different Geometries and Print Raster Patterns. Jornal of Failure Analysis and Prevention. 2016; 1–4:10–19. https://doi.org/10.1007/s11668-016-0067-4

[24] Liu X, Petinakis E, Long Yu, Cameron Way. Biodegradation and thermal decomposition of poly(lactic acid)-based materials reinforced by hydrophilic fillers. Polymer Degradation and Stability. 2010; 95(9):1704-1707. https://doi.org/10.1016/j.polymdegradstab.2010.05.027

[25] Chacón JM, Caminero MA, García-Plaza E, Núñez PJ. Additive manufacturing of PLA structures using FDM: Mechanical and thermal properties. Materials. 2017; 10:124. https://doi.org/10.1016/j.matdes.2017.03.065

[26] Chepushtanova TA, Merkibayev YS, Mamyrbayeva K K, Sarsenbekov T, Mishra B. Mechanism and technological results of sulfidation roasting of oxidized compounds. . Kompleksnoe Ispolzovanie Mineralnogo Syra = Complex Use of Mineral Resources. 2025; 332(1):119-132. https://doi.org/10.31643/2025/6445.11

[27] Chepushtanova TA, Merkibayev YS, Mamyrbayeva KK, Mishra B, Kuldeyev YI. Processing of the zinc-lead-bearing flotation middlings by sulfidizing roasting with pyrrhotites production by predicted properties. Non-Ferr. Met. 2022; 2: 15-24. https://doi.org/10.17580/nfm.2022.02.03

[28] Merkibayev YS, Chepushtanova TA, Berlibek AM, Tolegenova AK, Nugumarov ShT. Development of technology for the productio of aluminum castings using 3d printing of models and lost-was casting. Kompleksnoe Ispolzovanie Mineralnogo Syra=Complex Use of Mineral Resources. 2026; 337(2):108-116.https://doi.org/10.31643/2026/6445.22

Crossref
DOI: 10.31643/2028/6445.13
Metallurgy and Metallurgical Engineering

Deep Copper Recovery from Autogenous Smelting Slags under Strongly Reducing Conditions

[1]Altybayeva D. Kh., [1]Kenzhaliyev B.K., [1]Kvyatkovskiy S.A., [1*]Dyussebekova M.A., [1]Abdikerim B.E., [1]Semenova A.S., [2]Gemeal A.

[1] Institute of Metallurgy and Ore Beneficiation JSC, Satbayev University, Almaty, Kazakhstan
[2] Central Metallurgical Research &Development Institute, Cairo, Egypt

** Corresponding author email: m.dyussebekova@satbayev.university*

Received: *March 17, 2026*
Peer-reviewed: *April 21, 2026*
Accepted: *June 1, 2026*

ABSTRACT

Deep reduction of copper smelting slags is a promising route to recover entrained non-ferrous metals and to generate slags suitable for further processing. This work investigates the depletion of fayalite–magnetite slags formed during autogenous smelting of copper concentrates in conditions simulating the oxidation and reduction zones of a two-zone Vanyukov furnace. Laboratory charges of 100 g, containing 14.63–16.82 wt.% Cu, 25.6–27.6 wt.% Fe, 30 wt.% S and 15 wt.% SiO_2, were smelted at 1350 °C with controlled oxygen injection to produce slags containing 0.93–1.54 wt.% Cu, 30.05–32.30 wt.% SiO_2 and 7.8–9.8 wt.% Fe_3O_4. Subsequent reduction at 1300 °C was carried out with activated carbon in a fivefold stoichiometric excess relative to magnetite, at an oxygen-containing blast flow rate of 5 L/h and a 1 h holding time. Chemical analysis shows that Fe_3O_4 in slag decreases from 7.8–7.95 wt.% to 2.5–2.6 wt.%, while copper content drops from 0.93–1.033 wt.% to 0.43–0.50 wt.% under oxygen partial pressures of 10^{-12}–10^{-11} atm. X-ray diffraction and electron microscopic studies reveal a transition from fayalite–magnetite slags with dispersed metallic copper and sulfides to fayalite-dominated matrices containing ferruginous sphalerite, copper minerals of the bornite–chalcopyrite type, iron oxides and glassy phases. Simultaneous thermal analysis demonstrates that all major endothermic and exothermic events are completed by 1300 °C, supporting this as an optimal temperature for deep slag depletion. The results define an operating window—slag composition, temperature, reductant dosage and pO_2—under which copper losses to slag can be reduced to about 0.5 wt.% in industrially relevant fayalite slags.

Keywords: copper slag processing, pyrometallurgical treatment, copper-bearing sulfide materials, reductive melting, sem analysis, metallurgical waste.

Information about authors:

Altybayeva Dinara Khanatovna — *Master, Engineer of the Laboratory of Pyrometallurgy Heavy Non-Ferrous Metals, Institute of Metallurgy and Ore Beneficiation JSC, Satbayev University, 050010, Shevchenko str., 29/133, Almaty, Kazakhstan. Email: dinara.altybayeva.88@mail.ru; ORCID ID: https://orcid.org/0000-0002-2132-0076*

Kenzhaliyev Bagdaulet Kenzhaliyevich — *Doctor of Technical Sciences, Professor, General Director-Chairman of the Management Board of the Institute of Metallurgy and Ore Beneficiation JSC, Satbayev University, 050010, Shevchenko str., 29/133, Almaty, Kazakhstan. Email: bagdaulet_k@satbayev.university; ORCID ID: https://orcid.org/0000-0003-1474-8354*

Kvyatkovskiy Sergey Arkad'yevich — *Doctor of Technical Sciences, Chief of the Laboratory of Pyrometallurgy Heavy Non-Ferrous Metals, Institute of Metallurgy and Ore Beneficiation JSC, Satbayev University, 050010, Shevchenko str., 29/133, Almaty, Kazakhstan. Email: s.kvyatkovskiy@satbayev.university; ORCID ID: https://orcid.org/0000-0002-9686-8642*

Dyussebekova Maral Adel'bekovna — *Ph. D, Senior Researcher of the Laboratory of Pyrometallurgy Heavy Non-Ferrous Metals, Institute of Metallurgy and Ore Beneficiation JSC, Satbayev University, 050010, Shevchenko str., 29/133, Almaty, Kazakhstan. Email: m.dyussebekova@satbayev.university; ORCID ID: https://orcid.org/0000-0002-4359-9784*

Abdikerim Bekzat Erubaiuly — *Ph.D, Researcher of the Laboratory of Pyrometallurgy Heavy Non-Ferrous Metals, Institute of Metallurgy and Ore Beneficiation JSC, Satbayev University, 050010, Shevchenko str., 29/133, Almaty, Kazakhstan. Email: b.abdikerim@satbayev.university; ORCID ID: https://orcid.org/0000-0001-5551-2618*

Semenova Anastassiya Sergeyevna — *Master, Researcher of the Laboratory of Pyrometallurgy Heavy Non-Ferrous Metals, Institute of Metallurgy and Ore Beneficiation JSC, Satbayev University, 050010, Shevchenko str., 29/133, Almaty, Kazakhstan. Email: a.semenova@satbayev.university; ORCID ID: https://orcid.org/0000-0003-4054-8268*

Ahmad Gemeal — *Ph.D, Central Metallurgical Research & Development Institute, Cairo, Egypt. E-mail: agemeal@cmrdi.sci.eg, Gemil.Akhmad@kaznu.kz; ORCID ID: https://orcid.org/0000-0001-6663-2623*

Introduction

Intensive, or deep, reduction of metallurgical slags is increasingly important for maximising metal recovery and minimising waste. The effectiveness of such reduction processes is largely controlled by slag composition, process temperature and oxygen partial pressure, all of which influence phase equilibria, viscosity and metal solubility [[1],[2],[3],[4],[5],[6]].

The processing of metallurgical waste, including copper smelting slags, has been the subject of extensive research in many scientific communities. Researchers from Kazakhstan have investigated the thermodynamic modelling of mineral formation during the processing of toxic metallurgical waste, including the behaviour of zinc-containing phases [[7],[8]], and the utilisation of technogenic raw materials from South Kazakhstan metallurgical enterprises as secondary resources [[9],[10]]. These studies highlight the broader challenge of valorising metallurgical by-products — a context directly relevant to the present work.

Only a limited number of studies have explored deep slag reduction at extremely low oxygen potentials near 10^{-10} atm, leaving the kinetics and mass-transfer mechanisms under such conditions poorly constrained [11]. This knowledge gap is critical for autogenous copper smelting technologies, where copper losses to slag and magnetite build-up strongly depend on pO_2.

Available thermodynamic data suggest that decreasing pO_2 below 10^{-11} atm, and at the same time, at low iron contents in the alloy, leads to a noticeable reduction in copper activity and its solubility in slag [4]. Moreover, earlier studies [[12],[13],[14]] show that deep slag reduction is a complex and sensitive process that is strongly dependent on oxygen potential. This underlines the need for additional experimental and theoretical investigations to improve both the efficiency and economic performance of copper recovery [[15],[16],[17],[18]].

Several approaches have been proposed for copper recovery from smelting slags. Flotation is a widely used method; however, its efficiency is often limited by the fine dissemination of copper-bearing phases, and copper recovery under standard conditions typically does not exceed 45–50% [19], although higher values may be achieved with intensive grinding and optimised reagent conditions.

Electrothermal reduction represents an alternative route, yet it is constrained by the absence of bath agitation and the strongly endothermic nature of reduction reactions, which cause rapid temperature decrease, while electrode power is often insufficient to maintain stable thermal conditions, negatively affecting reaction kinetics and phase separation [[20],[21],[22]].

In contrast, the approach investigated in the present study employs intensive gas injection (bubbling) within a Vanyukov (PV) furnace configuration, which promotes bath mixing, enhances mass transfer, and stabilises the thermal regime. These conditions are more favourable compared to conventional methods, enabling more efficient reduction and improved separation of copper-containing phases.

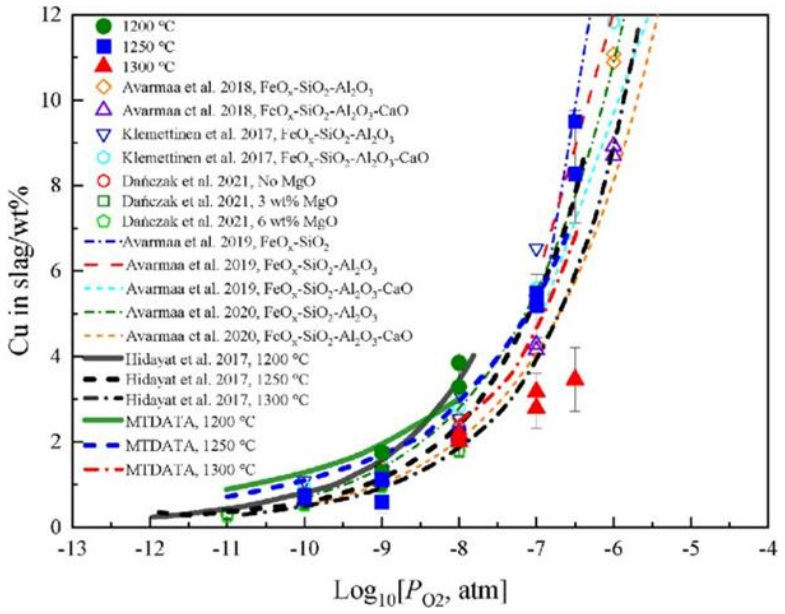

Figure 1 - Dependence of the copper content in the slag on the pO_2. Adapted from [23]

Figure 1 illustrates how the partial pressure of oxygen influences the copper concentration in the slag. In autogenous smelting, processes are conducted under oxidising conditions, with the oxygen partial pressure usually in the range of 10^{-6} to 10^{-8} atm. By contrast, establishing a deep reducing atmosphere (by adding coal or natural gas) significantly increases the thermodynamic possibility of reducing metal oxides.

For a Vanyukov (PV) furnace, achieving such deeply reducing conditions requires sufficient heat to enable effective interaction between the reducing agent and the slag. The present study focuses on experimentally defining the conditions for deep copper recovery from autogenous smelting slags, and on characterising the resulting slag structure and properties.

Experimental part

Laboratory experiments were conducted on 100 g charges smelted in a pre-calcined alund crucible (4) at 1350 °C in a silite furnace (1) designed to model autogenous smelting with gas purging (Figure 2). The charge consisted of copper concentrate containing 30 wt.% S and 27.0–27.6 wt.% Fe and a quartz flux with 70 wt.% SiO_2, added in an amount of 21.2 g per 100 g charge to form fayalite slags. For selected samples, experiments were carried out in triplicate to ensure reproducibility, and the reported values correspond to the average results.

After complete melting, oxygen was blown into the bath through an alund tube (3–5 mm inner diameter) at 1.0 L/min. The total oxygen input (43 L per 100 g charge) was calculated to oxidise iron sulfide and sulfur completely according to the reaction:

$$2FeS + 3O_2 \rightarrow 2FeO + 2SO_2 \quad (1)$$

and to convert FeO to fayalite in the presence of silica. After purging, the crucibles were held for 30 min and air-cooled.

Slags and mattes were studied using X-ray diffraction with a Bruker D8 Advance diffractometer (Cu Kα radiation); phase identification and quantification were carried out using DIFFRAC.SUITE EVA Version 5.2.0.5 (Bruker AXS, 2020) with the PDF-2 (2023) reference database applying the RIR-based S-Q method. Scanning electron microscopy with microanalysis (JEOL JXA-8230), simultaneous thermal analysis (NETZSCH STA 449 F3 Jupiter, processed with Proteus software), and reflected-light petrography (OLYMPUS BX-51, 50×–1000× magnification).

For depletion experiments simulating the reduction zone, slags obtained in the first stage were reheated to 1300 °C using activated carbon (74.3 wt.% C) as a reducing agent. The reduction of magnetite proceeds according to the reaction:

$$Fe_3O_4 + C \rightarrow 3FeO + CO\uparrow \quad (2)$$

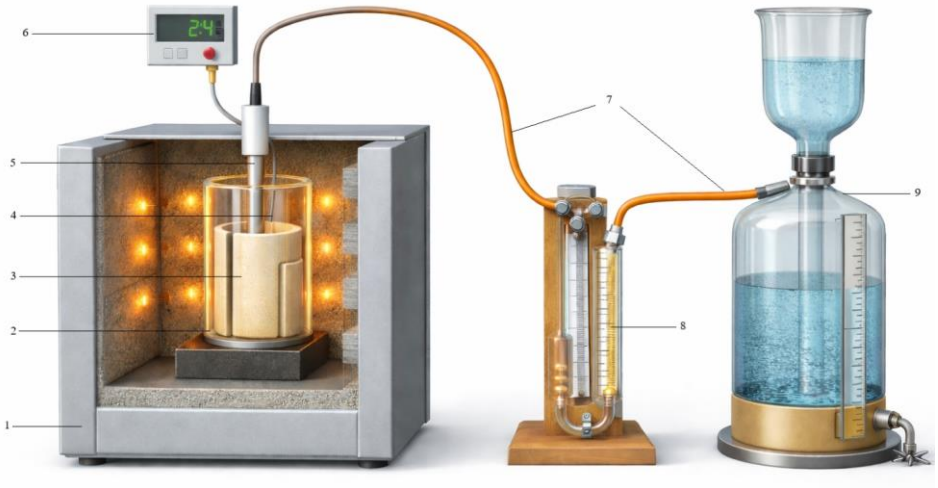

1 – silite furnace; 2 – alund glass; 3 – Pt-Pt-Rh thermocouple; 4 – alund crucible; 5 – alund tube; 6 – millivoltmeter; 7 – rubber hose; 8 – rheometer; 9 – gasometer

Figure 2 - Diagram of a laboratory installation for modelling autogenous melting with purging of a melt with an oxygen-containing mixture

The amount of carbon added (2.5 wt.%) corresponds to approximately a fivefold excess relative to the stoichiometric requirement for magnetite reduction, considering the Fe_3O_4 content of the slag and the carbon purity of the reducing agent. An oxygen-containing blast of 5 L/h was maintained, and the melt was held for 1 h before cooling. The experimental procedure was based on our previous study [3], in which the reduction-stage methodology was described in detail.

Oxygen partial pressures were calculated from measured copper contents in slag using a published empirical relationship between Cu in slag and pO_2 for such systems [[13],[24]].

Results and Discussion

Table 1 summarises the compositions of charge, slag and matte. Each value represents the average of three independent experiments conducted for each sample. Within the narrow variation of charge composition, slag chemistry remained stable: 0.93–1.033 wt.% Cu, 31.3–32.05 wt.% SiO_2, 37.3–37.4 wt.% total Fe and 7.8–7.95 wt.% Fe_3O_4, with matte copper contents around 46 wt.% A modest increase in magnetite from 7.80 to 7.95 wt.% was accompanied by a rise in slag Cu from 0.93 to 1.03 wt.%. This relationship demonstrates a strong positive correlation (R^2 = 0.82), indicating that an increase in Fe_3O_4 content is associated with higher copper losses in slag (Figure 3), which is further supported by structural analysis. XRD of slag from test No. 2 (0.97 wt.% Cu) show a fayalite–magnetite matrix with small metallic copper inclusions (Figure 4). Elemental mapping reveals copper, lead and zinc sulfides dispersed in the silicate matrix, with magnetite associated with Fe–O-rich regions and fayalite prominent along grain boundaries (Figure 5).

Table 1 - Principal key components in the charge, slag, and matte (average values)

Test No.	Chemical composition, %							Slag mass, g
	Cu in charge	*Fe in charge*	*Cu in slag*	*SiO_2 in slag*	*Fe_{total} in slag*	*Fe_3O_4 in slag*	*Cu in matte*	
1	16.82	27.00	0.930	32.05	37.4	7.80	46.30	44.0
2	16.73	27.60	0.970	31.90	37.3	7.90	46.20	43.6
3	16.35	27.10	1.033	31.30	37.3	7.95	45.90	44.6

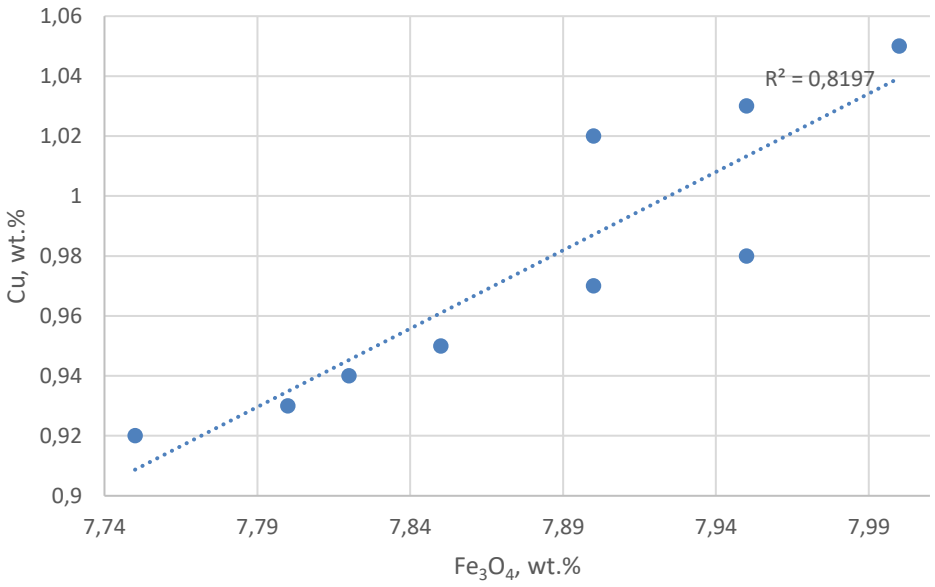

Figure 3 - Dependence of copper content in the slag on the magnetite content in the slag

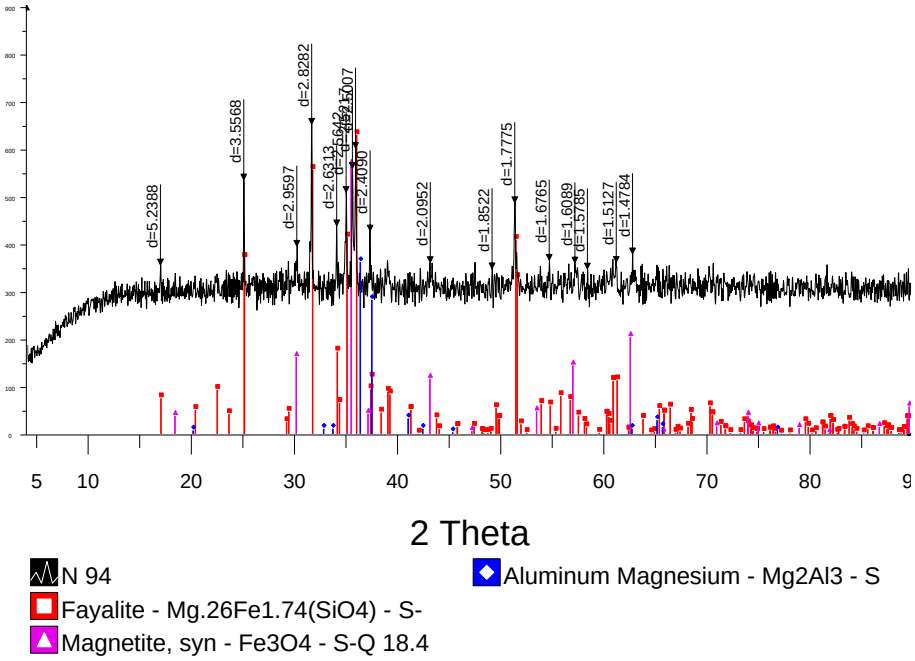

Figure 4 - Diffractogram of a slag sample containing 0.97% copper

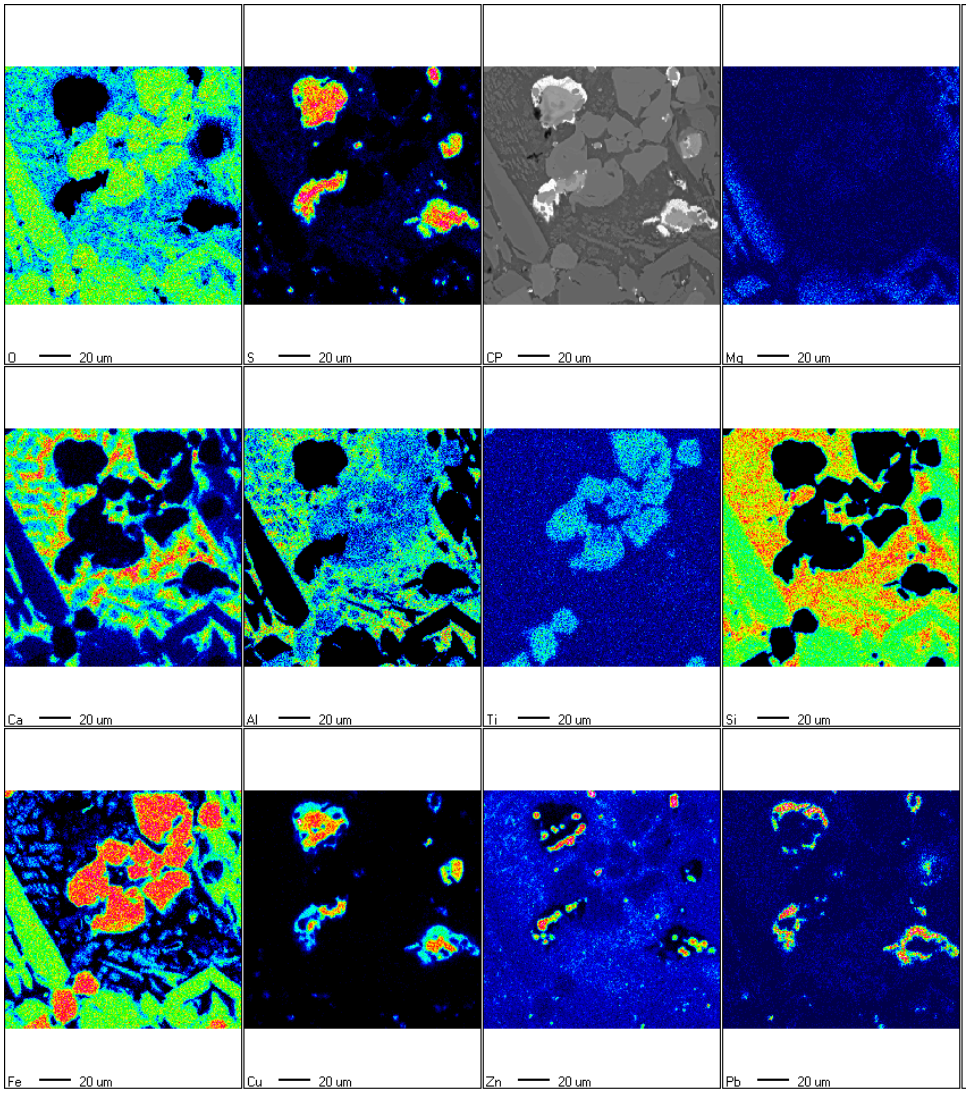

Figure 5 - Elemental mapping of the slag sample from test No. 2 containing 0.97% copper (WDS, x500)

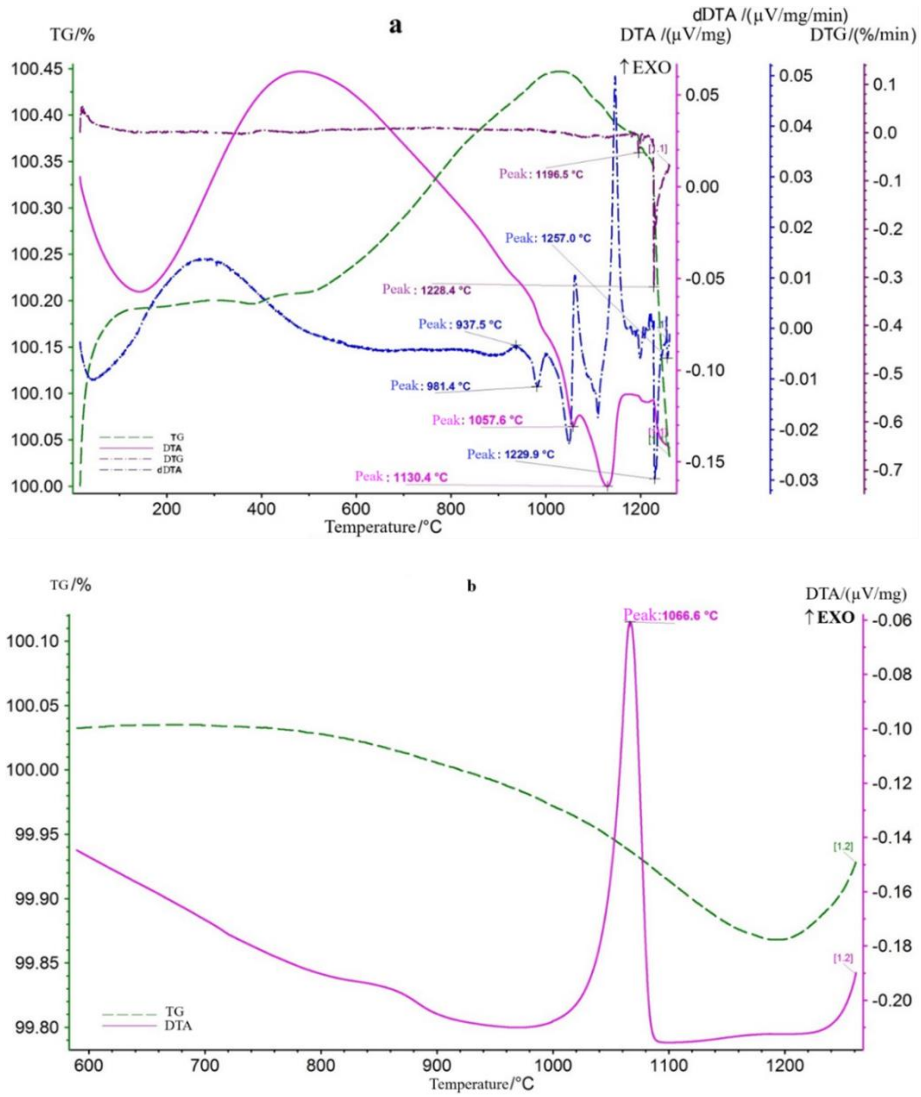

Figure 6 - Thermograms of a slag sample containing 0.97% Cu during heating (a) and cooling (b)

The distribution of elements within the slag sample obtained from test No. 2 is presented in Figure 5. The bright regions observed in the micrographs correspond to areas with elevated concentrations of specific elements. Based on these features, it can be inferred that the slag contains copper, lead, and certain zinc sulfides. The zones enriched in iron coincide with oxygen-rich areas, indicating the presence of magnetite. Fayalite is predominantly observed along the peripheral regions of the sample.

Thermal analysis of this slag indicates complete melting between 1280 and 1300 °C. Endothermic peaks at 1057.6 and 1130.4 °C correspond to the melting of major phases, with remaining phases liquefying around 1229.9 °C; during cooling, an exothermic effect near 1066.6 °C is accompanied by mass gain, consistent with crystallisation and oxidation (Figure 6).

Slags selected for depletion contained 0.93–1.54 wt.% Cu, 30.05–32.30 wt.% SiO_2 and 7.8–9.8 wt.% Fe_3O_4. Such slags require reduction treatment in order to decrease the content of non-ferrous metals.

During reduction at 1300 °C with activated carbon, two phases were formed: a slag phase and a bottom phase, whose compositions were similar to those of the matte phase formed during simulation of the oxidation zone of a two-zone PV furnace. Chemical composition of the obtained slag samples is presented in Table 2. These data indicate that magnetite was partially destroyed during smelting, with its content decreasing by 5.3–6.5 wt.%, which resulted in a lower copper concentration in the slag after reduction.

Table 2 – Chemical composition of major components after reduction of the slag

Test No.	Chemical composition, %			Coal consumption, g	pO_2, atm
	Cu	*SiO_2*	*Fe_3O_4*		
11	0.43	33.1	2.5	0.543	≈ 10^{-12}
12	0.47	32.9	2.6	0.545	≈ 10^{-11}
13	0.50	32.9	2.6	0.568	≈ 10^{-11}

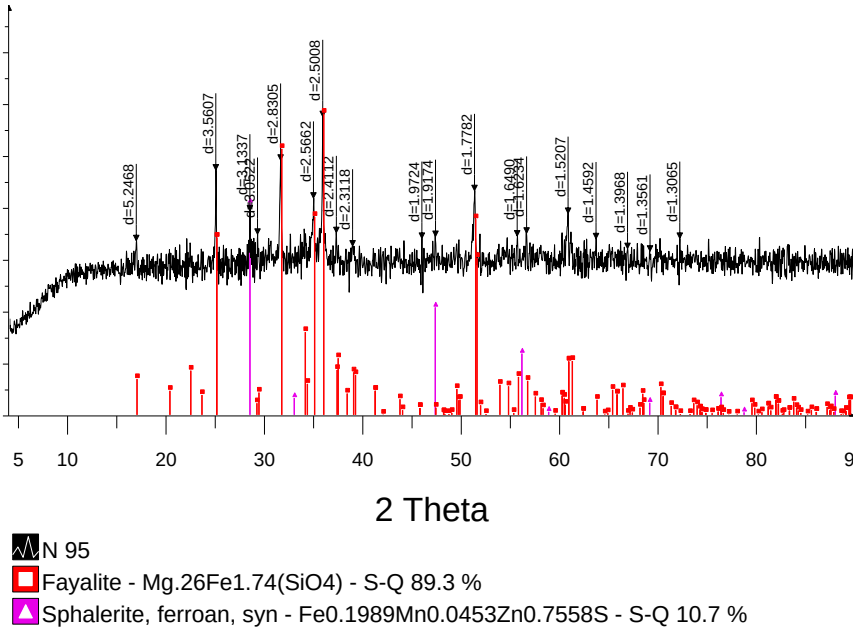

Figure 7 - Diffractogram of a sample of slag from test No. 12 containing 0.47% Cu

The results of the slag analysis after treatment with activated carbon revealed a substantial reduction in copper content, decreasing to 0.43–0.50 wt.% compared with the initial 0.93–1.033 wt.% in slags prior to reduction treatment. This decrease in copper concentration is attributed to the transformation of magnetite and other iron oxides into fayalite under reducing conditions. As a result, the magnetite content in the slag decreases to 2.5–2.6 wt.%, whereas before reduction it ranged from 7.8 to 7.95 wt.%.

Having calculated the partial pressure of oxygen according to the formula [13]:

$$\lg (Cu) = 0.221 \lg PO2 + 2.09 \quad (3)$$

where Cu is the copper content in the slag, % by weight, and pO_2 is the partial pressure of oxygen, atm., we obtain the pO_2 values (Table 2) in the slag under conditions of reducing the depletion of the slag by coal.

Based on the calculations performed, the obtained low oxygen partial pressure values indicate that the processes of depletion of copper slags occur under deeply reducing conditions, at $pO_2 < 10^{-11}$ atm. Under such conditions, the dissolved copper losses from the slag are restored, as well as the magnetite is restored. The reduction of magnetite has a beneficial effect on the viscosity of the slag. Reducing the viscosity of the slag, in turn, helps to reduce the mechanical losses of copper with the slag. Because, from studies conducted in the field of slag reduction treatment, it is known that the presence of magnetite in slag can increase its viscosity, which negatively affects the mechanical losses of copper [[25],[26],[27],[28],[29],[30],[31]]. However, the reduction processes occurring under deeply reducing conditions contribute to the transformation of magnetite and a decrease in thecontent of iron oxides, which favourably affects the physico-chemical properties of the slag, including its viscosity, which contributes to a more efficient removal of copper from the slag phase [[32],[33]].

X-ray diffraction analysis indicated that the slag sample of test No. 12, containing 0.47% Cu, consists of more than 85% fayalite with an admixture of iron-containing sphalerite (Figure 7).

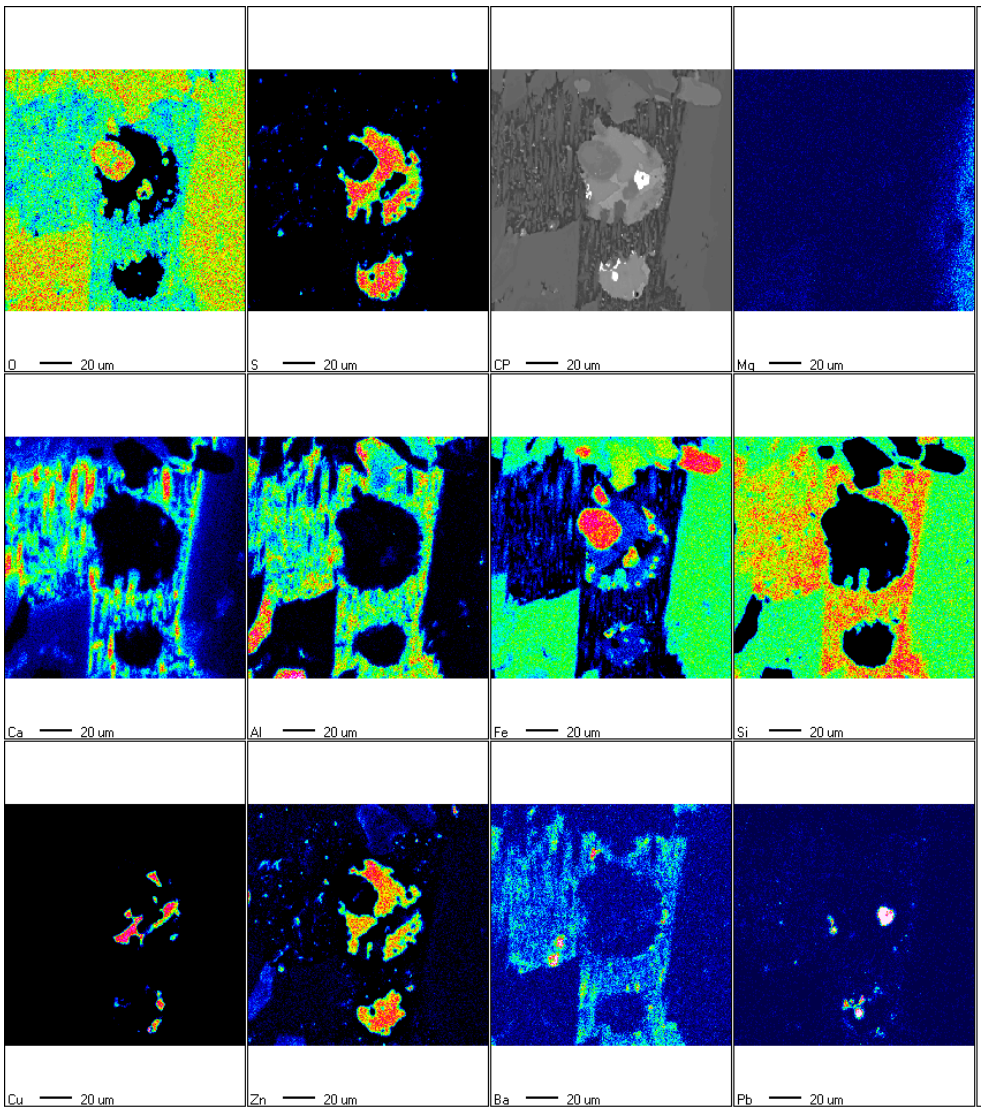

Figure 8 - Elemental mapping of the slag sample from test No. 12 containing 0.47% copper (WDS, x500)

According to the analysis data, the host matrix in the sample is fayalite, which contains iron oxides $FeCl_2$, FeO, Fe_2O_3, ferruginous sphalerite, and an isotropic glass phase in the form of inclusions. The distribution of the elements in the slag sample of test No. 12 is shown in Figure 8.

The presented thermograms (Figure 9) show that during heating, low-temperature effects (≈350–500 °C) are associated with minor structural changes and removal of physically bound components. At higher temperatures (≈870–980 °C), broader thermal effects indicate progressive phase transformations within the silicate system. More pronounced peaks in the range of ≈1090–1130 °C correspond to the onset of melting, while the strong effect near ≈1240–1250 °C is associated with the completion of melting and formation of a liquid phase.

During cooling, a distinct exothermic peak at ≈1067 °C corresponds to crystallisation of the melt.

It is observed that all significant endothermic and exothermic effects occur below 1300 °C. This is further supported by the absence of additional thermal effects above ≈1250 °C and the stabilisation of the thermal curves, indicating that the main phase transformations are completed within this temperature range. Therefore, this temperature range is considered optimal for the slag reduction process.

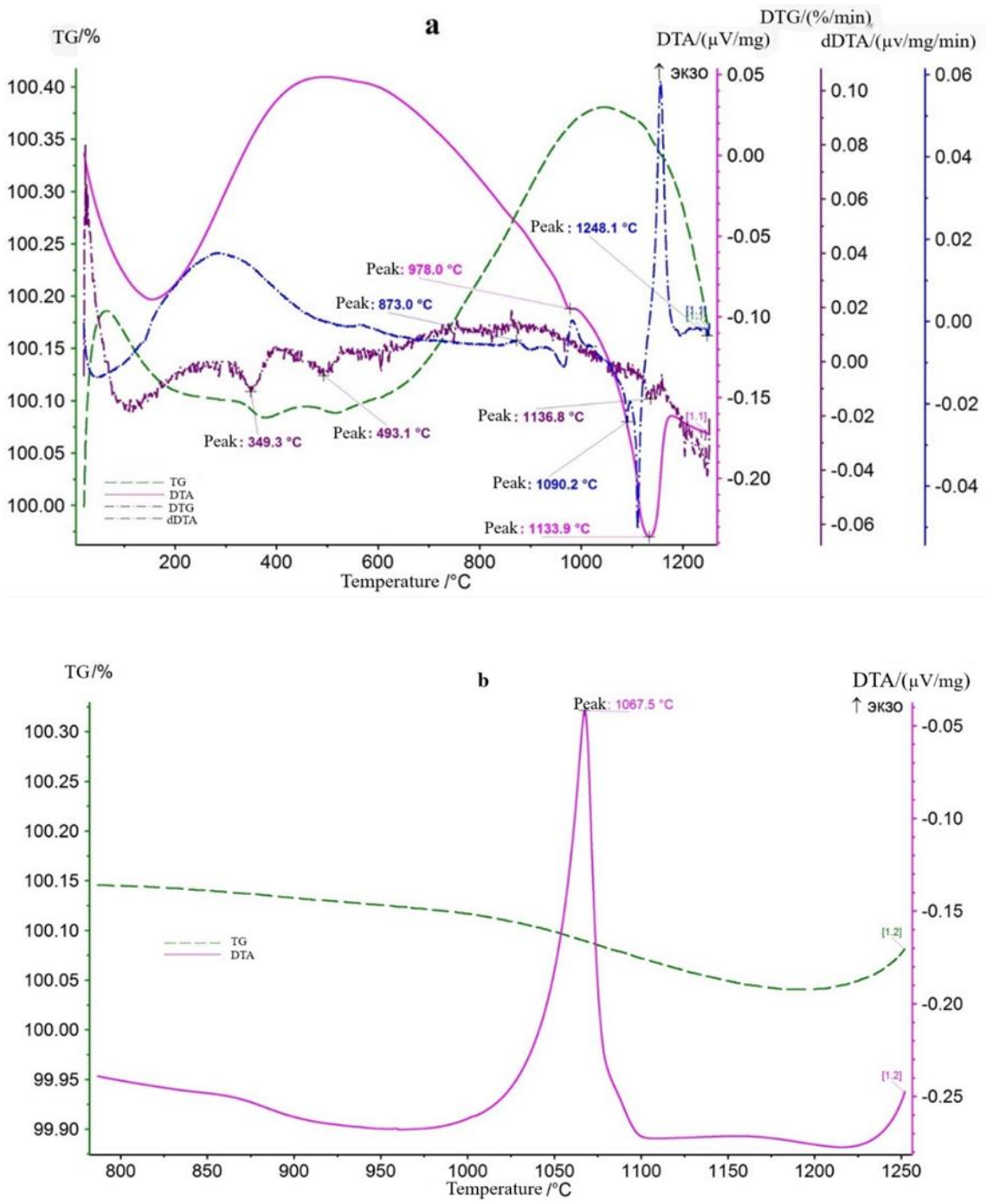

Figure 9 - Thermograms of the slag sample of test No. 12, during heating (a) and during cooling (b)

Conclusions

The study demonstrates that fayalite slags produced from the autogenous smelting of copper concentrates can be effectively depleted in a two-zone Vanyukov-type process when operated at 1300 °C and under strongly reducing conditions ($pO_2 < 10^{-11}$ atm). Slags with 0.93–1.54 wt.% Cu, 30.05–32.30 wt.% SiO_2 and 7.8–9.8 wt.% Fe_3O_4 are suitable feed for depletion; after reduction with activated carbon, magnetite decreases to 2.5–3.3 wt.% and copper to 0.43–0.80 wt.%.

The results revealed that ensuring sufficient heat input and controlling pO_2 are key to achieving deep reduction of metal oxides, lowering slag viscosity via magnetite destruction, and reducing both chemical and mechanical copper losses in industrial practice.

Conflicts of interest. On behalf of all authors, the corresponding author states that there is no conflict of interest.

CRediT author statement: **D. Altybayeva:** Writing draft preparation; **B. Kenzhaliyev**: Conceptualization, Project administration; **S. Kvyatkovskiy**: Supervision, Methodology; **M. Dyussebekova**: Data curation, Reviewing and Editing; **B. Abdikerim**: Visualization, Investigation; **A. Semenova**: Resources, Software, Validation; **A. Gemeal**: Validation, Formal analysis. All authors have read and agreed to the published version of the manuscript.

Funding. The research was funded by the Science Committee of the Ministry of Science and Higher Education of the Republic of Kazakhstan (Grant AP26101273).

Cite this article as: Altybayeva D Kh, Kenzhaliyev BK, Kvyatkovskiy SA, Dyussebekova MA, Abdikerim BE, Semenova AS, Gemeal A. Deep Copper Recovery from Autogenous Smelting Slags under Strongly Reducing Conditions. Kompleksnoe Ispolzovanie Mineralnogo Syra = Complex Use of Mineral Resources. 2028; 345(2):16-28. https://doi.org/10.31643/2028/6445.13

Жоғары тотықсыздандыру жағдайында автогенді балқыту қождарынан мысты терең бөліп алу

[1]Алтыбаева Д.Х., [1]Кенжалиев Б.К., [1]Квятковский С.А., [1]Дюсебекова М.А., [1]Әбдікерім Б.Е., [1]Семёнова А.С., [2]Gemeal A.

[1] Металлургия және кен байыту институты АҚ, Сәтбаев университеті, Алматы, Қазақстан
[2] Орталық металлургиялық ғылыми-зерттеу және дамыту институты, Каир, Мысыр

Мақала келді: *17 наурыз 2026*
Сараптамадан өтті: *21 сәуір 2026*
Қабылданды: *1 маусым 2026*

ТҮЙІНДЕМЕ

Мыс балқыту өндірісінің қождарын терең тотықсыздандыру олардың құрамындағы түсті металдарды бөліп алудың және әрі қарай қайта өңдеуге жарамды қождар алудың перспективалы тәсілі болып табылады. Бұл жұмыста екі аймақты Ванюков пешінің тотығу және тотықсыздану аймақтарын имитациялайтын жағдайларда мыс концентраттарын автогенді балқыту кезінде түзілетін фаялит-магнетитті қождарды жұтаңдануы зерттелді. Массасы 100 г шихта үлгілері (құрамында 14,63–16,82 % Cu, 25,6–27,6 % Fe, 30 % S және 15 % SiO_2) 1350 °C температурада оттегімен реттелген үрлеу жағдайында балқытылып, құрамында 0,93–1,54 % Cu, 30,05–32,30 % SiO_2 және 7,8–9,8 % Fe_3O_4 бар қождар алынды. Кейінгі тотықсыздандыру 1300 °C температурада магнетитке қатысты стехиометриялық мөлшерден бес есе артық енгізілген активтендірілген көмір қатысында, оттегі құрамды үрлеу шығыны 5 л/сағ және ұстау уақыты 1 сағат жағдайында жүргізілді. Химиялық талдау нәтижелері бойынша қождағы Fe_3O_4 мөлшері 7,8–7,95 %-дан 2,5–2,6 %-ға дейін, ал мыс мөлшері 0,93–1,033 %-дан 0,43–0,50 %-ға дейін төмендегені анықталды (оттегінің парциалдық қысымы ~10^{-12}–10^{-11} атм). Рентгенодифракциялық және SEM зерттеулер фаялит-магнетитті қождардың құрамындағы дисперсті металл мыс пен сульфидтерден темірлі сфалерит, борнит-халькопирит типті мыс минералдары, темір оксидтері және шынытәрізді фазалар бар фаялитті матрицаға өтуін көрсетті. Қосымша термиялық талдау барлық негізгі эндотермиялық және экзотермиялық процестердің 1300 °C дейін аяқталатынын көрсетті, бұл температураның қождарды терең жұтаңдануы үшін оңтайлы екенін дәлелдейді. Алынған нәтижелер қож құрамының, температураның, тотықсыздандырғыш мөлшерінің және оттегінің парциалдық қысымының жұмыс диапазонын анықтайды, бұл жағдайда қождағы мыс шығындарын шамамен 0,5 %-ға дейін төмендетуге болады, бұл өнеркәсіптік тұрғыдан маңызды.

Түйін сөздер: мыс қожын өңдеу, Пирометаллургиялық өңдеу, Құрамында мыс сульфидті материалдар, Тотықсыздандыру балқыту, SEM талдау, Металлургиялық қалдықтар.

Авторлар туралы ақпарат:

Алтыбаева Динара Ханатовна
Магистр, Металлургия және кен байыту институты АҚ, Сәтбаев университеті, Ауыр түсті металдар пирометаллургиясы зертханасының инженері, 050010, Шевченко көш., 29/133, Алматы, Қазақстан. Email: dinara.altybayeva.88@mail.ru; ORCID ID: https://orcid.org/0000-0002-2132-0076

Кенжалиев Багдаулет Кенжалиевич
Техника ғылымдарының докторы, профессор, Металлургия және байыту институты АҚ бас директоры және басқарма төрағасы, Сәтбаев университеті, 050010, Шевченко көш., 29/133, Алматы, Қазақстан. Email: bagdaulet_k@satbayev.university; ORCID ID: https://orcid.org/0000-0003-1474-8354

Квятковский Сергей Аркадьевич
Техника ғылымдарының докторы, Металлургия және кен байыту институты АҚ, Сәтбаев университеті, Ауыр түсті металдар пирометаллургиясы зертханасының меңгерушісі, 050010, Шевченко көш., 29/133, Алматы, Қазақстан. Email: s.kvyatkovskiy@satbayev.university; ORCID ID: https://orcid.org/0000-0002-9686-8642

Дюсебекова Марал Адельбековна	*Ph. D, Металлургия және кен байыту институты АҚ, Сәтбаев университеті, Ауыр түсті металдар пирометаллургиясы зертханасының аға ғылыми қызметкері, 050010, Шевченко көш., 29/133, Алматы, Қазақстан. Email: m.dyussebekova@satbayev.university; ORCID ID: https://orcid.org/0000-0002-4359-9784*
Әбдікерім Бекзат Ерубайұлы	*Ph.D, Ғылыми қызметкер, Металлургия және кен байыту институты АҚ, Сәтбаев университеті, Ауыр түсті металдар пирометаллургиясы зертханасы, 050010, Шевченко көш., 29/133, Алматы, Қазақстан. Email: b.abdikerim@satbayev.university, ORCID ID: https://orcid.org/0000-0001-5551-2618*
Семенова Анастасия Сергеевна	*Ғылым магистрі, ғылыми қызметкер, Ауыр түсті металдар пирометаллургиясы зертханасы, Металлургия және кен байыту институты АҚ, Сәтбаев университеті, 050010, Шевченко көш., 29/133, Алматы, Қазақстан. Email: a.semenova@satbayev.university; ORCID ID: https://orcid.org/0000-0003-4054-8268*
Ahmad Gemeal	*Ph.D, Орталық металлургиялық ғылыми-зерттеу институты, Каир, Египет. E-mail: agemeal@cmrdi.sci.eg, Gemil.Akhmad@kaznu.kz; ORCID ID: https://orcid.org/0000-0001-6663-2623*

Глубокое извлечение меди из шлаков автогенной плавки в условиях интенсивного восстановления

[1]Алтыбаева Д.Х., [1]Кенжалиев Б.К., [1]Квятковский С.А., [1]Дюсебекова М.А., [1]Абдикерим Б.Е., [1]Семёнова А.С., [2]Gemeal A.

[1] АО Институт металлургии и обогащения, Satbayev University, Алматы, Казахстан
[2] Центральный металлургический научно-исследовательский институт, Каир, Египет

Поступила: *17 марта 2026*
Рецензирование: *21 апреля 2026*
Принята в печать: *1 июня 2026*

АННОТАЦИЯ

Глубокое восстановление шлаков медеплавильного производства является перспективным способом извлечения содержащихся в них цветных металлов и получения шлаков, пригодных для дальнейшей переработки. В данной работе исследуется обеднение фаялит-магнетитовых шлаков, образующихся при автогенной плавке медных концентратов в условиях, имитирующих зоны окисления и восстановления двухзонной печи Ванюкова. Пробы шихты массой 100 г, содержащие 14,63–16,82% Cu, 25,6–27,6 % Fe, 30 % S и 15 % SiO_2, плавили при 1350 °C с контролируемой продувкой кислородом для получения шлаков, содержащих 0,93–1,54 % Cu, 30,05–32,30 % SiO_2 и 7,8–9,8 % Fe_3O_4. Последующее восстановление при 1300 °C проводилось с использованием активированного угля в пятикратном стехиометрическом избытке по отношению к магнетиту при потоке кислород содержащего дутья 5 л/ч и времени выдержки 1 ч. Химический анализ показал, что содержание Fe_3O_4 в шлаке снизилось с 7,8–7,95 % до 2,5–2,6 %, а содержание меди в шлаке с 0,93–1,033 % снизилось до 0,43–0,50 % при парциальном давлении кислорода ~10^{-12}–10^{-11} атм. Рентгенодифракционные и SEM исследования выявляют переход от фаялит-магнетитовых шлаков с диспергированной металлической медью и сульфидами к фаялитсодержащим матрицам, содержащим железистый сфалерит, медные минералы борнит-халькопиритового типа, оксиды железа и стеклообразные фазы. Одновременный термический анализ показывает, что все основные эндотермические и экзотермические процессы завершаются при температуре до 1300 °C, что подтверждает оптимальность этой температуры для глубокого обеднения шлаков. Результаты определяют рабочий диапазон — состав шлака, температуру, дозировку восстановителя и pO_2 — при котором потери меди в шлаке могут быть снижены примерно до 0,5 % шлаках, имеющих промышленное значение.

Ключевые слова: переработка медного шлака, пирометаллургическая обработка, медьсодержащие сульфидные материалы, восстановительная плавка, SEM-анализ, металлургические отходы.

Информация об авторах:

Алтыбаева Динара Ханатовна	*Магистр, Инженер Лаборатории пирометаллургии тяжелых цветных металлов, АО Институт Металлургии и Обогащения, Satbayev University, 050010, ул. Шевченко, 29/133, Алматы, Казахстан. Email: dinara.altybayeva.88@mail.ru; ORCID ID: https://orcid.org/0000-0002-2132-0076*
Кенжалиев Багдаулет Кенжалиевич	*Доктор технических наук, профессор, Генеральный директор-Председатель Правления АО Институт Металлургии и Обогащения, Satbayev University, 050010, ул. Шевченко, 29/133, Алматы, Казахстан. Email: bagdaulet_k@satbayev.university; ORCID ID: https://orcid.org/0000-0003-1474-8354*
Квятковский Сергей Аркадьевич	*Доктор технических наук, Заведующий лабораторией пирометаллургии тяжелых цветных металлов, АО Институт Металлургии и Обогащения, Satbayev University, 050010, ул. Шевченко, 29/133, Алматы, Казахстан. Email: s.kvyatkovskiy@satbayev.university; ORCID ID: https://orcid.org/0000-0002-9686-8642*

Дюсебекова Марал Адельбековна	*Ph. D, Старший Научный Сотрудник Лаборатории пирометаллургии тяжелых цветных металлов, АО Институт Металлургии и Обогащения, Satbayev University, 050010, ул. Шевченко, 29/133, Алматы, Казахстан. Email: m.dyussebekova@satbayev.university; ORCID ID: https://orcid.org/0000-0002-4359-9784*
Абдикерим Бекзат Ерубайұлы	*Ph.D, Научный Сотрудник Лаборатории пирометаллургии тяжелых цветных металлов, АО Институт Металлургии и Обогащения, Satbayev University, 050010, ул. Шевченко, 29/133, Алматы, Казахстан. Email: b.abdikerim@satbayev.university, ORCID ID: https://orcid.org/0000-0001-5551-2618*
Семенова Анастасия Сергеевна	*Магистр, Научный Сотрудник Лаборатории пирометаллургии тяжелых цветных металлов, АО Институт Металлургии и Обогащения, Satbayev University, 050010, ул. Шевченко, 29/133, Алматы, Казахстан. Email: a.semenova@satbayev.university; ORCID ID: https://orcid.org/0000-0003-4054-8268*
Ahmad Gemeal	*Ph.D, Центральный научно-исследовательский металлургический институт, Каир, Египет. E-mail: agemeal@cmrdi.sci.eg, Gemil.Akhmad@kaznu.kz; ORCID ID: https://orcid.org/0000-0001-6663-2623*

References

[1] Suh IK, Waseda Y, Yazawa A, Davenport WG. Some Interesting Aspects of Non-Ferrous Metallurgical Slags. High Temperature Materials and Processes. 1988; 8(1):65–88. https://doi.org/10.1515/HTMP.1988.8.1.65

[2] Wan X, Taskinen P, Shi J, Jokilaakso A. A potential industrial waste–waste co-treatment process of utilizing waste SO2 gas and residue heat to recover Co, Ni, and Cu from copper smelting slag. Journal of Hazardous Materials. 2021; 414:125541. https://doi.org/10.1016/j.jhazmat.2021.125541

[3] Kenzhaliyev BK, Kvyatkovskiy SA, Dyussebekova MA, Semenova AS, Nurhadiyanto D. Analysis of Existing Technologies for Depletion of Dump Slags of Autogenous Melting. Kompleksnoe Ispolzovanie Mineralnogo Syra = Complex Use of Mineral Resources. 2022; 323(4):23–29. https://doi.org/10.31643/2022/6445.36

[4] Rusen A, Derin B, Geveci A, Topkaya YA. Investigation of copper losses to synthetic slag at different oxygen partial pressures in the presence of colemanite. JOM. 2016; 68(9):2316-2322. https://doi.org/10.1007/s11837-016-1954-6

[5] Bellemans I, Cnockaert V, De Wilde E, Moelans N, Verbeken K. Metal Droplet Entrainment by Solid Particles in Slags: An Experimental Approach. Journal of Sustainable Metallurgy. 2018; 4(1):15-32. https://doi.org/10.1007/s40831-017-0145-1

[6] Kongoli F, McBow I, Yazawa A. Phase relations of ferrous calcium silicate slag and its possible application in the industrial practice. High Temperature Materials and Processes. 2011; 30(4):491–504. https://doi.org/10.1515/HTMP.2011.072

[7] Kolesnikov AS, Sapargaliyeva BO, Bychkov AY, Alferyeva YO, Syrlybekkyzy S, Altybaeva ZK, Suigenbayeva AZ. Thermodynamic modeling of the formation of the main minerals of cement clinker and zinc fumesin the processing of toxic technogenic waste of the metallurgical industry. Metallurgy. 2022; 15(3):2181-2187. https://doi.org/10.31788/RJC.2022.1536230

[8] Kenzhaliyev B, Berkinbayeva A, Baltabekova Z, Moldabayeva G, Smailov K, Saulebekkyzy S, Tolegenova N, Karim D, Omirbek T. Investigation of Phase Transformations in Technogenic Raw Materials Under Microwave Treatment for Enhanced Zinc Leaching. Processes. 2025; 13(4):1099. https://doi.org/10.3390/pr13041099

[9] Khudyakova TM, Kolesnikov AS, Zhakipbaev BE, Kenzhibaeva GS, Kutzhanova AN, Iztleuov GM, Mynbaeva E. Optimization of raw material mixes in studying mixed cements and their physicomechnical properties. Refractories and Industrial Ceramics. 2019; 60(1):76-81. https://doi.org/10.1007/s11148-019-00312-2

[10] Akhmadiyeva N, Abdulvaliyev R, Gladyshev S, Sukurov B, Abikak Y, Manapova A, Bakhytuly N. Optimizing technological parameters for chromium extraction from chromite ore beneficiation tailings. Minerals. 2025; 15(6):555. https://doi.org/10.3390/min15060555

[11] Ushakov AV, Karpov IV, Fedorov LY, Goncharova EA, Brungardt MV, Demin VG. Investigation of the Effect of Oxygen Partial Pressure on the Phase Composition of Copper Oxide Nanoparticles by Vacuum Arc Synthesis. Technical Physics. 2024; 69 (4):1069-1074. https://doi.org/10.1134/S106378422403040X

[12] Ulianov VV, Koshelev MM, Kremlyova VS, Kharchuk SE. Investigations of the regularities of the accumulation of slags reduced by hydrogen in the loops with lead-containing coolants. Izvestiya Wysshikh Uchebnykh Zawedeniy, Yadernaya Energetika. 2021; 2021(2):119–131. https://www.doi.org/10.26583/npe.2021.2.11

[13] Dosmukhamedov NK, Fedorov AN, Zholdasbay EE. Termodinamika vosstanovitel'nykh suspenzionnykh sistem CU-ME-FE-O-SIO2 (ME - PB, ZN, AS) na prirodnom gaze [Thermodynamics of Restorative Suspension CU-ME-FE-O-SIO2 (ME - PB, ZN, AS) Systems By Natural Gas]. Mezhdunarodnyy zhurnal prikladnykh i fundamental'nykh issledovaniy [International journal of applied and fundamental research]. 2019; 9:62–68. (in Russ.).

[14] Anindya A, Swinbourne DR, Reuter MA, Matusewicz RW. Distribution of elements between copper and FeOx–CaO–SiO2 slags during pyrometallurgical processing of WEEE: Part 1 – Tin: Part 1 – Tin. Mineral Processing and Extractive Metallurgy: Transactions of the Institutions of Mining and Metallurgy: Section C. 2013; 122(3):165-173. https://doi.org/10.1179/1743285513Y.0000000043

[15] Ospanov K, Smailov K, Nuruly Y. Patterns of non-traditional thermodynamic functions ΔrG0/n and ΔfG0(averaged) changes for cobalt minerals. Chemical Bulletin of Kazakh National University. 2020; 96(1):22-30. https://doi.org/https://doi.org/10.15328/cb1005

[16] Wang Y, Zhang SA, Wang L, Qin W, Han J. An unconventional approach for the efficient recovery of iron, cobalt, copper and silicon from copper slag. Journal of Hazardous Materials. 2024; 476:135168. https://doi.org/10.1016/j.jhazmat.2024.135168

[17] Abdulvaliev RA, Surkova TYu, Baltabekova ZhA, Yessimova DM, Stachowicz M, Smailov KM, Dossymbayeva ZD, Berkinbayeva AN. Effect of amino acids on the extraction of copper from sub-conditional raw materials. Kompleksnoe Ispolzovanie Mineralnogo Syra = Complex Use of Mineral Resources. 2025; 335(4):50-58. https://doi.org/10.31643/2025/6445.39

[18] Kenzhaliev BK, Kvyatkovskii SA, Kozhakhmetov SM. Determination of Optimum Production Parameters for Depletion of Balkhash Copper-Smelting Plant Dump Slags. Metallurgist. 2019; 63(7):759–765. https://doi.org/10.1007/s11015-019-00886-9

[19] Milanović D, Stanujkić D, Ignjatović MR. Comparative results of copper flotation from smelter slag and granulated smelter slag. Mining and Metallurgy Engineering Bor. 2013; (2):167-194. https://doi.org/10.5937/MMEB1302167M

[20] Svantesson J, Kojola N, Ersson M. Numerical study on the effect of material parameters and process conditions on the melting time of hydrogen-direct reduced iron. Metallurgical and Materials Transactions B. 2025; 56(3):2846-2872. https://doi.org/10.1007/s11663-025-03504-z

[21] Coursol P, Cardona VN, Mackey P, Bell S, Davis B. Minimization of copper losses in copper smelting slag during electric furnace treatment. Jom. 2012; 64(11): 305-1313. https://doi.org/10.1007/s11837-012-0454-6

[22] Pancnehko SV, Dli MI, Borisov VV, Panchenko DS. Analysis of thermalphysic processes in near-electrode zone of electrothermal reactor. Non-ferrous metals. 2016; 2:57-64.

[23] Chen M, Avarmaa K, Taskinen P, Michallik R, Jokilaakso A. An experimental study on the phase equilibria of FeOx-saturated iron silicate slags and metallic copper alloys at 1200–300°C. Calphad. 2022; 77:102418. https://doi.org/10.1016/j.calphad.2022.102418

[24] Yazawa A, Takeda Y. Equilibrium Relations between Liquid Copper and Calcium Ferrite Slag. Transactions of the Japan Institute of Metals. 1982; 23(6):328–333. https://doi.org/10.2320/matertrans1960.23.328

[25] Zuo Z, Yu Q, Wei M, Xie H. Thermogravimetric study of the reduction of copper slag by biomass: Reduction characteristics and kinetics. Journal of Thermal Analysis and Calorimetry. 2016; 126(2):481–491. https://doi.org/10.1007/s10973-016-5570-z

[26] Selivanov EN, Tyushnyakov SN, Gulyaeva RI. Viscosity of the Slags of the Autogenous Smelting of Copper–Zinc Concentrates. Russian Metallurgy (Metally). Pleiades journals. 2020; 2020(9):959–963.

[27] Zhou S, Wei Y, Zhang S, Li B, Wang H, Yang Y, Barati M. Reduction of copper smelting slag using waste cooking oil. Journal of Cleaner Production. 2019; 236:117668. https://doi.org/10.1016/j.jclepro.2019.117668

[28] Kucharski M, Nowak D, Czerwinski A, Saternus M. A study on the copper recovery from the slag of the Outokumpu direct-to-copper process. Metallurgical and Materials Transactions B: Process Metallurgy and Materials Processing Science. 2014; 45(2): 590–602.

[29] Sun J, Zhang T, Dong L, Zhu H, Shen P, Liu D. Eco-friendly recovery of copper from copper slag via magnetic separation followed by flotation: Experimental and mechanistic insights. Journal of Environmental Chemical Engineering. 2025; 13(2):115746. https://doi.org/10.1016/j.jece.2025.115746

[30] Zhang C, Zhang Y, Zhang Z, Zhang G. Effective separation and recovery of valuable metals from copper slag: A comprehensive review. Environmental Research. 2025; 283:122145. https://doi.org/10.1016/j.envres.2025.122145

[31] Akhmadiyeva N, Gladyshev S, Abdulvaliyev R, Abikak Y, Imangaliyeva L, Kasymzhanova A, Ruzakhunova G. Activation of Mineral Composition via Thermochemical Disintegration. Minerals. 2025; 15(9):1000. https://doi.org/10.3390/min15091000

[32] Zhang B, Xiao W, Yang Y, Zhou S, Wei Y, Li B, Wang H. Copper separation from slag in varying oxygen partial pressures during converting. Metallurgical and Materials Transactions B. 2024; 55(1):495-511. https://doi.org/10.1007/s11663-023-02972-5

[33] Ospanov YA, Kvyatkovskiy SA, Kozhakhmetov SM, Sokolovskaya LV, Semenova AS, Dyussebekova M, Shakhalov AA. Slag heterogeneity of autogenous copper concentrates smelting. Canadian Metallurgical Quarterly. 2023; 62(3):594-601. https://doi.org/10.1080/00084433.2022.2119495

Crossref
DOI: **DOI**: 10.31643/2028/6445.14
Metallurgy and Metallurgical Engineering

Influence of gas flow parameters on the velocity of bulk materials

[1*]Akhmetova S.S., [1]Kabiyeva G.K., [2]Rakhatova A.B.

[1]Abylkas Saginov Karaganda Technical University, Karaganda, Kazakhstan
[2]Saken Seifullin Kazakh Agro Technical Research University, Astana, Kazakhstan

** Corresponding author email: s.akhmetova@ktu.edu.kz*

Received: *April 18, 2026*
Peer-reviewed: *May 19, 2026*
Accepted: *June 5, 2026*

ABSTRACT
This article examines the flow patterns and kinetics of granular media interacting with ascending and descending gas flows. Bulk material release control is a critical aspect of shaft furnace and hopper operation Experimental studies were conducted on a flat transparent model and a close-up "hot" model using high-speed video recording (SK-16). With an error in the calculated values of the critical speed, amounting from to -30.0 to +28.8%, the main parameters varied within the following limits: specific gravity and viscosity of the gas, respectively, from 11.97 to 1.16 N/m³; from $8{,}9 \cdot 10^{-6}$ to $1.81 \cdot 10^{-5}$Pa · s; diameter, specific gravity and coefficient of internal friction of bulk material from $4{,}0 \cdot 10^{-4}$ to $15.0 \cdot 10^{-3}$m; from 14.3 to 39.2 kN/m³; from 0.55 to 0.95; coefficient taking into account the shape of the particles, from 6.0 to 7.8; outlet diameter from0.01 to 0.06 m; attitude $\frac{d}{R}$ equals $0{,}02 - 0{,}4$. The materials studied were agglomerate, lime, millet, and coke; the gas phases were air, helium, and hydrogen. It was established that the outflow mechanism is staged and determined by the frequency of destruction of dynamically unstable vaults. It was found that gas density is the key factor influencing the outflow rate, while the effect of viscosity is secondary. An analytical relationship was formulated for calculating the critical gas velocity that causes layer suspension. The obtained data make it possible to optimize the design parameters of outlet openings and blast supply modes in metallurgical units.

Keywords: bulk materials, gas flow, movement, speed, gas permeability.

Information about authors:

Akhmetova Sandugash Sovetovna — *Candidate of Technical Sciences, Associate Professor of the Department of Higher Mathematics, Abylkas Saginov Karaganda Technical University, 100027, Ave. Nursultan Nazarbayev, 56, Karaganda, Kazakhstan. E-mail: s.akhmetova@ktu.edu.kz; ORCID ID: https://orcid.org/0009-0003-7848-4463*

Kabiyeva Gulnar Kashkimbaevna — *Lecturer, Department of Higher Mathematics, Abylkas Saginov Karaganda Technical University, 100027, Ave. Nursultan Nazarbayev, 56, Karaganda, Kazakhstan. E-mail: g.kabiyeva@ktu.edu.kz; ORCID ID: https://orcid.org/0009-0003-4069-3569*

Rakhatova Aliya Beibutovna — *Doctoral Student, Saken Seifullin Kazakh Agro Technical Research University, 010011, Astana, Zhenis 62 Ave., Kazakhstan. E-mail: aliya-rahatova@mail.ru; ORCID ID: https://orcid.org/0009-0001-9086-232X*

Introduction

When discharged through a horizontal opening, particles of bulk material move across the layer at uneven speeds, causing it to become loosened. This creates the necessary conditions for intensifying heat exchange processes in the moving material layer.

Storage, transportation, and processing of bulk materials are the most common technological operations.

There are two known points of view on the bulk material model:

Firstly, the bulk material model is considered an isotropic conglomerate of tightly bound particles, and the movement of particles within the bulk of the material is possible only when the acting stresses exceed certain limit values. This representation of the bulk material is a consequence of considering the pressure of the material as the primary cause of its movement and flow through openings. This model is only valid for dispersed materials.

Secondly, the model of bulk material is represented as a set of solid, unchanging particles, the connection between which is carried out by dry friction forces.

Although modern numerical methods, such as coupled computational fluid dynamics and discrete element method (CFD-DEM), allow for detailed modeling of individual granule trajectories and local

gas pressure fields [[1], [2], [3], [4], [5]], they still rely heavily on the accuracy of micro-level boundary conditions (such as normal and tangential recovery coefficients, contact stiffness, and local porosity). Moreover, CFD-DEM models require significant computational power when scaled to the actual dimensions of metallurgical furnaces, and they may not always accurately represent the macroscopic analytical relationships of the vault mechanism.

In contrast to numerical simulations, this study proposes an analytical approach based on the fundamental laws of contact mechanics and the moments of friction forces acting directly on the boundary of a dynamically unstable vault. This allows for the derivation of direct criterion dependencies of macro parameters (mass release velocity, critical hover velocity) without the need for end-to-end discrete modeling of millions of particles, ensuring the invariance of the solution for engineering calculations of large-scale vehicles.

The scientific novelty of the work lies in the following:

1. A new analytical macro-model of the mechanics of the destruction of a dynamically unstable vault over an outlet is developed, based on the balance of moments of dry friction forces and the distributed aerodynamic effect of an oncoming or accompanying gas flow. Unlike existing approaches that only consider the gas influence as a volumetric resistance force to the layer, this work is the first to analytically describe the mechanism of changing the frequency of vault formation through changes in the torque acting on adjacent particles of the vault.

2. For the first time, the invariance of the mechanism of loose material release under the influence of gas in relation to gravitational release has been established and theoretically substantiated: it has been proven that the gas flow does not change the kinematic scheme of motion (staged destruction and formation of vaults), but acts as a regulator of the frequency of this process by pushing or dragging the boundary particles.

3. The physical phenomenon of asymmetry in the influence of gas parameters has been identified: it has been proven that the influence of gas viscosity on the critical release parameters is negligible in the developed turbulent regime, while the gas density and layer porosity nonlinearly determine the conditions for complete stagnation. A universal criterion dependence Eq. (12) has been obtained, which improves the accuracy of predicting the critical counterflow velocity by up to 30-50% compared to standard empirical models.

Experimental part

The destruction of a dynamically unstable vault above the outlet occurs as a result of the rolling of adjacent particles under the influence of the torque of frictional forces. In this case, with an increase in the velocity of the oncoming gas flow, one can expect a decrease in the velocity of the particles' rolling relative to each other, which, in turn, will lead to an increase in the lifetime of this vault, and consequently to a decrease in the mass velocity of the material flow [6]. Considering that the torque causing the rolling of two adjacent particles located on a dynamically unstable vault during gravity discharge is equal to:

$$M_1 = T_1 r_1 - T_2 r_2$$

accepting $r_1 = r_2 = r$, we get

$$M_1 = (T_1 - T_2) r$$

or

$$M_1 = T_1 \left(1 - \frac{T_2}{T_1}\right) r \quad (1)$$

where T_1 and T_2– frictional forces between adjacent particles of bulk material, r_1 and r_2 – particle radii.

When a gas flow from below uniformly impacts a dynamically unstable vault, i.e., its entire surface, an additional force appears F, coinciding in direction with the frictional force between particles, therefore:

$$M_2 = T_1 \left(1 - \frac{T_2 + F}{T_1 + F}\right) r. \quad (2)$$

Because $\frac{T_2+F}{T_1+F} < 1$, then with growth$F$this ratio increases, and the value $1 - \frac{T_2+F}{T_1+F}$ decreases. As a result, the torque, the speed of rolling of the material particles, the frequency of destruction (formation) of dynamically unstable arches and, consequently, the rate of flow of the material decrease [7]. The reduction in the rate of flow of the material is also facilitated by the braking of the particles falling out of the arch by the oncoming gas flow. Finally, upon reaching a certain gas velocity, when the ratio $\frac{T_2+F}{T_1+F} \to 1$, the magnitude of the torque will be zero and the release of material ceases. This is also facilitated by the gas flow

supporting the material particles forming the surface of the dynamically unstable vault against the material located above, preventing the particles from rolling [8]. In the limit, the effect of a uniform gas flow from below on the surface of the dynamically unstable vault leads to the layer hanging.

In the case of a layer moving with a co-current gas flow, an increase in its speed to a certain value causes a decrease in the ratio $\frac{T_2-F}{T_1-F}$, and consequently, an increase in torque, particle rolling speed, the frequency of destruction (formation) of dynamically unstable arches, and the rate of material flow. The rate of material flow also increases as a result of the aerodynamic effect of the accompanying gas flow on the descending particles.

To study in detail the mechanism of bulk material flow through a horizontal orifice exposed to counter and cocurrent gas flows, experiments were conducted on a flat transparent model measuring 250 mm in length, 50 mm in width, and 5 mm in depth (Fig.1). The thin depth (5 mm) makes the model virtually two-dimensional, simplifying observation and filming of the processes.

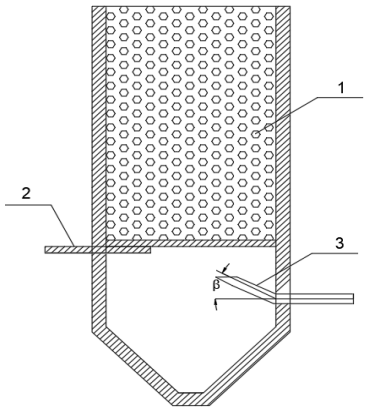

Figure 1 - Scheme of experimental «transparent» model: 1 – charge (шихта); 2 - diaphragm; 3 - nozzle

The experimental procedure involved the following technical specifications:

- Visual Recording: Process dynamics were captured using a high-speed SK-16 motion picture camera. This allowed for a precise frame-by-frame analysis of particle trajectories and the evolution of the dynamically unstable arch formed above the outlet.
- Gas Injection: Gas was introduced into the system in two modes: as a uniform flow exerting pressure on the arch surface, and as concentrated gas jets via specialized nozzles (3) positioned below the outlet [9].
- Flow Measurement: Air flow rates were regulated and monitored using RS-type rotameters, ensuring instantaneous volumetric control with a measurement accuracy of ±3%.
- Experimental Materials: Experiments were conducted using millet, limestone, and agglomerate fractions with particle sizes ranging from 1.45 to 2.44 mm. The material layer height was maintained at 200 mm (±3 mm).
- Data Acquisition: The mass flow rate was determined gravimetrically with a precision of ±50 mg, complemented by visual observations of the flow regime transitions.

Initial observations across all material types indicated that at relatively low gas injection velocities through the nozzles specifically when the velocity ratio (V_1 is the speed of gas movement througt the nozzle and V_2 is the gas velocity ay the outler; S_1 is outlet area, S_2 is the cross section on the gas jet upon meeting the surface):

$$\frac{V_1}{V_2} \leq 20 \text{ and } \frac{S_1}{S_2} \geq 0.38,$$

the system maintains a stable discharge pattern governed by the cyclic collapse of the arch structure.

Here V_1 – the speed of gas movement through the nozzle, V_2 – the gas velocity at the outlet, upon reaching which the material hangs above the outlet, S_1 – outlet area, S_2 – the cross-section of the gas jet upon meeting the surface of a dynamically unstable structure.

As a result of reviewing the filming materials, it was established that as the gas velocity is exceeded, the speed of rolling of the material particles relative to each other decreases, as well as a decrease in the mass velocity of the outflow through the outlet [10].

The mechanism of bulk material flow, both in counter- and co-current gas flows, across the entire studied range of pressure and gas velocity changes, corresponds to gravity release and proceeds through stages of destruction and formation of dynamically unstable vaults. The analysis revealed a dependence of the frequency of destruction (formation) of dynamically unstable vaults on the direction and velocity of the gas flow (Table 1).

Visual observations confirmed that the mechanism of outflow, both in the opposite and in the following flows, retains its staged nature (destruction/formation of arches).

Table 1 -Mechanism of bulk material flow

Flow mode	Frequency of vault failure	Expiration rate	System status
Gravitational	Basic	Standard	Stable
Counter (↑)	It's decreasing	Falls	Risk of hangs
Passing (↓)	It's growing	It's growing	Intensive

It was found that as the counterflow velocity increases, a critical point is reached where the frequency of arch failure becomes minimal, leading to a complete halt of the process. The outflow velocity in the coflow was higher than in the counterflow across the entire pressure range, confirming theoretical calculations on the contribution of aerodynamic forces to particle roll dynamics [11].

To ensure the scalability of laboratory data to industrial processes, fundamental modeling laws were strictly observed [[12], [13]]. To eliminate wall effects and ensure stable granular flow, the following geometric ratios were maintained:

-The ratio of the model shaft diameter to the equivalent particle diameter was >20

-The ratio of the outlet diameter to the particle diameter was >5.

-The ratio of the bed height to the shaft diameter was maintained at ≥ 2

Discussion of the results

Experiments were performed across a wide range of geometric variations, with the outlet-to-shaft diameter ratio ranging from 0.1 to 0.7. The gas flow dynamics, characterized by the Reynolds criterion, included regimes corresponding to the self-similar region. The investigations utilized both «cold» and «hot» laboratory models (Fig. 2 and 3). In the «cold» model, a replaceable diaphragm at the shaft base allowed for outlet diameter variations from 10 to 60 mm. The shaft was mounted on a sealed receiving bin (height: 800 mm, diameter: 250 mm). Gas, with properties detailed in Table 2, was supplied to the system at flow rates up to 60 m³/h via three symmetrically distributed pipes (8 mm diameter) to ensure uniform pressure distribution. The gas supply system was designed to ensure uniform pressure distribution across the material bed. Pipes for gas injection were evenly spaced around the circumference in a horizontal plane, located at distances of 150 mm below and 30 mm above the discharge orifice. In co-current flow experiments (gas and material moving in the same direction), gas was introduced through a sealed plug at the top of the shaft, with subsequent discharge through the receiving hopper [14]. To monitor system pressure, measurement points were flush-mounted with the internal walls of the shaft and hopper. The mass flow rate of the granular medium was recorded with a high precision of ±50 mg.

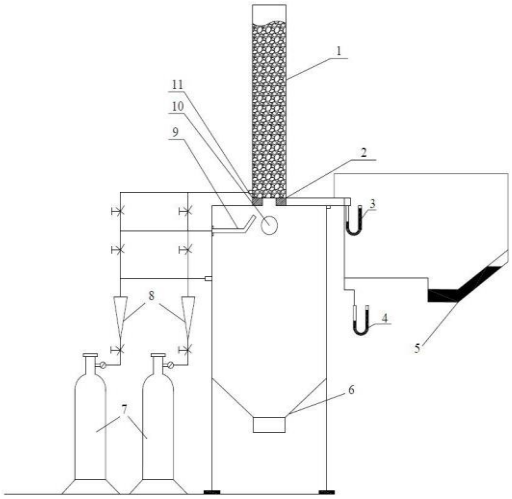

Figure 2 - Model diagram: 1 - shaft; 2 - replaceable diaphragm; 3 and 4 - U-shaped pressure gauges; 5 - micromanometer type MMN; 6 - receiving hopper; 7 - cylinders with compressed gas; 8 - glass rotameters; 9 - gas nozzle; 10 - peephole; 11 - regulating device (damper)

Gas (Table 2), with a flow rate varying within the range of 0 to 60 m³/h, was supplied to the hopper and shaft through three 8 mm diameter pipes, installed evenly around the circumference in the horizontal plane at a distance of 150 mm below and 30 mm above the outlet opening, respectively. When the gas and material moved in the same direction, the gas was supplied through a pipe passed through a plug hermetically sealing the top of the shaft; in this case, the gas was removed from the receiving hopper [[15], [16]]. The ends of the pipes for sampling gas pressure in the receiving hopper and shaft were installed at the level of their walls.

The accuracy of measuring the mass flow rate of bulk material was ± 50 mg.

The «hot» model (Fig. 3) is constructed from individual steel sections lined with fireclay bricks. To ensure a tight seal, the detachable joints are sealed with asbestos gaskets.

Table 2 - Physical properties of the gases used

Gas	Specific gravity, N/m³	Viscosity 10^{-5} Pa· s ·
Hydrogen	1.16	0.89
Helium	1.57	1.95
Air + 62% helium	5.49	1.89
Air + 34% helium	8.44	1.86
Air	11.97	1.81

A lid was attached to the top of the furnace shaft, with steel strip rings welded to the inner surface to divide the gas flow. The cylindrical shaft had an internal diameter of 300 mm, a height of 500 mm, a shoulder height of 200 mm, and a lower diameter of 173 mm. A refractory conical nozzle with the required outlet diameter (60-100 mm) was inserted into the lower part of the shoulders.

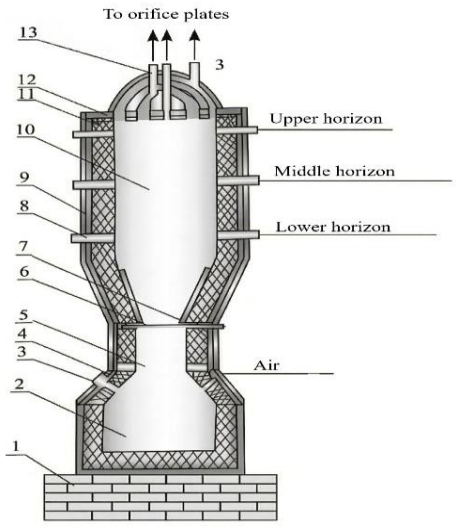

Figure 3 - Schematic diagram of the enlarged model: 1 - foundation; 2 - hearth; 3 - peephole; 4 - hearth dome; 5 - steam; 6 - damper; 7 - refractory cup; 8 - pipes for measuring equipment; 9 - lining; 10 - shaft; 11 - connecting flanges; 12 - gas distribution cover; 13 - pipes for gas outlet

During preparation for and after the experiment, the exhaust port was sealed with a lined damper with holes for gas passage. A hermetically sealed hatch for material release was located in the furnace hearth [17]. The operation of the furnace consists of forced air supply (blast) into the fuel combustion zone to quickly achieve the operating temperature. Air was supplied to the model from the factory line, and hydrogen from cylinders.

Table 3 - Characteristics of bulk materials

Material	Fraction, mm	Equivalent diameter 10^{-3}, m	Coefficient of internal friction
Agglomerate I	3.0 - 10.0	5.48	0.67
Agglomerate II	3.4 - 4.7	4.06	0.67
Agglomerate III	1.6 - 2.5	2.00	0.65
Millet	1.6 - 2.5	2.00	0.55
Limestone I	2.5 - 3.8	3.08	0.57
Limestone II	0.4 - 1.0	0.64	0.56
Coke	1.6 - 2.5	2.00	0.95
Pellets I	5.0 - 15.0	8.66	0.58
Pellets II	4.0 - 6.0	4.90	0.60

The model is equipped with gas flow and pressure control systems using measuring diaphragms, U - shaped pressure gauges and RS type rotameters.

Experiments were conducted on materials with significantly different physical and mechanical properties (Table 3). To determine the mass flow rate of the bulk material, a specific gas flow rate was set and a damper (regulating device) was opened. The material poured into a sealed receiving bin or model forge was weighed, and the mass flow rate was calculated.

Based on the difference in gas pressure below and above the outlet, the pressure drop on the dynamically unstable vault was calculated using the relationship $\Delta P_0 = \Delta P \cdot \frac{d_{eq}}{l_0}$. Where: ΔP is the measured gas pressure drop across the bed; d_{eg} is the equivalent diameter of the material particles; l_0 is the characteristic length (height) of the granular layer.

The freezing of bulk material in the models was determined by a sharp increase in the gas pressure drop and the cessation of pulsations of the working fluid in the pressure gauges, as well as visually through the viewing devices.

Experiments on a «cold» model showed that feeding gas above the outlet and diverting it through the top of the model (Fig. 4, a) has virtually no effect on the material flow rate (Fig. 5, curve a). Feeding gas above the outlet and diverting it through the top of the model and the receiving bin (Fig. 4, b) is more effective, the lower the porosity of the layer in the model. If the material layer has high porosity, then feeding gas has very little effect on the flow rate (Fig. 5, curve b).

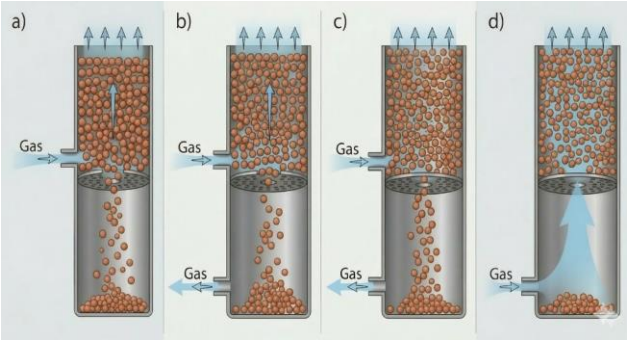

Figure 4- Gas supply diagram for the model: a - gas supply is above the outlet, the top of the model is open, the bottom is closed; b - the same, the top and bottom of the model are open; c - the same, the top of the model is closed, the bottom is open; d - gas supply is below the outlet, the top of the model is open

Reducing the layer's porosity and gas permeability, particularly by replacing the agglomerate layer with millet, results in an increasingly larger portion of the gas flow being directed downward and diverted from the model through the outlet, while the flow rate of the bulk material increases (Fig. 5, curve d). This is explained by the additional downward impact of the gas flow on the descending bulk material in the area of the outlet.

In the case of gas supply to the model above the outlet opening and its removal through the latter (Fig. 4, c), an increase in the gas flow rate or its pressure gradient in the layer in a certain range (Fig. 5, curve c) leads to an increase in the flow rate of bulk materials, which is in good agreement with the results of previously published studies. The lower the gas permeability of the material, the higher its flow rate at a constant gas flow pressure at the inlet (Fig. 6). Changes in the amount of gas supplied to the model, and consequently, its pressure in the bulk material layer, affect the nature of the action of the gas flow passing through a dynamically unstable arch, causing its destruction. In this regard, the conclusion of the authors of the studies about an increase in the flow rate of bulk material with an increase in the pressure gradient in the layer or an equivalent amount of gas supplied to the model becomes clear. The increase in excess pressure above the layer of material increased the additional load from top to bottom on the surface of the dynamically unstable vault, which, in turn, contributed to an increase in the frequency of its destruction, an increase in the initial velocity of movement of particles after the destruction of this vault and an increase in the mass velocity of the outflow of material.

The experimentally recorded dependencies (Fig. 5 and 6) clearly confirm the proposed hypothesis about the mechanism of particle rolling. An increase in the counterflow gas velocity F leads to an asymptotic approach of the moment ratio to unity Eq. (2), which is physically expressed in the stabilization of the dynamic vault and a decrease in its collapse frequency. This refutes the common assumption in simpler empirical models that the release is uniformly slowed down throughout the entire height of the material column, as the key critical resistance is concentrated at the lower boundary of the vault.

From graph 5, it can be seen that the individual series behave differently. Series c and d show a pronounced increase in W_t/W_0 as Q_r/Q_{kr} increases. Series c has the most intense increase, reaching approximately 1.4 at Q_r/Q_{kr} = 4. Series d also increases, but more gradually, reaching a value of approximately 1.2. Series a remains almost unchanged and has a slight downward trend, indicating a slight decrease in W_t/W_0 relative to the initial level. Series b changes slightly and is around 1.0-1.1. Series e decreases sharply when the Q_r/Q_{kr} rises to 1, which indicates a strong difference between this series and the others.

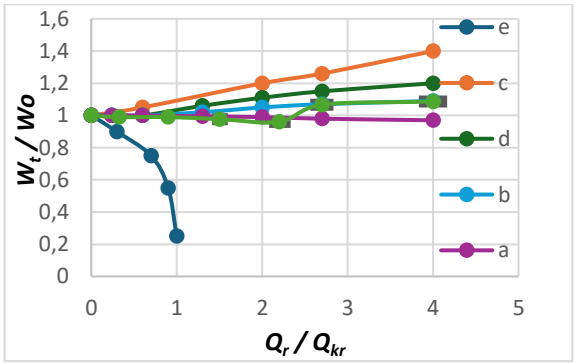

Figure 5 - Dependence of the of the mass flow rate ratio (W_t/W_0) on the normalized gas flow rate (Q_r/Q_{kr}) for different gas supply above the outlet with: (*a*) top removal; (*b*) combined removal (high porosity); (*c*) removal through the orifice; (*d*) combined removal (low porosity); (*e*) counter-current flow (gas supply below the outlet)

The middle line shows the overall average change in the indicator. In general, it is around 1.0-1.1, which indicates a moderate change in W_t/W_0. The error limits show the spread of data relative to the average value: the longer the whiskers, the higher the heterogeneity of the results at a given point. An increase in Q_r/Q_{kr} leads to a different change in W_t/W_0 in individual series.

The most noticeable increase is observed for series c and d, while the most significant decrease is

observed for series e. The average line shows the overall trend, and the error limits reflect the variation between the measurement series.

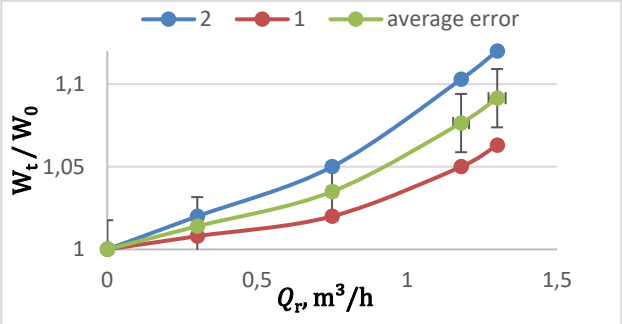

Figure 6 - Dependence of the relative velocity of material flow (W_t/W_0) from the amount of gas (Q_r, m³/h), fed into the model. The diameter of the outlet is 15 mm.
1 - millet; 2 - agglomerate III

The graph 6 shows the dependence of the relative value of W_t/W_0 on the ratio of Q_r.

Lines 1 and 2 represent the minimum and maximum values of the indicator, and the middle line shows the average value. The error limits are plotted on the middle line and show the deviation of the average value from the extreme values.

As Q_r increases from 0 to 1.3, there is a steady increase in the W/W_o value in all data series. This means that there is a direct relationship between the values: the higher the value of Q_r, the higher the relative value of W_t/W_0. For series 1, the W_t/W_0 value increases from 1.000 to 1.063. For series 2, the increase is more pronounced, from 1.000 to 1.120. The average value increases from 1.000 to 1.0915.

It can also be seen that as Q_r increases, the difference between series 1 and 2 increases. At the beginning of the graph, the error is almost non-existent, and at Q_r = 1.3, it reaches its maximum value of ±0.0285. This shows that at higher values of Q_r, the spread of results becomes more noticeable.

Therefore, for the point Q_r = 1.3, the error limit is ±0.0285.

An increase in Q_r leads to an increase in W_t/W_0. At the same time, the average value of W_t/W_0 increases smoothly, and the error value increases as Qr increases, which indicates a greater spread of results at high values of the parameter.

The extreme nature of the dependence of the bulk material flow rate on the amount of air supplied to the model is explained by the change in the distance from the nozzle through which air was supplied to the model to the mouth of the discharge funnel, and consequently to the dynamically unstable arch above the outlet. This distance determines the magnitude of the kinetic energy of the air stream acting on the dynamically unstable arch, which affects the frequency of its destruction (formation) and the rate of material outflow, which is confirmed by the change in the maximum material flow rate depending on the nozzle position [18]. With an increase in the amount of air entering the model, and, accordingly, its velocity, an air channel is apparently formed in the layer of bulk material, passing through the outlet. A decrease in the flow rate of bulk material is explained by the compaction of the material located around the rigid air stream. The probability of the formation of a channel passage of gas is greater, the higher the density of the layer. Naturally, with relatively small dimensions of the outlet opening and high excess air pressure of 9.8 - 29.4 kPa, a complete cessation of material release is expected.

The mass flow rate (G, kg/s) is most often calculated using empirical formulas as the product of the cross-sectional area (S, m²) and the density (ρ, kg/m³) and flow rate (v, m/s), taking into account the flow coefficients: $G=\mu S \rho v$.

Gas outflow:

$$G = C_d \cdot A \cdot \sqrt{2\rho \cdot \Delta P} \qquad (3)$$

where C_d - flow coefficient (empirical); A - hole area; ΔP - pressure drop.

A comparison of the experimental data when gas is supplied to the model according to the scheme shown in Fig. 4 b, c, with the results of calculating the mass flow rate of bulk material using empirical equations shows that the error in the calculated values fluctuates within a fairly wide range: from -25.2 to +47.0%; from -32.5 to +55.6%; from +9.0 to +79.6% respectively. The increased error in the latter case is explained by the different shapes of the outlet openings, which, in our opinion, is consistent with the data from the study.

With increasing gas flow rate supplied below the discharge zone (Fig. 4, d), the flow rate of various bulk materials gradually decreases to 60 – 20% relative to the mass flow rate corresponding to gravity discharge. With a further increase in gas flow rate, the material discharge ceases (Fig. 5, curve d). The wide range of the lower limit of flow rate regulation is explained by the significant differences in the physical and mechanical properties of the bulk materials studied, primarily in particle size distribution, electrical properties, moisture content, adhesion, etc.

A comparison of experimental data with the results of calculating the mass flow rate of bulk materials using empirical equations shows that the error in the calculated values varies widely and amounts to: from -21.0 to +176.0%; from -99.0 to -0.6%; from -100.0 to +67.2 %. The average error is about $\pm 40\%$ and increases sharply when the gas velocity in the outlet approaches the critical value at which the bulk material freezes.

Supplying a certain amount of gas through a nozzle of a smaller diameter allows for a higher velocity of the gas flow and a relatively local nature of its impact on the bulk material adjacent to the point where the jet enters the layer [19].

The kinetic energy of a gas flow acting on the surface of a dynamically unstable vault alters the conditions of its collapse and, consequently, determines the rate of material flow. Therefore, a dependence of the material flow rate on the gas flow parameters was expected.

Experiments have shown that decreasing gas density and viscosity significantly increases the flow rate of the material through the outlet (Fig. 7). The effect of gas viscosity on the flow rate of the bulk material can be clearly seen by comparing the effects of countercurrent flows of hydrogen and helium, which, under the experimental conditions, are similar in density but differ greatly in viscosity (Table 1). Figure 7 shows that the effect of gas viscosity is insignificant, and changes in the flow rate of the material are determined by the density of the gas flow.

Figure 7 shows the dependence of the values of three measurement series and the average error on the speed (V_0), m/s. As the speed increases, there is a general decrease in all the values, but the pattern of decrease varies for each series. The first series shows the most pronounced decrease: at (V_0 = 0), the value is 1, but at (V_0 = 4.9), it decreases to 0.05; at (V_0 = 6.3), the value almost reaches zero. The second row decreases more smoothly: from 1 at the initial speed value to 0.21 at (V_0 = 8.4). The third row is characterized by the most stable decrease: its values remain relatively high for most of the interval and decrease to 0.20 only at (V_0 = 10.4).

The average error also has a downward trend. It decreases from 1 to 0.06, indicating a gradual decrease in the average value of the indicator as the speed increases. The most noticeable decrease in the average error is observed after (V_0 = 3.7), when the differences between the individual rows become more pronounced. Overall, the graph shows that an increase in speed (V_0) leads to a decrease in the indicator under consideration, with the first row being the most sensitive to changes in speed and the third row being the most stable.

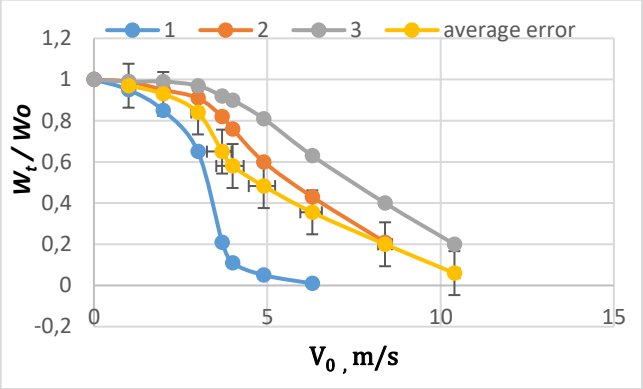

Figure 7 – Dependence of the relative flow rate of agglomerate III (W_t/W_0) from the gas velocity at the outlet (V_0, m/s) with a diameter of 30 mm. 1 - air; 2 - helium; 3 – hydrogen

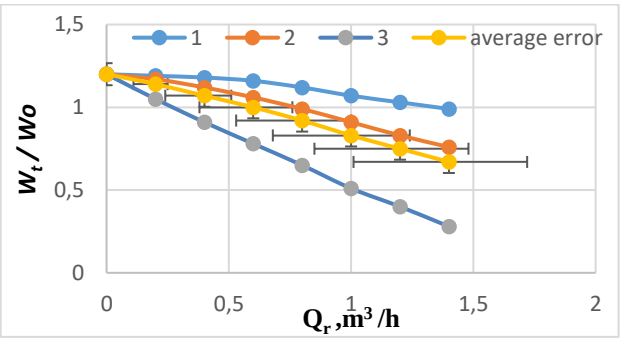

Figure 8 - Dependence of the relative velocity of material flow (W_t/W_0) from its density in air countercurrent (Q_r, m³/h).1 - agglomerate; 2 - limestone; 3 – millet

The fact that in the self-similar (turbulent) region the influence of gas viscosity is leveled out (Fig. 7), indicates the dominance of the inertia forces of the gas jet over the viscous friction forces in the interparticle channels directly at the moment of the vault destruction. This opens up the fundamental possibility of scaling the obtained equations to industrial units working with complex gas mixtures (hydrogen, helium, metallization technological gases) without complicating the calculation algorithms.

When studying the process of controlling the release of a layer in a counter-current gas flow, it was found that the physical properties of the gas do not affect the lower limit of the mass flow rate of the material (Fig. 7). This undoubtedly expands the possibilities for the practical application of methods for controlling the release of bulk materials using a gas flow [20].

The effect of bulk material density on its flow rate is clearly demonstrated in Fig. 8.

Figure 8 shows a graph of the change in the values of three measurement series and the average error. The x-axis shows the argument values from 0 to 1.4 in increments of 0.2, and the y-axis shows the corresponding values of the indicator. All three series show a decreasing trend, but the rate of decrease varies: the first series decreases more smoothly, the second series decreases more pronouncedly, and the third series shows the sharpest decrease. The average error also gradually decreases from 1.20 to 0.67. For the average error line, we have built whiskers that reflect the spread of values between the minimum and maximum values among the three-measurement series at each point. The longer the whiskers, the greater the difference between the individual values. In the initial section, there is almost no spread, as all the values are equal to 1.20. As the argument value increases, the length of the whiskers gradually increases, indicating a growing discrepancy between the measurement series.

It was found that the nature of the material's flow is independent of its physical and mechanical properties. As the size of the material piece used in the experiments increases, the flow rate increases significantly (Fig. 9). Characteristically, as the ratio of the model and outlet diameters decreases, not only does the absolute flow rate of the layer increase, but its lower limit decreases to a certain value at equal gas flow rates, i.e., it becomes possible to control the material release over a wider range.

Figure 9 shows the dependence of two series of values and the average error on the flow rate (Q_r), m³/h. Both series have a decreasing trend, but the rate of decrease differs. The first series decreases smoothly, from 1 at (Q_r = 0) to 0.80 at (Q_r = 12) m³/h. The second series decreases much faster, from 1 to 0 at (Q_r = 8.8) m³/h, indicating a higher sensitivity to changes in flow rate.

The average error also decreases consistently: from 1 to 0.43. The whiskers on the graph reflect the spread between the minimum and maximum values of the two series at each point. At the beginning of the interval, there is no spread because the values of the series are the same. Then, the length of the whiskers gradually increases, indicating an increase in the differences between the first and second series as (Q_r) increases.

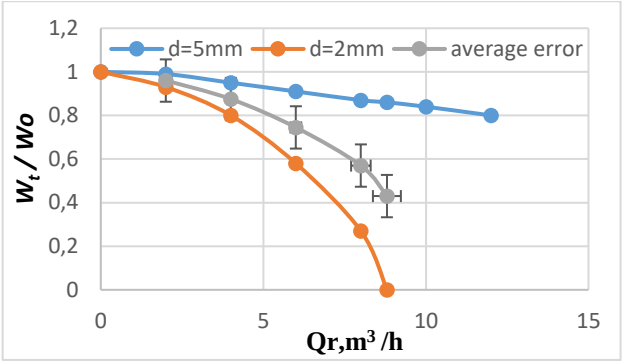

Figure 9 - Dependence of the relative velocity of pellet outflow (W_t/W_0) from the size of the piece (d_{eq}, mm) with air counterflow (Q_r, m³/h).

The physical mechanism of the influence of oncoming and associated gas flows on the kinetics of the outflow, recorded using high-speed video filming SK-16, has a pronounced stage character and is determined by the frequency of destruction of dynamically unstable arches. The observed change in the relative exhaust velocity (W_t/W_0) is due to the redistribution of stress chains inside the dense layer above the outlet (Fig. 8 and 9). The oncoming gas flow passing through the interparticle channels creates an upward aerodynamic pressure, which increases the normal compressive forces between the layer elements. This leads to an increase in the forces of interparticle friction and, as a result, to an increase in the holding torque of the forces acting on the particles in the support nodes of the dynamic vault. The stabilization of the vault blocks the gravitational displacement of the material, causing a decrease in flow rate up to complete stagnation. On the contrary, the oncoming flow reduces the apparent adhesion of the particles, reducing the critical radius of vault formation, which intensifies the release of material due to an increase in the frequency of vault pulsations. The extremum identified in Figure 9 (maximum velocity at d_{eq}=2.0÷2.5 mm) reflects the bifurcation point, where the geometric factor of jamming of large pieces is balanced by the optimal aerodynamic transparency of the pore channels for fluid filtration.

Mathematical analysis of the experimental data allowed for the ranking of investigated parameters based on their influence on the material discharge rate. Under standard conditions, the factors are arranged in the following descending order of significance:

1. Direction of the gas flow;
2. Diameter of the discharge orifice;
3. Bulk density of the granular material;
4. Gas flow rate;

5. Physical properties of the gas (density and viscosity).

Notably, this hierarchy can shift under specific dynamic conditions. For instance, a 30% increase in the gas flow rate causes this parameter to exert a more dominant influence on the discharge rate than the intrinsic bulk density of the material.

To consolidate the experimental findings for both counter-current and co-current gas flow regimes, a unified empirical equation was developed):

$$W_0 = 0.05\gamma_n \frac{D_0^{2.5}}{\sqrt{d_{eq}}} \sqrt{1 \pm \frac{\Delta P}{0.6\gamma_n D_0}} \quad (4)$$

The error associated with this generalized model ranges from **−**19.8% to +23.1%**,** which is significantly lower than the deviations observed when using classical empirical equations. As previously noted, traditional models exhibit errors ranging from −25.1% to +176.1%**,** especially near critical regimes. This confirms that the proposed Eq. (9), which explicitly accounts for the gas-dynamic pressure drop ΔP and orifice geometry rate (D_0) provides a much more reliable tool for industrial design. Comparing the experimental results with calculations of the material mass flow rate under pressure discharge using empirical equations shows that the error in the calculated values varies within a wide range, namely: from −25.1% to +47.1%, from −32.6% to +55.5%, and from +9.8% to +79.5%, respectively.

The limitations of conventional empirical models become even more apparent under counter-current gas flow conditions. For such regimes, the error in mass flow rate calculations using standard equations escalates significantly, with deviations ranging from −21.1% to +176.1%, −99.1% to −0.7%, and −100.0% to +67.1%. On average, the predictive error is approximately ±50%. Notably, this discrepancy increases sharply when transitioning from air typically used in the baseline experiments of previous authors to gases with significantly different physical properties, such as hydrogen or helium (as detailed in Table 1). Such high levels of uncertainty underscore that purely empirical correlations, which do not account for the internal structural mechanics of the granular bed, are unsuitable for complex gas-solid systems. Consequently, there is a clear necessity for a more rigorous theoretical description of the discharge process. By integrating the results of this experimental study with the proposed torque-balance mechanism, it becomes possible to establish a physically consistent model that remains accurate across a wide range of gas-dynamic and material conditions

$$W_0 = \frac{1}{2}\sqrt{2g\mu\left[R + d\left(\frac{1}{2} + \frac{1-\mu}{\sqrt{1+\mu^2}}\right)\right]\left[1 \pm \frac{\Delta P_0}{d\gamma_k f\left(\mu;\frac{d}{R}\right)}\right]} \quad (5)$$

by the area of the outlet opening and the bulk density of the material, we find the mass velocity of its outflow:

$$W_0 = \frac{1}{2}\gamma_n \frac{\bar{n}D_0^2}{4}\sqrt{2g\mu\left[R + d\left(\frac{1}{2} + \frac{1-\mu}{\sqrt{1+\mu^2}}\right)\right]\left[1 \pm \frac{\Delta P_0}{d\gamma_k f(\mu;\frac{d}{R})}\right]} \quad (6)$$

Comparison of experimental data with the results of calculations using dependence (6) shows that the error in the calculated values is within the range from -28.5 to 28.8%.

A comparison of empirical relationships for the critical velocity of a counter-current gas flow demonstrates the varying roles assigned by researchers not only to gas density and viscosity, but also to bulk material density, particle diameters, and the outlet opening [21]. A consequence of this, apparently, is a sharp increase in the error in calculating critical velocity values when processing experimental data using the aforementioned equations, even in the case of an air counter-current [22]. At the same time, gas flow parameters in shaft metallurgical furnaces, and especially in metallization furnaces, can vary widely.

To determine the critical velocity of the counter-flowing gas, a series of experiments were conducted on a «cold» model. The values of the variables were varied within the following limits: outlet diameter $0{,}035 - 0{,}055$m, equivalent diameter of a piece 0.002-0.006 m, specific gravity of gas from 1.2 to 9.2 N/m³ and apparent specific gravity of the material (from 14.5 to 43.5)· 10^3 N/m³.

Assuming equilibrium between the aerodynamic forces and the resisting forces within the granular structure, the following dimensionless relationship can be defined:

$$V'_{kr} = \frac{1}{0.557\sqrt{\gamma_r}} \quad (7)$$

Further transformation of the experimental data into generalized dimensionless coordinates yields:

$$V''_{kr} = \sqrt{\frac{\gamma_k}{437}} \quad (8)$$

Analysis of the experimental datasets demonstrated an approximately linear dependence between the dimensionless critical velocity and the

equivalent flow cross-sectional area. Consequently, the final empirical expression was expressed:

$$V'''_{kr} = \sqrt{\frac{d_{eq}}{0{,}0048} - 0.4} + 0.5 \qquad (9)$$

It has been established that the outlet diameter does not affect the critical velocity of the gas counterflow. In general, the critical velocity of the gas counterflow takes the form:

$$V_{kr} = 0.087\sqrt{\frac{\gamma_k}{\gamma_r}}\left(\sqrt{\frac{d_{eq}}{0.048} - 0.4} + 0.5\right) \qquad (10)$$

The experiment shows that the error in the calculated values ranges from +16.7 to -35.4% and from -28.4 to +24.9%, respectively. Consequently, equation (9) has satisfactory accuracy and is quite acceptable for practical calculations. The influence of gas parameters, the physical and mechanical properties of the bulk material, and the outlet size on the critical velocity of the oncoming gas flow was further studied using volumetric models with gases and materials, the characteristics of which are presented in Tables 1 and 2.

The dependence of the critical counter-current gas velocity V_{kr} on the gas specific weight γ_r is illustrated in Fig. 10. The experimental data for different materials pellets II (1), agglomerate III (2), and millet (3) show a strong correlation with the values calculated using Eq. (17).

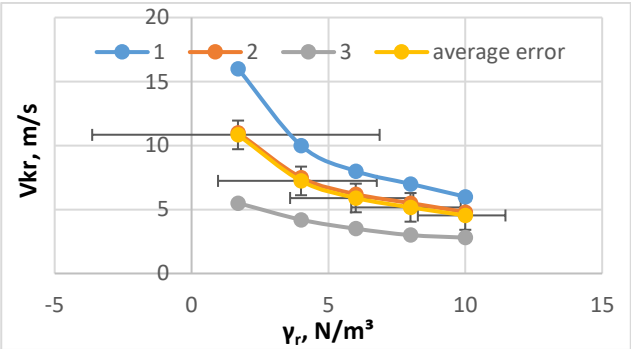

Figure 10 - Dependence of the critical velocity of the counter gas flow (V_{kr}, m/s) from its specific gravity (γ_r, N/m^3). 1 - pellets II; 2 - agglomerate III; 3 - millet; curves - results of calculation according to equation (16)

Figure 10 shows the dependence of three series of values and the average error on the change in the parameter under consideration. All the curves are decreasing, indicating a gradual decrease in the value as the argument increases. The highest values are observed in the first series, which decreases from 16 to 6. The second series also shows a consistent decrease from 11 to 4.8, while the third series has the lowest values and decreases from 5.5 to 2.8.

The average error decreases from 10.83 to 4.533, which confirms the general trend of decreasing the studied indicator. The whiskers on the graph reflect the spread between the minimum and maximum values among the three rows at each point. In the initial section, the spread is the most pronounced, as the difference between the first and third rows is the greatest. As the argument increases, the length of the whiskers gradually decreases, indicating a reduction in the differences between the individual measurement rows.

Thus, the known empirical formulas obtained based on experiments with air flow are valid for calculating the critical gas velocity only within certain limits.

The analytical dependence (5) has been experimentally verified only in the case of air flow. When a loose material is suspended, its flow rate becomes zero when

$$1 - \frac{\Delta P_0}{d\gamma_k f\left(\mu;\frac{d}{R}\right)} = 0 \qquad (11)$$

Revealing the meanings ΔP_0, after substitution and transformations we obtain for the counter gas flow:

$$V_{kr} = m\sqrt{\frac{gd\cdot d_{eq}\gamma_k f\left(\mu;\frac{d}{R}\right)}{2\lambda H\gamma_r}} \qquad (12)$$

Substituting λ and R into equation (12), we obtain

$$V_{kr} = m^{2-n}\sqrt{\frac{g^{1-n}d_{eq}^{1+n}\gamma_k f\left(\mu;\frac{d}{R}\right)}{2cH\gamma_r^{1-n}\eta^n}} \qquad (13)$$

In the case of unstable turbulent motion of the oncoming gas flow ($c = 3.8; n = 0.2$):

$$V_{kr} = m^{1.8}\sqrt{\frac{g^{0.8}d_{eq}^{1.2}\gamma_k f\left(\mu;\frac{d}{R}\right)}{7.6H\gamma_r^{0.8}\eta^{0,2}}} \qquad (14)$$

In turbulent conditions (c=0.55, n=0):

$$V_{kr} = \sqrt{\frac{gd\cdot d_{eq}\gamma_k f\left(\mu;\frac{d}{R}\right)}{1{,}1H\gamma_r}} \qquad (15)$$

Taking $d = d_{eq}$, we obtain for an unstable turbulent regime:

$$V_{kr} = m^{1.8}\sqrt{\frac{g^{0.8}d^{2.2}\gamma_k f\left(\mu;\frac{d}{R}\right)}{7.6H\gamma_r^{0.8}\eta^{0.2}}\cdot\left[\frac{4m}{k(1-m)}\right]^{1.2}} \qquad (16)$$

and for the turbulent regime

$$V_{kr} = md\sqrt{\frac{g\gamma_k f\left(\mu;\frac{d}{R}\right)}{1{,}1H\gamma_r}\cdot\frac{4m}{k(1-m)}} \qquad (17)$$

A comparison of the calculated values of the critical velocities of the counter-current gas flow according to equation (16) and the obtained experimental data showed their satisfactory agreement. The error lies within the range: from -36.4 to +17.1%. Dependence (16) with an accuracy of -25.6 to -35.0% and from -26.3 to -38.4%.

Calculation of critical speeds using formula (16) allows us to reduce the magnitude of the error, which is from -13.9 to +28.8% (Fig. 10) compared with the experimental data. At the same time, the error for the critical velocities of the oncoming air flow, calculated using Eq. (17), is reduced -19.6 to -30.1% and from -18.1 to -32.4% accordingly. This is explained by the significant turbulence of the gas flow in the layer, especially before it freezes.

With an error in the calculated values of the critical speed, amounting from to -30.0 to +28.8%, the main parameters varied within the following limits: specific gravity and viscosity of the gas, respectively, from 11.97 to 1.16 N/m^3; from $8{,}9\cdot 10^{-6}$ to $1.81\cdot 10^{-5}$Pa · s; diameter, specific gravity and coefficient of internal friction of bulk material from $4{,}0\cdot 10^{-4}$ to $15.0\cdot 10^{-3}$m; from 14.3 to 39.2 kN/m^3; from 0.55 to 0.95; coefficient taking into account the shape of the particles, from 6.0 to 7.8; outlet diameter from0.01 to 0.06m; attitude $\frac{d}{R}$ equals $0{,}02-0{,}4$.

A critical finding of this study is the shift in factor significance during the transition to a turbulent counter-current flow. As the system approaches the blockage limit, the influence of gas density increases substantially. Concurrently, the impact of bed porosity, particle size, and shape decreases, while the role of gas viscosity practically disappears. This confirms that at high velocities, the aerodynamic drag acting on the arch structure becomes the primary governing force.

The developed analytical Eq. (12) is universal and demonstrates high accuracy in predicting the critical velocity of counter-current gas flows. It effectively integrates the influence of outlet geometry, solid-phase characteristics, and gas-dynamic parameters. This provides a robust tool for the design and optimization of bulk material flow in horizontal-plane discharge systems, ensuring stable operation in industrial metallurgical furnaces.

Conclusions

Based on the theoretical analysis and a set of experimental studies on "cold" and "hot" models, the following key conclusions were obtained, which constitute the scientific contribution of the work:

1. A physical and mathematical explanation of the mechanism of regulation of the speed of dispersion media by gas flows is proposed, based on the change in the torque of the friction forces during the rolling of particles that form a dynamically unstable vault. It is analytically proven that an oncoming flow minimizes the resulting torque (up to zero at the point of suspension), while a tailing flow maximizes it.

2. The boundaries of applicability of classical empirical release equations have been established, which, as shown in the work, give an error of up to ±50% or more when the gas density and viscosity parameters exceed the normal air conditions. In contrast, the proposed generalized semi-analytical model Eq. (12) stably describes the release kinetics and hover conditions with an error that does not exceed +17.1÷−36.0% in a wide range of changes in the physical and mechanical properties of the phases.

3. The spectrum of factors affecting the controlled release of granular media has been determined and ranked according to their significance: gas velocity vector → hole geometry → bulk density of the material → aerodynamic flow parameters (flow rate, density). It has been revealed that in conditions of developed turbulence, before the layer freezes, the gas density becomes the dominant factor, completely suppressing the influence of the media's viscous characteristics.

4. The practical value of the results lies in the fact that the established macroscopic patterns and criterion equations allow for the precise design of the release and dosing units of hopper systems and counterflow shaft furnaces without conducting expensive and resource-intensive CFD-DEM simulations for each individual particle size.

Conflict of interest. On behalf of all the authors, the correspondingauthor declares that there is no conflict of interest.

CRediT author statement: **S. Akhmetova:** conceptualization, designed the experimental methodology, writing – originaldraft, supervision; **G. Kabiyeva:** methodology and editing; **A. Rakhatova:** writing -review and editing, literature review.

Cite this article as: Akhmetova SS, Kabiyeva GK, Rakhatova AB. Influence of gas flow parameters on the velocity of bulk materials**.** Kompleksnoe Ispolzovanie Mineralnogo Syra = Complex Use of Mineral Resources. 2028; 345(2):29-43. https://doi.org/10.31643/2028/6445.14

Газ ағыны параметрлерінің сусымалы материалдардың ағу жылдамдығына әсері

[1] Ахметова С.С., [2] Кабиева Г.К., [3] Рахатова А.Б.

[1]Ә. Сағынов атындағы Қарағанды техникалық университеті, Қарағанды, Қазақстан
[2]С.Сейфуллин атындағы Қазақ агротехникалық зерттеу университеті, Астана, Қазақстан

Мақала келді: *18 сәуір 2026*
Сараптамадан өтті: *19 мамыр 2026*
Қабылданды: *5 маусым 2026*

ТҮЙІНДЕМЕ

Мақалада жоғары және төмен бағытталған газ ағындарымен өзара әрекеттесу кезінде түйіршікті орталардың ағу заңдылықтары мен қозғалыс кинетикасы зерттеледі. Сусымалы материалдарды тиімді жәшығару процесін басқару шахталық пештер мен бункерлік құрылғыларды пайдалануда маңызды аспект болып табылады. Зерттеулер жазық мөлдір және үлкейтілген «ыстық» модельдерде жылдам бейнетүсірілімді (СК-16) қолдана отырылып жүргізілді. Критикалық жылдамдықтың есептелген мәндеріндегі қателік -30,0-ден +28,8%-ға дейін ауытқыған кезде негізгі параметрлер келесі шектерде өзгерді: газдың меншікті тығыздығы мен тұтқырлығы, тиісінше, 11,97-ден 1,16 Н/м³; $8{,}9\cdot10^{-6}$ бастап $1{,}81\cdot10^{-5}$ Па·с дейін; диаметрі, меншікті тығыздығы және сусымалы материалдың ішкі үйкеліс коэффициенті $4{,}0\cdot10^{-4}$-ден $15{,}0\cdot10^{-3}$ м дейін; 14,3-тен 39,2 кН/м³-ге дейін; 0,55-тен 0,95-ке дейін; бөлшектердің пішінін ескеретін коэффициент, 6,0-ден 7,8-ге дейін; шығыс диаметрі 0,01-ден 0,06 м-ге дейін; d/R қатынасы 0,02-0,4. Зерттелетін материалдар ретінде агломерат, әк, тары және кокс пайдаланылды; газ фазасы ретінде – ауа, гелий және сутегі қолданылды. Ағу механизмі динамикалық тұрақсыз күмбездердің (свод) бұзылу жиілігімен анықталатын сатылы сипатқа ие екені анықталды. Шығару жылдамдылығына әсер ететін негізгі фактор газдың тығыздығы екені, ал тұтқырлықтың әсері екінші дәрежелі екені анықталды. Қабаттың кептелуін (іркілуін) тудыратын газдың критикалық жылдамдығын есептеуге арналған аналитикалық тәуелділік тұжырымдалды. Алынған нәтижелер металлургиялық агрегаттарда шығару тесіктерінің конструктивтік параметрлерін және үрлеу режимдерін оңтайландыруға мүмкіндік береді.

Түйін сөздер: сусымалы материалдар, газ ағыны, қозғалыс, жылдамдық, газөткізгіштік.

Авторлар туралы ақпарат:

Ахметова Сандуғаш Советовна — *Техника ғылымдарының кандидаты, Жоғары математика кафедрасының қауымдастырылған профессоры, Ә. Сағынов атындағы Қарағанды техникалық университеті, 100027, Нұрсұлтан Назарбаев даңғ. 56, Қарағанды, Қазақстан. E-mail: s.akhmetova@ktu.edu.kz; ORCID ID: https://orcid.org/0009-0003-7848-4463*

Кабиева Гульнар Кашкимбаевна — *Жоғарғы математика кафедрасының оқытушысы, Ә. Сағынов атындағы Қарағанды техникалық университеті, 100027, Нұрсұлтан Назарбаев даңғ. 56, Қарағанды, Қазақстан. E-mail: g.kabiyeva@ktu.edu.kz; ORCID ID: https://orcid.org/0009-0003-4069-3569*

Рахатова Алия Бейбутовна — *PHD докторант, Сәкен Сейфуллин атындағы Қазақ агротехникалық зерттеу университеті, 010011, Жеңіс 62 даңғылы, Астана, Қазақстан. E-mail: aliya-rahatova@mail.ru; ORCID ID: https://orcid.org/0009-0001-9086-232X*

Влияние параметров газового потока на скорость истечения сыпучих материалов

[1] Ахметова С.С., [2] Кабиева Г.К., [3] Рахатова А.Б.

[1] Карагандинский технический университет имени А. Сагинова, Караганда, Казахстан
[3] Казахский агротехнический исследовательский университет им. С. Сейфуллина, Астана, Казахстан

Поступила: *18 апреля 2026*
Рецензирование: *19 мая 2026*
Принята в печать: *5 июня 2026*

АННОТАЦИЯ

Статья посвящена исследованию закономерностей истечения и кинетики движения зернистых сред при взаимодействии с восходящими и нисходящими газовыми потоками. Управление выпуском сыпучих материалов является критическим аспектом эксплуатации шахтных печей и бункерных устройств. Экспериментальные исследования проведены на плоской прозрачной и укрупненной «горячей» моделях с использованием скоростной видеосъемки (СК-16). При погрешности в расчетных значениях критической скорости, составляющей от -30,0 до +28,8%, основные параметры изменялись в следующих пределах: удельная плотность и вязкость газа, соответственно, от 11,97 до 1,16 Н/м³; от 8,9 ·

	10^{-6} до $1.81 \cdot 10^{-5}$ Па·с; диаметр, удельная плотность и коэффициент внутреннего трения сыпучего материала от $4{,}0 \cdot 10^{-4}$ до $15{,}0 \cdot 10^{-3}$м; от 14,3 до 39,2 кН/м³; от 0,55 до 0,95; коэффициент, учитывающий форму частиц, от 6,0 до 7,8; диаметр выходного отверстия от 0,01 до 0,06 м; отношение d/R равно 0,02-0,4. В качестве исследуемых материалов использованы агломерат, известь, пшено и кокс; в качестве газовой фазы — воздух, гелий и водород. Установлено, что механизм истечения носит стадийный характер и определяется частотой разрушения динамически неустойчивых сводов. Выявлено, что ключевым фактором, влияющим на скорость выпуска, является плотность газа, в то время как влияние вязкости вторично. Сформулирована аналитическая зависимость для расчета критической скорости газа, вызывающей зависание слоя. Полученные данные позволяют оптимизировать конструктивные параметры выпускных отверстий и режимы подачи дутья в металлургических агрегатах.
	Ключевые слова: сыпучие материалы, газовый поток, движение, скорость, газопроницаемость.
Ахметова Сандугаш Советовна	***Информация об авторах:*** *Кандидат технических наук, ассоциированный профессор кафедры Высшая математика, Карагандинский технический университет им. А.Сагинова, 100027, пр. Нурсултана Назарбаева, 56, Караганда, Казахстан. E-mail: s.akhmetova@ktu.edu.kz; ORCID ID: https://orcid.org/0009-0003-7848-4463*
Кабиева Гульнар Кашкимбаевна	*Преподаватель кафедры Высшая математика, Карагандинский технический университета им. А.Сагинова, 100027, пр. Нурсултана Назарбаева, 56, Караганда, Казахстан. E-mail: g.kabiyeva@ktu.edu.kz; ORCID ID: https://orcid.org/0009-0003-4069-3569*
Рахатова Алия Бейбутовна	*Докторант PHD, Казахский агротехнический исследовательский университет имени Сакена Сейфуллина 010011, пр. Жеңіс, 62, Астана, Казахстан. E-mail: aliya-rahatova@mail.ru; ORCID ID: https://orcid.org/0009-0001-9086-232X*

References

[1] Guo C, Liu G, Wang X. CFD-DEM coupling analysis of EPB screw conveyor muck discharge in water-rich sandy cobble strata // Scientific Reports. 2026; 16(1):12407. https://doi.org/10.1038/s41598-026-41903-7

[2] Xiao F, Luo M, Huang F, et al. CFD–DEM investigation of gas-solid flow and wall erosion of vortex elbows conveying coarse particles. Powder Technology. 2023; 424:118524. https://doi.org/10.1016/j.powtec.2023.118524

[3] Heng Zhou, Kun Xu, Xu Tian, et al. Influence of burden profile on gas-solid distribution in COREX shaft furnace with center gas supply by CFD-DEM model. Powder Technology. 2021; 392:672–679. https://doi.org/10.1016/j.powtec.2021.07.039

[4] Fei Xiao, Min Luo, Fayuan Huang, et al. CFD – DEM investigation of gas-solid flow and wall erosion of vortex elbows conveying coarse particles. Powder Technology. 2023; 424:118524. https://doi.org/10.1016/j.powtec.2023.118524

[5] Banik R K, Das H J. MFIX – DEM simulation of gas-solid flow dynamics in a dual fluidized bed system. IOP Conference Series: Earth and Environmental Science. 2024; 1372(1):012100. https://doi.org/10.1088/1755-1315/1372/1/012100

[6] Maksimov E V, Bekbaev K S, Tarabaev B K, et al. Issledovaniye protsessa porchi sypuchikh materialov v szhatykh usloviyakh [Investigation of the expiration of bulk materials in summary conditions]. Vestnik nauki Kazakhskogo agrotekhnicheskogo universiteta im. S. Seyfullina [Herald of Science of S. Seifullin Kazakh Agrotechnical University]. 2012; 4(75):94–98. (In Russ.).

[7] Mankoc C, Janda A, Arévalo R, et al. The flow rate of granular materials through an orifice. Granular Matter. 2007; 9(6):407–414. https://doi.org/10.1007/s10035-007-0062-2

[8] Amanbaev T R, Antony S J. Modeling the Outflow of Particulate Solids from a Container Taking into Account the Effect of Adhesion to the Wall. 2022; 57:954–966. https://doi.org/10.1134/S0015462822070023

[9] Chen J, Ge M, Li L, Zheng G. Material transport and flow pattern characteristics of gas–liquid–solid mixed flows. Processes. 2023; 11(8):2254. https://doi.org/10.3390/pr11082254

[10] Tingwen Li, Erik Delsman, Sreekanth Pannala. Mass flow rate prediction for gas-controlled hopper discharge of free-flowing granular materials. Powder Technology. 2026; 473:122190. https://doi.org/10.1016/j.powtec.2026.122190

[11] Ferrari G, Poletto M. Arch-Free flow in aerated silo discharge of cohesive powders. Powder Technology. 2009; 191(1-2):118–125. https://doi.org/10.1016/j.powtec.2008.10.013

[12] Zhanxia D, Yan B, Huang M, Cheng B. Numerical simulation of reduction behavior in shaft furnace based on DEM and CFD // International Journal of Chemical Reactor Engineering. – 2025. – Vol. 23, No. 3. – P. 373–391. https://doi.org/10.1515/ijcre-2024-0109

[13] Xu T, Zhou H, Zhang Y, et al. Numerical simulation of hydrogen-enriched shaft furnace. International Journal of Hydrogen Energy. 2024; 55:1131–1142. https://doi.org/10.1016/j.ijhydene.2023.11.277

[14] Zhou H, Xu K, Tian X, et al. Influence of burden profile on gas-solid distribution in COREX shaft furnace with center gas supply by CFD-DEM model. Powder Technology. 2021; 392:672–679. https://doi.org/10.1016/j.powtec.2021.07.039

[15] Wan Q, Zhao Z, Wang R, Tang M, Wang D, Zhang S, Hu B. Characteristics of Gas–Solid Flow in an Intermittent Countercurrent Moving Bed. Processes. 2022; 10(10):2116. https://doi.org/10.3390/pr10102116

[16] Vynnycky M, Rangavittal B V, Glaser B. An Asymptotic Model for Gas-Solid Flow in a Countercurrent Moving Bed Reactor. SIAM Journal on Applied Mathematics. 2023; 83(2):605–631. https://doi.org/10.1137/22M1496293

[17] Chen X, Chen J, Cai C, Liang X. Discharge characteristics of granular coal with wide size distribution from aeration silo. Journal of Chemical Industry and Engineering. China. 2011; 62(6):1654–1661. https://doi.org/10.3969/j.issn.0438-1157.2011.06.031

[18] Chen J, Ge M, Li L, Zheng G. Material transport and flow pattern characteristics of gas–liquid–solid mixed flows. Processes. 2023; 11(8):2254. https://doi.org/10.3390/pr11082254

[19] Li T, Delsman E, Pannala S. Mass flow rate prediction for gas-controlled hopper discharge of free-flowing granular materials. Powder Technology. 2026; 473:122190. https://doi.org/10.1016/j.powtec.2026.122190

[20] Zhu X, Dong P, Tu Q, Zhu Z, Wang H. Investigation of gas–solids flow characteristics in a pressurised circulating fluidised bed by experiment and simulation. Powder Technology. 2020; 366:420–433. https://doi.org/10.1016/j.powtec.2020.02.047

[21] Zhang X, Yu Y, Hu Y. Experimental study on gas–liquid–solid interaction characteristics in the launch tube. Journal of Marine Science and Engineering. 2022; 10(9):1239. https://doi.org/10.3390/jmse10091239

[22] Yang S-C, Hsiau S-S. The simulation and experimental study of granular materials discharged from a silo with the placement of inserts. Powder Technology. 2001; 120(3):244–255. https://doi.org/10.1016/S0032-5910(01)00277-7

Crossref
DOI: 10.31643/2028/6445.15
Metallurgy and Metallurgical Engineering

Elemental Assessment of Lead–Bismuth Sludge from Copper Smelting with Emphasis on Tellurium Recovery

[1*]Tulaganova M., [1]Matkarimov S., [1]Ismailov J., [2]Matkarimov Z., [3]Alamova G.

[1]Tashkent State Technical University, Tashkent, Uzbekistan
[2]Tashkent Institute of Chemical Technology, Tashkent, Uzbekistan
[3]Uzbek-Japan Innovation Center of Youth, Tashkent, Uzbekistan

** Corresponding author email: tulaganovamunisa1512@gmail.com*

Received: *March 26, 2026*
Peer-reviewed: *May 13, 2026*
Accepted: *June 9, 2026*

ABSTRACT

Industrial by-products generated during copper smelting are increasingly regarded as promising secondary sources of strategically important and critical elements. Among such technogenic materials, lead–bismuth sludge formed during wet gas cleaning of sulfur-bearing gases represents a potentially valuable reservoir of selenium and tellurium. The present study provides a comprehensive elemental assessment of lead–bismuth sludge obtained from the Almalyk Mining and Metallurgical Complex (Uzbekistan). Prior to analysis, representative sludge samples were subjected to acid digestion using freshly prepared aqua regia, followed by elemental determination using inductively coupled plasma optical emission spectroscopy (ICP-OES). Particular attention was devoted to the distribution behavior of selenium and tellurium due to their technological importance as critical raw materials. The analytical results demonstrated that the investigated sludge is characterized by a pronounced polymetallic composition dominated by lead (20.0%), together with significant concentrations of iron (6.76%), copper (5.34%), and zinc (4.40%). Tellurium was detected at a concentration of 0.33%, indicating its selective accumulation in the lead–bismuth residue, whereas selenium was not detected under the selected analytical conditions. Based on elemental composition data and thermodynamic considerations, the investigated sludge may be considered a promising secondary source for tellurium recovery. The obtained results contribute to understanding the physicochemical behavior of chalcogen elements during copper smelting and wet gas-cleaning processes and may serve as a basis for the development of integrated recycling approaches for technogenic metallurgical waste.

Keywords: copper smelting, secondary tellurium source, critical raw materials, technogenic waste, wet gas cleaning, elemental composition, ICP-OES.

Information about authors:

Munisa Tulaganova Abdulla kizi — *PhD student, Department of Metallurgy, Tashkent State Technical University, 2, University str., 100098, Tashkent, Uzbekistan. Email: tulaganovamunisa1512@gmail.com; ORCID ID: https://orcid.org/0009-0007-4089-2217*

Sokhibjon Matkarimov Turdalievich — *Doctor of Technical Sciences, Professor, Head of Career Center, Tashkent State Technical University, 2, University str., 100098, Tashkent, Uzbekistan. Email: sohibtm@gmail.com; ORCID ID: https://orcid.org/0000-0003-2393-6576*

Ismailov Jonibek Bakhadyrovich — *PhD, Assistant professor, Head of the Department of Metallurgy, Tashkent State Technical University, 2, University str., 100098, Tashkent, Uzbekistan. Email: jonibekismailov1001@gmail.com; ORCID ID: https://orcid.org/0009-0001-8065-5773*

Zaynobiddin Matkarimov Turdalievich — *PhD, Assistant professor, Department of technology of silicate materials and noble, rare metals, Tashkent Institute of Chemical Technology, 32, Navoiy str., 100011, Tashkent, Uzbekistan. Email: zaynobiddin1986@mail.ru; ORCID ID: https://orcid.org/0000-0002-5650-7404*

Alamova Gulbahor Khamroevna — *PhD student, Department of Mining and deep processing os mineral resources, Uzbek-Japan innovation center of youth, 2, University str., 100098, Tashkent, Uzbekistan. Email: alamovagulbahor1903@gmail.com; ORCID ID: https://orcid.org/0009-0006-4917-488X*

Introduction

In recent years, waste generated during copper smelting has attracted increasing attention not only as an environmentally hazardous material, but also as a potential secondary source of economically and strategically important elements [[1], [2], [3], [4], [5]]. Among such technogenic products, lead–bismuth sludge formed during wet gas cleaning represents a chemically complex polymetallic system whose composition depends on the mineralogical characteristics of raw materials and the physicochemical conditions of pyrometallurgical processing [[6], [7], [8]].

Particular interest has recently been directed toward selenium and tellurium because these

elements are classified as critical raw materials due to the limited availability of primary deposits and their growing demand in photovoltaic technologies, thermoelectric materials, semiconductor manufacturing, and advanced energy systems [[9], [10], [11], [12]]. Copper smelting processes are considered one of the major industrial sources of secondary tellurium recovery because chalcogen elements tend to redistribute into dusts, sludges, and gas-cleaning products during high-temperature processing [[13], [14], [15]].

Despite the growing industrial importance of tellurium, reliable information concerning its distribution in lead–bismuth sludge generated during wet gas cleaning remains limited. Existing studies indicate that selenium and tellurium exhibit significantly different physicochemical behavior under oxidizing smelting conditions, which directly influences their volatility, phase stability, and accumulation in technogenic products [[16], [17], [18]].

Selenium is characterized by the formation of volatile oxide compounds that can migrate with process gases or transfer into liquid phases during gas purification. In contrast, tellurium tends to form more stable and less volatile compounds, favoring its accumulation in condensed solid residues [19]. Consequently, the enrichment degree of selenium and tellurium in individual waste streams may differ substantially from values predicted solely from ore composition [[20], [21]].

The growing demand for tellurium and other critical elements significantly increases the importance of identifying alternative secondary resources suitable for their recovery [[22], [23]]. In this context, technogenic products generated during copper smelting may represent an important raw material base for future extraction of valuable elements.

Therefore, the present study is aimed at evaluating the elemental composition of lead–bismuth sludge obtained from the Almalyk Mining and Metallurgical Complex (Uzbekistan), with particular emphasis on the distribution behavior and selective accumulation of tellurium in wet gas-cleaning residues.

Experimental part

Lead–bismuth sludge samples investigated in this study were obtained from the Almalyk Mining and Metallurgical Complex (Uzbekistan). The material represents a solid technogenic product formed after wet gas cleaning of sulfur-bearing gases generated during copper smelting operations.

Prior to analysis, the samples were dried under laboratory conditions, homogenized, and mechanically crushed to ensure representative sampling. For preliminary characterization, two independent subsamples (S_o) with a mass of approximately 1000 g each were prepared. One subsample was used for primary analytical measurements, whereas the second was employed to evaluate analytical reproducibility.

For elemental analysis, representative portions of approximately 0.5–1.0 g were subjected to acid digestion using freshly prepared aqua regia ($HCl:HNO_3$ = 3:1). The digestion process was carried out in glass vessels at approximately 90 °C for 1–2 h under controlled laboratory conditions until complete dissolution of the solid matrix was achieved. After cooling, the obtained solutions were diluted with distilled water to a final volume of 50 mL and filtered when necessary to remove residual insoluble particles (Fig.1).

Figure 1 - Dissolved sample

The elemental composition of the prepared solutions was determined using inductively coupled plasma optical emission spectroscopy (ICP-OES) performed on a Genesis Spectrum ICP-OES instrument. Calibration of the instrument was carried out using standard reference solutions under standard operating conditions. The analysis included determination of major and trace elements, with particular emphasis on selenium and tellurium as critical elements of technological interest.

All measurements were performed in duplicate, and analytical reproducibility was evaluated based on repeated measurements of independently prepared samples. The obtained analytical data

demonstrated satisfactory repeatability for polymetallic technogenic materials. Element concentrations are reported as mass percentages (%).

Special attention was devoted to the determination of selenium because its concentration in the investigated sludge was close to or below the instrumental detection limit under the selected analytical conditions. The applied analytical methodology allowed reliable determination of tellurium and major accompanying elements in the investigated technogenic residue.

Results and Discussion

The elemental composition of the investigated lead–bismuth sludge was determined using ICP-OES analysis (Fig.2). The obtained results confirmed the pronounced polymetallic nature of the studied technogenic material. The analytical data are summarized in Table 1. Lead was identified as the dominant component with a concentration of approximately 20.0%, indicating its significant accumulation in the investigated residue. Considerable concentrations of iron (6.76%), copper (5.34%), and zinc (4.40%) were also detected, reflecting the transfer of volatile metal compounds and fine dispersed particles during copper smelting and subsequent wet gas-cleaning processes.

Bismuth and antimony were detected at concentrations of 0.20% and 0.34%, respectively, while nickel was present only in trace quantities (0.02%). The obtained results additionally confirmed the presence of noble metals in the investigated sludge. Palladium was detected at 0.003%, whereas platinum was identified in minor quantities within the analyzed material.

Particular attention was devoted to the distribution behavior of selenium and tellurium because these elements are considered technologically important critical raw materials. Tellurium was detected at a concentration of 0.33%, indicating its selective accumulation in the lead–bismuth sludge. In contrast, selenium was not detected under the selected analytical conditions, suggesting either its absence in the solid residue or concentrations below the instrumental detection limit.

Repeated measurements of independently prepared subsamples demonstrated satisfactory analytical reproducibility for the investigated polymetallic material.

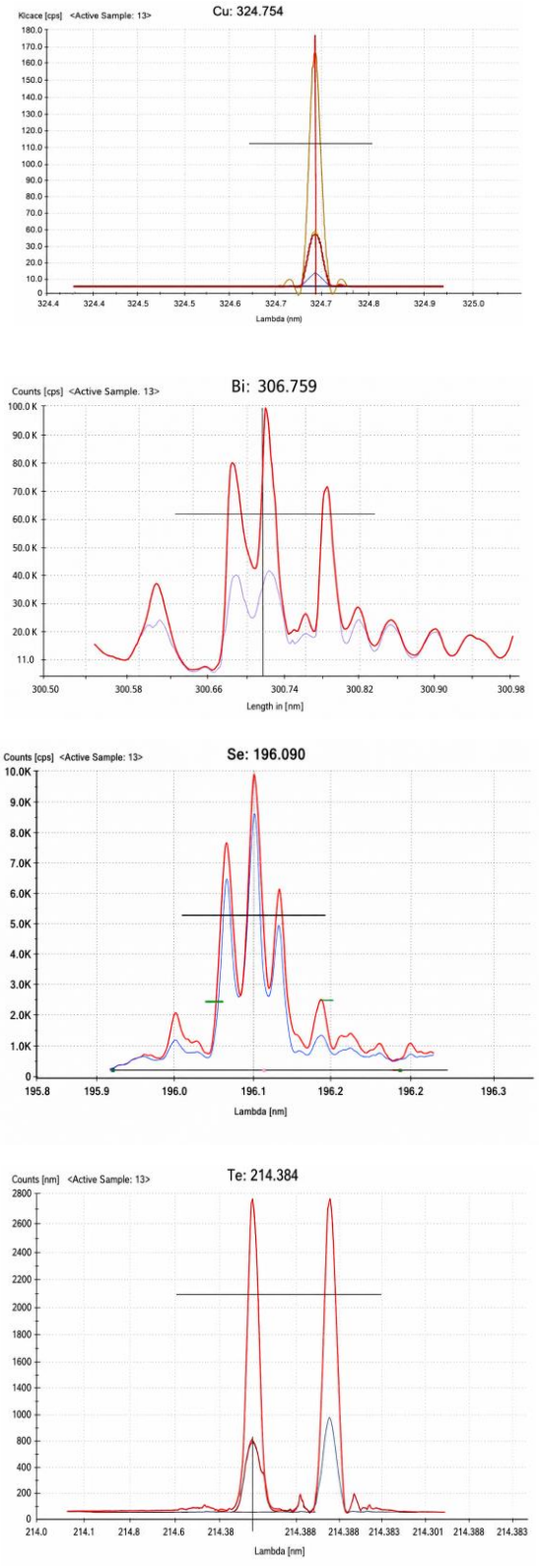

Figure 2 - Representative emission spectra recorded using a Genesis ICP-OES instrument

The obtained results demonstrate substantial differences in the physicochemical behavior of selenium and tellurium during copper smelting and wet gas-cleaning processes. Despite their chemical similarity, these elements exhibit different volatility

and redistribution characteristics under oxidizing high-temperature conditions.

According to previously published studies, selenium is generally characterized by the formation of more volatile compounds capable of transferring into gaseous or liquid process streams during gas purification. In contrast, tellurium demonstrates a greater tendency toward accumulation in condensed technogenic products generated during copper smelting.

The observed enrichment of tellurium in the investigated sludge indicates that wet gas-cleaning residues may serve as important secondary resources for tellurium recovery from metallurgical waste. At the same time, the absence of detectable selenium in the solid residue suggests its redistribution into alternative technological streams, including associated dusts and liquid gas-cleaning products.

The present investigation was primarily focused on elemental characterization of lead–bismuth sludge using ICP-OES analysis. Therefore, additional investigations involving X-ray diffraction (XRD), scanning electron microscopy coupled with energy-dispersive spectroscopy (SEM-EDS), and mineralogical analysis are required for direct identification of phase associations and distribution forms of tellurium and accompanying elements in the investigated technogenic material.

Behavior and Distribution of Elements in Lead–Bismuth Sludge

The established elemental composition allows evaluation of the possible distribution behavior of elements in the investigated sludge, taking into account their physicochemical properties and previously published data concerning similar technogenic materials [[24], [25], [26]]. The obtained analytical results indicate that lead-containing compounds represent a significant component of the investigated residue formed during wet gas cleaning of sulfur-bearing gases generated in copper smelting processes.

The presence of bismuth together with elevated lead concentrations indicates accumulation of these elements in the solid fraction of the sludge. Earlier studies have demonstrated that lead and bismuth exhibit similar redistribution tendencies during pyrometallurgical processing and subsequent gas-cleaning operations. The measured tellurium concentration (0.33%) indicates selective retention of this element in the investigated technogenic material. Previous investigations have shown that tellurium demonstrates lower volatility under oxidizing smelting conditions compared with selenium, promoting its accumulation in condensed metallurgical products. Iron, copper, and zinc identified in the investigated sludge are associated with transfer of volatile metal compounds and fine dispersed particles during smelting and gas purification processes. Their presence confirms the polymetallic nature of the investigated residue.

The obtained results demonstrate substantial differences in the distribution behavior of selenium and tellurium during copper smelting and wet gas-cleaning processes. Despite their chemical similarity, these elements exhibit different redistribution characteristics under high-temperature oxidizing conditions. Selenium is generally characterized by formation of more volatile compounds capable of transferring into gaseous or liquid process streams during gas purification. In contrast, tellurium demonstrates a greater tendency toward accumulation in condensed technogenic products due to formation of relatively stable low-volatility compounds. The observed enrichment of tellurium in the investigated sludge indicates that wet gas-cleaning residues may represent promising secondary resources for tellurium recovery from metallurgical waste.

The present investigation was primarily focused on elemental characterization using ICP-OES analysis. Therefore, additional investigations involving X-ray diffraction (XRD), scanning electron microscopy coupled with energy-dispersive spectroscopy (SEM-EDS), and mineralogical analysis are required for direct confirmation of phase composition and elemental associations in the investigated technogenic material.

Implications for Secondary Resource Potential

The results of the analysis indicate that lead-bismuth sludge formed during wet gas cleaning has selective absorption capacity. It cannot be considered a universal matrix for the simultaneous concentration of selenium and tellurium. Nevertheless, the measured concentration of tellurium indicates that this man-made material is a promising secondary resource for tellurium extraction. The absence of selenium in the solid residue confirms its predominant removal in associated technological cycles. In this regard, additional study of alternative flows in the smelting and gas cleaning system is required to identify the main accumulation zones of this element

Table 1 - Elemental composition of lead–bismuth technogenic sludge formed during wet gas cleaning

Element	Content, %
Pb	20.00
Cu	5.34
Fe	6.76
Zn	4.40
Bi	0.20
Sb	0.34
Ni	0.02
Te	0.33
Se	Not detected
Pd	0.003
Pt	1.11

Conclusions

This paper presents a detailed polymetallic characterization of anthropogenic lead-bismuth slag formed during copper smelting. The experimental results confirm that the material under study is a complex multicomponent system. Lead acts as the main carrier matrix, associated with significant concentrations of copper, iron, zinc, as well as a number of impurities and trace elements. During the study, a distinct selectivity in the distribution of target components was observed. The tellurium content was 0.33%, which confirms its preferential accumulation in the lead-bismuth residue, while the presence of selenium was not detected using the analytical methods employed. These results reflect fundamental differences in the physicochemical behavior of selenium and tellurium during high-temperature smelting and subsequent wet gas cleaning.

Based on the data obtained on the elements and previously published studies, it can be concluded that tellurium in the sludge is mainly associated with the oxide phases of lead and bismuth.

Due to its high volatility and increased migration ability, selenium is redistributed into alternative technological cycles. Thus, lead-bismuth sludge exhibits selectivity and is not a universal medium for the simultaneous concentration of both elements.

From a practical point of view, the man-made material under study should be considered as a promising secondary source of tellurium. At the same time, for the effective utilization of selenium, it is necessary to identify and study alternative areas of its accumulation in the smelting and gas purification system. The methodology used and the data obtained allow for a more accurate assessment of the value of secondary raw materials. This opens up opportunities for the creation of rational schemes for the utilization and processing of waste generated during copper smelting.

Conflicts of interest. On behalf of all authors, the corresponding author states that there is no conflict of interest.

CRediT author statement: **M. Tulaganova**: Conceptualization, Methodology, Software; **J. Ismailov**: Data curation, Writing draft preparation; **Z. Matkarimov**: Visualization, Investigation; **G. Alamova**: Supervision; Software, Validation; **S. Matkarimov**: Reviewing and Editing.

Cite this article as: Tulaganova MA, Matkarimov ST, Ismailov JB, Matkarimov ZT, Alamova G. Elemental assessment of lead–bismuth sludge from copper smelting with emphasis on tellurium recovery. Kompleksnoe Ispolzovanie Mineralnogo Syra = Complex Use of Mineral Resources. 2028; 345(2):44-51. https://doi.org/10.31643/2028/6445.15

Теллурды мыс балқыту арқылы алуда қорғасын-висмут шламының қарапайым бағалауы

[1] Тулаганова М., [1] Маткаримов С., [1] Исмаилов Ж., [2] Маткаримов З., [3] Аламова Г.

[1]Ташкент мемлекеттік техникалық университеті, Ташкент, Өзбекстан
[2]Ташкент химия-технологиялық институты, Ташкент, Өзбекстан
[3]Өзбек-жапон жастарының инновациялық орталығы, Ташкент, Өзбекстан

ТҮЙІНДЕМЕ

Мыс балқыту кезінде түзілетін өнеркәсіптік жанама өнімдер стратегиялық маңызды және критикалық элементтердің перспективалы екінші реттік көздері ретінде жиірек қарастырылуда. Осындай техногендік материалдардың бірі — құрамында күкірті бар газдарды ылғалды тазарту кезінде түзілетін қорғасын-висмут шламы, ол селен мен теллурдың әлеуетті құнды көзі болып табылады. Бұл зерттеу Алмалық тау-кен металлургия

Мақала келді: *26 наурыз 2026*
Сараптамадан өтті: *13 мамыр 2026*
Қабылданды: *9 маусым 2026*

комбинатында (Өзбекстан) алынған қорғасын-висмут шламының элементтік құрамын кешенді бағалау ұсынылған. Талдау алдында шламның өкілдік үлгілері жаңадан дайындалған патша сұйығымен қышқылдық ыдыратуға ұшыратылып, содан кейін элементтік құрамы индуктивті байланысқан плазмалы оптикалық-эмиссиялық спектроскопия (ICP-OES) әдісімен анықталды. Селен мен теллур маңызды шикізат ретінде технологиялық маңыздылығына байланысты олардың таралу заңдылықтарына ерекше назар аударылды. Талдау нәтижелері зерттелген шламның қорғасынның басымдығымен (20,0%) айқын полиметалдық құраммен, сондай-ақ темір (6,76%), мыс (5,34%) және мырыштың (4,40%) %) айтарлықтай концентрациясымен сипатталатынын көрсетті. Теллур мөлшері 0,33% құрады, бұл оның қорғасын-висмут қалдығында селективті жинақталуын көрсетеді, ал таңдалған аналитикалық жағдайларда селен анықталмады. Элементтік құрам деректері мен термодинамикалық түсініктер негізінде зерттелген шлам теллурды алудың перспективалы екінші реттік шикізат көзі ретінде қарастырылуы мүмкін. Алынған нәтижелер мыс балқыту және ылғалды газ тазарту процестеріндегі халькоген элементтерінің физика-химиялық жағдайын түсінуге ықпал етеді және техногендік металлургиялық қалдықтарды кешенді қайта өңдеу тәсілдерін әзірлеуге негіз бола алады.

Түйін сөздер: мыс балқыту, екіншілік теллур көзі, критикалық шикізат, техногендік қалдықтар, ылғалды газды тазарту, элементтік құрам, ICP-OES.

Авторлар туралы мәлімет:

Муниса Тулаганова Абдулла кизи — *PhD студент, Ташкент мемлекеттік техникалық университеті металлургия кафедрасы, Университетская көшесі 2, 100098, Ташкент, Өзбекстан. Email: tulaganovamunisa1512@gmail.com; ORCID ID: https://orcid.org/0009-0007-4089-2217*

Сохибжон Маткаримов Турдалиевич — *Техника ғылымдарының докторы, профессор, Ташкент мемлекеттік техникалық университеті, Карьера орталығының жетекшісі, Университет көшесі, 2, 100098, Ташкент, Өзбекстан. Email: sohibtm@gmail.com; ORCID ID: https://orcid.org/0000-0003-2393-6576*

Исмаилов Жонибек Бахадирович — *PhD, доцент, Металлургия кафедрасының меңгерушісі Ташкент мемлекеттік техникалық университеті, Университетская 2, 100098, Ташкент, Өзбекстан. Email: jonibekismailov1001@gmail.com; ORCID ID: https://orcid.org/0009-0001-8065-5773*

Зайнобиддин Маткаримов Турдалиевич — *PhD, доцент, Силикат материалдары және асыл және сирек металдар технологиясы кафедрасы, Ташкент химия-технологиялық институты, Навои көшесі, 32, 100011, Ташкент, Өзбекстан. Email: zaynobiddin1986@mail.ru; ORCID ID: https://orcid.org/0000-0002-5650-7404*

Аламава Гулбахор Хамроевна — *Өзбек-Жапон инновациялық жастар орталығы, Тау-кен өнеркәсібі және минералды ресурстарды терең өңдеу зертханасының докторанты, Университетская 2б, 100098, Ташкент, Өзбекстан. Email: alamovagulbahor1903@gmail.com; ORCID ID: https://orcid.org/0009-0006-4917-488X*

Элементарная оценка свинцово-висмутового шлама при выплавке меди с акцентом на извлечение теллура

[1] Тулаганова М., [1] Маткаримов С., [1] Исмаилов Ж., [2] Маткаримов З., [3] Аламова Г.

[1]Ташкентский государственный технический университет, Ташкент, Узбекистан
[2]Ташкентский институт химической технологии, Ташкент, Узбекистан
[3]Узбекско-японский инновационный центр молодежи, Ташкент, Узбекистан

Поступила: *26 марта 2026*
Рецензирование: *13 мая 2026*
Принята в печать: *9 июня 2026*

АННОТАЦИЯ

Промышленные побочные продукты, образующиеся при выплавке меди, все чаще рассматриваются как перспективные вторичные источники стратегически важных и критических элементов. Среди таких техногенных материалов свинцово-висмутовый шлам, образующийся при мокрой очистке серосодержащих газов, представляет собой потенциально ценный источник селена и теллура. В настоящем исследовании представлена комплексная оценка элементного состава свинцово-висмутового шлама, полученного на Алмалыкском горно-металлургическом комбинате (Узбекистан). Перед проведением анализа представительные образцы шлама подвергались кислотному разложению свежеприготовленной царской водкой с последующим определением элементного состава методом оптико-эмиссионной спектроскопии с индуктивно связанной плазмой (ICP-OES). Особое внимание было уделено характеру распределения селена и теллура в связи с их технологической значимостью как критически важных видов сырья. Результаты анализа показали, что исследуемый шлам характеризуется выраженным полиметаллическим составом с преобладанием свинца (20,0%), а также значительными концентрациями железа (6,76%), меди (5,34%) и цинка (4,40%). Содержание теллура составило 0,33%, что свидетельствует о его селективном накоплении в свинцово-висмутовом остатке, тогда как селен в выбранных аналитических условиях обнаружен не был. На основании данных

элементного состава и термодинамических представлений исследуемый шлам может рассматриваться как перспективный вторичный источник для извлечения теллура. Полученные результаты способствуют пониманию физико-химического поведения халькогенных элементов в процессах выплавки меди и мокрой газоочистки, а также могут служить основой для разработки комплексных подходов к переработке техногенных металлургических отходов.

Ключевые слова: плавка меди, вторичный источник теллура, критическое сырье, техногенные отходы, мокрая очистка газов, элементный состав, ICP-OES.

Информация об авторах:

Муниса Тулаганова Абдулла кизи *PhD студент, кафедра Металлургии Ташкентского государственного технического университета, ул. Университетская 2, 100098, Ташкент, Узбекистан. Email: tulaganovamunisa1512@gmail.com; ORCID ID: https://orcid.org/0009-0007-4089-2217*

Сохибжон Маткаримов Турдалиевич *Доктор технических наук, профессор, руководитель Центра карьеры Ташкентского государственного технического университета, 2, ул. Университетская, 100098, Ташкент, Узбекистан. Email: sohibtm@gmail.com; ORCID ID: https://orcid.org/0000-0003-2393-6576*

Исмаилов Жонибек Бахадирович *PhD, доцент, заведующий кафедрой металлургии Ташкентского государственного технического университета, ул. Университетская 2, 100098, Ташкент, Узбекистан. Email: jonibekismailov1001@gmail.com; ORCID ID: https://orcid.org/0009-0001-8065-5773*

Зайнобиддин Маткаримов Турдалиевич *PhD, доцент кафедры технологии силикатных материалов и благородных, редких металлов, Ташкентский химико-технологический институт, ул. Навои 32, 100011, Ташкент, Узбекистан. Email: zaynobiddin1986@mail.ru; ORCID ID: https://orcid.org/0000-0002-5650-7404*

Аламава Гулбахор Хамроевна *Докторант лаборатории горнодобывающей промышленности и глубокой переработки минеральных ресурсов, Узбекско-Японский инновационный молодежный центр, ул. Университетская 2б, 100098, Ташкент, Узбекистан. Email: alamovagulbahor1903@gmail.com; ORCID ID: https://orcid.org/0009-0006-4917-488X*

References

[1] Habashi F. Handbook of extractive metallurgy. Wiley-VCH. 1997.

[2] Matkarimov S T, Yusupkhodjayev A A, Berdiyarov B T, Nosirkhujayev S Q U, & Matkarimov Z T. Technology of deep processing of copper slags by method of active thermal gravity. International Journal of Advanced Science and Technology. 2020; 29(3):5633–5639.

[3] Matkarimov S T, Yusupkhodjaev A A, Khojiev S T, Berdiyarov B T, & Matkarimov Z T. Technology for the complex recycling slags of copper production. Journal of Critical Reviews. 2020; 7(5):214–220. https://doi.org/10.31838/jcr.07.05.38

[4] George M W, et al. Tellurium: Properties, processing, and applications. Minerals Engineering. 2015; 70:35–45.

[5] Guo Z, Pan J, Zhu D, & Zhang F. Recovery of iron from copper slag by deep reduction and magnetic separation. Journal of Iron and Steel Research International. 2013; 20(1):24–28.

[6] Saidova MS, Aribdjonova DE, Mirzajonova SB, Karimova TP, Bakhodirova NK. Development of resource-based technology for production of blue vitriol from industrial products. Metal 2021 - 30th Anniversary International Conference on Metallurgy and Materials, Conference Proceedings. 2021, 1155 – 1159. https://doi.org/10.37904/metal.2021.4254

[7] Jha M K, Kumar V, & Singh R J. Review of hydrometallurgical recovery of selenium and tellurium from secondary resources. Hydrometallurgy. 2012; 111–112:1–9.

[8] Khojiev S T, & et. al. The technology for the reduction of metal oxides using waste polyethylene materials. In METAL 2020: 29th International Conference on Metallurgy and Materials, Conference Proceedings. 2020, 971–978. https://doi.org/10.37904/metal.2020.3592

[9] Li X, Deng Z, & Wei C. Recovery of valuable metals from copper slag by hydrometallurgical methods. Transactions of Nonferrous Metals Society of China. 2017; 27(6):1283–1292.

[10] Berdiyarov B. Method for oxidative roasting of sulfide zinc concentrates in an air oxygen stream in fluidized bed furnaces. IOP Conference Series: Earth and Environmental Science. 2023; 1142(1). https://doi.org/10.1088/1755-1315/1142/1/0120

[11] Moskalyk R R, & Alfantazi A M. Processing of copper smelter slags. Minerals Engineering. 2003; 16(10):893–902.

[12] Schlesinger M E, King M J, Sole K C, & Davenport W G. Extractive metallurgy of copper (5th ed.). Elsevier. 2011.

[13] Umarova I, et al. Study of the form of minerals in copper porphyry ores of Yoshlik-I deposit. E3S Web of Conferences. 2021; 304:7. https://doi.org/10.1051/e3sconf/202130402003

[14] Wang S, & Chen Y. Behavior of minor elements during copper smelting and converting. Journal of Materials Research and Technology. 2018; 7(3):321–329.

[15] Zhang L, & Ostrovski O. Reduction of lead oxide from smelting slags. Metallurgical and Materials Transactions B. 2002; 33(3):431–439.

[16] Zhao Y, & Stanforth R. Extraction of zinc from zinc ferrites by alkaline leaching. Hydrometallurgy. 2000; 56(3):237–249.

[17] Nassar N T, Brainard J, Gulley A, et al. Critical minerals and materials sustainability. Proceedings of the National Academy of Sciences. 2022; 119(5). https://doi.org/10.1073/pnas.2118933119

[18] Zhang Y, Wang S, & Chen Y. Recovery of tellurium from copper anode slimes and secondary resources: A review. Hydrometallurgy. 2022; 213. https://doi.org/10.1016/j.hydromet.2022.105938

[19] Matkarimov ST. Heat treatment processes of steel-smelting slags in the recovery environment. Metal 2020 - 29th International Conference on Metallurgy and Materials, Conference Proceedings. 2020, 105–112. https://doi.org/10.37904/metal.2020.3439

[20] Li J, Zhao Z, & Wei C. Tellurium supply, demand, and recovery technologies: A review. Journal of Cleaner Production. 2023; 388. https://doi.org/10.1016/j.jclepro.2023.135989

[21] Wang H, Li X, & Deng Z. Distribution behavior of minor elements during copper smelting processes. Journal of Sustainable Metallurgy. 2022; 8(4):1452–1465. https://doi.org/10.1007/s40831-022-00552-9

[22] Chen Q, Zhou T, & Li B. Recovery of valuable metals from copper smelting dusts and sludges: Current status and future perspectives. Minerals Engineering. 2023; 198. https://doi.org/10.1016/j.mineng.2023.108083

[23] Luo Y, Pan J, & Guo Z. Secondary recovery of critical metals from copper metallurgy residues. Resources, Conservation and Recycling. 2024; 201. https://doi.org/10.1016/j.resconrec.2023.107332

[24] Park J, Kim H, & Lee S. Thermodynamic behavior of selenium and tellurium during non-ferrous smelting. Metallurgical and Materials Transactions B. 2022; 53(6):4120–4132. https://doi.org/10.1007/s11663-022-02620-4

[25] Zhao L, Wang Y, & Chen X. Selective enrichment of tellurium in copper smelting by-products. Minerals. 2023; 13(7):944. https://doi.org/10.3390/min13070944

[26] Sun W, Li G, & Deng T. Critical metal recovery from metallurgical secondary resources: Challenges and opportunities. Separation and Purification Technology. 2024; 337. https://doi.org/10.1016/j.seppur.2024.126312

Crossref
DOI: 10.31643/2028/6445.16
Earth and Planetary Sciences: Earth-Surface Processes

Placer formation processes in the cenozoic of Northern and Eastern Kazakhstan

[1]Poezzhaev I.P., [1]Nigmatov D.F., [1]Imangalieva M.Zh., [2]Gavrilenko O.D., [2]Temirbekov N.M., [2*]Mustafina Z.A., [2]Zimanovskaya N.A.

[1]LLP Innova Engineering Service, Almaty, Kazakhstan
[2]National Engineering Academy of the Republic of Kazakhstan (NEA RK), Almaty, Kazakhstan

** Corresponding author email: zinurrka86@gmail.com*

Received: *March 18, 2026*
Peer-reviewed: *April 20, 2026*
Accepted: *June 9, 2026*

ABSTRACT
The article is devoted to the generalization of data on the entire geological and genetic range of placers in Eastern and Northern Kazakhstan: from the weathering of the kaolin profile at the root sources of ore minerals Au, Ni, Co, RM, Ti, Zr, Nb, TR, through polyfacial and alluvial placers of the near demolition of the Zaisan depression to coastal-marine titanium-zirconium placers Northern Kazakhstan and Pavlodar Irtysh region. The sections and patterns of ore localization for gold- and nickel-bearing weathering crusts of the Rudny Altai are considered in more detail. An idea is given of the different conditions of formation of the Paleocene-Miocene ilmenite placers of the Zaisan Depression, depending on the tectonic regime – rifting in the Paleocene-Eocene and orogeny in the Lower Miocene. The dating of titanium-zirconium placers of the Pavlodar Irtysh region has been clarified due to the large-scale removal of silicon from the eluvium of the Kazakh shield. The relationship of the processes of coastal-marine placer formation with regional paleogeographic changes in Central Eurasia, starting with the collision of Hindustan and Eurasia and the Paleocene-Lower Eocene temperature maximum, is shown. The role of the completion of water exchange between the Tethys and Arctic shelf seas in the occurrence of constant westerly winds from the Tarim and Gobi, which played a major role in the formation of placers in the northern border of the Kazakh Shield, is shown.

Keywords: Weathering crust, titanium, rare metals, inshore placer.

Information about authors:

Poezzhaev Igor Pavlovich — *Candidate of Geological and Mineralogical Sciences, Chief Geologist, LLP Innova Engineering Service, 050026, Ayteke Bi 187, Almaty, Kazakhstan. Email: ipoyezzhayev@gmail.com; ORCID ID: https://orcid.org/0000-0002-5689-1063*

Nigmatov Dias Farkhadovich — *Master of Technical Sciences, Project Manager, LLP Innova Engineering Service, 050026, Ayteke Bi 187, Almaty, Kazakhstan. Email: d.nigmatov@ieservice.kz; ORCID ID: https://orcid.org/0009-0007-3215-437X*

Imangalieva Mariyash Zharylkasynovna — *Engineering Geologist, LLP Innova Engineering Service, 050026, Ayteke Bi 187, Almaty, Kazakhstan. Email: mary7468@yandex.ru; ORCID ID: https://orcid.org/0000-0002-5429-0854*

Gavrilenko Oleg Dmitrievich — *Candidate of Geological and Mineralogical Sciences, Leading Researcher, National Engineering Academy of the Republic of Kazakhstan (NEA RK), 050060, 67 Khodzhanova St., Almaty, Kazakhstan. Email: ogavrilenko8@gmail.com*

Temirbekov Nurlan Mukhanovich — *Doctor of physical and mathematical sciences, professor, Al-Farabi KazNU, National Engineering Academy of the Republic of Kazakhstan (NEA RK), 050060, 67 Khodzhanova St., Almaty, Kazakhstan. Email: ntemirbekov314@gmail.com; ORCID ID: https://orcid.org/0000-0001-7542-3778*

Mustafina Zinura Agzamovna — *PhD candidate, D. Serikbayev East Kazakhstan Technical University, Ust-Kamenogorsk, Kazakhstan; Researcher, National Engineering Academy of the Republic of Kazakhstan, 050060, 67 Khodzhanova St., Almaty, Kazakhstan. Email: zinurrka86@gmail.com; ORCID ID: https://orcid.org/0009-0001-6233-2479*

Zimanovskaya Nataliya Aleksandrovna — *PhD, associate professor D. Serikbayev East Kazakhstan Technical University, 070004, Serikbayev str., 19, Ust-Kamenogorsk, Kazakhstan. Email: nzimanovskaya@edu.ektu.kz; ORCID ID: https://orcid.org/0000-0002-9881-690X*

Introduction

This article is devoted to a review of the processes of placer formation that occurred from the Late Cretaceous to the Late Eocene, and their results in the form of placers of various genotypes that were widespread in the eastern part of Northern Kazakhstan and Kazakh part of Altai. In this article, we will consider the features of predominantly eluvial (Au, Ni, реже Ti и-REE) and coastal-marine (Ti, Zr, REE) placers. Special attention is paid to regional climatic factors that contributed

to the enrichment of sands with heavy minerals in the coastal zone of the Middle and Upper Eocene seas, primarily to the formation of a system of coastal currents that played an important role in the formation of placers.

The territory described is located at the junction of two geostructures of the 1st order: the Kazakh Shield, in the zone of its immersion under the Cretaceous-Paleogene rocks of the West Siberian Depression, and the Altai collision-shear system, which also sinks under the loose formations of Western Siberia in a northwesterly direction (Fig. 1). The territory under consideration is characterized by the presence of a full range of placer formations, depending on the degree of connection with indigenous sources. A series of placer formations begins with metalliferous weathering crusts with minerals Au, Nb, Ta, Li, Sn, W, Ti, Zr, Ni, and Co, in some cases with epigenetic infiltration and enrichment with REE phosphates. This is followed by alluvial placers with minerals Au, Sn, W, less often Ti and TR, which are directly related to the indigenous sources. The third representative of the series is coastal-marine and lake placers with a predominance of Ti-Zr-TR in the heavy fraction.

The main sources of placer minerals were regionally developed weathering crusts on a substrate of different ages, or intermediate reservoirs, from Late Cretaceous to Early Eocene alluvial and deltaic facies. And, if the connection between the placer and the source for eluvial formations is obvious, for alluvial formations it is easily detectable, then for coastal formations it is usually not detectable due to the vastness of the drift area drained by river systems

Considering that the purpose of the article is to summarize the data obtained by the authors for many years of research on Northern and Eastern Kazakhstan placers, the results are presented in the form of a consistent description of individual deposits in a single genetic series, from eluvial metal-bearing formations and products of their migration and enrichment, to coastal-marine placers in final demolition basins.

Materials and methods

This article is the result of author's research on off-shore Ti-Zr placers and rare-metal-bearing weathering crusts, using numerous publications on mineralogy and paleogeography of North Kazakhstan, Western Siberia, Tarim and Chinese Altai. For certain areas of placer genesis in Northern and Eastern Kazakhstan, the main method of forecasting placer formations was the method of facies analysis, with the identification of various accumulative shelf forms of Eocene seas, paleoroussels, delta channels, etc. The methods of material analysis are widely used, first of all, the granulometry of ore and non-ore sands, the results of which were published earlier [[1], [2]] and are summarized in this paper (Table 1), in comparison with Ti-Zr placers of other areas and other age levels. Data on the fractional composition of the Druzhba deposit Eocene sands in Pavlodar Irtysh, Obukhovsky and other placers in Northern Kazakhstan, served as a starting point for recognizing the conditions of formation of the main ore bodies as shelf, in contrast to modern coastal-marine placers formed mainly on beaches. Such interpretations determine the possibility of finding new ore bodies south of known deposits zone, as discussed in more detail below.

The Altai Hercynid is characterized by a system of parallel structural zones extending to the northwest (Rudno-Altaiskaya, Irtyshskaya, Kalba-Narymskaya, Charskaya and Zharma-Saurskaya), which differ in geodynamic evolution, geology and metallogeny and are separated by deep faults (fig 2). Large-scale magmatism appeared in Eastern Kazakhstan in the Late Carboniferous-Late Permian period, i.e. at the post-orogenic stage. The orogenic stage was invaded by sub-alkaline gabbro and large granitoid massifs [[3], [4]], including monzonites and biotite-amphibole granites of the multiphase Karaotkel-Preobrazhenskaya intrusion, dated 290 ± 2 million years ago, and which was the source of eluvial and alluvial placers ilmenite known as Karaotkel and Satpayevskoye deposits [[3], [5]].

The period of active orogeny was followed by a stage of relative tectonic quiescence, with relief alignment and rifting, resulting in the formation of the Zaisan Depression, between the Altai Hercynides and the Chingiz-Tarbagatai caledonides [[6], [7]].

In the Late Cretaceous, under conditions of relative tectonic rest, a crust of weathering of a humid profile was formed on the formations of the Paleozoic and Mesozoic.

Figure 1 - Study area location map

The upper age limit of the weathering crust dates back to fairly well-faunistically characterized deposits of the Danish stage in the Semipalatinsk Irtysh region [[8], [9]]. To the west, in the Pavlodar Irtysh region, marine formations of the Middle and Upper Eocene lie on the weathering crust formations with a clear angular discrepancy [[2], [9], [10], [11]].

Eluvial formations are known in depressions inherited by river valleys and in rare remnants of peneplene, usually developed on effusions of medium-basic composition and in crumpling zones formed by ophiolite complexes (Ekibastuz-Shidertinsky and Charsky belts) in the small-scale area of the Kazakh Shield. In the areas of transition of the Kazakh upland to the plains of Western Siberia, weathering crusts are preserved in depressions of the Paleozoic basement and in the bases of scarcely pronounced ledges in the modern relief tracing the stepwise immersion of the Paleozoic basement under the cover of Cenozoic formations of the West Siberian Depression.

In the areas of the Rudny Altai low mountains, eluvial formations are represented by fragments of foam in the interfluves, usually in the altitude range 450-650 m [[12], [13], [14]]. Significant areas of alignment surfaces in the watershed spaces are characterized by incompleteness of the eluvium section due to later erosion, when only zones of disintegration and clay-sand-gravel formations are represented. Less often, there are fairly complete sections, with 20-30 meters or more of eluvium thickness, with an exposure of complete kaolinite, kaolinite-mica and gravel-gravelly types of section. Most often, such situations occur at the junctions of faults of different orders, along zones of crumpling, fracturing, and other superimposed endogenous processes leading to the disintegration of the source. rocks. Known deposits of gold and rare metals are confined to such zones [[7][15], [16], [17], [18]].

The distribution of weathering crusts and their processed products in the form of placers of various genotypes is shown in Fig. 3. The areas of eluvium are taken into account in the case of clay neoplasms typical of hypergenic conditions. If only the gravelly and gravelly part of the profile is preserved in the section, such an area was not shown.

In the humid subtropical climate of the Upper Cretaceous-Lower Eocene, different types of weathering crusts were formed from Paleozoic and older rocks. In the Charsky and Ekibastuz-Shidertinsky belts, Ni-Co weathering crusts of the nontronite type were formed from serpentinized hyperbasites, and gold-bearing kaolinite-mica crusts were formed from greysens and veins and other metasomatites in the Semipalatinsk Irtysh region at the Suzdalskoye, Mukur, Sekisovskoye, Mirage, and others deposits [[7], [15], [19]]. In the Kalba-Narym granite belt, alkaline and subalkaline granites of late collisional stages, pegmatites and aplites, have developed weathering crusts of kaolinite profile with Zr, Sn, W, TR, Be, Ta, Li [[7], [19]].

The Cimmerian cycle was generally destructive. Huge masses of loose material, along with scattered ore matter, were carried down into the Kulundinsk and Zaisan depressions, the West Siberian Lowland and into shallow intermountain depressions, which contributed to the formation of placers of gold, cassiterite, wolframite, monazite and other minerals.

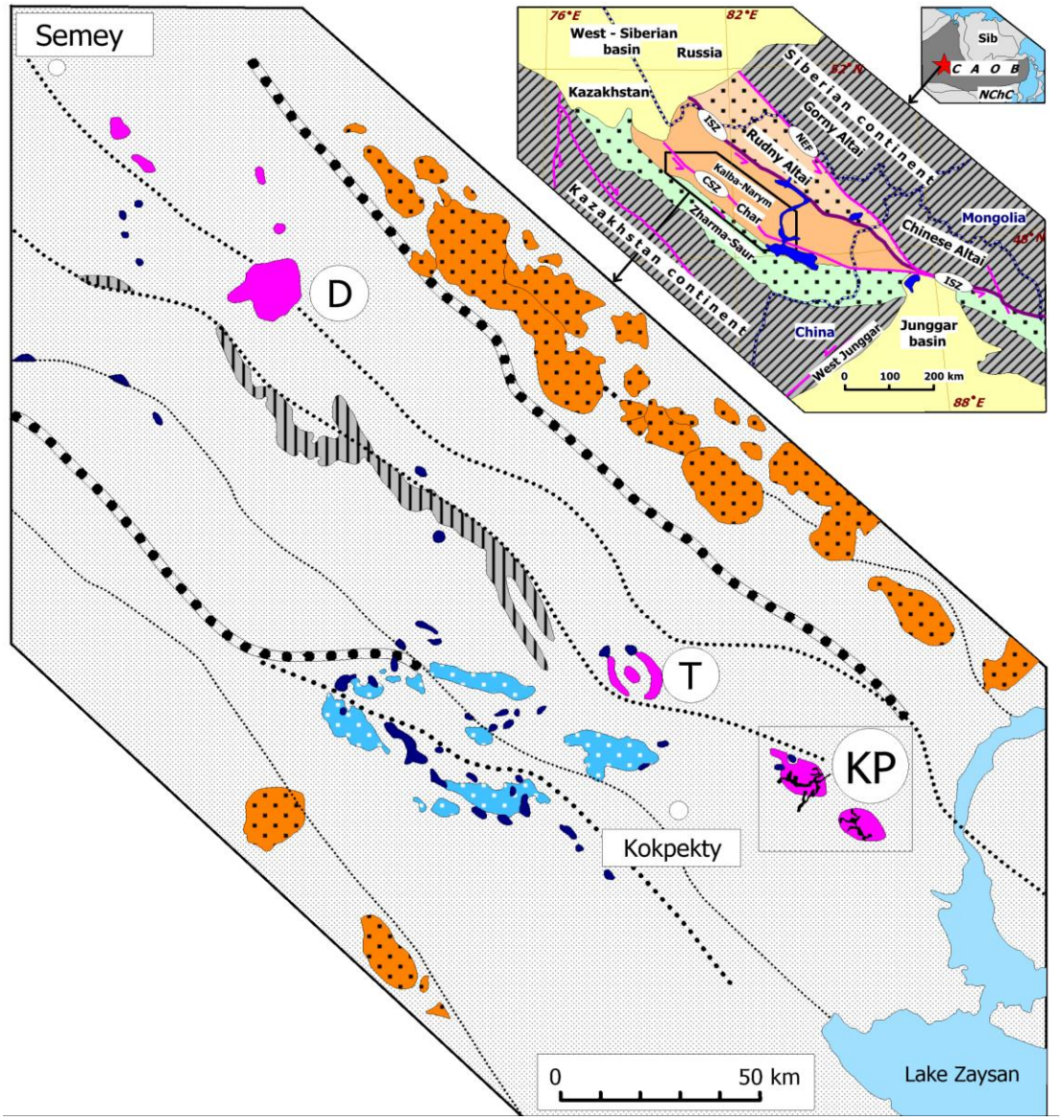

Figure 2 - Scheme of magmatic formations within the Char zone, modified after [3]. 1 - sedimentary structural and compositional complexes, 2 - Char ophiolite belt, 3 - massifs of granitoids P1, undivided, 4 - andesite-basalt series (C2-P1), 5 - massifs of subalkaline gabbro and picrite gabbro - granitoid intrusions: D -, 6 - Delbegetey, T - Tastau, KP - Karaotkel- Preobrazhenka massifs, 7 – faults, 8 - Ti-Zr placers

The eluvial complexes are formed by the initial ore zones of deposits of nickel, gold, titanium and rare metals. The processes of hypergenesis played the role of relative enrichment, due to the decomposition and removal of a significant mass of rock-forming minerals. At the same time, hydration, hydrolysis, and oxidation during hypergenesis at latitudes corresponding to Northern and Eastern Kazakhstan in the Cretaceous-Lower Eocene, led to a kaolinite or kaolinite-hydromica profile of the weathering crust. Laterite profiles of eluvial formations are known in the Turgai trough, and in isolated areas of the northern slope of the Kazakh Shield, where geomorphological conditions of crust formation contributed to deep washing of elevated parts of the foam, with lateritization of products [10]. But these regions are outside the research area.

An example of a gold deposit where residual weathering crusts are considered as a separate enrichment object is the Suzdal deposit (Fig. 4). The indigenous mineralization is confined to mineralized zones of quartz-carbonate-sulfide composition localized in carbonate-terrigenous deposits of the lower-middle Vis. The gold in the bedrock is concentrated in arsenopyrite, pyrite, pyrrhotite, and chalcopyrite.

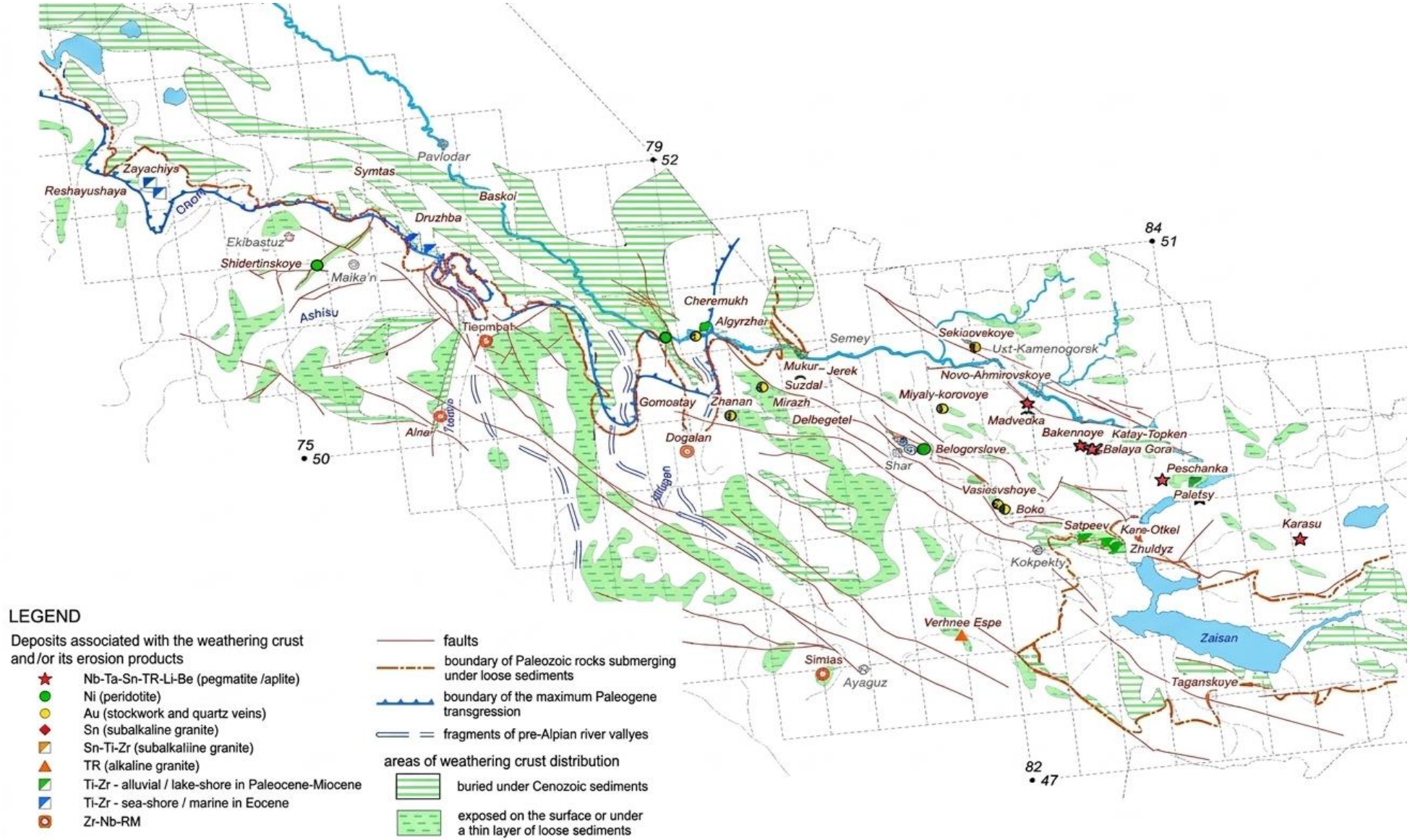

Figure 3 - The spread of ore-bearing weathering crust and their redeposition products. Based on the author's materials, using data from [11], [15], [19], [20], [21], [22].

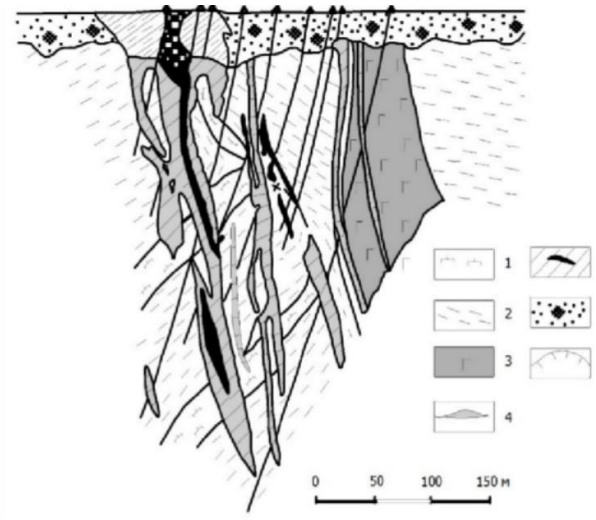

Figure 4 - A section through the ore zones of the Suzdal gold deposit, according to [15].
1, 2 – Lower carboniferous terrigenous-carbonate (1) and siltstone-sandstone (2) formations, 3 – lower-middle carboniferous gabbro-diabases, 4 – upper carboniferous dikes of acid composition, 5 – linear and linear-areal weathering crusts, 6 – cover loams and sands, 7 – carrier border line

The deposit has developed a linear and linear-area type weathering crust with a thickness of up to 80 m and a typical section, according to [[15], [18]]:

1. Variegated eluvium containing up to 50% kaolinite, 10-20% mixed-layer minerals and montmorillonite.
2. Structural eluvium of kaolinite-hydro-micaceous composition, with siliceous-goethite veins.
3. A sandstone in a clay aggregate (up to 40% clay of a hydro-micaceous composition) with a well-preserved structure of the initial rocks. Hydrogetite and hydrohematite accumulations and deposits of manganese hydroxides are characteristic.

A characteristic feature of the hypergenesis of the kaolinite stage in gold deposits, where it is associated with sulfides and has a clear correlation with SiO2 and As, the authors [[18], [23]] consider the formation of high-grade hypergenic gold due to large-scale dissolution of gold-bearing minerals (arsenopyrite, pyrite, etc.), local redistribution along the weathering crust profile, and redeposition under oxidative conditions, which is accompanied by an increase in the size of native gold towards the upper horizons of the weathering crust.

Nickel–bearing weathering crusts are known from the Gornostaevskoye and Belogorskoye deposits in the Charsky hyperbasite belt, and the Shidertinskoye deposits in the Ekibastuz-Shidertinsky belt. An example is the Belogorskoye deposit, where ore nontronites are mined on an industrial scale.

The main ore deposits of the Belogorskoye deposit (Fig. 5) are concentrated in the fractured linear type of the weathering crust of serpentinites, listvenites and metasomatic quartzites. Three separated deposits of nickel ores have been identified and contoured at the deposit. The ores are mostly of the silicate type, but there is also nickel sulfide mineralization of a non-industrial nature, spatially and probably genetically related to larch rocks [24].

A wide development of nontronite eluvium with an average thickness of 8.5 m has been revealed on the deposit area, where the main ore minerals are nontronite, kerolite, psilomelan, asbolan and magnesite, with a Ni content of 0.5-6.8%. Concentrations of Au, Ag, Sb and weight samples of Pt, Pd, Hf were revealed [24] in ochreous eluvial formations, which indicates a potential expansion of the spectrum of ore components of the weathering crust according to the hyperbasites of Eastern Kazakhstan.

Somewhat apart from the above-mentioned deposits of the weathering crust is titanium-rare metal-feldspar deposit Kara-Otkel, which is a two-tiered eluvial (in the lower part) and alluvial-proluvial (in the upper part of section) placer.

Alluvial titanium deposits are known worldwide (Ariadnenskoye deposit in Far East, RF, Appalachian River placers, US, intracontinental placers in India, sites in Mozambique and Madagascar) and, in general, have low industrial value [[1], [22]] due to low concentrations of industrial minerals and small placer sizes. The industrial value of individual objects may increase due to the peculiarities of mineralization (rare-metal minerals, tin or gold as related metals, or ceramic feldspar, like Kara-Otkel).

The Kara-Otkel deposit consists of several placers of three age generations [[5], [13], [25]] with a complex fan-shaped morphology of valleys. Placers of a two-tiered structure, where the lower tier was formed in the Late Cretaceous weathering profile with a predominance of kaolin, the upper tier in the sediments of the North Zaisan Paleogene formation (Fig. 6).

The Karaotkel placer deposit is confined to a horseshoe-shaped depression, open to the southeast, closed on three sides along the periphery by a low shaft, clearly expressed in the modern relief and confined to the contact of the multiphase Karaotkel-Preobrazhenskaya intrusion with sedimentary rocks of the lower Carboniferous Serpukhov stage and the Bukon formation of the Middle Carboniferous.

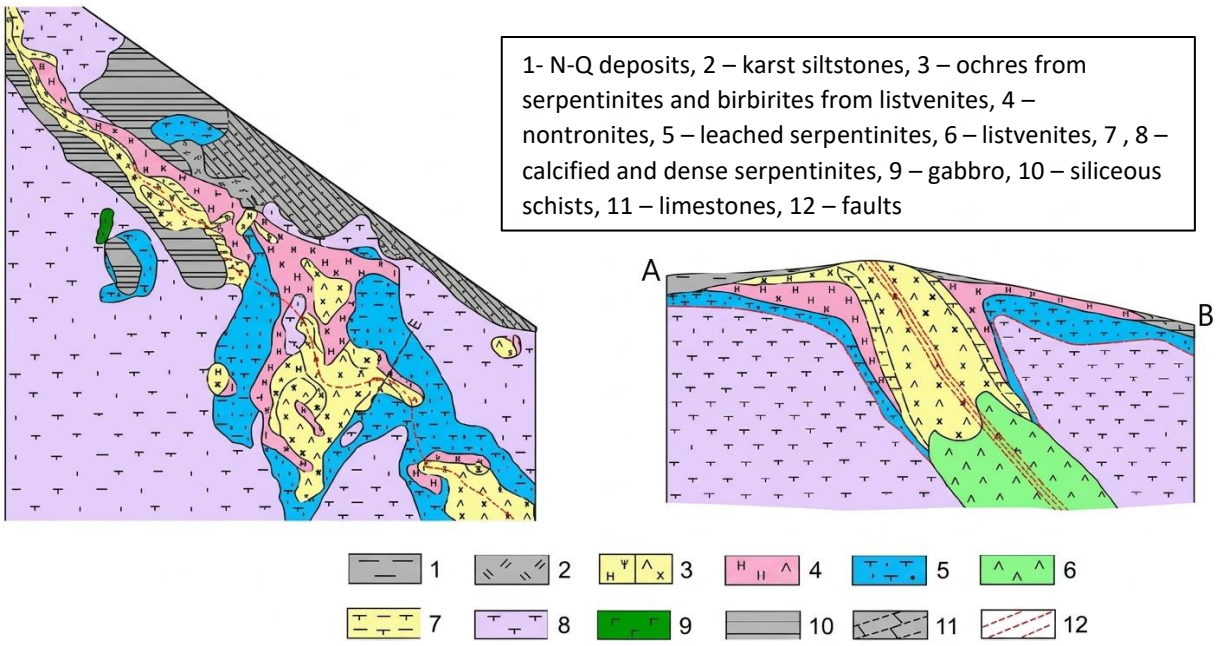

Figure 5 - Geological diagram of the Belogorskoye field and generalized section along the A-B line

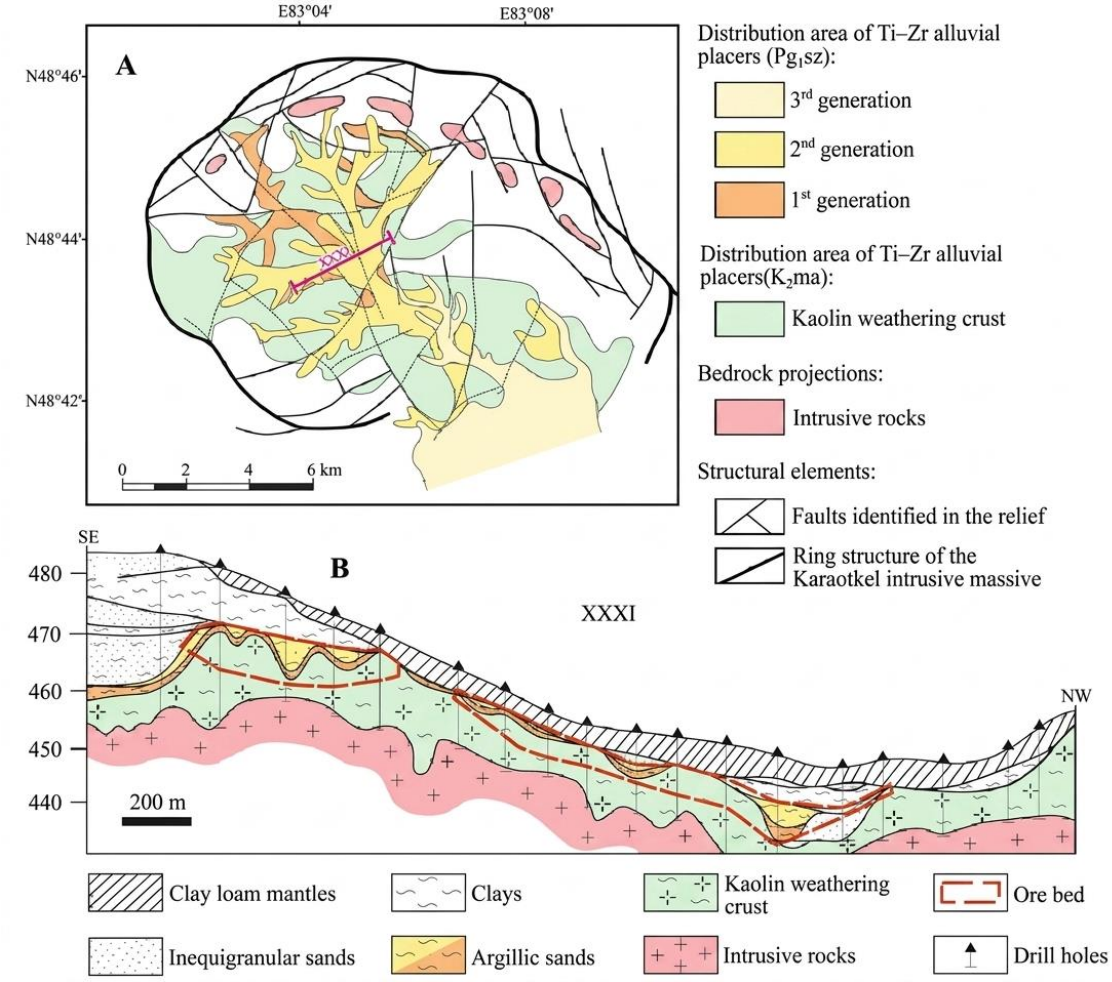

Figure 6 - Geological and structural sketch of the Kara-Otkel deposit, according to [5]

Several main channels with a width of 1-1.6 km and a length of up to 12 km are known in the field. The tributaries are 0.3 to 0.6 km wide and 1-3 km long. The thickness of the productive deposit is up to 14 m, on average it is 4-7 m.

The lower part of the ore section of the deposit is confined to the weathering crust of gabbro, diorites, granosienites and more alkaline differences in acid magmatism. The upper subzone of the kaolin-type weathering crust (thickness from 2-3 to 8 m) is represented by loams with rounded uneven patches of brownish-red calcification. In the lower parts of the subzone, the clay component is 50- 70% hydrous, kaolinite – up to 15%, in the upper parts - the content of hydrous varies between 20- 30%, kaolinite – 40-50%. The composition of loams contains 55% siltstone-clay fractions, and 45% - sandy. Macroscopically, the lower part of the ore section is made of variegated and light sandy clays and loams, the ore component is represented by ilmenite, in the form of uniform inclusions and sharply enriched nests and interlayers, with a content of up to 4-15%.

The upper part of the ore section in the main channel is represented by unevenly granular arkose obliquely layered sands of the North Zaisan formation [5], consisting of quartz (12-48%), potassium feldspar (5-30%), plagioclase - up to 7%, fragments of kaolinized sandstones and siltstones of the lower and Middle Carboniferous (up to 15%), with inclusions ilmenite and zircon.

Ore minerals represented by ilmenite, zircon, leucoxene, and rutile undergo the following changes in composition and appearance:

- ilmenite: average contents in the weathering crust of 1.72%, in the sands of the North Zaisan formation - 2.96%, zircon: in the weathering crust – 0.15%, in the sands – 0.6%, leucoxene – 0.63% in the weathering crust, 0.46% in the sands.

Ilmenite and zircon experience obvious enrichment in alluvial-proluvial conditions, the leucoxene content decreases, apparently due to the low mechanical strength of the grains. In terms of the chemical composition of ilmenite, as the initial ore–bearing formations matured, the bedrock – the crust of chemical weathering - the products of the redeposition of the weathering crust accumulated titanium oxide with the loss of total iron [5]. Judging by the geological position of the deposit (Fig.7), the root sources of the placer ore minerals appear to be quite clear. Studies of the composition of ilmenite and zircon from the Karaotkel-Preobrazhenskaya intrusion, eluvium and redeposition products performed by one of the authors of the article indicate that the chemical composition of ilmenite from the weathering crust and Paleogene sands has a similar composition to the indigenous intrusive rocks of four of the five phases of the Karaotkel-Preobrazhenskaya intrusion, with the lowest discrepancies in the content of basic elements (TiO2 and FeO) between ilmenite from gabbro of the 4th phase, weathering crust and Paleogene sands [13].

The Satpayevskoye titanium deposit, located 18 km north of Kara Otkel, is confined to the zone of transition from an accumulative plain to a low mountain and is localized in alluvial deposits of the Aral formation of the Miocene, lying with a sharp angular discrepancy on the surface of Paleozoic rocks or their weathering crusts.

The mineralization plan has a ribbon-like elongated shape, with maximum thickness in the central part with a gradual decrease towards the flanks. The areas of alluvial mineralization in the plan follow the contours of the faults, which are manifested in the form of crushing zones, intense fracturing and linear weathering crusts (Fig. 8). The beds of Neogene watercourses clearly inherit fragments of discontinuous tectonics. There are 5 placer sites in the field with a similar geological structure, with valleys ranging from 8.7 to 12.6 km long and widths from the first hundred to 900 m. The thickness of the ore sands is from 1 to 14.8 m.

Ilmenite mineralization is concentrated in sandy clays and in poorly sorted medium- and multigrained, often clay sands. The fraction content of -0.05 mm is from 13 to 84%, with a kaolinite-hydrous composition. Sand fractions are represented by quartz (60%), potassium feldspar, and oxides- iron hydroxides. Ilmenite occurs in the form of poorly and moderately rounded grains, flat and tabular precipitates and their fragments. Zircon is found in insignificant concentrations, which determines the specialization of the deposit as purely titanium. A comparison of the ilmenite placers of the Satpayevsky deposit and the Preobrazhenskaya intrusion [[13], [26]], as well as the structural position of the Satpayevsky ore field along the boundary of the intrusion and zones of tectonic disturbances inherited by placer watercourses, indicates that the Preobrazhenskaya intrusion served as a source of placer ore material.

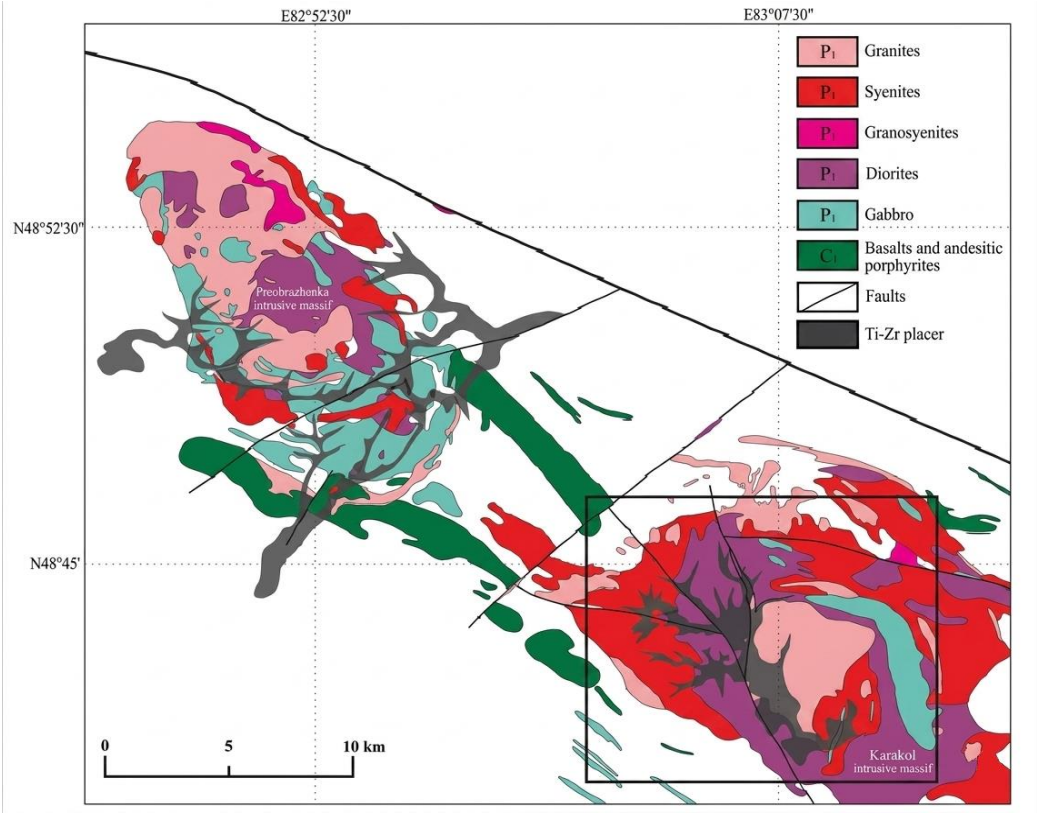

Figure 7 - Geological map of the Karaotkel-Preobrazhenskaya multiphase intrusion, by [[3], [4], [5]]

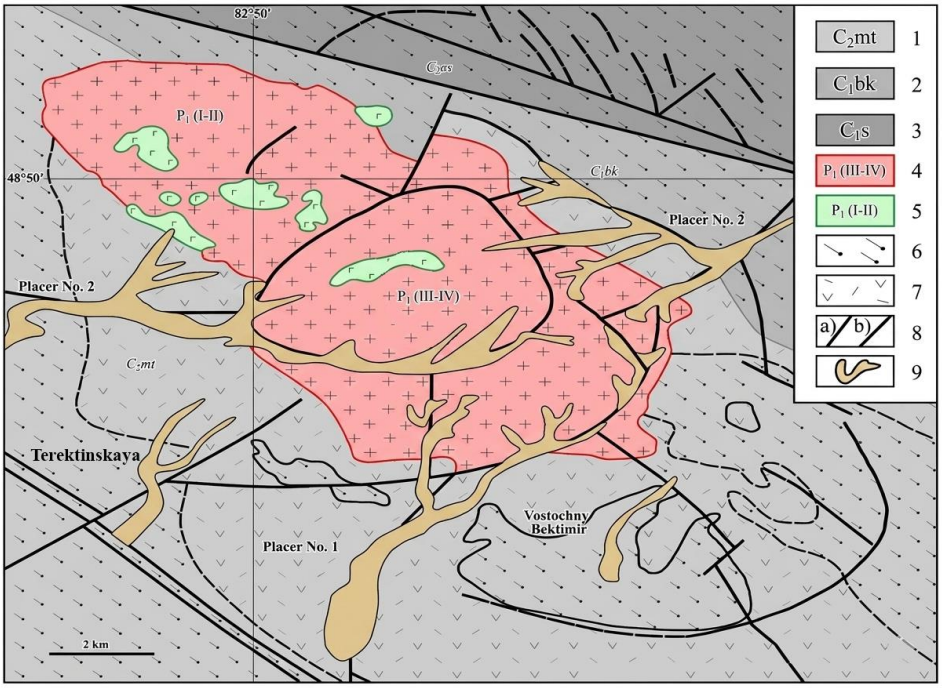

1 - Maityuba suite, volcanomictic sandstone and tuff, 2- Bukon suite, interbedding of clayey, argillaceous aleurolite, 3- visean suite, polymoctic calcareous sandstone, siltstone, shale, covers of lava and tuff, 4- Delbegetei complex, alkaline granite, syenite, granosyenite, 5- Maksut complex, gabbro, gabbro-norite, diorite, monzonite, 6- Siltstone, sandstone, shale, 7- Lava, tuff of andesite porphyrite, 8 – Deep faults, regional established (a) or proposed (b), 9 - Ti-Zr placers

Figure 8 - Geological scheme of the Satpayev Deposit of Ti-Zr placers, according to [26]

In the vertical section, the ore-bearing horizon demonstrates a transgressive cycle of the Early Miocene [[26], [27], [28]], beginning with alluvial-proluvial quartz-feldspar sand with gravel, less often sandstone and sand-gravel material. Above the section there are sandy-clay deposits, which are alluvial according to the conditions of formation. The thickness of productive sediments ranges from 2.4 to 15.6 m, with an average of 7.8 m (Fig. 9).

Industrial ilmenite mineralization is confined to the lower sandy part of the Aral formation, with a mineral content of 20-200 (120 on average) kg/m3. Clays deposited on the sands of the ore- bearing horizon contain only rare inclusions of very fine ilmenite and form the off-balance sheet part of the deposit's reserves [29].

In general, the geological and genetic position of the two described deposits in the north-west of the Zaisan depression differs in the features of ore material mobilization. In both cases, the formation of placers is associated with the redeposition of the crust by chemical weathering. However, in the case of the Kara-Otkel, the Paleocene-Eocene saw the beginning of deflection of the Zaisan Depression with weak tectonic movements of the Altai peneplain, which led to the initial stage of erosion of the Cretaceous weathering crusts [[27], [29]]. The area of the Satpayevsky deposit in the Paleocene-Eocene remained a weakly hilly peneplenized plain.

The beginning of the Alpine orogeny at the end of the Lower Miocene is associated with the involvement of the Satpayevsky deposit area in differentiated tectonic movements. At the same time, a wide lacustrine transgression of Zaisan develops in a northwesterly direction [[13], [25], [27]], forming the lower (balanced) sand-gravel horizon of the deposit's placers. The stabilization of the erosion base, at the maximum of lake transgression in the Middle Miocene, is associated with the formation of sandy-clay formations forming the upper (off-balance) ore horizon.

Placer genesis in the Quaternary period is associated with the erosion of Paleozoic formations, which were poorly affected by the hypergenic effect, since the main part of the eluvium was recycled at the beginning of the Alpine movements. This determined the polymictic composition of the clastic material of quaternary placers of gold and rare metals in the river valleys of the Kalba-Narym zone.

The next region with Cenozoic placer generation is the northern slope of the Kazakh Shield. The formation of the Middle-Upper Eocene coastal-marine titanium-zirconium placers is known here, traced as an intermittent strip of fine-grained sands for about 400 km, from the northern slope of the Kokshetau massif to the Irtysh Valley. There are known some placer deposits, from west to east: Obukhovskaya Group (Ti-Zr-TR), Orlinogorskoye (Ti-Zr-Sn), Kara-Agash, Letovochnoye (Ti-Zr), Zayachye, (Ti-Zr), Druzhba (Zr-Ti).

These deposits have a complex titanium-rare metal specialization, with an ilmenite-to-zircon ratio of 2-3:1. The last of these placers, Druzhba– is characterized by a predominance of zircon in the heavy fraction, with an ilmenite/zircon ratio of 1:2-2.5 [[2], [10], [30]], which reflects the zirconium-rare metal specialization of the indigenous sources – sub-alkaline and alkaline collisional granites south and southeast of the placer (Fig. 10, 11).

All Eocene placer complexes of Northern Kazakhstan and the Pavlodar Irtysh region are united under the name of the Obukhov strata and are characterized by a three-member structure.

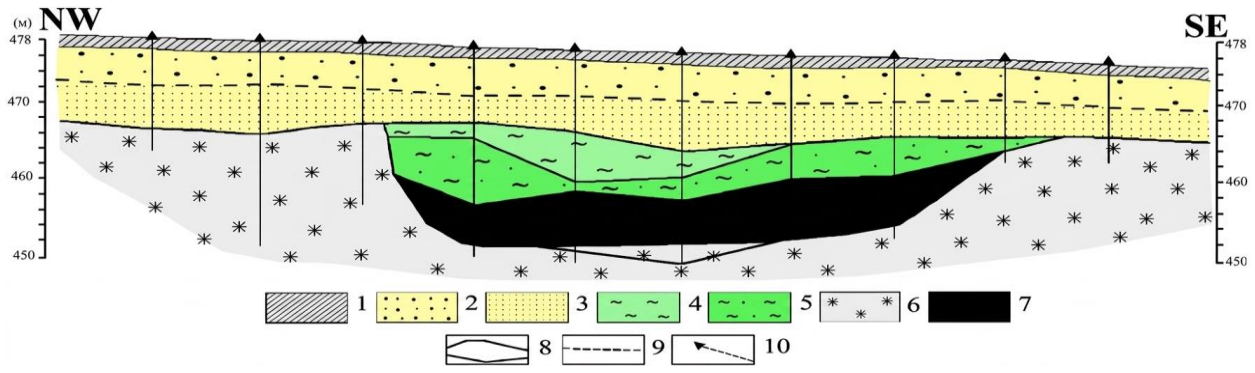

Figure 9 - Geologic al section of Satpayevskoye Deposit along the A-A line, pic. 1 – Quaternary sediments, sandy loams (QIII- IV); 2 – sandy-gravel-pebble deposits, and 3 – sands (QI); 4 – Aral formation, N 1-2, clays; 5 – sandy clays containing subeconomic ores; 6 – weathering crusts from sedimentary rocks of the Bukon formation (C2); 7– economic ore; 8 – contour of the ore-bearing zone; 9 – static groundwater level; 10 – exploration drillholes

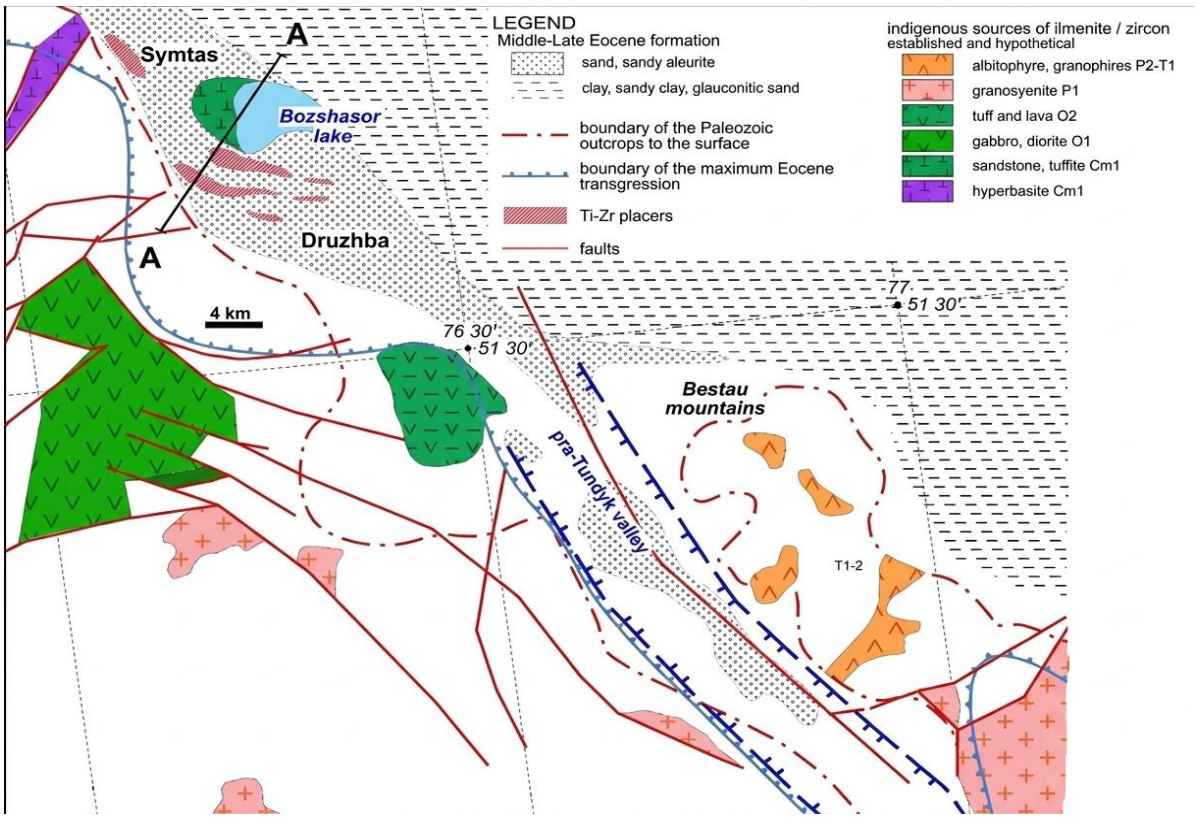

Figure 10 - Geological scheme of the Druzhba placer area showing probable sources of ore material

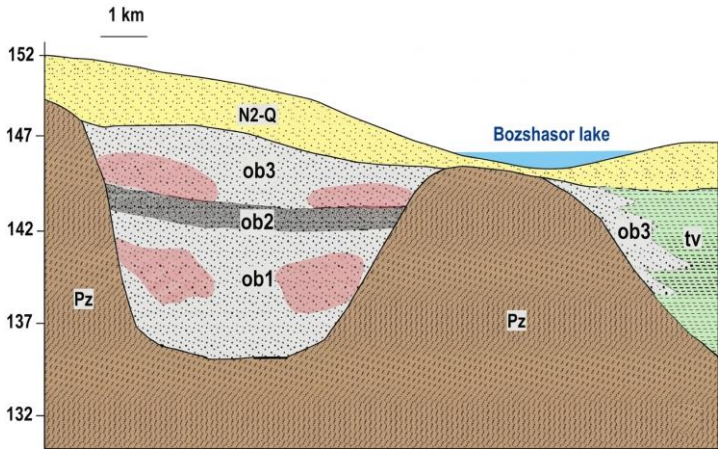

Pz – Paleozoic formations (without separation),
tv – clays of the Lyulinvor formation of the Middle-Upper Eocene,
ob1, ob2, ob3 –sediments of the Obukhov strata of the Middle-Upper Eocene, along the horizons: 1 – lower, 2- middle (false raft), 3- upper,
N2-Q – cover loams and clays.

Figure 11 - Druzhba generalized section along the A-A line on fig. 10

The ob1 horizon with a thickness of 2-15 m lies directly on Paleozoic formations, less often on their weathering crust, consists of fine–grained gray or greenish-gray quartz sands with a characteristic admixture of glauconite and spicules of three-ray sponges, in rare cases shark teeth are found.

These deposits are paralleled with the maximum Paleogene transgression in the Middle Eocene, corresponding to the middle part of Lyulinvor formation of Western Siberia [[2], [13], [31], [32]]. Ob1 ores are represented by ore minerals dispersed in the total thickness, without concentrations in the form of black sludge layers. The texture of the sands is indistinctly layered, often with a slightly pronounced horizontal layering formed by thin (up to 1-2 cm) layers of larger sands. Above, with a sharp transition, there are large sands of the ob2 horizon with a thickness of 1- 2 m, carrying insignificant concentrations of heavy sludge – 1-3 kg/ton.

The ob3 horizon contains the main mineralization on all placers of the northern slope of the Kazakh Shield, lying directly on the clays or coarse sands of the false raft. It is represented by fine- grained yellow, gray-yellow sands with

scattered well-rounded gravel and a content of siltstone particles of up to 25% [2]. The texture of ob3 sands is emphasized by gently undulating and subhorizontal-wavy, undulating layers of slurry. The concentrations of ore minerals are in the range of 5-65 kg/t of the heavy fraction, 90% represented by ore minerals of titanium and zirconium, with a ratio of zircon to ilmenite of 2-2.5:1.

The genetic features of the Druzhba placer [[1], [32]], which distinguish it from other deposits of the northern slope of the Kazakh Shield, consist, as already noted above, in:

1- Zircon ore specialization,

2- the sand-gravel composition of the false raft, in contrast to the clay composition of the other placers,

3- very fine-grained composition of ore-bearing horizons and ore minerals.

The zircon specialization of the placer is explained by the widespread development of subalkaline and alkaline granite intrusions, which are characterized by zirconium-rare metal mineralization in the southern and SE fringes of the placer. Ore minerals were brought by the river (Pra-Tundyk), which drained the areas of development of zircon-bearing granites with a developed weathering crust.

The rough composition of the false raft, unlike the clay composition of other deposits, is explained by the deflection of the Irtysh syneclise inherited from the beginning of the Eocene, which was reflected in the deep depression of the Middle Eocene Sea, with penetration into the valley of the Great Tundyk by 40-50 km. This fact is justified by the presence of well-rounded sands cemented into quartzite-like sandstones with leaf prints of the Middle-Upper Eocene flora [[32], [34], [35], [36]].

The zircon source was Late Carboniferous and Early Permian granosienite massifs drained by the Great Tundyk (Bestau, Kalmak-Kurgan, etc.), the distance to which is 40-100 km. Zircon-malacons of the Early Triassic liparite-dacite Bestau massif (Fig. 10), despite the significant content of zircon in rocks (up to 1.5%) and the relatively short distance to the Druzhba placer, took little part in the formation of zircon concentrations [[2], [32]]. This fact is explained both by the low resistance of the malacons themselves to river and coastal-marine transport, and by the characteristic western direction of longshore transport from river deltas, as the main suppliers of placer material, whereas the Bestau massif is located east of Tundyk delta. The western direction of transfer has been reliably diagnosed in the Obukhov placer group, Zayachye, and Druzhba [[1], [2], [22], [28]].

A characteristic difference between the material composition of Druzhba and other placers of the northern slope of the Kazakh Shield and, especially, Western Siberia, is the extremely small size of ore minerals and the corresponding quartz grains in hydraulic size [[32], [36]]. Ore minerals of titanium-zirconium placers in Western Siberia have the dimension of fine-grained sand up to the upper boundary of coarse siltstone, Druzhba - the dimension of coarse siltstone (55%) and fine siltstone and pelite (45%), Table 1.

Table 1 - The dimension of heavy fraction minerals from Sublittoral and Alluvial Cenozoic placers in Northern Kazakhstan, southern part of West Siberia, Zaisan Depression, and modern placers. According to the [[2], [13], [22], [30], [33]]

Ti-Zr minerals dimension, mm	Modern placers (Aynemer & Konshin, 1982)	Zaisan *Early Miocene*	North Kazakhstan and Pavlodar-Irtysh *Middle-Late Eocene*		South of West Siberia (Rikhvanov et al., 2001) *Early Oligocene*	
		Satpayevskoe	Obukhovskaya	Druzhba	Tuganskaya	Tarskaya
+1.0		0	0	0	0	0
-1.0+0.5	0.3	0	0	0	4.6	1.2
-0.5+0.25	2.5	3.5	0.8	1.0	5.1	1.9
-0.25+0.1	60.1	20.9	5.7	3.3	44	12.2
-0.1+0.05	30.1	60.8	52.9	50.1	29	51
-0.05+0.01	5.2	13.8	23.3	25.1	2.6	16.5
-0.01	1.4	1.0	16.5	20.3	14	14.4

So, modern placers are concentrated in medium-grained beach sands with fine and medium-grained dimensions of ore minerals. Placers of Western Siberia are found in fine–to-medium–grained sands with fine-grained ore minerals, with a significant - up to 30% - content of ilmenite in the siltstone-clay fraction. The Satpayevskoye field of the Zaisan depression is characterized by similar dimensional parameters. The placers of the northern slope of the Kazakh Shield are characterized by fine-grained sand and ore minerals of coarse siltstone (0.1-0.05 mm), fine siltstone and clays (less than 0.05 mm).

Discussion

Sequence of processes of placer deposition and ore bodies facies diagnostic

Genetically, the placers of these provinces differ in their facies type:

- North Kazakhstan placers (Obukhov, Kara-Agash, Zayachya, etc.) are composed of Eocene fine-grained sands. Facies diagnostics [[1], [2]] indicate sublittoral formation conditions with a predominance of longshore accumulative sands in the lower part of the Obukhov sequence and a complex polyfacies sequence with the participation of deposits of longshore ridges, delta channels, bars, and embankments in the upper part of the Obukhov sequence. Clays of the false raft coincide with a short-term retreat of the sea, with the formation of a lagoon or delta in place of the open coast. The texture of the sands is mainly wavy, the series alternate with horizontally layered, formed by thin layers of rich sludge (1-3 cm), coarse sands or siltstones. Such features of the ore-bearing stratum indicate the absence of classical beach deposits, which are characteristic of modern placers of the oceanic coasts of Australia, India, South Africa, etc. [[1], [2], [37], [38]].

- Placers of the Pavlodar Irtysh region was formed in less active conditions of the sublittoral (off-shore placers). Fine-grained sands with fine (silty) ore minerals predominate, having an indistinctly stratified or weakly expressed wavy texture. Such formations are typical for delta islands, lagoon beaches, and, in general, coasts where water exchange with the open sea is difficult [[2], [10], [32], [38]]. The false raft is also considered, as in the placers of Northern Kazakhstan, as a product of short-term regression, but due to the beginning of the activation of the formations of the Chingiz-Tarbagatai zone, which was drained by watercourses supplying placer components to the Druzhby region, and the inherited deflection of the Irtysh syneclise, coarser-grained material was supplied to the coastal zone [2]. The actual sands of the false raft appear to be alluvial or alluvial-deltaic.

- Placers of the Zaisan region are polyfacies formations (deluvial-proluvial-alluvial, with the inclusion of eluvium of the primary source in the lower sections) (Kara-Otkel), or alluvial, which drained the rich primary source of ilmenite directly [[5], [6], [26], [29]]. The formation of the Kara-Otkel placer deposit is associated with the onset of rifting, which manifested itself in the subsidence of the Zaisan Basin and the renewal of the river network on its northwestern margin. In contrast, the topography of the Kara-Otkel-Preobrazhenskaya multiphase intrusive region, like that of the entire Rudny Altai, retains a weakly defined undulating character with a developed weathering crust throughout the Paleocene. The onset of peneplain destruction likely occurred during the Danian-Ypresian interval.

By the end of the Miocene, Altai was a medium-low mountain country, including the northwestern periphery of the Zaisan Depression [[15], [34], [39]]. This process directly influenced the formation of placers of the Satpayevsky deposit. Unlike the Kara-Otkiel basin, the reason is not rifting with the deflection of the Zaisan Depression, but the growth of mountains that began in the Early Miocene and peaked in the Early Quaternary [34]. The sediments of the lower part of the Aral formation correlate with the growth of the mountains. It is obvious that orogeny took place in a pulsating mode – the Lower Miocene stage took place, after which the Altai Mountain were leveled. The next was the lower Quaternary stage of large-scale mountain growth associated with the continuation of the collision of Hindustan and Asia, when there was a significant increase in the Himalayas, Kunlun, Pamir and the general uplift of Tibet [[39], [40], [41]].

The placers age estimation in Northern Kazakhstan and the Pavlodar Irtysh region is ambiguous due to the rare finds or uncertainty of any faunal or floristic remains in the placer strata.

Since the extensive exploration of Ti-Zr placers in northern Kazakhstan and southern Western Siberia (late 1950s – mid-1960s), the formation of coastal-marine placers has been considered to be of Middle Eocene – Lower or Middle Oligocene age, with reference to the coastal facies of the Tavda Formation. Some of this view remains valid today [[11], [22], [30]].

At the same time, in the late 1970s, V. A. Dargevich identified the first spore-pollen assemblages, allowing for a more precise age

determination of the ore-bearing sands, as corresponding to the upper reaches of the Lyulinvor Formation, or the upper part of the Middle Eocene [[42]]. Subsequent work by the authors on assessing the rare-metal potential of Kazakhstan's placers confirmed these views [[2], [10], [32]], leading to a refinement of the geological and genetic position of the placers and, ultimately, to an increase in the prospects of the eastern part of Northern Kazakhstan, with a likely strengthening of the mineral resource base of the Republic of Kazakhstan for titanium, zirconium, and rare earth elements.

The placers framing the Kokshetau Proterozoic massif – Obukhovskaya group, Letovochnaya, Kara-Agash, and others - have been dated fairly reliably. The Obukhov formation (ob1-3) is compared with the middle-upper part of the Lyulinvor formation of Western Siberia, late Lutetian-Bartonian [[10], [22], [36]].

As for the placers of the Pavlodar-Irtysh region, the question of the age dating and the relationship of ore-bearing formations in the Pavlodar Irtysh region and Northern Kazakhstan remains controversial. The following should be noted:

1. The influx of huge masses of dissolved silicic acid and silica gel into the coastal waters of the Lyulinvor basin, with the simultaneous development of radiolariae, sponges, and diatoms in deeper parts of the sea. Well-known sections of the Lyulinvor in the valley of the Olenty River, at the confluence with the lake Auliekol are formed by chemo- and biogenic opoka [36].

2. A site of alluvial formations was identified by one of the authors 40 km south-east of the Druzhba placer, in an ancient river valley inherited by the modern Tundyk River. The section shows a gradual transition from the bottom up, from coarse-grained sands through gradual silicification to almost pure quartzite. The thickness of the sands is 3.5 m, sandstones, from loose to dense, on ferruginous-siliceous cement – 1.2 m, quartzite with a thickness of 0.1-0.15 m lies on top.

The entire complex lies in a local Paleozoic depression, which preserved the sands from erosion during the latestactivation. This section corresponds the formations of the false raft of the Druzhba placer due to the identity of the composition and dimension of the sands [[32], [36]].

3. It seems possible to assume epigenetic silicification of the sands and to draw a parallel with the time of accumulation of siliceous rocks in the middle part of the Lyulinvor formation of Western Siberia, respectively, the Tundyk alluvium is older than the placers of the North Kazakhstan, probably the late Ypres-early-middle Lutetian. In this case, the main ore horizon of the Druzhba placer, correlating with the upper Obukhov strata (ob3), can be dated as Early-Middle Lutet. With this interpretation, Druzhba looks like a slightly older placer, in comparison with the deposits of Northern Kazakhstan: Lutetian age of Druzhba versus late Lutetian - Bartonian age of the placers of Northern Kazakhstan.

The question of why ore formations are shown in lutetian sands is also controversial.

Below, we will consider our hypothesis about the occurrence of a special wind circulation in Central Asia at the end of the Iperlutetia, which contributed to high concentrations of heavy fraction in coastal accumulative forms.

The movement of sediments along the coast is the main factor in the classification of material by hydraulic size and the formation of placers in sublittoral conditions. [[1], [22], [32], [37]. The presence of steady winds is assumed to be a prerequisite for the formation of coastal placers. This does not negate the formation of classical beach placers (black sands), which are most common in modern conditions, but in most cases, examples of Eocene beach formations have not been reliably confirmed.

Since sublittoral placers themselves are indicators of the direction of coastal transport [[1], [32], [33], [38]] and are always located west of river deltas that served as the main suppliers of ore minerals, it would be logical to assume a northwesterly direction of coastal currents and, accordingly, a westerly or northwesterly direction of prevailing winds.

It is assumed [[31], [43]] that the high-pressure zone in Tarim has existed since the end of the Cretaceous period, and the high-pressure zone in the Gobi appeared with the onset of global cooling in the middle to the end of the Eocene. Due to the non-contrasting climate of Central Eurasia, until the middle of the Eocene, there were no conditions for the occurrence of strong winds [[28], [31], [44], [45]]. Starting from Lutet, with a general cooling, there is an expansion of high-pressure zones in Tarim and Gobi (Fig. 12). This is facilitated by the cessation of water exchange between the Tethys and the Arctic, which was carried out through the Turgai Strait and leveled the climatic conditions of Eurasia in the range of 35-55 degrees north latitude. [[35], [43], [46]].

At the same time, the structures of Altai and Dzungaria were shallow hills and hilly plains that did not interfere with the western winds [40]. On the

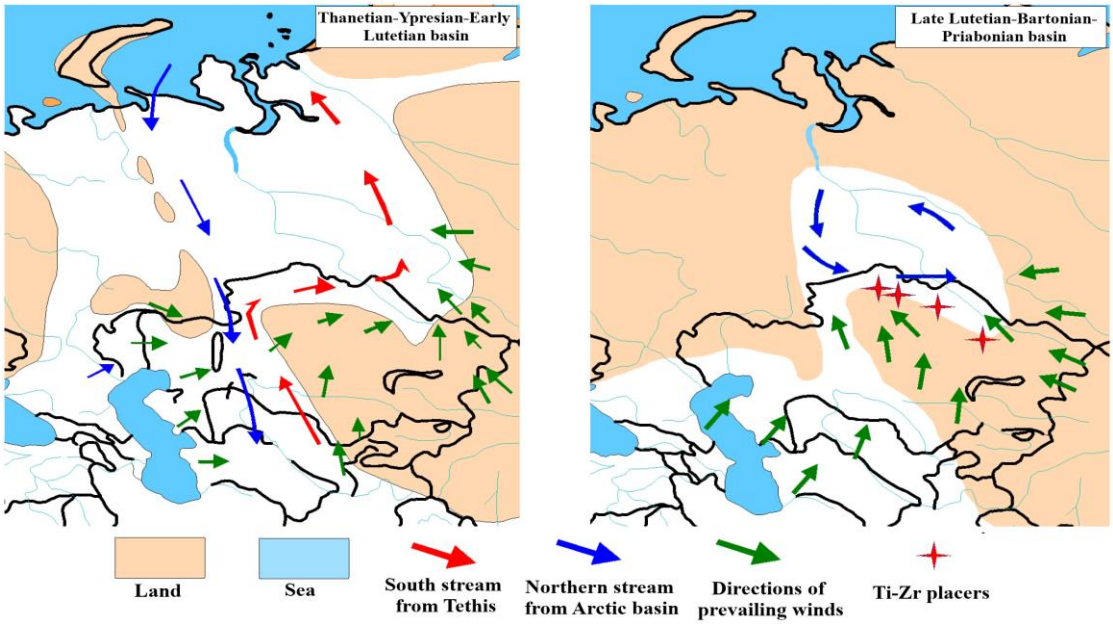

Figure 12 - Palaeogeographical scheme of the Central Eurasia for early Eocene (leftward) and mid- late Eocene (on the right), according to [[35], [46]]. Atmospheric circulation - author's views

other hand, the beginning of large-scale erosion of the weathering crust of the Kazakh shield contributed to the penetration of silica compounds into the adjacent regions of the West Siberian basin, which led to the formation of a Lulinvor formation, siliceous in composition (opoka, siliceous clays, quartz sand). In coastal and subtidal conditions, concentrations of a heavy fraction of industrial scale are formed during Lutet, which was facilitated by:

- deep chemical weathering of the primary sources of placers - formations of different ages forming the Kazakh shield, Dzungaria and Altai;
- the existence of river systems - ways of transferring ore minerals to final runoff basins,
- the emergence of a stable system of atmospheric circulation in the form of westerly and northwesterly winds, which led to constant coastal currents in the West Sobir Sea and, in turn, to the formation of various coastal accumulative forms containing increased concentrations of heavy fraction, which became the basis for the formation of placers. The formation of beach placers proper most likely took place, but the vast majority of them were destroyed by subsequent erosion.

The above reasons for the generation of industrial accumulations of the heavy fraction expand the prospects for the discovery of new titanium-zirconium placers in the Pavlodar Irtysh region. The results of paleogeographic reconstructions given in this article, as well as in other works of the authors [[1], [2], [32], [38]], suggest that new placer ore bodies can be found south of the placer mining belt, which extends more than 400 km along on the northern slope of the Kazakh shield and in the Pavlodar Irtysh region.

We believe that the formation of ore bodies in the main (upper) ore horizon of the Druzhba placer does not correspond to the maximum transgression level of the Ipresian-Lutetian basin, but rather indicates stabilization.

The deepest penetration of the sea into the Kazakhstan shield is shown by blue boundary on (fig 3) and marked by fields of medium- and coarse-grained sands covered by quartzites. It dated by the Eocene on geological maps, more precisely, in our opinion, by the early Lutetian. These formations are widespread from the valley of the Shiderta River in the west to the valley of the Tundyk River in the east, forming separate sand lenses up to 3-10 km long and 1-2 km wide, preserved from subsequent denudation in the depressions of the Paleozoic basement.

In some of these areas, quartzite-like sandstones lie directly on Paleozoic complexes; in others, sands up to 10-12 meters thick lie between sandstones and Paleozoic rocks, and reveal increased contents of heavy minerals up to 10-12 kg per ton [32]. From our point of view, such formations can be the remains of beach placers of Eocene basins [2]. In addition, east of the Bestau Mountains, within the western slope of the Irtysh syneclise, sands correlating with the lower ore layer of the Druzhba placer are possible. These sands are traced by single wells at a depth of 10-50 meters and are covered by Pliocene clays and Quaternary sands. The above considerations significantly expand the

prospects for the discovery of titanium-zirconium placers along the eastern part of the northern slope of the Kazakh Shield.

Conclusion

In preparing this article, the authors sought not only to describe individual objects of the placer series of formations in the series "weathering crust - alluvial placer - coastal-basin placer", but also to show the features of the processes of placer genesis for each of the members of this series, both locally and regionally. In particular, this applies to Ti-Zr placers of the Zaysan depression, Northern Kazakhstan and Pavlodar Irtysh region, the subject of authors's many years research.

The issue of correlation of Northern Kazakhstan single coastal-marine formation with classical marine formations of Western Siberia - the Lyulinvor and Tavda formations of the Eocene is considered. The older age of the Obukhov stratum for the Pavlodar Irtysh region is being substantiated in comparison with the northern slope of the Kazakh shield.

For the first time, we consider the factor of regional atmospheric circulation as one of the decisive for the formation of the Eocene placer-bearing coastal-marine formation. The sequence of tectonic-climatic changes in the Late Cretaceous-Eocene of Central Asia is substantiated as the reason for the subsequent placer formation.

The chain of events originates in the collision of the Indian subcontinent and Eurasia, which was reflected in Northern Kazakhstan by a complex of block movements and the beginning of a large-scale erosion of eluvium formed during the Dat-Eocene climatic optimum. At the same time, there is a shallowing of the Turgai Strait with the cessation of communication between the Arctic and Tethys basins. The result is an increase in climate contrast, with the activation of intracontinental high-pressure zones in Tarim and Gobi, with the emergence of a system of stable westerly and northwesterly winds. We believe that such climatic events led to the generation of constant alongshore currents, which became the main agent of coastal placer generation in the Middle, and to a lesser extent in the Late Eocene. At the same time, classic beach placers could form, but, most likely, were destroyed by subsequent denudation, and their finds are not reliably known.

This interpretation of the tectonic and climatic events of the Early Paleogene explains the location of placers on the northern slope of the Kazakh Shield and in the Pavlodar Irtysh region. Placers are always located to the west of the paleodeltas, which determines the leading role of rivers in the supply of ore material, unlike modern coastal-marine placers, where the main role in the ore material suppling belongs to coastal abrasion.

At the same time, prospects are expanding for the discovery of new ore placer deposits south of the border of Paleogene deposits continuous distribution at Northern Kazakhstan and Pavlodar Irtysh region. We believe that there is reason to expect the discovery of beach and delta placers in the depressions of the Paleozoic basement, made by Eocene sands and armored quartzite-like sandstones.

Conflict of interest: The authors declare that they have no known competing financial interests or personal relationships that could have appeared to influence the work reported in this paper

CRediT author statement: **I.Poezzhaev:** supervision, conceptualization, investigation, writing-original draft; **D.Nigmatov** and **M. Imangalieva:** writing -original draft, writing -review & editing, supervision; **O. Gavrilenko, N. Temirbekov, Z.Mustafina, N. Zimanovskaya:** conceptualization, writing -review & editing.

Acknowledgement: The authors have no acknowledgements to declare.

Funding information: This research was funded by the Committee of Science of the Ministry of Science and Higher Education of the Republic of Kazakhstan (No. BR 27100483 "Development of predictive exploration technologies for identifying ore-prospective areas based on data analysis from the unified subsurface user platform "Minerals.gov.kz" using artificial intelligence and remote sensing methods").

Data availability statement: The data that support the findings of this study are available on request from the corresponding author. The data are not publicly available due to privacy or ethical restrictions.

Cite this article as: Poezzhaev IP, Nigmatov DF, Imangalieva MZh, Gavrilenko OD, Temirbekov NM, Mustafina ZA, Zimanovskaya NA. Placer formation processes in the cenozoic of Northern and Eastern Kazakhstan. Kompleksnoe Ispolzovanie Mineralnogo Syra = Complex Use of Mineral Resources. 2028; 345(2):52-71. https://doi.org/10.31643/2028/6445.16

Солтүстік және Шығыс Қазақстан Кайнозойындағы шашылымдардың түзілу процестері

[1]Поезжаев И.П., [1]Нигматов Д.Ф., [1]Имангалиева М.Ж., [2]Гавриленко О.Д., [2]Темирбеков Н.М., [2]Мустафина З.А., [2]Зимановская Н.А.

[1] Innova Engineering Servic» ЖШС, Алматы, Казахстан
[2] Қазақстан Республикасының Ұлттық инженерлік академиясы (ҚР ҰИА), Алматы, Қазақстан

Мақала келді: *18 наурыз 2026*
Сараптамадан өтті: *20 сәуір 2026*
Қабылданды: *9 маусым 2026*

ТҮЙІНДЕМЕ

Мақала Шығыс және Солтүстік Қазақстан аумағындағы шашылымдардың түзілуінің толық геологиялық-генетикалық қатары бойынша деректерді жалпылауға арналған. Онда Au, Ni, Co, RM, Ti, Zr, Nb, TR кен минералдарының түпкі көздерінде қалыптасқан каолиндік профильдегі үгілу қыртыстарынан бастап, Зайсан ойысындағы жақын тасымалданған полифациялық және аллювиалдық шашылымдар арқылы Солтүстік Қазақстан мен Павлодар Ертіс маңының жағалау-теңіздік ильменит-цирконды шашылымдарына дейінгі түзілу кезеңдері қарастырылады. Рудный Алтайдағы алтын және никельге бай үгілу қыртыстарының қималары мен кендердің локализация заңдылықтары неғұрлым егжей-тегжейлі талданған. Тектоникалық режимнің ерекшеліктеріне байланысты Зайсан ойысындағы палеоцен–миоцен кезеңіндегі ильменит шашылымдарының қалыптасу жағдайлары сипатталады: палеоцен–эоцендегі рифтогенез және төменгі миоцендегі орогенез. Қазақ қалқанының элювийінен кремнийдің ауқымды шайылуына байланысты Павлодар Ертіс маңы шашылымдарының жасы нақтыланған. Жағалау-теңіздік шашылым түзілу процестерінің Орталық Еуразиядағы аймақтық палеогеографиялық өзгерістермен байланысы көрсетілген. Бұл өзгерістер Индостан мен Еуразия плиталарының соқтығысуынан және палеоцен–төменгі эоцен кезеңіндегі температуралық максимумнан бастау алады. Сонымен қатар Тетис пен Арктика шельфтік теңіздері арасындағы су алмасудың тоқтауы нәтижесінде Тарим мен Гоби аймақтарынан батыс бағыттағы тұрақты желдердің қалыптасуы және олардың Қазақ қалқанының солтүстік шетінде сублиторальдық шашылымдардың түзілуіне ықпалы көрсетілген.

Түйін сөздер: Үгілу қыртысы, титан, сирек металдар, жағалау-теңіздік шашылымдар.

Авторлар туралы ақпарат:

Поезжаев Игорь Павлович — *Геология-минералогия ғылымдарының кандидаты, басты геолог, Innova Engineering Service ЖШС, Әйтеке би к-сі 187, Алматы, Қазақстан. Email: ipoyezzhayev@gmail.com; ORCID ID: https://orcid.org/0000-0002-5689-1063*

Нигматов Диас Фархадович — *Техникалық ғылым магистрі, жоба менеджері, Innova Engineering Service ЖШС, Әйтеке би к-сі 187, Алматы, Қазақстан. Email: d.nigmatov@ieservice.kz; ORCID ID: https://orcid.org/0009-0007-3215-437X*

Имангалиева Марияш Жарылкасыновна — *Инженер-геолог, Innova Engineering Service ЖШС, Әйтеке би к-сі 187, Алматы, Қазақстан. Email: mary7468@yandex.ru; ORCID ID: https://orcid.org/0000-0002-5429-0854*

Гавриленко Олег Дмитриевич — *Геология-минералогия ғылымдарының кандидаты, жетекші ғылыми қызметкер, Қазақстан Республикасының Ұлттық инженерлік академиясы (ҚР ҰИА), 050060, Ходжанов көшесі, 67, 6-қабат, Алматы, Қазақстан. Email: ogavrilenko8@gmail.com*

Темирбеков Нурлан Муханович — *Физика-математика ғылымдарының докторы, профессор, Қазақстан Республикасының Ұлттық инженерлік академиясы (ҚР ҰИА),, Әл-Фараби атындағы Қаз¥У, 050060, Ходжанов көшесі, 67, Алматы, Қазақстан. Email: ntemirbekov314@gmail.com; ORCID ID: https://orcid.org/0000-0001-7542-3778*

Мустафина Зинура Агзамовна — *PhD докторанты, Д. Серікбаев атындағы Шығыс Қазақстан техникалық университеті, Өскемен, Қазақстан; ғылыми қызметкер, Қазақстан Республикасының Ұлттық инженерлік академиясы, 050060, Ходжанов көшесі, 67, Алматы, Қазақстан. Email: zinurrka86@gmail.com; ORCID ID: https://orcid.org/0009-0001-6233-2479*

Зимановская Наталья Александровна — *PhD, қауымдастырылған профессор, Д. Серікбаев атындағы Шығыс Қазақстан техникалық университеті, 070004, Серікбаев көшесі, 19, Өскемен, Қазақстан. Email: nzimanovskaya@edu.ektu.kz; ORCID ID: https://orcid.org/0000-0002-9881-690X*

Процессы Россыпеобразования в Кайнозое Северного и Восточного Казахстана

[1]Поезжаев И.П., [1]Нигматов Д.Ф., [1]Имангалиева М.Ж., [2]Гавриленко О.Д., [2]Темирбеков Н.М., [2]Мустафина З.А., [2]Зимановская Н.А.

[1]ТОО Innova Engineering Service, Алматы, Казахстан
[2]Национальная инженерная академия Республики Казахстан (НИА РК), Алматы, Казахстан

Поступила: *18 марта 2026*
Рецензирование: *20 апреля 2026*
Принята в печать: *9 июня 2026*

АННОТАЦИЯ

Статья посвящена обобщению данных по всему геолого-генетическому ряду россыпегенеза в Восточном и Северном Казахстане: от образования кор выветривания каолинового профиля на коренных источниках рудных минералов Au, Ni, Co, RM, Ti, Zr, Nb, TR, через полифациальные и аллювиальные россыпи ближнего сноса Зайсанской впадины до прибрежно-морских ильменит-цирконовых россыпей Северного Казахстана и Павлодарского Прииртышья. Более подробно рассмотрены разрезы и закономерности локализации руд для золота- и никеленосных кор выветривания Рудного Алтая. Дано представление о различных обстановках формирования палеоцен-миоценовых ильменитовых россыпей Зайсанской впадины, в зависимости от тектонического режима – рифтогенеза в палеоцен-эоцене и орогенеза в нижнем миоцене. Уточнена датировка россыпей Павлодарского Прииртышья, в связи с масштабным выносом кремния из элювия Казахского щита. Показана связь процессов прибрежно-морского россыпегенеза с региональными палеогеографическими изменениями в Центральной Евразии, начиная с коллизии Индостана и Евразии и палеоцен-нижнеэоценового температурного максимума. Показана роль завершения водообмена между шельфовыми морями Тетиса и Арктики в возникновении постоянных ветров западного направления из Тарима и Гоби в возникновении сублиторальных россыпей северного обрамления Казахского щита.

Ключевые слова: Кора выветривания, титан, редкие металлы, прибрежные россыпи.

Информация об авторах:

Поезжаев Игорь Павлович — *Кандидат геолого-минералогических наук, главный геолог, ТОО Innova Engineering Service, 050026, Айтеке би 187, Алматы, Казахстан. Email: ipoyezzhayev@gmail.com; ORCID ID: https://orcid.org/0000-0002-5689-1063*

Нигматов Диас Фархадович — *Магистр технических наук, менеджер проекта, ТОО Innova Engineering Service, 050026, Айтеке би 187, Алматы, Казахстан. Email: d.nigmatov@ieservice.kz; ORCID ID: https://orcid.org/0009-0007-3215-437X*

Имангалиева Марияш Жарылкасыновна — *Инженер-геолог, ТОО Innova Engineering Service, 050026, Айтеке би 187, Алматы, Казахстан. Email: mary7468@yandex.ru; ORCID ID: https://orcid.org/0000-0002-5429-0854*

Гавриленко Олег Дмитриевич — *Кандидат геолого-минералогических наук, ведущий научный сотрудник, Национальная инженерная академия Республики Казахстан (НИА РК), 050060, ул. Ходжанова, 67, Алматы, Казахстан. Email: ogavrilenko8@gmail.com*

Темирбеков Нурлан Муханович — *Доктор физико-математических наук., профессор, КазНУ имени Аль-Фараби; Национальная инженерная академия Республики Казахстан (НИА РК), 050060, Ходжанова, 67, Алматы, Казахстан. Email: ntemirbekov314@gmail.com; ORCID ID: https://orcid.org/0000-0001-7542-3778*

Мустафина Зинура Агзамовна — *Аспирант (PhD докторант), Восточно-Казахстанский технический университет имени Д. Серикбаева, Усть-Каменогорск, Казахстан; Научный сотрудник, Национальная инженерная академия Республики Казахстан, 050060, ул. Ходжанова, 67, Алматы, Казахстан. Email: zinurrka86@gmail.com; ORCID ID: https://orcid.org/0009-0001-6233-2479*

Зимановская Наталья Александровна — *PhD, ассоциированный профессор, Восточно-Казахстанский технический университет имени Д. Серикбаева, 070004, ул. Серикбаева, 19, Усть-Каменогорск, Казахстан. Email: nzimanovskaya@edu.ektu.kz; ORCID ID: https://orcid.org/0000-0002-9881-690X*

Reference

[1] Poezzhayev IP, Imangaliyeva MZh. K probleme fatsial'noi diagnostiki drevnikh pribrezhno-basseinovykh otlozhenii [On facies diagnostics of ancient coastal-basin deposits]. In: Geologiya i zakonomernosti razmeshcheniya tverdykh poleznykh iskopaemykh Kazakhstana [Geology and Patterns of Distribution of Solid Minerals in Kazakhstan]. Alma-Ata. 1994, 39–54. (in Russ.).

[2] Poyezzhayev IP. Osobennosti obrazovaniya titan-tsirkonievykh rossypei v eotsene (Severnyi i Zapadnyi Kazakhstan) [Some peculiarities of formation of titan-zirconium placers in the Eocene of North and West Kazakhstan]. Geologiya Kazakhstana = Kazakhstan Geology. 1999; 3:68–84. (in Russ.).

[3] Khromykh SV, Burmakina GN, Tsygankov AA, Kotler PD, Vladimirov AG. Vzaimodeistvie gabbroidnoi i granitoidnoi magm pri formirovanii Preobrazhenskogo intruziva, Vostochnyi Kazakhstan [Interactions between gabbroid and granitoid magmas during formation of the Preobrazhensky intrusion, East Kazakhstan]. Geodinamika i tektonofizika = Geodynamics & Tectonophysics. 2017; 8(2):311–330. (in Russ.). https://doi.org/10.5800/GT-2017-8-2-0243

[4] Suiekpaev ES. Titan-tsirkonievye rossypi i kory vyvetrivaniya Vostochnogo Kazakhstana i ikh prakticheskoe znachenie. [Titanium-zirconium placer deposits and weathering crusts in East Kazakhstan and their practical importance]. PhD Thesis, 6D070600, VKTGU, Ust-Kamenogorsk. 2021. (in Russ.).

[5] Suiekpayev YS, Sapargaliyev YM, Dolgopolova AV, Pirajno F, Seltmann R, Khromykh SV, Bekenova GK, Kotler PD, Kravchenko MM, Azelkhanov AZh. Mineralogy, geochemistry and U-Pb zircon age of the Karaotkel Ti-Zr placer deposit, Eastern Kazakhstan and its genetic link to the Karaotkel-Preobrazhenka intrusion. Ore Geology Reviews. 2021; 131:(104015). https://doi.org/10.1016/j.oregeorev.2021.104015

[6] Sapargaliev EM, Azelkhanov AZh, Kravchenko MM et al. Prospects for practical significance of complex development of low-grade Ti-Zr placers and weathering crusts in Kazakhstan. Nedropolzovanie 2021; 21(1):17–22. https://doi.org/10.15593/2712-8008/2021.1.3

[7] Dyachkov BA, Chernenko ZI, Mataybayeva IE, Frolova OV. Raionirovanie i tipy mestorozhdenii Vostochnogo Kazakhstana [Zoning and types of deposits in East Kazakhstan]. Vestnik KazNTU = Bulletin of KazNTU 2015; 4:101–109. (in Russ.).

[8] Mikhailov BM. Izuchenie i kartirovanie zon gipergeneza [Studies and Mapping of the Hypergene Zones]. Nedra. St. Petersburg, 1995, 189. (in Russ.).

[9] Mysnik AM, Bochkova OI, Kravchenko MM. Vozrastnye rubezhi formirovanija kor vyvetrivanija Vostochnogo Kazahstana. [Age Boundaries of Weathering Crust Formation in Eastern Kazakhstan]. Mater. II Int. Sci.-Tech. Conf. Pt. I. Ust'-Kamenogorsk. 2003; 46-49. (in Russ.).

[10] Dolgopolov VF, Dolgopolova AV, Seltmann R. Ore formations of the platform cover of Kazakhstan. NHM London: CERCAMS Report. 2009, 159.

[11] Patyk-Kara NG. Minerageniya rossypei: tipy rossypnykh provintsii [Minerageny of placers: types of placer provinces]. IGEM RAS Moscow: 2008, 528. (in Russ.).

[12] Dyachkov BA, Mataybayeva IE, Frolova OV, Gavrilenko OD. Tipy redkometal'nykh mestorozhdenii Vostochnogo Kazakhstana i ikh otsenka [Types of rare metal deposits in East Kazakhstan and their appraisal]. Gornyi Zhurnal = Mining Journal. 2017; 8:45–50. (in Russ.). https://doi.org/10.17580/gzh.2017.08.08

[13] Volkova VS, Kul'kova IA, Kuz'mina OV. Palinostratigrafiya paleogenovykh i neogenovykh otlozhenii Barabinsko-Kulundinskoi fatsial'noi zony Zapadnoi Sibiri [Palynostratigraphy of Paleogene and Neogene deposits of the Baraba-Kulunda facies zone of Western Siberia]. Geologiya i geofizika = Geology and Geophysics. 2002; 43(11):1017–1037. (in Russ.).

[14] Dyachkov BA, Bisatova AE, Mizernaya MA, Zimanovskaya NA, Oitesva TA, Amralinova BB, Aitbaeva SS, Kuzmina ON, Orazbekova GB. Specific Features of Geotectonic Development and Ore Potential in Southern Altai (Eastern Kazakhstan). Geology of Ore Deposits. 2021; 63(5):383–408. https://doi.org/10.1134/S1075701521050020

[15] Dyachkov BA, Mochalkina LN, Kuzmina ON. Tipy mestorozhdeniy kor vyvetrivaniya Vostochnogo Kazakhstana [Types of weathering-crust deposits of East Kazakhstan]. Seriya: Geologiya, gornoe delo i metallurgiya. Vestnik VKTGU = Series: Geology, Mining and Metallurgy. Bulletin of EKSTU. 2005; 4:6–13. (in Russ.).

[16] Zhevago IV, Karlova GS. Mezozoiskaya kaolinovaya kora vyvetrivaniya Semipalatinskogo Priirtysh'ya i ee geokhimicheskie osobennosti [Mesozoic kaolin weathering crust in the Semipalatinsk Irtysh region and its geochemical peculiarities]. In: Litologiya i osadochnye poleznye iskopaemye Kazakhstana [Lithology and Sedimentary Mineral Resources of Kazakhstan]. Alma-Ata: Nauka. 1973, 89–95. (in Russ.).

[17] Kalinin YA, Kovalev KR, Naumov EA, Kirillov MV. Gold of the weathering crust of the Suzdal deposit (Kazakhstan). Russian Geology and Geophysics. 2009; 50(3):241–257. https://doi.org/10.1016/j.rgg.2008.09.002

[18] Parilov YuS, Bespaev KhA. Problemy Bakyrchika i vsego Zapadno-Kalbinskogo zolotorudnogo poyasa (Vostochnyi Kazakhstan) [Problems of Bakyrchik and the entire West Kalba gold belt (Eastern Kazakhstan)]. Izvestiya NAN RK. Seriya geologii i tekhnicheskikh nauk = News of the NAS RK. Series of Geology and Technical Sciences. 2015;6(414):46–56. (in Russ.).

[19] Shcherba GN (ed.). Bol'shoi Altai (Geologiya i metallogeniya) [Great Altai (Geology and Metallogeny)]. Almaty: VAC Publishing House. 2000. (in Russ.).

[20] Bespaev KhA, Polyanskiy NV, Ganzhenko GD, et al. Geology and Metallogeny of the Southwestern Altai (within the territories of Kazakhstan and China). Gylym. 1997, 288.

[21] Gorelov SK. Osnovnye etapy vyravnivaniya rel'efa SSSR i ikh sootnoshenie s drevnimi epokhami vyvetrivaniya [Main stages of relief leveling of the USSR and correlation with ancient weathering epochs]. Geomorfologiya = Geomorphology. 1971; 4:9–20. (in Russ.).

[22] Patyk-Kara NG, Benevolsky BI, Bykhovsky LZ, et al. Rossypnye mestorozhdeniya Rossii i drugikh stran SNG [Placer Mineral Deposits of Russia and Other CIS Countries]. Moscow: Nauchnyi Mir, 1997, 479. (in Russ.).

[23] Khromykh SV, Tsygankov AA, Burmakina GN, Kotler PD, Sokolova EN. Mantle–crust interaction in petrogenesis of gabbro–granite association in Preobrazhenka intrusion, Eastern Kazakhstan. Petrology. 2018; 26(4):368–388. https://doi.org/10.1134/S0869591118040045

[24] Amralinova BB. Formirovanie zakonomernostei i otsenka perspektiv nikelevo-kobal'tovykh kor vyvetrivaniya Vostochnogo Kazakhstana [Formation patterns and assessment of the prospects for nickel–cobalt weathering crusts in East Kazakhstan]. PhD Dissertation, VKGTU, Ust-Kamenogorsk. (in Russ.). https://elib.kstu.kz/en/lib/document/AVTOR/D5AFDBAA-2387-4F00-8A74-9E6BB8A698CD/ (Accessed 24 May 2026)

[25] Suiekpayev Ye, Sapargaliyev Ye, Dolgopolova A, Seltmann R, Raspopov A, Bekenova G. Prognoznaya otsenka Ti–Zr rossypnykh mestorozhdenii v mezozoiskikh i kainozoiskikh otlozheniyakh severo-zapadnoi okrainy Zaisanskogo basseina, Vostochnyi Kazakhstan [Predictive estimate of Ti–Zr placer deposits in Mesozoic and Cenozoic sediments in the northwestern margins of the Zaisan Basin, East Kazakhstan]. News of the Academy of Sciences of the Republic of Kazakhstan. 2019; 2(434):6–14. (in Russ.). https://doi.org/10.32014/2019.2518-170X.32

[26] Suiekpayev Ye, Sapargaliyev Ye, Bekenova G, Kravchenko M, Dolgopolova A, Seltmann R. Mineralogicheskie i geokhimicheskie osobennosti Satpaevskogo Ti–Zr rossypnogo mestorozhdeniya, Vostochnyi Kazakhstan [Mineralogical and geochemical features of the Satpayev Ti–Zr placer deposit, East Kazakhstan]. News of the Academy of Sciences of the Republic of Kazakhstan. 2019; 1(433):6–22. (in Russ.). https://doi.org/10.32014/2019.2518-170X.1

[27] Trikhunkov YaI, Tesakov AS, Bachmanova DM, Syromyatnikov EV, Latyshev AV, Bulanov SA, Azelkhanov AZh, Suyekpaev ES. Stratigrafiya kainozoiskikh otlozhenii i istoriya poslednego etapa geologicheskogo razvitiya Zaisanskoi vpadiny (Vostochnyi Kazakhstan) [Stratigraphy of Cenozoic deposits and the history of the latest stage of geological development of the Zaisan Depression (Eastern Kazakhstan)] Stratigraphy and Geological Correlation. 2023; 6:92–112. (in Russ.). https://doi.org/10.31857/S0869592X23060121

[28] Patyk-Kara NG, Kolodochko VI. Paleostrukturnye usloviya formirovaniya titan–tsirkonievykh rossypei Obukhovskoi gruppy, Severnnyi Kazakhstan [Palaeostructural conditions for the formation of titanium–zirconium placers of the Obukhov Group, North Kazakhstan]. Geologiya rudnykh mestorozhdenii = Geology of Ore Deposits. 1994; 1(36):57–67. (in Russ.).

[29] Kravchenko MM, Dyachkov BA, Suiekpaev ES, et al. Perspektivy ukrepleniya i razvitiya titanovoi syr'evoi bazy Vostochnogo Kazakhstana [Prospects for strengthening and developing the titanium raw-material base in East Kazakhstan]. Vestnik Permskogo Universiteta. Geologiya = Perm University Herald. Geology. 2016; 1(30):78–86. (in Russ.).

[30] Rikhvanov LP, Kropotkin SS, Babenko SA, Solovyev AI, Sovetov VM, Usova TY, Polyakova MA. Tsirkon-il'menitovye rossypnye mestorozhdeniya kak potentsial'nyi istochnik razvitiya Zapadno-Sibirskogo regiona [Zircon–ilmenite placer deposits as a potential source for the development of the West Siberian region]. Kemerovo. 2001, 214. (in Russ.).

[31] Oreshkina TV. Evidence of Late Paleocene–Early Eocene hyperthermal events in biosiliceous sediments of Eastern Siberia and adjacent areas. Austrian Journal of Earth Sciences. 2012; 105(1):145–153. https://www.ajes.at/images/AJES/archive /Band%20105_1/oreshkina_ajes_v105_1.pdf (Accessed 24 May 2026).

[32] Poezzhayev IP. Tsirkonienosnye formatsii platformennogo chekhla Kazakhstana: genezis, zakonomernosti razmeshcheniya, perspektivy [Zirconium-bearing formations of the platform cover of Kazakhstan: genesis, distribution patterns, prospects]. PhD Thesis, Reg. 0499RK01255. Almaty. 1999. (in Russ.).

[33] Aynemer AI, Konshin GI. Rossypnye mestorozhdeniya shel'fovykh zon Mirovogo okeana [Placer deposits in the shelf zones of the World Ocean]. Leningrad: Nedra. 1982, 263. (in Russ.).

[34] Tsekhovsky YuG. Litogenez kontinental'noi pestrotsvetno-kremnisto-getit-kaolinovoi formatsii (Vostochnyi Kazakhstan) [Lithogenesis of the continental variegated siliceous-goethite-kaolin formation (East Kazakhstan)]. Trudy. 242. Moscow: Nauka. 1973. (in Russ.).

[35] Akhmetiyev MA. Problems of Paleogene stratigraphy and paleogeography in the middle latitudes of Eurasia. Russian Geology and Geophysics. 2011; 52(10):1075–1091. https://doi.org/10.1016/j.rgg.2011.09.004

[36] Abdulkabirova MA, Abdulin AA (eds.). Geologiya Severnogo Kazakhstana (Stratigrafiya) [Geology of Northern Kazakhstan (Stratigraphy)]. Almaty: Nauka. 1987, 224. (in Russ.).

[37] Lalomov AV. Lokal'nye faktory formirovaniya pribrezhno-morskikh redkometall'no-titanovykh rossypei [Local factors in the formation of coastal-marine rare-metal titanium placers]. Litologiya i poleznye iskopaemye = Lithology and Mineral Resources. 2023; 4:407–420. (in Russ.). https://doi.org/10.31857/S0024497X23700143

[38] Lalomov AV, Tabolich SE. Mekhanizmy formirovaniya kontsentratsii titan-tsirkonievykh mineralov pribrezhno-morskikh rossypei sublitoral'noi zony [Mechanisms of formation of titanium-zirconium mineral concentrations in coastal-marine placers of the sublittoral zone]. Uchenye zapiski Kazanskogo universiteta. Seriya: Estestvennye nauki = Scientific Notes of Kazan University. Series: Natural Sciences. 2011; 153(4):232–242. (in Russ.). https://kpfu.ru/portal/docs/F_1169592903/153_4_est_15.pdf (Accessed 24 May 2026).

[39] Caves JK, Bayshashov BU, Zhamagara AI, Ritch AJ, Ibarra DE, Sjostrom DJ, Mix HT, Winnick MJ, Chamberlain CP. Late Miocene uplift of the Tian Shan and Altai and reorganization of Central Asia climate. GSA Today. 2017; 27(2):19–26. https://www.geosociety.org/gsatoday/archive/27/2/article/GSATG305A.1.htm (Accessed 24 May 2026).

[40] Huangfu P, Fan W, Li ZH, Zhang H, Zhao J, Shi Y. Linkage between the India–Asia collision and far-field reactivation of the Altai Mountains. Palaeogeography, Palaeoclimatology, Palaeoecology. 2023; 616. https://doi.org/10.1016/j.palaeo.2023.111478

[41] De Grave J, Buslov MM, Van den Haute P. Distant effects of India–Eurasia convergence and Mesozoic intracontinental deformation in Central Asia: Constraints from apatite fission-track thermochronology. Journal of Asian Earth Sciences. 2007; 29(2–3):188–204. https://doi.org/10.1016/j.jseaes.2006.03.001

[42] Dargevich VA. K voprosu o vozraste maksimal'noi transgressii paleogena v yuzhnoi chasti Zapadno-Sibirskoi plity [On the age of the maximum Paleogene transgression in the southern part of the West Siberian Plate]. In: Paleogen i neogen Sibiri [Paleogene and Neogene of Siberia]. Novosibirsk: Nauka. 1978, 82–85. (in Russ.).

[43] Zhang R, Jiang D, Li X, Shi J, Shen T. East Asian climate evolution during the Cenozoic: A review from the modeling perspective. Fundamental Research. 2025; 5(6):2684–2692. https://doi.org/10.1016/j.fmre.2023.09.011

[44] Brunet M-F, Sobel ER, McCann T. Geological evolution of Central Asian Basins and the western Tien Shan Range. Geological Society, London, Special Publications. 2017; 427:1–17. https://doi.org/10.1144/SP427.17

[45] Cramwinckel MJ, van der Ploeg R, van Helmond NAGM, Waarlo N, et al. Deoxygenation and organic carbon sequestration in the Tethyan realm associated with the Middle Eocene Climatic Optimum. GSA Bulletin. 2023; 135(5–6):1280–1296. https://doi.org/10.1130/B36280.1

[46] Akhmetiev MA, Zaporozhets NI, Benyamovskiy VN, Aleksandrova GN, Iakovleva AI, Oreshkina TV. The Paleogene history of the Western Siberian seaway – a connection of the Peri-Tethys to the Arctic Ocean. Austrian Journal of Earth Sciences. 2012;105(1):50–67. https://www.ajes.at/images/AJES/archive/Band%20105_1/akhmetiev_et_al_ajes_v105_1.pdf (Accessed 24 May 2026).

Crossref
DOI: 10.31643/2028/6445.17
Earth and Planetary Sciences: Earth-Surface Processes

Identification of Methane-Bearing Coal Seams in Borehole Sections of the Karaganda Basin Using Geophysical Logging Data

[1]Portnov V.S., [1]Golik A.V., [1]Duganova G.K., [1]Khuangan N., [1]Kenetayeva A.A., [1*]Rabatuly M., [2]Peng Hou

[1]Abylkas Saginov Karaganda Technical University, Karaganda, Kazakhstan
[2] Wuhan University Wuhan, China

** Corresponding author email: mukhammedrakhym@mail.ru*

Received: *March 17, 2026*
Peer-reviewed: *March 19, 2026*
Accepted: *June 9, 2026*

ABSTRACT

The Karaganda coal basin is one of the most gas-bearing in the world. Its feature is that there are no large accumulations of free gas in it, while the natural gas content reaches up to 25-30 m³/t; this is confirmed by a large volume of gas sampling, gas logging data, and gas survey data in operating mines. Methane from coal seams enters the atmosphere through natural migration through overlying rocks, as well as at the places where seams outcrop under overburden and through the shafts of closed mines. During degassing of coal seams in the Karaganda basin during the opening of seams by mine workings, including during open-pit mining, seam outcrops to the surface, degassing of the worked-out space of closed mines, part of the extracted methane is used at the mines for obtaining thermal and electrical energy, and the larger part enters the atmosphere during degassing of coal seams. It is known that methane entering the atmosphere retains the Earth's heat significantly higher, by 25-30 times, than carbon dioxide. The extraction of methane from unloaded coal seams for its industrial use in obtaining thermal and electrical energy is an important task in the development of technologies for the integrated development of coal-methane deposits, as well as for reducing the environmental load on the regions where they are located. The purpose of the research is the identification in the section of gas-bearing coal seams for assessing the potential of methane extraction from unloaded seams for its industrial use and reducing emissions into the atmosphere. Methods. A complex of geophysical methods for studying exploration wells to investigate the physico-mechanical and filtration-capacity properties of coal seams and host rocks, sampling and analysis of coal seam samples in mine workings. Results. Patterns of changes in the complex of physical properties of coal seams determining their gas content have been established, geological justification for these changes and changes in the physico-mechanical properties of host rocks has been given. Application. The gas-bearing coal seams identified in the section can be used in planning methane extraction from all gas-bearing seams of the geological section, including coal seams being developed by mines, and the patterns of changes in physico-mechanical and filtration-capacity properties of coal seams prepared for development or being developed can be used in geomechanical calculations. The factual materials for conducting the research were obtained from the results of laboratory and geophysical studies of exploration wells, materials from geological and production reports.

Keywords: coal suites, metamorphism physico-mechanical characteristics of coal and host rocks, gas content, forms of methane occurrence in coals, ecology, geomechanics.

Information about authors:

Portnov Vasily Sergeevich — *Doctor of Technical Sciences, Professor of Abylkas Saginov Karaganda Technical University, 100027, Ave. Nursultan Nazarbayev, 56, Karaganda, Kazakhstan. E-mail: vs_portnov@mail.ru; ORCID ID: https://orcid.org/0000-0002-4940-3156*

Golik Andrey Vasilyevich — *PhD student of Abylkas Saginov Karaganda Technical University, 100027, Ave. Nursultan Nazarbayev, 56, Karaganda, Kazakhstan. E-mail: andrey.golik@i-geo.kz; ORCID ID: https://orcid.org/ 0009-0008-5179-0002*

Duganova Gulden Kanatovna — *PhD student Abylkas Saginov Karaganda Technical University, 100027, Ave. Nursultan Nazarbayev, 56, Karaganda, Kazakhstan. E-mail: dgulden_k@mail.ru; ORCID ID: https://orcid.org/0009-0008-0368-4619*

Khuangan Nurbol — *Ph.D., Associate Professor, Department of Development of Mineral Deposits Abylkas Saginov Karaganda Technical University, 100027, Ave. Nursultan Nazarbayev, 56, Karaganda, Kazakhstan. E-mail: n.khuangan@ktu.edu.kz; ORCID ID: https://orcid.org/0000-0001-9609-6649*

Kenetayeva Aigul Akanovna — *Master of Technical Sciences, specialty Geology and Exploration of Mineral deposits, lecturer, Abylkas Saginov Karaganda Technical University, 56 Nursultan Nazarbayev Ave., 100027, Karaganda, Kazakhstan. E-mail: aigul_tate2@bk.ru; ORCID ID: https:// orcid.org/0000-0001- 7943-3279*

Rabatuly Mukhammedrakhym — *Ph.D., Associate Professor, Department of Development of Mineral Deposits of Abylkas Saginov Karaganda Technical University, 100027, Ave. Nursultan Nazarbayev, 56, Karaganda, Kazakhstan. E-mail: mukhammedrakhym@mail.ru; ORCID ID: https://orcid.org/0000-0002-7558-128X*

Peng Hou — *Doctor of Engineering, Professor, Wuhan University, Wuchang District, Wuhan, Hubei, 430072, No. 299 Bayi Road, Wuchang District, China. E-mail: penghou@whu.edu.cn; ORCID ID: https://orcid.org/0000-0002-2621-8943*

Indroduction

The gas content of coal seams in the Karaganda Basin is studied to ensure safe working conditions during mining operations in underground mines. As the depth of mining increases, both the gas content and gas pressure in coal seams rise, and their physico-mechanical as well as filtration-capacity characteristics undergo significant changes.

These factors govern the mechanism of coal and gas outbursts, which encompass a complex sequence of physical processes: destruction of the coal mass, gas desorption, diffusion and seepage of gas, and transport of pulverized coal within the gas flow [[1], [2], [3]].

Investigations of gas-dynamic phenomena in the basin's mines indicate the synergistic influence of several key factors, including: in-situ stress and gas pressure within the coal seam, physico-mechanical properties of the coal, its micro- and macrostructure, and the surface energy of coal particles. The latter increases markedly with the degree of tectonic pulverization of coal in zones of tectonic dislocations and abrupt changes in seam hypsometry [[4], [5], [6]].

Analysis of the factors controlling the manifestation of gas-dynamic events — and their implications for safe mining practices — highlights the necessity of comprehensive studies of the physical properties of coal seams and host rocks, not only under natural (undisturbed) conditions but also in areas already prepared for extraction [[7], [8]].

The development of fracture networks during pre-mine degasification, as well as fracturing induced by mining-induced destressing of the coal seam (including that created by boreholes drilled from development workings and in-seam boreholes), substantially enhances the effectiveness of coal seam degasification operations. All these processes lead to alterations in the physico-mechanical characteristics of the coal-rock mass, which must be duly accounted for in geomechanical calculations [[9], [10]].

In recent years, there has been growing global interest in the exploration and development of unconventional hydrocarbon resources [[11], [12]]. A promising direction for the development of Kazakhstan’s fuel and energy sector is the integrated development of coal-methane deposits, among which the Karaganda Basin holds a prominent position. One of the key components of this raw material is coalbed methane — an environmentally friendly and highly efficient energy and chemical feedstock [[13], [14]].

Methane extracted during coal seam degasification is utilized for industrial purposes. This reduces its emissions into the atmosphere, thereby mitigating its contribution to global warming, climate change, and adverse effects on human health [[15], [16]]. It is used for the generation of thermal and electrical energy, and its utilization promotes the intensive socio-economic development of the coal-methane deposit region.

Experimental part

The object of the study is the Karaganda Coal Basin, which includes the following districts: Karaganda, Sherubai-Nurinsky, Tenteksky, and Verkhne-Sokursky. The most productive and workable coal-bearing suites are the Karaganda and Dolinskaya formations.

Coal samples for laboratory investigations were collected in accordance with GOST R ISO 18283-2010 “Hard coal and coke. Manual sampling”.

It is well known that the gas content of coals is determined by the degree of metamorphism. In this regard, the studied stages of metamorphism were determined based on vitrinite reflectance (R^o), volatile matter yield (A^{daf}), carbon content in the coals, heat of combustion, and caking properties. These analyses were performed in the specialized laboratory of LLP "Scientific Research Center " Ugol’ l" in Karaganda.

It was established that the coals of the basin belong predominantly to the III and IV stages of metamorphism, with vitrinite reflectance (R^o) ranging from 0.52% to 2.8% [17].

Studies on the forms of methane occurrence in coals were carried out using the DMT method (Germany) at the “Spetsmontazhdegazatsiya” department of the Mining Department of JSC “Qarmet”. It was found that a dynamic equilibrium exists in the coal matter between adsorbed methane, absorbed methane, and methane in the free phase. The measurements were performed on 250 coal samples taken from boreholes in seam D6 at the “Kazakhstanskaya” and “Lenina” mines in underground workings. During the studies, the ash content, volatile matter yield, and moisture content of the coals were also determined.

Geophysical logging in open exploration boreholes (GLB) was performed by the companies Weatherford and IGeo.

To investigate the density and volumetric clay content of coal seams within the Tentek (T) and Dolinsk (D) formations at the Kazakhstanskaya mine (boreholes Nos. 1/2, 2, and 3) and the Lenin mine

(boreholes Nos. 1–4), studies were conducted under conditions of the natural stress–strain state. The research was carried out using an integrated suite of well-logging (geophysical logging) methods, including gamma–gamma density logging (GGDL), gamma-ray logging (GR), and broadband acoustic logging (BAL), employing calibrated borehole instruments.

Coal seams in the borehole sections were identified using gamma–gamma density logging (GGDL), characterized by lower density relative to the surrounding host rocks, as well as by borehole-derived clay content values from gamma-ray logging (GR). Additional criteria included elevated electrical resistivity obtained from the apparent resistivity method (AR). Gas-bearing intervals were delineated using the neutron–neutron logging method based on thermal neutrons.

Drilling regimes for 128 mm diameter boreholes adhered to the recommendations specified for the Karaganda Basin in references [[18], [19]].

Results and Discussion

For the Karaganda coal basin, a general relationship has been established between the gas content of coal seams and the degree of coal metamorphism, as well as changes in their physical properties [[20], [21], [22]], including their association with tectonically weakened coals [[23], [24], [25]]. Table 1 presents the systematic relationship between the thickness of coal-bearing formations in the Karaganda basin and the stages of metamorphism.

Table 2 presents the balance of volatile products generated during metamorphism of organic matter. The intensity of volatile release varies across different stages. Carbon dioxide emissions increase during the transition from peat to lignite, whereas hydrogen sulfide is released in minimal amounts. With increasing degree of metamorphism—particularly during the transition from bituminous coal to anthracite and from anthracite to graphite—the maximum amount of methane is generated [[26], [27], [28]].

The results presented in Tables 1 and 2 confirm that variations in the gas content of coal seams within the basin depend on both burial depth and the degree of metamorphism. The general pattern of metamorphic influence is expressed in the increase in methane content with stratigraphic depth, rising within a formation from the upper seams to the lower ones (Table 3).

Table 1 - Thicknesses of coal-bearing sequences and stages of coal metamorphism by districts and coal-bearing suites

Districts and deposits	Formation thickness, m (stage of metamorphism)		
	Karagandinskaya	Dolinskaya	Karagandinskaya, Nadkaragandinskaya, Dolinskaya, Tentekskaya
Tentek District	750 (IV-II)	520 (IV-II)	2400
Samarskoe Deposit	600 (II-III)	390 (II)	1965
Zavyalovskoe Deposit	650 (III)	450 (III)	2100

Table 2 - Balance of metamorphism products in organic matter, % [20]

Volatile component	The metamorphic series of coals			
	Peat brown coal	Brown coal bituminous coal	Bituminous coal anthracite	Anthracite graphite
H_2O	4.7	14.4	15.0	7.6
CO_2	74.8	53.6	18.4	9.3
CH_4	11.6	26.3	57.6	65.1
H_2S	0.2	5.4	2.8	9.0
NH_3	8.7	0.3	6.2	9.0
Total volatiles released at each stage	28.8	29.6	18.7	10.5

Table 3 - Average values of in-seam methane pressure, volatile matter yield, gas content, and permeability in coal seams K10 and K12 of the Karaganda Basin

Coal seam	Depth, m	Volatile matter yield, %	Coal rank	Thickness of surface layer d, nm	Change in in-seam pressure, MPa	Methane content, m^3/t	Gas permeability, mD
K12	600	29.5	G	190.0	6.2	19.2	0.35-0.2
K10	370	27.5	G	198.5	3.8	15.0	1-1.4
	510	23.0	GF	180.7	4.0	17.5	0.90-0.55
	610	26.0	CF	158.1	4.2	18.5	0.30-0.20
	680	21.5	C	161.8	4.9	18.2	0.15-0.10

Table 4 - Components of methane occurrence forms in coal seams

Depth, m	Moisture, W, %	Ash Ad, %	Volatile matter r, %	Methane content, m^3/t					Desorbable gas D
				Total Q	q_1	q_2	q_3	q_{1bar}	
-30	0.76	21.6	27.80%	15.9	1.1	11.6	3.2	2.3	13.6
-25	0.99	9.9	24.70%	17.2	1.2	13.7	2.3	2.7	14.5
-25	0.84	22.5	25.70%	13.9	0.9	10.7	2.3	2.5	11.4
-25	0.79	24	27.30%	12.7	0.7	6.9	5.1	2.5	10.2
-165	0.58	14.1	28.80%	11.6	0.9	6.2	4.5	2.3	9.3
-170	0.67	17.3	27.10%	15.8	1.4	10.4	4	2.4	13.4
0	0.66	19.6	28.30%	18.6	1.5	15.6	1,5	2.3	16.3
-100	0.9	14.7	28.80%	19.1	1.5	15.6	2	2.4	16.7
-13	0.99	14.7	26.00%	7.6	0.4	3.2	4	2.4	5.2
-80	1.02	26.8	24.50%	13.8	1	8.9	3.9	2.4	11.4
-76	0.98	21.2	27.50%	5.9	0.3	2.6	3	2.4	3.5
-70	0.91	18.4	27.20%	5.9	0.3	2.5	3.1	2.3	3.6
-40	0.9	10	25.80%	6.7	0.3	4.3	2.1	2.5	4.2
Average	0.85	18.06	26.88%	12.67	0.88	8.63	3.15	2.12	10.25

The results presented in Table 3, including the evaluation of volatile yield, thickness of the near-surface coal layer, reservoir pressure, methane content, and gas permeability across coal ranks at different depths, indicate that methane reservoir pressure in coal seams increases with depth. For example, in seam K11 "Felix," methane pressure at a depth of 320 m is 2.80 MPa with a gas content of 15 m^3/t, whereas at a depth of 690 m these values increase to 4.90 MPa and 18.2 m^3/t, respectively.

Methane in coal seams occurs predominantly in sorbed and free states, accumulated within micro- and macropores. The ratio between these forms varies with depth depending on changes in porosity.

The natural gas pressure within micropores and natural microfractures of the coal matrix determines the volume of methane in the sorbed state, whereas the content of free gas increases slightly with depth and subsequently stabilizes. This behavior is associated with metamorphic processes classified as first-order phase transitions: one part of the coal substance forms an activated complex, another contributes to the growth of the aromatic carbon network, and a third transitions into the gaseous

phase, which migrates from the coal seam toward the surface.

During marine regression, the coal-bearing strata are uplifted toward the surface (in this case, the Ashlyarik Formation coals), leading to changes in the thermodynamic parameters of the coal substance. Under these conditions, coal macromolecules become more electrically neutral due to ion diffusion within the coal matrix. The degree of electrical neutrality of coal macromolecules is governed by time, ion concentration, and the structure and size of the coal substance, including its surface layer.

The key factors controlling the preservation and migration of gases through coal seams and surrounding rocks include methane reservoir pressure, coal permeability, sorption properties, and the porosity of both coal seams and host rocks [[29], [30]].

The results of studies on the forms of gas occurrence in coal seam D6, prepared for extraction, are presented in Table 4, where:

q_1 — denotes the amount of gas lost during borehole drilling and prior to placing the sample into a sealed container;

q_2 — gas measured in the container;

q_3 — gas released after sample grinding;

$q_1$bar — gas desorbed after equilibration at laboratory (atmospheric) pressure.

The sum of the first three values (Table 4) corresponds to the total gas content of the sample Q. Subtracting q_{1bar} from this sum yields the amount of desorbed gas in the sample (D). Analysis of Table 4 and Figure 1 shows that the contents of q_1, q_3, and q_{1bar} remain practically unchanged and correspond to the following mean statistical values (m³/t): q_1 = 0.88, q_3 = 3.15, and q_{1bar} = 2.12.

At the same time, the contents of q_2 and D correlate with the total gas content of the sample Q, and the difference between them represents the average content of free gas, which is 2.42 m³/t.

The desorbable gas content, amounting to 10.25 m³/t, is determined by two main factors: the adsorption surface of micropores and microfractures (including the microfracturing of the coal surface layer) and the gases absorbed by the coal matter.

Based on Schlumberger logging results using neutron-neutron logging (NNL) in combination with gamma-gamma density logging (GGL-D), gas-bearing coal seams were identified (see Tables 5 and 6).

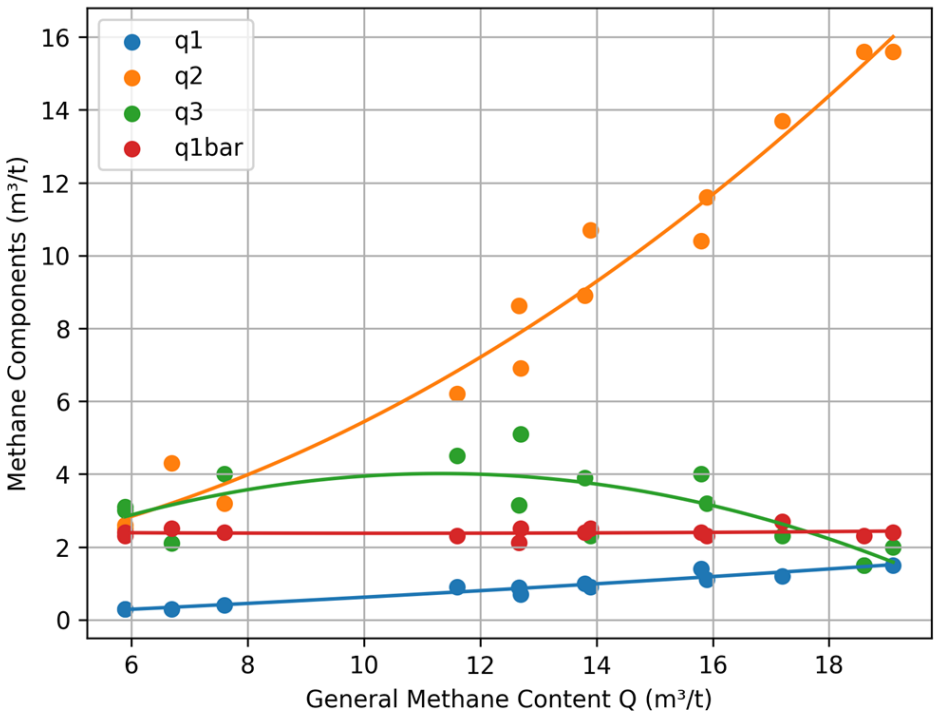

Figure 1 - Methane Components with Average Trend Lines

Table 5 - Average density, volumetric clay content, and lithology of coal seams in the Tentek and Dolinskaya suites

Borehole №	Depth interval, m	Number of seam intersections	Coal seams	Average thickness, m	Density ρ, g/cm³	Volumetric clay content K_{CC}, %	Lithology
	Lenina Mine						
1	109.1-	12	T_1-$T_{1/2}$	0.79	1.71	9.13	coals
	489.3			0.53	1.74	13.6	coals
	516.6-647.0	2	D_8-D_{11}	0.70	1.35	2.23	gas-bearing
	515.3-702.3	3	D_6-D_{11}				
2	202.7-400.7	18	T_1-T_9	0.87	1.88	21.15	coal
	536.0-68.7	12	D_7-D_{11}	0.81	2.02	23.32	coals
	254.6-391.0	6	T_2-T_8	1	1.64	3.17	gas-bearing
	722.7-727.9	2	6	5.20	1.40	2.40	gas-bearing
3	96.9-445.7	18	T_1-T_{16}	0.80	1.78	14.57	coal
	636.7-727.9	5	D_7-D_9	0.54	1.93	13.36	coal
	186.9-447.3	4	T_1-T_{12}	0.93	1.68	5.40	gas-bearing
	618.9-770.7	3	D_6-D_{11}	1.90	1.55	2.33	gas-bearing
4	94.8-673.6	24	T_1-T_{13}	0.72	1.885	29.30	coal-fired
	676.9-753.7	2	D_8	0.70	1.92	35.30	coal-fired
	552.3-555.7	1	D_{10}-D_{11}	2.57	1.37	3.10	gas-bearing
2	Kazakhstanskaya Mine						
	261.3-321.0	6	T_4-T_6	0.60	1.89	33.85	coals
	505.6-703.2	9	D_6-D_{11}	0.60	1.87	25.48	coals
	347.2-347.9	1	T_3	0.7	1.41	9.70	gas-bearing
	520.4-706.5	7	D_6-D_{10}	1.06	1.55	6.31	gas-bearing

Table 6 - Average characteristics of coal seams by suite

Suite	Density ρ, g/cm³		Volumetric clay content Kcc, %	
	non-gas-bearing	gas-bearing	non-gas-bearing	gas-bearing
	Lenina Mine			
Dolinskaya	1.51 ±0.03	1.41 ± 0,03	17.90 ± 0.21	2.44 ± 0.12
Tentek	1.81±002	1.66 ± 002	21.40 ± 0.22	4.28 ± 0.12
Difference	0.30	0.25	3.50	1.84
Kazakhstanskaya Mine				
Dolinskaya	1.89 ± 0.01	1.55 ±001	26.85 ±0.13	6.30 ±0.14
Tentek	1.81 ± 0.02	1.41 ± 0.02	23.48 ± 0.13	9.70±0.14
Difference	0.08	0.14	3.37	3.40

Table 7 - Average physico-mechanical properties of gas-bearing coal seams in the Tentek and Dolinskaya suites at Kazakhstanskaya and Lenina mines

Seam	Depth interval, m	Density (GGL-D), g/cm³	K_{CC} (GL), %	Poisson's ratio	Modules, GPa			Gas presence
					Young's	Shear	Bulk	
				BAL				
T_3	347.2-347.9	1.91	9.7	0.41	3.88	1.37	7.52	gas
D_8, D_9, D_{10}	520.4-656.9	1.88	10.2	0.37	6.98	2.55	8.78	gas
D_6	701.1-706.5	1.68	4.8	0.41	6.10	2.16	1.38	gas
		1.48	9.9	0.40	4.34	1.55	7.31	gas
		1.41	0.5	0.41	3.92	1.39	7.11	gas
		1.29	3.3	0.35	5.58	2.11	5.92	gas

Analysis of Tables 5 and 6 shows that the non-gas-bearing coal seams of the underlying Dolinskaya Formation at the Lenina mine have an average density 0.30 g/cm³ lower than that of the Tentek seams. The average density of the gas-bearing Dolinskaya coals is 0.25 g/cm³ lower compared to the Tentek coals. This difference is attributed to variations in volumetric clay content. Specifically, for non-gas-bearing coal seams the difference in volumetric clay content is 3.50 %, while for gas-bearing seams it is 1.84 %.

At the Kazakhstanskaya mine site, the average density of non-gas-bearing coal seams from both formations differs only slightly (by 0.08 g/cm³), whereas for gas-bearing seams the difference is 0.14 g/cm³. The ratio of volumetric clay content values for gas-bearing and non-gas-bearing seams at the Kazakhstanskaya mine is similar to that observed at the Lenina mine: 3.37 % and 3.40 %, respectively.

A decrease in both density and clay content in gas-bearing coal seams is a characteristic feature. For reliable identification of such seams, the results of neutron-neutron logging based on thermal neutrons were used. The readings of this method are lower in gas-bearing seams compared to non-gas-bearing ones due to their lower hydrogen content.

Based on the integrated interpretation of geophysical well logging data (gamma-gamma density logging (GGL-D) and cross-dipole acoustic imager) in the depth interval of 284–765 m at the Kazakhstanskaya and Lenina mines, the average values of the physico-mechanical properties of gas-bearing coal seams were determined (Table 7).

The results presented in Table 7 confirm the lower density of gas-bearing coal seams compared to non-gas-bearing ones, while following the general trend of density increasing with depth. For non-gas-bearing coal seams of both formations, there is a characteristic increase in physico-mechanical properties (Young's modulus, shear modulus, and bulk modulus) compared to gas-bearing seams.

Overall, the gas content of coal seams in the Karaganda Basin increases with depth of occurrence, starting from the lower boundary of the gas weathering zone. The rate of gas content increase per 100 m of depth decreases with increasing degree of coal metamorphism. Thus, at a depth of 1000 m, the calculated methane content is expected to reach 22–29 m³/t (Ermekov M.A., 1968), and the Langmuir pressure ranges from 1.08 to 1.41 MPa, with an average of 1.27 MPa. This is explained by the fact that the calculated methane quantity according to the Langmuir model is lower than the maximum sorption capacity of the seam, which may be associated with the fracturing of the coal seams and surrounding rocks.

Particular importance is attached to geophysical studies of the physico-mechanical and filtration-capacity properties of coal seams and host rocks in areas prepared for mining, as these parameters change during the implementation of all degasification measures.

As can be seen from Tables 2 and 4, the free gas concentration of 2.42 m³/t is lower than the known values reported in the literature (2–12 m³/t). This is due to the influence of advance degasification of seam D6, during which mainly free gas is extracted from natural macropores and macrofractures, as well as from fractures formed during hydraulic fracturing of the seam. The research results confirmed the elevated methane content in prepared loose coals of seam D6, which is associated with a significant increase in the specific surface area of coal particles and microfractures in the surface nanosized layer of the coal.

From Tables 2 and 4, free gas concentration (2.42 m³/t) is lower than typical literature values (2–12 m³/t), attributable to pre-mine degasification,

Table 8 - Average values of C_u (%), W (%), C_p (J/(kg·K)), and V^{daf} (%) for coals of the Karaganda Basin

Coal rank	d(I), nm	C_u, %	W, %	C_p,	A^{daf}, %
B	214.2	50-77	До 40	1440	42-52
LF	198.7	70-80	17-19	1380	43-46
C	180.8	88-90	2-5	1050	26-29
A	151.5	92-98	1-3	815	<10

which primarily extracts free gas from natural macropores, macrofractures, and hydrofracturing-induced fractures. Gas composition in seam D6 from vertical boreholes (%): H_2 0.01–30, O_2 0.3–6.0, N_2 1.3–42.0, CH_4 25.0–98.0, CO_2 0.12–11.8. These findings confirm elevated methane in loose, tectonically disturbed coals of seam D6, linked to increased specific surface area of microfractures in the surface layer and macrofractures in tectonically pulverized coal.

A critical factor in gas regime formation during coal extraction and storage is spontaneous combustion, governed by specific heat capacity C_p (J/(kg·K)), ash content A (%), carbon content C_u (%), moisture W (%), and volatile matter yield V^{daf} (%) (see Table 8).

The data presented in Table 8 indicate that as the degree of metamorphism increases (coal ranks progressing from B to A), the thickness of the surface coal layer decreases, the carbon content increases, while moisture content, specific heat capacity, and volatile matter yield decrease.

The established regularities can be used in planning operations for the industrial extraction of methane from coal seams identified in the well sections of the basin.

Conclusions

An optimal suite of geophysical logging methods for open-hole wells has been selected to study the physico-mechanical and filtration-capacity properties of coal seams and surrounding rocks.

Characteristic features for identifying gas-bearing coal seams have been established based on a comprehensive set of physico-mechanical and filtration-capacity measurements obtained through well logging methods.

Using the example of the Kazakhstanskaya and Lenina mine sites, gas-bearing coal seams were identified throughout the entire well sections for potential methane extraction, with subsequent aggregation of gas volumes obtained during coal seam degasification.

Regularities in the variation of physico-mechanical and filtration-capacity properties of coal seams in the overlying Tentek Formation and the underlying Dolinskaya Formation have been established, as well as for coal seam sections prepared for mining. These findings are an important factor used in geomechanical calculations to ensure efficient coal extraction while maintaining safe working conditions.

It is recommended to conduct a comprehensive suite of geophysical logging in the open hole of all vertical exploration and drainage wells to monitor the variability of physical properties along the dip and strike of coal seams when planning hydraulic fracturing operations. The results should be used for geomechanical calculations during coal mining. This approach will enable monitoring of changes in the strength and filtration properties of the coal massif, as well as the intensity of gas emission, thereby contributing to the assessment of risks associated with gas-dynamic phenomena.

To standardize and improve the accuracy of studies on the physico-mechanical and filtration-capacity properties of rocks and coal seams, it is necessary to establish a specialized laboratory in the Karaganda Basin. This laboratory should include a well logging crew (party) dedicated to geophysical investigations.

Conflict of interest. On behalf of all the authors, the correspondent author declares that there is no conflict of interest.

***CRediT author statement*: V. Portnov, M. Rabatuly:** Conceptualization, Methodology, Software; **N. Khuangan, A. Kenetayeva:** Data curation, Writing-Original draft preparation; **G. Duganova, A. Golik:** Visualization, Investigation; **Peng Hou:** Software, Validation.

Cite this article as: Portnov VS, Golik A V, Duganova G K, Khuangan N, Kenetayeva A A, Rabatuly M, Peng Hou. Identification of Methane-Bearing Coal Seams in Borehole Sections of the Karaganda Basin Using Geophysical Logging Data. Kompleksnoe Ispolzovanie Mineralnogo Syra = Complex Use of Mineral Resources. 2028; 345(2):72-83. https://doi.org/10.31643/2028/6445.17

Қарағанды бассейні ұңғымалары кесіндісінде метаны мол көмір қабаттарын геофизикалық каротаж деректері бойынша бөліп шығару

[1]Портнов В.С., [1]Голик А.В., [1]Дуганова Г.К., [1]Хуанган Н., [1]Кенетаева А.А., [1]Рабатулы М., [2]Peng Hou

[1]Әбілқас Сағынов атындағы Қарағанды техникалық университеті, Қарағанды, Қазақстан
[2]Ухань Университеті, Ухань, Қытай

Мақала келді: *17 наурыз 2026*
Сараптамадан өтті: *19 наурыз 2026*
Қабылданды: *9 маусым 2026*

ТҮЙІНДЕМЕ

Қарағанды көмір бассейні әлемдегі ең газға бай бассейндердің бірі болып табылады. Оның ерекшелігі – оның құрамында бос газдың көп мөлшерде жиналмауы, ал табиғи газдылық 25-30 м³/т-қа жетеді; бұл газдық сынамалаудың үлкен көлемімен, газдық каротаж деректерімен және жұмыс істеп тұрған шахталардағы газдық түсірілім деректерімен расталады. Көмір қабаттарының метаны атмосфераға жоғарыдағы жыныстар арқылы табиғи миграция жолымен, сондай-ақ қабаттардың қабыршақ астында шығу орындарында және жабық шахталардың оқпандары арқылы түседі. Қарағанды бассейнінің көмір қабаттарын газсыздандыру кезінде, тау-кен жұмыстарымен қабаттарды ашуда, соның ішінде ашық карьерлік өндіру кезінде, қабаттар жер бетіне шыққан кезде және жабық шахталардан шығатын газды газсыздандырылған кезде, өндірілген метанның бір бөлігі шахталарда жылу мен электр энергиясын алу үшін пайдаланылады, ал көп бөлігі көмір қабаттарын газсыздандыру кезінде атмосфераға шығарылады. Атмосфераға шығарылатын метан Жердің жылуын көмірқышқыл газына қарағанда 25-30 есе тиімдірек - сақтайтыны белгілі. Өңделмеген көмір қабаттарынан метанды өнеркәсіптік пайдалану мақсатында жылу және электр энергиясын алу үшін, көмір-метан кен орындарын кешенді игеру, технологияларын дамытудың маңызды міндеті болып табылады, сондай-ақ олар орналасқан өңірлердегі экологиялық жүктемені төмендету болып табылады. Зерттеулердің мақсаты – қабат кесіндісінде газға бай көмір қабаттарын бөліп шығару, оны өнеркәсіптік мақсатта пайдалану үшін өңделмеген қабаттардан метанды алу және атмосфераға шығарындыларды азайту мүмкіндігін бағалау. Әдістер. Барлау ұңғымаларын зерттеудің геофизикалық әдістерінің кешені көмір қабаттары мен қоршаған жыныстардың физика-механикалық және сүзгі-қуыстық қасиеттерін зерттеу үшін, тау-кен жұмыстарындағы көмір қабаттарының сынамаларын алу және талдау. Нәтижелер. Көмір қабаттарының газ құрамын анықтайтын физикалық қасиеттер кешенінің өзгеру заңдылықтары анықталды және осы өзгерістер мен негізгі қоршаған жыныстардың физика-механикалық қасиеттерінің өзгеруіне геологиялық негіздеме берілді. Қолдану. Кесіндіде бөлінген газға бай көмір қабаттары геологиялық кесіндінің барлық газға бай қабаттарынан, соның ішінде көмір қабаты шахталары игеріп жатқан қабаттардан метанды алуды жоспарлау кезінде пайдалануға болады, ал игеруге дайындалған немесе игеріліп жатқан көмір қабаттарының физикалық-механикалық, сүзу-сыйымдылық қасиеттерінің өзгеру заңдылықтарын геомеханикалық есептеулерде пайдалануға болады.

Түйін сөздер: көмір свиталары, метаморфизм көмір мен қоршаған жыныстардың физика-механикалық сипаттамалары, газдылық, көмірлердегі метанның болу пішіндері, экология, геомеханика.

Авторлар туралы ақпарат:

Портнов Василий Сергеевич *Техника ғылымдарының докторы, Әбілқас Сағынов атындағы Қарағанды техникалық университетінің профессоры, 100027, Нұрсұлтан Назарбаев даңғ. 56, Қарағанды, Қазақстан. E-mail: vs_portnov@mail.ru; ORCID ID: https://orcid.org/0000-0002-4940-3156*

Голик Андрей Васильевич *Әбілқас Сағынов атындағы Қарағанды техникалық университетінің PhD докторанты, 100027, Нұрсұлтан Назарбаев даңғ. 56, Қарағанды, Қазақстан. E-mail: andrey.golik@i-geo.kz; ORCID ID: https://orcid.org/ 0009-0008-5179-0002*

Дуганова Гульден Канатовна *Әбілқас Сағынов атындағы Қарағанды техникалық университетінің PhD докторанты, 100027, Нұрсұлтан Назарбаев даңғ. 56, Қарағанды, Қазақстан. E-mail: dgulden_k@mail.ru; ORCID ID: https://orcid.org/0009-0008-0368-4619*

Хуанган Нұрбол *PhD докторы, Әбілқас Сағынов атындағы Қарағанды техникалық университетінің Пайдалы қазбалар кенорындарын өндіру кафедрасының қауымдастырылған профессоры, 100027, Нұрсұлтан Назарбаев даңғ. 56, Қарағанды, Қазақстан. E-mail: n.khuangan@ktu.edu.kz; ORCID ID: https://orcid.org/0000-0001-9609-6649*

Кенетаева Айгуль Акановна *Техника ғылымдарының магистрі, Геология және пайдалы қазбалар кен орындарын барлау мамандығы бойынша, Әбілқас Сағынов атындағы Қарағанды техникалық университетінің оқытушысы, 100027, Нұрсұлтан Назарбаев даңғ. 56, Қарағанды, Қазақстан. E-mail: aigul_tate2@bk.ru; ORCID ID: https://orcid.org/0000-0001-7943-3279*

Рабатұлы Мұхаммедрахым *PhD докторы, Әбілқас Сағынов атындағы Қарағанды техникалық университетінің Пайдалы қазбалар кенорындарын өндіру кафедрасының қауымдастырылған профессоры, 100027, Нұрсұлтан Назарбаев даңғ. 56, Қарағанды, Қазақстан. E-mail: mukhammedrakhym@mail.ru; ORCID ID: https://orcid.org/0000-0002-7558-128X*

Peng Hou *Инженерлік ғылымдарының докторы, Профессор, Ухань Университеті, Вучан Ауданы, Ухань, Хубэй, 430072, Қытай,, № 299 Байи Жолы, Вучан Ауданы. E-mail: penghou@whu.edu.cn; ORCID ID: https://orcid.org/0000-0002-2621-8943*

Выделение метаноносных угольных пластов в разрезе скважин Карагандинского бассейна по данным геофизического каротажа

[1]Портнов В. С., [1]Голик А. В., [1]Дуганова Г. К., [1]Хуанган Н.., [1]Кенетаева А. А., [1]Рабатулы М., [2]Peng Hou

[1]Карагандинский технический университет имени Абылкаса Сагинова, Караганда, Казахстан
[2]Уханьский университет, Ухань, Китай

Поступила: *17 марта 2026*
Рецензирование: *19 марта 2026*
Принята в печать: *9 июня 2026*

АННОТАЦИЯ

Карагандинский угольный бассейн является одним из наиболее газоносных в мире. Его особенностью является то, что в нем нет крупных скоплений свободного газа, а природная газоносность достигает до 25-30 м3/т, это подтверждается большим объемом газового опробирования, по газовому каротажу и данными газовой съемки в действущих шахтах. Метан угольных пластов попадает в атмосферу путем естественной миграции через вышележащие породы, а также в местах выхода пластов под наносы и через стволы закрытых шахт. При дегазации угольных пластов Карагандинского бассейна при вскрытии пластов горными выработками в том числе при открытой разработке, выхода пластов к поверхности, дегазации отработанного пространстве закрытых шахт часть извлеченного метана используется на шахтах, для получения тепловой и электрической энергии, а большая часть попадает в атмосферу при дегазации угольных пластов. Известно, то, что метан, попавший в атмосферу, удерживает тепло Земли значительно выше, в 25-30, раз, чем диоксид углерода. Извлечение метана из неразгруженных угольных пластов для его использовния в промышленности при получении тепловой и электрической энергии, является важной задачей развития технологий комплексной разработки углеметановых месторождений, но и снижением экологической нагрузки на регионы, где они располагаются. Целью исследований является выделение в разрезе газоносных угольных пластов для оценки потенциала извлечения метана из неразгруженных пластов для его промышленного использования и снижения выброса в атмосферу. Методы. Комплекс геофизических методов исследований разведочных скважин для изучения физико-механических и фильтрационно емкостных свойств угольных пластов и вмещающих пород, отбори анализ проб угольных пластов в горных выработках. Результаты. Установлены закономерности изменения комплекс физических свойств угольных пластов, определяющих их газоностность, дано геологическое обоснование этих изменений и изменений физико-механических свойств вмещающих пород. Применение. Выделенные в разрезе газоносные угольные пласты могут быть использованы при планировании добычи метана из всех газоносных пластов геологического разреза, включая разрабатываемые шахтами угольного пласта, а закономерности изменения физико-механических, фильтрационно-емкостных свойств, подготовленных к разработке или разрабатываемых угольных пластов, могут быть использованы при геомеханических расчетах. Фактические материалы, для проведения исследований получены по результатам лабораторных, геофизических исследований разведочных скважин, материалов геологических и производственных отчетов.

Ключевые слова: угольные свиты, метаморфизм физико - механические характеристики угля и вмещающих пород, газоносность, формы нахождения метана в углях, экология, геомеханика.

Информация об авторах:

Портнов Василий Сергеевич — *PhD, ассоциированный профессор кафедры Разработки месторождений полезных ископаемых, Карагандинский технический университет имени Абылкаса Сагинова, 100027, пр. Нурсултана Назарбаева, 56, Караганда, Казахстан. E-mail: vs_portnov@mail.ru; ORCID ID: https://orcid.org/0000-0002-4940-3156*

Голик Андрей Васильевич — *PhD докторант, Карагандинский технический университет имени Абылкаса Сагинова, 100027, пр. Нурсултана Назарбаева, 56, Караганда, Казахстан. E-mail: andrey.golik@i-geo.kz; ORCID ID: https://orcid.org/ 0009-0008-5179-0002*

Дуганова Гульден Канатовна — *PhD докторант, Карагандинский технический университет имени Абылкаса Сагинова, 100027, пр. Нурсултана Назарбаева, 56, Караганда, Казахстан. E-mail: dgulden_k@mail.ru; ORCID ID: https://orcid.org/0009-0008-0368-4619*

Хуанган Нұрбол — *PhD, ассоциированный профессор кафедры Разработки месторождений полезных ископаемых, Карагандинский технический университет имени Абылкаса Сагинова, 100027, пр. Нурсултана Назарбаева, 56, Караганда, Казахстан. E-mail: n.khuangan@ktu.edu.kz; ORCID ID: https://orcid.org/0000-0001-9609-6649*

Кенетаева Айгуль Акановна — *Магистр технических наук, специальность Геология и разведка месторождений полезных ископаемых, преподаватель Карагандинского технического университета имени Абылкаса Сагинова, 100027, пр. Нурсултана Назарбаева, 56, Караганда, Казахстан. E-mail: aigul_tate2@bk.ru; ORCID ID: https://orcid.org/0000-0001-7943-3279*

Рабатулы Мухаммедрахым — *PhD, ассоциированный профессор кафедры Разработки месторождений полезных ископаемых, Карагандинский технический университет имени Абылкаса Сагинова, 100027, пр. Нурсултана Назарбаева, 56, Караганда, Казахстан. E-mail: mukhammedrakhym@mail.ru; ORCID ID: https://orcid.org/0000-0002-7558-128X*

Peng Hou — *Доктор технических наук, профессор Уханьского университета, округ Учан, Ухань, провинция Хубэй, 430072, улица Байи-роуд, 299, район Учан, Китай. E-mail: penghou@whu.edu.cn; ORCID ID: https://orcid.org/0000-0002-2621-8943*

References

[1] Fu G, Xie X, Jia Q, Tong W, Ge Y. Accidents analysis and prevention of coal and gas outburst: Understanding human errors in accidents. Process Saf. Environ. Prot. 2020; 134:1–23.

[2] Yuan L, Wang E, Ma Y, Liu Y, Li X. Research progress of coal and rock dynamic disasters and scientific and technological problems in China. J. China Coal Soc. 2023; 48:1825–1845.

[3] Zhang C, Wang P, Wang E, Xu J. Coal and gas outburst mechanism: Research progress and prospect in China over the past 70 years. Coal Geol. Explor. 2023; 51:59–94.

[4] Gazaliyev AM, Portnov VS, Kamaov RK, Maussymbayeva AD, Yurov VM. Geophysical research of areas with increased gas content of coal seams. Naukovyi Visnyk Natsionalnoho Hirnychoho Universytetu. 2015.

[5] Mussin R, Portnov V, Golik A, Zamaliyev N, Akhmatnurov D, Ganyukov N, Skrzypkowski K, Zagórski K, Efremova S. Assessment of Strength Characteristics and Structural Heterogeneity of Coal Seams in the Karaganda Basin by Geophysical Methods for Enhancing Mining Safety. Mining. 2026; 6(1):21. https://doi.org/10.3390/mining6010021

[6] Maussymbayeva AD, Mindubaev AB, Imanbaeva SB, Portnov VS, Rabatuly M. A force model of a sudden coal and gas outburst. Ugol. 2024; 11:44–50. http://dx.doi.org/10.18796/0041-5790-2024-11-44-50

[7] Portnov V, Mindubaev A, Golik A, Sulemenov N, Zakharov A, Madisheva R, Kolikov K, Imanbaeva S. Risk Assessment of Sudden Coal and Gas Outbursts Based on 3D Modeling of Coal Seams and Integration of Gas-Dynamic and Tectonic Parameters. Fire. 2025; 8:234. https://doi.org/10.3390/fire8060234

[8] Suleimenov N, Sattarova G, Sarsenbekov N, … Zakharov A, Abdirashit A. Recognition of Stages of Endogenous Fire Outbreak and Development in Coal Mines. Applied Sciences. 2025; 15(20):11114.

[9] Maussymbayeva AD, Portnov VS, Imanbaeva SB, Rabatuly M, Rakhimova GM. Influence of Rock Shear Processes on the Methane Content of Longwall Faces. Naukovyi Visnyk Natsionalnoho Hirnychoho Universytetu. 2024; 4:11–17. https://doi.org/10.33271/nvngu/2024-4/011

[10] Maussymbayeva AD, Yurov VM, Portnov VS, Rabatuly M, Rakhimova GM. Assessment of the Influence of the Surface Layer of Coals on Gas-Dynamic Phenomena in the Coal Seam. Naukovyi Visnyk Natsionalnoho Hirnychoho Universytetu. 2024; 2:5–11. https://doi.org/10.33271/nvngu/2024-2/005

[11] Zheng S, Liu Y, Huang F, Liu S, Sang S, Dai X, Wang M. Pore Structure Evolution of Coal After Supercritical CO_2–Water–Rock Treatment: A Multifractal Analysis. Fractal Fract. 2025; 9:144.

[12] Liu D, Qiu F, Liu N, Cai Y, Guo Y, Zhao B, Qiu Y. Pore Structure Characterization and Its Significance for Gas Adsorption in Coals: A Comprehensive Review. Unconv. Resour. 2022; 2:139–157.

[13] Yu S, Bo J, Fengli L, Jiegang L. Structure and Fractal Characteristic of Micro- and Meso-Pores in Low, Middle-Rank Tectonic Deformed Coals by CO_2 and N_2 Adsorption. Microporous Mesoporous Mater. 2017; 253:191–202.

[14] Liu X, Nie B. Fractal Characteristics of Coal Samples Utilizing Image Analysis and Gas Adsorption. Fuel. 2016; 182:314–322.

[15] Technical Regulations on the Safety of Coals and Production Processes of Their Extraction, Processing, Storage and Transportation. Resolution of the Government of the Republic of Kazakhstan. 2010; 731.

[16] Fakhrullin RF, Tursunbayeva A, Portnov VS, L'vov Yu. Ceramic nanotubes for polymer composites with stable anticorrosion properties. Crystallography Reports. 2014; 59:1107–1113. https://doi.org/10.1134/S1063774514070104

[17] Filimonov EN, Portnov VS, Egorov VV, Steflyuk YuYu, Kenetaeva AA. Nekotoryye aspekty izucheniya gazonosnosti plasta K10 v usloviyakh shakhty «Abayskaya» Gornogo upravleniya AO AMT. Karaganda [Some aspects of the study of gas content of seam K10 under the conditions of the Abayskaya mine of the Mining Department of JSC AMT. Karaganda]. 2016, 98. (In Russ.).

[18] Alikulov Sh, Toshov J, Mussin R, Rabatuly M, Tolovkhan B, Bogzhanova Zh, Gabitova A. Study of rational solution parameters during in-situ uranium leaching. Mining of Mineral Deposits. 2025; 19(1):37–46. https://doi.org/10.33271/mining19.01.037

[19] Rabatuly M, Demin VF, Kenetaeva AA, Steflyuk YuYu, Toshov JB. Evaluation of modern methods and techniques for calculating parameters during coal bed degassing. Kompleksnoe Ispolzovanie Mineralnogo Syra = Complex Use of Mineral Resources. 2025; 334(3):110–120. https://doi.org/10.31643/2025/6445.33

[20] Seravkin I B. Metamorphism of caustobiolites of the Karaganda Basin. Nauka, Metallogeny of the Southern Urals and Central Kazakhstan. 1970, 135.

[21] Chen Y, Liu R, Wang G, Ma J, Wu J, Wang P, Wu K, Guo X. Pore and gas desorption characteristics of primary coal with different degrees of metamorphism. Energy Sci. Eng. 2023; 11:3185–3203.

[22] Maussymbayeva AD, Yurov VM, Portnov VS, Rabatuly M, Rakhimova GM. Assessment of the Influence of the Surface Layer of Coals on Gas-Dynamic Phenomena in the Coal Seam. Naukovyi Visnyk Natsionalnoho Hirnychoho Universytetu. 2024; 2:5–11. https://doi.org/10.33271/nvngu/2024-2/005

[23] Guo H, Yu Y, Wang K, Yang Z, Wang L, Xu C. Kinetic characteristics of desorption and diffusion in raw coal and tectonic coal and their influence on coal and gas outburst. Fuel. 2023; 343:127883.

[24] Kopobayeva AN, Portnov VS, Kim SP, Amangeldykyzy A, Askarova NS. Tectonic factors of impurity elements accumulation at the Shubarkol coal deposit (Kazakhstan). Naukovyi Visnyk Natsionalnoho Hirnychoho Universytetu. 2021; 5:11–15. https://doi.org/10.33271/nvngu/2021-5/011

[25] Wang C, Yang S, Li X, Li J, Jiang C. Comparison of the initial gas desorption and gas-release energy characteristics from tectonically-deformed and primary-undeformed coal. Fuel. 2019; 238:66–74.

[26] Portnov VS, Kamarov R, Mausymbaeva A, Yurov V. Link of specific electric resistance with qualitative and strength characteristics of ores. In Progressive Technologies of Coal, Coalbed Methane, and Ores Mining. 2014. https://doi.org/10.1201/b17547

[27] Portnov VS, Yurov VM, Mausymbaeva AD. Influence of Surface Properties of Minerals on Rebellious Ore Disintegration. Journal of Mining Science. 2018; 54:681–689. https://doi.org/10.1134/S1062739118044600

[28] Lei D, Wang Y, Meng H, Ma S, Ma T, Yan L. Experimental study on response characteristics of coal adsorption and desorption under electric field enhancement. Energy Sources Part A Recovery Util. Environ. Eff. 2021, 1–14.

[29] Kenetayeva AA, Kenetayeva ZhK, Tokusheva ZhT, Rabatuly M. Methane content of coal seams of Karaganda basin. IOP Conference Series: Materials Science and Engineering. 2019; 516(1). https://doi.org/10.1088/1757-899X/516/1/012020

[30] Ross DJK, Marc Bustin R. The Importance of Shale Composition and Pore Structure upon Gas Storage Potential of Shale Gas Reservoirs. Mar. Pet. Geol. 2009; 26:916–927.

Crossref
DOI: 10.31643/2028/6445.18
Mining & Mineral Processing

Technological, economic and environmental aspects of the production of sulfate-resistant Portland cement clinker based on the mineral resources of Karakalpakstan

[1*]Khadzhiev A.Sh., [2]Wang L., [3]Atabaev F.B., [3]Makhsudova N.D., [1]Atashev E.A.

[1] Urgench State University named after Abu Rayhon Beruni, Urgench, Uzbekistan
[2]College of Energy Engineering, Zhejiang University, Hangzhou, Zhejiang
[3] Institute of General and Inorganic Chemistry of the Academy of Sciences of Uzbekistan, Tashkent

** Corresponding author email: azamat.x@urdu.uz*

Received: *December 1, 2025*
Peer-reviewed: *May 20, 2026*
Accepted: *June 10, 2026*

ABSTRACT

This study focuses on the production of sulfate-resistant Portland cement clinker using local raw materials found in the Aral Sea region of the Republic of Uzbekistan and on its properties. The obtained results highlight the technological, economic, and environmental advantages. The raw material mixtures consisted of limestone, barren sand, kaolin, and iron-containing industrial waste, resulting in a clinker with an optimized oxide composition (LSF = 0.82, SR = 2.15, AP = 0.94). X-ray phase analysis reveals a high content of alite (C_3S ≈ 38.6%) and belite (C_2S ≈ 41.0%) phases, which ensures high mechanical strength. Low tricalcium aluminate content (tricalcium aluminate < 5%) and sufficient ferrite content (C_4AF ≈ 16.2%) increased sulfate resistance and phase dominance. Sulfate resistance tests conducted in accordance with ASTM C1012/C1012M showed that sulfate-resistant Portland cement had the lowest swelling index among samples immersed in a 5% Na_2SO_4 solution, demonstrating its superior stability compared to conventional Portland cement and mixed cement types. The experimental results demonstrate the feasibility of producing high-quality sulfate-resistant Portland cement clinker using local raw materials and demonstrate its potential for use in the sulfate-rich conditions of the Aral Sea region. From an economic perspective, the use of local raw materials reduces production costs, the need for imports, and increases the competitiveness of the cement industry in our region. From an environmental perspective, the long service life of sulfate-resistant Portland cement and the ability to utilize industrial waste align with the principles of a "green economy" and promote waste reduction and sustainable growth.

Keywords: clinker synthesis, mineral resources, sulfate resistance, green economy, sustainability of sulfate-resistant Portland cement.

Information about authors:

Khadzhiev Azamat Shamuratovich — *Doctor of Philosophy in Technical Sciences, Associate Professor at the Faculty of Chemical Technology, Urgench State University named after Abu Rayhon Beruni, Urgench, H. Olimjon Street 14, 220100, Uzbekistan. Email: xadjiyev2019@mail.ru; ORCID ID: https://orcid.org/0000-0003-2131-8256*

Lei Wang — *Professor, College of Energy Engineering, Zhejiang University, Hangzhou, Zhejiang, 310027, PR China. Email: wanglei.leo@zju.edu.cn; ORCID ID: https://orcid.org/0000-0002-0336-7241*

Atabaev Farrukh Bakhtiyarovich — *Doctor of Technical Sciences, Professor, Chief Scientific Researcher, STROM Research Laboratory, Institute of General and Inorganic Chemistry, Academy of Sciences of Uzbekistan, Tashkent, Uzbekistan. Email: atabaev_farruh@mail.ru; ORCID ID: https://orcid.org/0009-0004-4941-5060*

Makhsudova Nozima Djaparxonovna — *PhD, Junior Researcher, STROM Research Laboratory and Testing Center, Institute of General and Inorganic Chemistry, Academy of Sciences of Uzbekistan, Tashkent, Uzbekistan. Email: nazima-25@mail.ru; ORCID ID: https://orcid.org/0000-0003-4579-6551*

Atashev Elyor Atashevich — *Doctor of Philosophy in Technical Sciences, Associate Professor at the Faculty of Chemical Technology, Urgench State University named after Abu Rayhon Beruni, Urgench, H. Olimjon Street 14, 220100, Uzbekistan. Email: elyor.a@urdu.uz; ORCID ID: https://orcid.org/0000-0003-4070-5665*

Introduction

The rapid development of the construction industry—particularly the expansion of hydraulic structures, industrial facilities, and residential infrastructure—has significantly increased the global demand for strong and durable cements and concretes. However, in some regions, specific natural and geographical conditions pose particular challenges for building materials. In the Republic of Karakalpakstan, particularly in the Aral Sea region, soils and groundwater are characterized by high salinity: high concentrations of sulfate ions (SO_4^{2-}) pose a serious threat to concrete and reinforced

concrete structures. In a sulfate environment, ordinary Portland cement quickly degrades: sulfate ions react with the three aluminate phases of calcium (C_3A), forming expanding ettringite, which leads to cracking and reduced strength. Therefore, the production of sulfate-resistant Portland cement has become a pressing technical challenge for this region.

According to UzM St 337:2024 and GOST 22266-2013, the C_3A content in cement clinker should not exceed 5%, and should be reduced to 3% under aggressive conditions. This limitation is due to the fact that C_3A reacts with sulfate ions, forming harmful expanding products. Reducing the amount of Al_2O_3 in the raw mix or increasing the amount of Fe_2O_3 are the most effective ways to suppress C_3A formation and improve sulfate resistance.

The Republic of Karakalpakstan possesses significant scientific and practical potential in this area. The region possesses reserves of raw materials necessary for cement production: limestone ($CaCO_3$ ≈ 85–90%), kaolin (Al_2O_3 ≈ 36–38%), basalt, and iron-rich rocks. Rational use of these resources not only ensures economic efficiency but also enables the production of high-quality sulfate-resistant Portland cement (SRC) clinker, adapted to the region's aggressive sulfate conditions. Therefore, the production and use of such cement has become an important requirement for the construction of reservoirs, sewer systems, and other engineering structures in the Aral Sea region.

International and regional standards set clear requirements for the mineralogical composition of cement clinker to ensure sulfate resistance. The C_3A content is one of the most important controlled parameters: the higher its proportion, the faster the sulfate attack and the greater the risk of expansive failure in concrete. Reducing C_3A by precisely adjusting the Al_2O_3/Fe_2O_3 ratio requires careful selection of raw materials and accurate calculation of batch ratios.

The main objective of this study is to synthesize sulfate-resistant Portland cement clinker from mineral raw materials from the Aral Sea region, determine its chemical and mineralogical composition, and examine the relationship between phase composition and sulfate resistance.

The problem of sulfate corrosion in cement-based materials has attracted extensive research attention internationally, as concrete made from ordinary Portland cement rapidly deteriorates in a sulfate environment, significantly reducing the service life of engineering and hydraulic structures [1]. Many studies are aimed at improving the mineralogical composition of sulfate-resistant clinker, in particular, minimizing the C_3A phase [2]. Studies have shown that reducing the amount of Al_2O_3 or increasing the amount of Fe_2O_3 effectively suppresses the formation of C_3A. Clinkers with a high iron-to-aluminum ratio and a predominance of the ferrite phase demonstrated a sharp reduction in C_3A content and an increase in sulfate resistance [[3], [4]].

It has been shown that optimization of batch composition can reduce the C_3A content below 5% [5], with iron-rich admixtures shown to be particularly effective. Thermodynamic modeling has confirmed the high sulfate resistance of clinkers with a predominance of ferrite phases [[6], [7], [8]]. Mechanistic studies have shown that C_3A phases form expanding products in a two-stage reaction with sulfate ions; long-term observations of the microstructure of sulfate-exposed concrete have confirmed that low-C_3A cements have high strength. The addition of mineral admixtures such as limestone powder, upper kiln slag, and pozolanic materials has also been noted to significantly improve sulfate resistance [[9], [10], [11], [12], [13]].

It has also been noted that sulfate-resistant Portland cement can deteriorate under prolonged moisture conditions and exposure to highly aggressive sulfate. Among the proposed strategies for combating this problem, increasing the Fe/Al ratio with iron-rich mineral additives and using additional cementitious materials such as slag and limestone have been shown to be the most effective [14].

Research conducted in Spain examined the technical and environmental performance of sulfate-resistant clinkers containing new mineral components such as iron-rich sand, slag, and "albero" [15]. The results showed that partial replacement with slag (up to 30%) increases sulfate resistance without compromising mechanical strength. Additional research has confirmed that optimal use of additional cementitious materials in Portland cements improves sulfate resistance [16]; the amount of SO_3 generated by the clinker-gypsum interaction has been found to have a measurable effect on sulfate resistance [17].

In addition to compositional optimization, the use of mineral additives and recycled materials in clinker production improves environmental performance, reduces production costs, and lowers CO_2 emissions [18].

Research conducted in regions neighboring Uzbekistan also explored the potential for

producing sulfate-resistant cement using local mineral resources, focusing on batch optimization, phase analysis, and durability testing in sulfate environments. Practical trials conducted at Karakalpak Cement LLC confirmed that silicon additives improve physical and mechanical properties and enhance sulfate resistance [[19], [20], [21], [22], [23]]. Buriev et al. noted that a high degree of substitution with pozolane materials—for example, fly ash—has a positive effect on sulfate resistance [[24], [25]]. Iskandarova and her colleagues identified innovative directions for the development of composite Portland cement in the region. Kazakhstani scientists who synthesized ferrite-phase cements using manganese- and iron-rich ores confirmed that increasing the C_4AF content reduces C_3A, improving sulfate resistance [26].

From an economic perspective, the use of local limestone, loose sand, kaolin, and iron-rich industrial waste reduces dependence on imported raw materials and lowers production costs, strengthening the competitiveness of the cement industry in the region. Rational use of local resources not only improves technological efficiency but also reduces production costs, contributing to the sustainable development of industry in the Aral Sea region [27].

From an environmental perspective, sulfate-resistant Portland cement clinker, by resisting sulfate corrosion, extends the service life of hydraulic and civil engineering structures, reduces the need for repairs and reconstruction, thereby reducing resource consumption and environmental impacts. These principles are fully consistent with the concepts of a "green economy" and "circular economy," which prioritize sustainability and the efficient use of industrial waste [28]. The inclusion of iron-rich industrial waste in the batch further supports waste recycling and helps reduce CO_2 emissions in the cement industry.

Overall, sulfate-resistant Portland cement clinker synthesized from local raw materials from Karakalpakstan offers a harmonious combination of technological advantages, cost efficiency, and environmental sustainability, making it a material of high practical importance for the Aral Sea region.

Experimental part

Materials and Methods

Sulfate-resistant Portland cement clinker was synthesized using local raw materials sourced from the Lower Aral Sea region. The base raw material mixture included limestone, barren sand, and kaolin, while gypsum and iron-containing industrial waste were used as adjusting components to achieve the target oxide balance. Laboratory samples were prepared at Karakalpak Cement LLC, and all analytical measurements were conducted at the STROM Research and Testing Center of the Institute of General and Inorganic Chemistry of the Academy of Sciences of Uzbekistan.

Chemical Composition

The chemical composition of the synthesized clinker was determined in accordance with UzM St 337:2024 and GOST 5382-2019 by classical titration and gravimetric methods [[28], [29]]. The results (wt.%) were as follows: CaO - 61.09; SiO_2 22.10; Al_2O_3 - 4.98; Fe_2O_3 5.32; MgO - 2.07; SO_3 - 0.80; LOI - 1.14; Free CaO - 0.94. The calculated modulus values (LSF = 0.82; SR = 2.15; AR = 0.94) were within the standard values established for sulfate-resistant Portland cement clinker.

Mineralogical composition (XRD)

X-ray diffraction (XRD) analysis was performed using a Rigaku MiniFlex diffractometer (Cu-Kα radiation), and phase quantification was carried out using the Rietveld refining method. The main mineralogical phases identified in the clinker were: C_3S - 38.6%; C_2S - 38.0%; C_3A - 4.2%; C_4AF - 14.8%. These results are in close agreement with Bogue's calculations and meet the standard requirements for the phase composition of sulfate-resistant Portland cement clinker.

Sulfate Resistance Testing

Sulfate resistance was assessed in accordance with ASTM C1012/C1012M [31]. Test specimens were immersed in a 5% Na_2SO_4 solution, their dimensional expansion was measured, and they were compared to reference specimens stored in distilled water. To ensure the reliability of the results and accurately quantify the effect of sulfate ions on dimensional stability and mechanical strength, two control specimens were used for each test condition. All analyses were conducted in full compliance with the requirements of UzM St 337:2024 and GOST 5382-2019 [[29], [30]].

Results and Discussion

The selection of raw materials for the production of sulfate-resistant Portland cement clinker is of particular scientific and practical importance. Therefore, the economical use of local raw materials is an urgent issue. In the Republic of Karakalpakstan, dune sands, kaolin, iron-rich industrial waste and limestone deposits are

considered promising sources of raw materials. By analyzing their chemical composition, it is possible to determine the mineralogical composition of sulfate-resistant Portland cement clinker.

The ratio of the main oxides in the raw material mixture is an important factor in the synthesis of sulfate-resistant Portland cement clinker. Calcium oxide (CaO) serves to form alite (C_3S) and belite (C_2S) phases, and silicon dioxide (SiO_2) is the basis for silicate phases; aluminum oxide (Al_2O_3) serves to form tricalcium aluminate (tricalcium aluminate). Also, to ensure sulfate resistance, it is necessary to reduce the content of tricalcium aluminate to ≤5%, preferably to 3%. Iron oxide (Fe_2O_3) is part of the ferrite phase (C_4AF) and is important in reducing the content of tricalcium aluminate.

Also, achieving the correct distribution of oxides is an important factor in ensuring the strength and long-term stability of cement in sulfate environments. The chemical composition of local raw materials in the Republic of Karakalpakstan by main oxides is presented in (Table 1).

The chemical composition of these raw materials is suitable for ensuring the optimal balance required in the synthesis of sulfate-resistant Portland cement clinker. Barkhan sands are characterized by a very high SiO_2 content (89.22%), which provides a primary source for silicate phases (e.g., C_3S and C_2S) and contributes to improved mechanical strength of clinker. However, due to their relatively low Al_2O_3 (3.15%) and Fe_2O_3 (0.97%) contents, these sands are mainly useful for increasing the silica modulus (SM).

The iron-rich by-product contains a high Fe_2O_3 content (45.24%), which plays a critical role in forming the ferrite phase (C_4AF) and thus contributes to sulfate resistance by reducing three calcium aluminate content. Meanwhile, its SiO_2 (40.40%) and Al_2O_3 (6.00%) levels are moderate, allowing adjustment of the iron modulus (IM) in the raw mix. Low levels of alkaline oxides such as Na_2O and K_2O ensure that adverse effects occur during clinker hydration. Kaolin is high in Al_2O_3 (16.47%) and SiO_2 (54.07%), and acts as the main raw material for the formation of aluminate phases. However, due to the relatively high Al_2O_3 content, kaolin consumption must be carefully controlled, otherwise the tricalcium aluminate content in the clinker may exceed 5%. Kaolin has moderate Fe_2O_3 (9.93%) and Na_2O (1.72%) levels, and it is suitable for adjusting the aluminum modulus (AM). The low content of SO_2 (0%) and TiO_2 (0.17%) does not adversely affect the quality of sulfate-resistant clinker.

Limestone is the main source of CaO (53.14%), which is essential for the formation of alite and belite phases. The almost complete absence of SiO_2 and Al_2O_3 (0% and 0.15%) in it proves that it is a pure calcium source. The low content of MgO (2.56%) and Fe_2O_3 (0.12%) does not cause problems during the clinker hydration process. The loss on heat (LOI, ≈ 42.49%) proves the carbonate nature of the limestone and indicates the release of CO_2 during the calcination process.

In general, the mixture of these raw materials provides the ratio of oxides necessary for the synthesis of sulfate-resistant Portland cement clinker. It is recommended to conduct laboratory tests to determine the main composition. According to preliminary calculations, the optimal batch composition may be as follows: barren sand 15–20%, iron-rich industrial waste 5–10%, kaolin 10–15% and limestone 60–70%. This approach allows for the maximum use of local raw materials and increases the resistance of cement to sulfate environments by 20–30%. In addition to these raw materials, gypsum plays an important role in the cement production process. It is mainly used as a component that regulates the rate of hardening at the cement setting stage.

Table 1 - Chemical composition of local raw materials selected for the synthesis of sulfate-resistant portland cement

Raw Material	**Chemical composition by major oxides (wt.%)**									
	SiO_2	**Al_2O_3**	**CaO**	**MgO**	**Fe_2O_3**	**Na_2O**	**K_2O**	**TiO_2**	**SO_2**	**LOI**
Limestone	–	0.15	53.14	2.56	0.12	–	–	–	–	42.49
Barxan sand	89.22	3.15	0.68	2.32	0.97	0.94	0.70	0.24	0.20	1.61
Kaolin	54.07	16.47	0.85	2.57	9.93	1.72	–	0.17	–	9.23
Iron-rich by-product	40.40	6.00	2.05	4.00	45.24	–	0.40	–	0.22	3.10
gypsum stone	2.80	0.49	30.98	–	–	–	2.63	2.80	42.80	20.30
	$CaSO4 \times 2H_2O = 42.80 \times 2.15 = 85.6\%$									

According to the results of chemical analysis, gypsum from the Tashaba deposit in the Republic of Karakalpakstan contains 42.80% SO_3, which is approximately 85.6% $CaSO_4 \cdot 2H_2O$. Such a very high purity and very low content of SiO_2 (2.80%), Al_2O_3 (0.49%), MgO and Fe_2O_3 indicate that Tashaba gypsum is an ideal raw material for the cement industry. Such a pure chemical composition of Tashaba gypsum ensures the stable formation of ettringite during the hydration process, prevents secondary reactions and increases the sulfate resistance of cement. The low content of impurities in the mixture has a positive effect on the friability, color and stability of the composition of the cement. Therefore, the use of Tashaba gypsum in the production process of sulfate-resistant clinker not only improves the quality of cement, but also serves to effectively use local mineral resources, reduce production costs, and ensure the environmental sustainability of the cement industry (Fig. 1).

Figure 1 - gypsum stone sourced from the Tashaba deposit, Karakalpakstan

The successful balance of the above raw material components is reflected in the mineralogical composition of the synthesized sulfate-resistant Portland cement clinker, since the ratio of oxides directly affects the phases formed (Table 2).

According to the data from the table, the clinker contains CaO (61.09%). It is mainly derived from limestone and is important in the formation of the main part of the alite (C_3S) and belite (C_2S) phases, which determine the strength of the cement and the hydration process. The SiO_2 content (22.1%) is moderate, which plays an important role in the formation of silicate phases in particular. This oxide is mainly derived from barren sands and kaolin. The amounts of Al_2O_3 (4.98%) and Fe_2O_3 (5.32%) serve to form the aluminate and ferrite phases in the clinker due to kaolin and iron-rich industrial waste. Small amounts of oxides such as MgO (2.07%) and SO_3 (0.80%) improve the stability of the clinker in sulfate environments and at the same time prevent undesirable reactions. The absence of Cl^- (0.0%) and the low content of free CaO (0.935%) greatly increase corrosion resistance. The low heat loss (1.14%) confirms the very good quality of the raw materials. The total oxide content of 100.0% indicates that the clinker composition is optimal and fully balanced.

In the mineralogical composition, the clinker is dominated by C_3S (38.64%) and C_2S (41.03%) phases, which primarily determine its mechanical properties. The relatively low content of tricalcium aluminate (4.17%, ≤5%) is the main indicator of sulfate resistance, since it greatly reduces the formation of ettringite. This is directly related to the low content of Al_2O_3 in the raw materials. The presence of the C_4AF (16.16%) phase indicated a high ferrite content in the clinker. This phase is formed due to Fe_2O_3 introduced through iron-rich industrial waste and, replacing part of the tricalcium aluminate, increases the strength of sulfate-resistant cement clinker. The calculated modulus values once again prove that the raw material mixture is in equilibrium. The CaO/SiO_2 ratio (2.76) — the silicon modulus — provides high mechanical strength of the cement. The lime saturation factor (LSF = 0.86) indicates that the firing process was carried out under optimal conditions. The aluminum modulus n (2.15) and iron modulus p (0.94) confirm that the oxides have a stable ratio. These results prove that it is possible to effectively produce sulfate-resistant Portland cement clinker based on local raw materials such as barren sand, iron-rich industrial waste, kaolin and limestone.

Table 2 - Chemical and mineralogical composition of sulfate-resistant portland cement clinker

Material name	**LOI**	**SiO_2**	**Al_2O_3**	**Fe_2O_3**	**CaO**	**MgO**	**SO_3**	**Cl^-**	**CaO (Free CaO)**	**Σ**
Portland cement clinker	1.14	22.1	4.98	5.32	61.09	2.07	0.8	0.0	0.935	100.0
	Mineralogical composition (%) and module indices									
		C_3S=38.64; C_2S=41.03; C_3A=4.17; C_4AF=16.16; CaO/SiO_2=2.76; LSF=0.86; SR=2.15; AR=0.94								

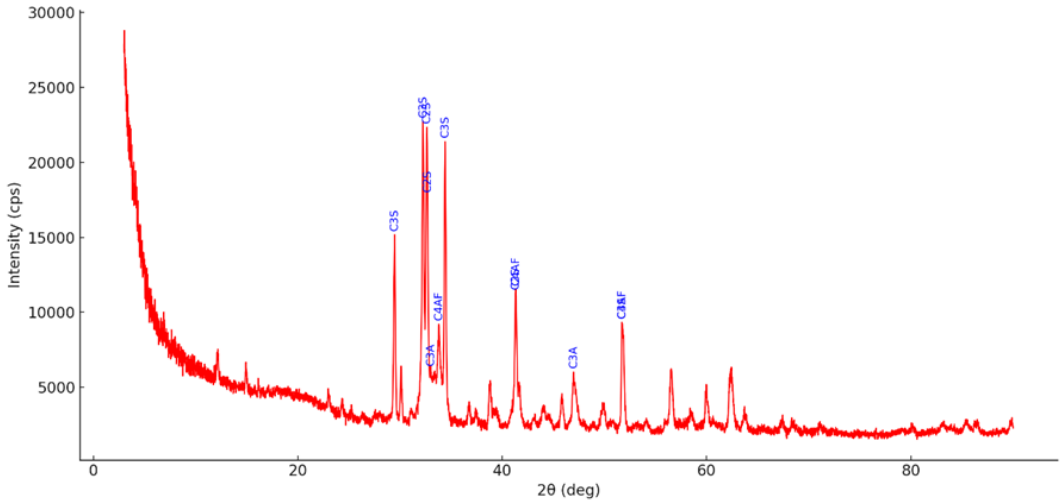

Figure 2 - XRD pattern of SRC clinker showing the main phases (C_3S, C_2S, C_3A, C_4AF)

Reducing the amount of tricalcium aluminate can reduce the expansion and erosion of cement in sulfate environments by 15–25%, resulting in increased long-term durability of structures. However, to maintain optimal modulus values, it is necessary to precisely control the firing temperature in the range of 1350–1450 °C, as well as the time of burning the clinker in the kiln. In future studies, it is proposed to study the mineralogy of the raw material mixture in depth, analyze the hydration kinetics, and conduct mechanical tests in order to improve the efficiency of the synthesized clinker. The chemical composition and phase structure of the clinker were evaluated by X-ray phase analysis along with tabular data. The XRD diffractogram showed clear peaks corresponding to the main crystal phases, the presence of which confirmed the results obtained by the Bogue method (Fig. 2). The strongest diffraction peaks observed between 2θ ≈ 29–34° and 51–52° indicate the dominance of the C_3S and C_2S phases.

The high content of alite and belite phases is an mportant factor determining the main mechanical properties of clinker. The Alite mineral, which makes up the mineralogical composition of clinker, actively participates in the early days of the hydration process, ensuring rapid hardening of the cement stone from the first days. Belite, on the other hand, exhibits a very slow hydration property compared to allite and serves to increase the long-term strength of the cement stone in the period of 28 days and beyond. The high content of these two phases is the main reason for the rapid and very high-quality mechanical strengthening of the cement.

The results of the above data were found to be in full agreement with the analysis of the X-ray diffractogram. The most intense diffraction peaks were recorded in the range of 2θ = 28–350 and 50–530, which were found to correspond to the alite (C_3S) and belite (C_2S) phases. These indicators confirm the quantitative data obtained from Bogue calculations. The peaks around 2θ = 32–340 and 480 correspond very well to the tricalcium aluminate phase (C_3A = 4.2%) and indicate that its content in the clinker is very low. The low content of tricalcium aluminate clearly indicates that it is an important factor in increasing sulfate resistance. The peaks observed at 2θ = 32–340, 41–420 and 520 also correspond to the tricalcium aluminoferrite phase (C_4AF = 16.2%), which is in full agreement with the results of chemical and mineralogical analyses.

The fact that free CaO is lower than the required standard indicates the efficiency of the synthesis process. These results scientifically justify the possibility of using the obtained sulfate-resistant Portland cement clinker in the production of sulfate-resistant cement in accordance with the standards of the Republic of Uzbekistan St 337:2024 and GOST 22266-2013.

Sulfate resistance tests conducted according to the ASTM C1012/C1012M standard showed significant differences in cement samples. The degree of expansion observed in a Na_2SO_4 solution for 28 days was directly related to the composition of the mineral phases of the cement (Table 3).

Table 3 - ASTM C1012 sulfate resistance test – 28-day results

Sample	Medium	Length (mm)
1.1	Distilled Water	16.1
1.2	Distilled Water	16.1
1.3	5% Na_2SO_4	16.1
2.1	Distilled Water	16.1
2.2	Distilled Water	16.1
2.3	5% Na_2SO_4	16.1
3.1	Distilled Water	16.0
3.2	Distilled Water	16.0
3.3	5% Na_2SO_4	16.0

The 28-day exposure results clearly show that the cement based on sulfate-resistant Portland cement clinker showed significantly higher durability than OPC (ordinary Portland cement) and blended cements (Figure 3).

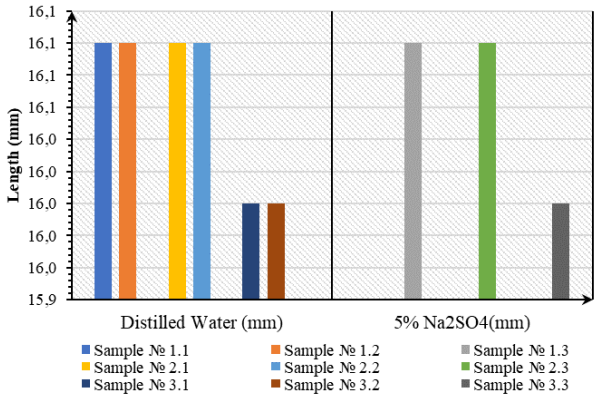

Figure 3 - Expansion of cement samples (SULFATE RESISTANT PORTLAND CEMENT, OPC, and blended cement) after 28 days of exposure to 5% Na_2SO_4 solution

First, the cement based on sulfate-resistant Portland cement clinker had the lowest expansion values. This is explained by the limited content of tricalcium aluminate in the composition (tricalcium aluminate ≤ 5%). Due to the low calcium aluminate, it reduces the reaction with sulfate ions and reduces the formation of excess ettringite or secondary gypsum. As a result, sulfate-resistant Portland cement exhibits long-term durability.

Second, ordinary Portland cement (OPC) showed high expansion. At the end of 28 days, the deformation values approached or exceeded the limit values specified in the ASTM C1012 standard. This is explained by the high content of three calcium aluminates in the OPC composition. Tricalcium aluminate actively reacts with sulfate ions, forming expansive ettringite.

Third, the mixed cements obtained from local raw materials showed lower expansion than OPC, but did not reach the level of sulfate-resistant Portland cement. This indicates that local mineral additives (kaolin, clay derivatives, iron-rich additives) have a partially limiting effect on the reaction with sulfate ions.

In general, experiments have shown that sulfate-resistant Portland cement, which can be produced in Karakalpakstan, has significantly higher resistance to sulfate-rich conditions - in particular, in the conditions of high-sulfate groundwater of the Aral Sea region - than ordinary Portland cement. These scientific results confirm the increased resistance of sulfate-resistant Portland cement to the effects of sulfate ions and its possible use as a promising construction material in aggressive environments.

Conclusions

This study comprehensively assessed the feasibility of producing sulfate-resistant Portland cement clinker from local raw materials in Karakalpakstan, specifically limestone, barren sand, kaolin, and iron-containing industrial waste. This represents a new use for regionally available resources, which have not previously been explored in combination for this purpose.

Chemical analysis confirmed that the raw mix achieved an optimal oxide balance of CaO, SiO2, Al2O3, and Fe2O3, resulting in modulus values (LSF = 0.82; SR = 2.15; AR = 0.94) fully compliant with standard regulatory requirements for sulfate-resistant Portland cement clinker. The significant belite content is particularly significant, as C2S promotes long-term strength development and a reduction in the heat of hydration—properties particularly beneficial in sulfate-resistant systems. Critically, the tricalcium aluminate (C3A ≈ 4.2%) content remained below the 5% regulatory threshold, which is the primary mineralogical basis for sulfate resistance. The increased C4AF content, achieved through the intentional inclusion of iron-rich industrial waste, further enhanced clinker stability.

X-ray diffraction analysis, consistent with Bogue's calculations, confirmed that the free lime content (0.32%) was significantly below the regulatory level, indicating that the clinkerization process was complete and thermally efficient.

Sulfate resistance tests conducted in accordance with ASTM C1012/C1012M demonstrated clear differences in performance between cement types. Ordinary Portland cement demonstrated the highest expansion (approaching the standard limit after 28 days), the blended cements yielded intermediate results, and the sulfate-resistant Portland cement clinker synthesized in this study achieved the lowest expansion value, confirming its excellent resistance to sulfate attack. The exact expansion values for all cement types tested are presented in Table 3.

In conclusion, sulfate-resistant Portland cement clinker of standard quality can be successfully synthesized from local raw materials from Karakalpakstan, with optimized modulus values specifically tailored to the mineral properties of these regional resources. The use of iron-containing industrial waste as a corrective additive not only met the compositional requirements but also facilitated the recycling of industrial waste, reduced dependence on primary raw material extraction, and minimized emissions associated with the transportation of imported raw materials. These results demonstrate both the technical viability and the environmental and economic benefits of localized sulfate-resistant cement production.

Conflicts of interest. On behalf of all authors, the corresponding author states that there is no conflict of interest.

CRediT author statement: **A. Khadzhiev**: Conceptualization, Methodology, Software; **A. Khadzhiev**: Data curation, Writing draft preparation; **L Wang**: Visualization, Investigation; **F. Atabaev**: Supervision; **N. Makhsudova**: Software, Validation; **E. Atashev**: Reviewing and Editing.

Acknowledgements. We express our deep gratitude to **Atabaev Farrukh Bakhtiyarovich**, Chief Scientific Researcher at the "STROM" Research Laboratory and Testing Center of the Institute of General and Inorganic Chemistry of the Academy of Sciences of Uzbekistan, for his practical assistance in conducting the experiments for this research. We also extend our sincere appreciation to **Jumaniyazov Arslon G'anibek o'g'li** for his support in translation and language-related matters, as well as to the co-authors for their contributions to the writing and editing of the article.

Formatting of funding sources. This research did not receive any specific grant from funding agencies in the public, commercial, or not-for-profit sectors.

Cite this article as: Khadzhiev ASh, Wang L, Atabaev FB, Makhsudova ND, Atashev EA. Technological, economic and environmental aspects of the production of sulfate-resistant Portland cement clinker based on the mineral resources of Karakalpakstan. Kompleksnoe Ispolzovanie Mineralnogo Syra = Complex Use of Mineral Resources. 2028; 345(2):84-94. https://doi.org/10.31643/2028/6445.18

Қарақалпақстанның минералдық ресурстары негізінде сульфатқа төзімді портландцемент клинкерін өндірудің технологиялық, экономикалық және экологиялық аспектілері

[1]Хаджиев А.Ш., [2]Wang L., [3]Атабаев Ф.Б., [3]Махсудова Н.Ж., [1]Аташев Э.А.

[1] Әбу Райхон Бируни атындағы Ургенч мемлекеттік университеті, Ургенч, Өзбекстан
[2]Чжэцзян университеті, Энергетикалық инженерия колледжі, Ханчжоу, Қытай
[3]Өзбекстан Республикасы Ғылым академиясы Жалпы және бейорганикалық химия институты, Ташкент

Мақала келді: *1 желтоқсан 2025*
Сараптамадан өтті: *20 мамыр 2026*
Қабылданды: *10 маусым 2026*

Бұл зерттеу Өзбекстан Республикасының Арал теңізі өңірінен табылған жергілікті шикізат негізінде сульфатқа төзімді портландцемент клинкерін өндіруге және оның қасиеттерін зерттеуге арналған. Алынған нәтижелер технологиялық, экономикалық және экологиялық артықшылықтарды көрсетеді. Шикізат қоспалары әктас, құнарсыз құм, каолин және темірге бай өндірістік қалдықтардан тұрды, нәтижесінде оңтайландырылған оксидті құрамы бар клинкер алынды (LSF = 0,82, SR = 2,15, AR = 0,94). Рентгендік фазалық талдау жоғары механикалық беріктікті қамтамасыз ететін алит (C_3S ≈ 38,6%) және белит (C_2S ≈ 41,0%) фазаларының жоғары құрамын көрсетеді. Үшкальций алюминатының төмен мөлшері (үшкальций алюминатының < 5%) және ферриттің жеткілікті мөлшері (C_4AF ≈ 16,2%) сульфатқа төзімділігі мен фазалық басымдылығын арттырды. ASTM C1012/C1012M стандартына сәйкес жүргізілген сульфатқа төзімділік сынақтары сульфатқа төзімді портландцементтің 5% Na_2SO_4 ерітіндісіне салынған үлгілер арасында ісіну индексінің ең

	төмен екенін көрсетті, бұл қарапайым портландцемент пен аралас цемент түрлерімен салыстырғанда оның жоғары төзімділігін дәлелдеді. Алынған нәтижелер жергілікті шикізат негізінде сульфатқа төзімді жоғары сапалы портландцемент клинкерін шығаруға және оның Орал өңірінің сульфатқа бай жағдайларына жарамдылығын көрсетуге мүмкіндік береді. Экономикалық тұрғыдан жергілікті шикізатты пайдалану өндіріс шығындарын азайтады, импортқа қажеттілікті азайтады, цемент өнеркәсібінің бәсекеге қабілеттілігін арттырады. Экологиялық тұрғыдан алғанда, сульфатқа төзімді портландцементтің ұзақ қызмет ету мерзімі және өнеркәсіптік қалдықтарды пайдалану жасыл экономикаға сәйкес келеді, қалдықтарды азайтуға көмектеседі және тұрақты дамуға ықпал етеді.
	Түйінді сөздер: сульфатқа төзімді портландцемент, клинкер синтезі, минералды ресурстар, сульфатқа төзімділік, жасыл экономика, тұрақтылық.
Хаджиев Азамат Шамуратұлы	***Авторлар туралы ақпарат:*** *Техника ғылымдары бойынша философия докторы (PhD), Ургенч мемлекеттік университеті, Абу Райхон Беруни атындағы университеттің Химиялық технология факультетінің доценті, 220100, Х. Олимжон көшесі, 14, Ургенч, Өзбекстан. Email: xadjiyev2019@mail.ru; ORCID ID: https://orcid.org/0000-0003-2131-8256*
Lei Wang	*Профессор, Энергетикалық инженерия колледжі, Чжэцзян университеті, Ханчжоу, Чжэцзян, Қытай Халық Республикасы. Email: wanglei.leo@zju.edu.cn; ORCID ID: https://orcid.org/0000-0002-0336-7241*
Атабаев Фаррух Бахтияруллы	*Техника ғылымдарының докторы, профессор, Өзбекстан Ғылым академиясының Жалпы және бейорганикалық химия институтының жанындағы STROM ғылыми-зерттеу зертханасының бас ғылыми қызметкері, Ташкент, Өзбекстан. Email: atabaev_farruh@mail.ru; ORCID ID: https://orcid.org/0009-0004-4941-5060*
Махсудова Нозима Жапарханқызы	*PhD, кіші ғылыми қызметкер, Өзбекстан Ғылым академиясының Жалпы және бейорганикалық химия институтының жанындағы STROM ғылыми-зерттеу зертханасы мен сынақ орталығы, Ташкент, Өзбекстан. Email: nazima-25@mail.ru; ORCID ID: https://orcid.org/0000-0003-4579-6551*
Аташев Элёр Аташевич	*Техника ғылымдары бойынша философия докторы, Әбу Райхон Беруни атындағы Үргеніш мемлекеттік университетінің химия-технология факультетінің доценті, 220100, Х.Олимжон, 14, Үргеніш, Өзбекстан. Email: elyor.a@urdu.uz; ORCID ID: https://orcid.org/0000-0003-4070-5665*

Технологические, экономические и экологические аспекты производства сульфатостойкого портландцементного клинкера на основе минеральных ресурсов Каракалпакстана

[1]Хаджиев А.Ш., [2]Wang L., [3]Атабаев Ф.Б., [3]Махсудова Н.Ж., [1]Аташев Э.А.

[1] Ургенчский государственный университет имени Абу Райхона Беруни, Ургенч, Узбекистан
[2] Чжэцзянский университет, Колледж энергетического машиностроения, Ханчжоу, Китай
[3]Институт общей и неорганической химии Академии наук Узбекистана, Ташкент

Поступила: *1 декабря 2025*
Рецензирование: *20 мая 2026*
Принята в печать: *10 июня 2026*

АННОТАЦИЯ

Данное исследование посвящено получению сульфатостойкого портландцементного клинкера на основе местного сырья, обнаруженного в регионе Аральского моря Республики Узбекистан, и изучению его свойств. Полученные результаты подчеркивают технологические, экономические и экологические преимущества. В качестве сырьевых смесей использовались известняк, пустые пески, каолин и богатые железом промышленные отходы, что позволило получить клинкер с оптимизированным оксидным составом (LSF = 0,82, SR = 2,15, AR = 0,94). Рентгенофазовый анализ показывает высокое содержание фаз алита (C_3S ≈ 38,6%) и белита (C_2S ≈ 41,0%), что обеспечивает высокую механическую прочность. Низкое содержание трикальцийалюмината (трикальцийалюминат < 5%) и достаточное содержание феррита (C_4AF ≈ 16,2%) повысили сульфатостойкость и фазовое доминирование. Испытания на сульфатостойкость, проведенные в соответствии со стандартами ASTM C1012/C1012M, показали, что сульфатостойкий портландцемент имел самый низкий индекс набухания среди образцов, помещенных в 5% раствор Na_2SO_4, что подтверждает его высокую стойкость по сравнению с обычным портландцементом и смешанными видами цемента. Полученные результаты открывают возможность производства высококачественного сульфатостойкого портландцементного клинкера на основе местного сырья и демонстрируют его пригодность для условий региона Орал с высоким содержанием сульфатов. С экономической точки зрения использование местного сырья снижает производственные затраты, уменьшает потребность в импорте и повышает конкурентоспособность цементной промышленности. С экологической точки зрения длительный срок службы сульфатостойкого портландцемента и использование промышленных отходов совместимы с «зеленой» экономикой, способствуют сокращению отходов и устойчивому развитию.

Ключевые слова: сульфатостойкий портландцемент, синтез клинкера, минеральные ресурсы, сульфатостойкость, зелёная экономика, устойчивое развитие.

Хаджиев Азамат Шамуратович	***Информация об авторах:*** *Доктор философии в области технических наук, доцент факультета химической технологии Ургенчского государственного университета имени Абу Райхона Беруни, 220100, улица Х. Олимжона, 14, Ургенч, Узбекистан. Email: xadjiyev2019@mail.ru; ORCID ID: https://orcid.org/0000-0003-2131-8256*
Lei Wang	*Профессор, Колледж энергетического машиностроения, Чжэцзянский университет, Ханчжоу, Чжэцзян, Китайская Народная Республика. Email: wanglei.leo@zju.edu.cn; ORCID ID: https://orcid.org/0000-0002-0336-7241*
Атабаев Фаррух Бахтиярович	*Доктор технических наук, профессор, главный научный сотрудник научно-исследовательской лаборатории STROM при Институте общей и неорганической химии Академии наук Узбекистана, Ташкент, Узбекистан. Email: atabaev_farruh@mail.ru; ORCID ID: https://orcid.org/0009-0004-4941-5060*
Махсудова Нозима Джапархановна	*PhD, младший научный сотрудник Научно-исследовательской лаборатории и испытательного центра STROM при Институте общей и неорганической химии Академии наук Узбекистана, Ташкент, Узбекистан. Email: nazima-25@mail.ru; ORCID ID: https://orcid.org/0000-0003-4579-6551*
Аташев Элёр Аташевич	*Доктор философии в области технических наук, доцент факультета химической технологии Ургенчского государственного университета имени Абу Райхона Беруни, 220100, улица Х. Олимжона, 14, Ургенч, Узбекистан. Email: elyor.a@urdu.uz; ORCID ID: https://orcid.org/0000-0003-4070-5665*

References

[1] Sharma A, & Chaudhary S. Time-resolved rheological characterization of cement paste using a distinct shear protocol: Quantifying thixotropic and hydration-driven structuration. Innovative Infrastructure Solutions. 2025; 10:487. https://doi.org/10.1007/s41062-025-02273-7

[2] Mehta PK, & Monteiro PJM. Concrete: Microstructure, Properties, and Materials (4th ed.). McGraw-Hill, New York. 2014, 704.

[3] Thomas M. Supplementary Cementing Materials in Concrete. CRC Press, Boca Raton. 2013, 208. https://doi.org/10.1201/b14493

[4] Shao Y, Chen X, & Li W. Study on the preparation and sulfate resistance of Portland cement clinker with the high Fe/Al ratio of ferrite phase. Cement and Concrete Composites. 2022; 134:104699. https://doi.org/10.1016/j.cemconcomp.2022.104699

[5] Labidi I. Optimization of sulfate resistant Portland cement raw mixes. Journal of Building Materials and Structures. 2017; 4(1):53–61.

[6] Labidi I, Megriche A, & Benazzouk S. Natural resources exploitation in sulfate-resisting Portland cement manufacturing. Frontiers in Chemistry. 2022; 10:806433. https://doi.org/10.3389/fchem.2022.806433

[7] Khalifa SA, & AlSadig DY. Adjustment of clinker raw mix design to produce sulfate resisting cement. International Journal of Trend in Research and Development. 2017; 4(5):187–193.

[8] Costa ARD, Figueiredo M, & Canda L. Thermodynamic modelling of the clinkering process in sulfate resistant cements. Scientific Reports. 2023; 13:16542. https://doi.org/10.1038/s41598-023-44078-7

[9] Santhanam K, Cohen MD, & Olek J. Mechanism of sulfate attack: Part I. Experimental study. Cement and Concrete Research. 2002; 32(6):915–921. https://doi.org/10.1016/S0008-8846(02)00724-X

[10] Santhanam K, Cohen MD, & Olek J. Mechanism of sulfate attack: Part II. Numerical simulation. Cement and Concrete Research. 2003; 33(3):341–346. https://doi.org/10.1016/S0008-8846(02)00925-6

[11] Whittaker M, Black J, & Jones S. A review of external sulfate attack in concrete. Advances in Cement Research. 2015; 27(9):519–529. https://doi.org/10.1680/adcr.14.00089

[12] González MA, Ros F, & Blanco MT. The effect of limestone filler on the sulfate resistance of low C_3A Portland cements. Cement and Concrete Research. 1998; 28(11):1653–1667. https://doi.org/10.1016/S0008-8846(98)00144-1

[13] Higgins DD. The use of ground granulated blastfurnace slag to improve the sulfate resistance of concrete. Cement and Concrete Composites. 2003; 25(8):913–919. https://doi.org/10.1016/S0958-9465(03)00148-3

[14] Abubaker F. Long-term durability of concrete in sulfate environment: Role of sulfate resisting Portland cement. Construction and Building Materials. 2014; 72:272–278. https://doi.org/10.1016/j.conbuildmat.2014.10.079

[15] Martínez Infante MA, Rosales J, & Morón MA. Sulfate-resistant clinker based cement with new secondary main constituents: Technical, economic and environmental assessment. Buildings. 2025; 15(3):479. https://doi.org/10.3390/buildings15030479

[16] Tiburzi NB, Le Saout P, & Damidot D. Performance of portland-limestone cements with supplementary cementitious materials in sulfate exposure. Construction and Building Materials. 2019; 220:187–197. https://doi.org/10.1016/j.conbuildmat.2019.06.009

[17] Neto R, Cincotto A, & Fernandes L. Influence of sulfates on the hydration and durability of Portland cement systems. Construction and Building Materials. 2021; 302:122188. https://doi.org/10.1016/j.conbuildmat.2021.122188

[18] Khadzhiev A, Atabaev F, & Tursunova G. Influence of sandstone on physical and chemical processes of interaction of components and genetic formation of cement composite. E3S Web of Conferences. 2024; 563:02027. https://doi.org/10.1051/e3sconf/202456302027

[19] Iskandarova M, Atabaev F, Tursunova G, Tursunov Z, Khadzhiev A. Composite Portland cements: Innovations and future directions in cement technology. Innovative Infrastructure Solutions. 2025. https://doi.org/10.1007/s41062-025-02067-x

[20] Iskandarova MI, Atabaev FB, Khadzhiev AS. Utilization of natural silicate rocks to reduce the carbon footprint in the cement industry. Kompleksnoe Ispolzovanie Mineralnogo Syra = Complex Use of Mineral Resources. 2026; 338(3):40–50.

https://doi.org/10.31643/2026/6445.27

[21] Khadzhiev A, Abdullaev M, Yakubov Y, Jumaniyozov J. The effect of hybrid mineral additives on the genetic formation and physico-chemical processes of cement composites. E3S Web of Conferences. 2025; 633:08003. https://doi.org/10.1051/e3sconf/202563308003

[22] Atabaev FB, Aripova MKh, Khadzhiev ASh, Tursunova GR, Tursunov ZR. Effect of multicomponent mineral additives on the microstructure and strength of composite cement. Kompleksnoe Ispolzovanie Mineralnogo Syra = Complex Use of Mineral Resources. 2025; 1(322):45–57. https://doi.org/10.31643/2027/6445.05

[23] Khadzhiev A, & Atabaev F. Influence of silica-containing additives on physical and mechanical properties of Portland Cement Co. Ltd Karakalpaksement. E3S Web of Conferences. 2023; 401:05051. https://doi.org/10.1051/e3sconf/202340105051

[24] Buriev AI, Iskandarova MI, & Begzhanova GB. Influence of a high degree of filling on the properties of pozzolanic cement. RA Journal of Applied Research. 2023; 9(2):60–65. https://doi.org/10.47191/rajar/v9i2.02

[25] Buranova D. Main characteristics of quartz-feldspar sands from the Khiva deposit, and the physico-chemical and technological fundamentals of obtaining an enriched concentrate. *Kompleksnoe Ispolzovanie Mineralnogo Syra = Complex Use of Mineral Resources.* 2025; *340*(1):37–44. https://doi.org/10.31643/2027/6445.04

[26] Bagdaulet B, & Aitkulov N. Application of regional mineral resources for the synthesis of sulfate resisting cements. Kompleksnoe Ispolzovanie Mineralnogo Syra = Complex Use of Mineral Resources. 2023; 4:33–42. https://doi.org/10.31643/2023/6445.18

[27] Xalimbetov F B, & Reyimberdiyev B A. The role of innovative entrepreneurship in the digital economy. Tashkent State University of Economics. 2021; 85:53–58.

[28] Xalimbetov F B. Development of small business and private entrepreneurship in Uzbekistan: Problems and solutions. Tashkent State University of Economics. 2020; 1509:40–45.

[29] O‘zM St 337:2024. Sulfatga chidamli portlandsement. Texnik shartlar [Sulfate-resistant Portland cement. Technical conditions]. O‘zbekiston milliy standarti. (in Uzb.). 2024.

[30] GOST 22266-2013. Sulfatstoykiy portlandtsement i shlakoportlandtsement. Tekhnicheskiye usloviya [Sulfate-resistant Portland cement and slag Portland cement. Technical conditions]. Mezhgosudarstvennyy standart. 2013. https://meganorm.ru/Data/592/59275.pdf.

[31] ASTM International. ASTM C1012/C1012M–24: Standard Test Method for Length Change of Hydraulic-Cement Mortars Exposed to a Sulfate Solution. West Conshohocken, PA: ASTM International. 2024. https://www.astm.org/c1012_c1012m-24.html

Crossref
DOI: 10.31643/2028/6445.19
Mining & Mineral Processing

Mathematical modeling and ecological assessment of fluoride release in a mixture of mineralized phosphorite waste and wastewater from the fat and oil industry

[1]Kurambayev Sh.R., [1]Qodirova S.R., [1*]Achilova S.S., [1]Ollaberganova A.M., [1]Abdullayeva F.B., [2]Matmuratov A.A.

[1]Urgench State University named after Abu Rayhon Biruni, Uzbekistan
[2]Mamun university, Khiva, Uzbekistan

Corresponding author email: sanobar.a@urdu.uz

Received: *December 25, 2026*
Peer-reviewed: *January 27, 2026*
Accepted: *June 11, 2026*

ABSTRACT

This study investigates fluoride loss in a mixture of mineralized mass (MM) extracted from the Central Kyzylkum phosphorite deposits and acidic wastewater (AWW) generated by the fat-and-oil industry. The research aimed to evaluate fluoride release and its retention stability under various conditions. Experimental trials were conducted using AWW:MM mass ratios ranging from 100:10 to 100:40. The experiments were carried out at 333 K for 30 minutes, employing ionometric analysis. The theoretical fluoride content varied from 1.23 g to 4.90 g, while the experimental values ranged from 0.88 g to 3.68 g. The lowest fluoride loss was observed at the 100:20 ratio, amounting to 0.34 g. The highest loss, 1.22 g, was recorded at the 100:40 ratio. The 100:25 ratio (pH 5.90), with a fluoride loss of 0.40 g and an experimental retention of 2.66 g, was identified as optimal. At pH values between 6.33 and 7.30, fluoride levels stabilized between 3.08 g and 3.68 g. An exponential regression model demonstrated a high degree of correlation (R^2 = 0.9767). The standard deviation ranged from ±0.002 g to ±0.008 g. Ions in AWW (SO_4^{2-}: 48,145 mg/L and Cl^-: 38,116 mg/L) significantly accelerated fluoride volatilization. The emission of HF gas contributed to atmospheric pollution; however, the 100:25 ratio minimized environmental impact. The results aligned with literature-reported fluoride loss ranges of 0.3–1.5 g. This research contributes to the development of effective and environmentally safe approaches to waste reutilization.

Keywords: fluoride loss, pH value, Ionometric analysis, exponential regression, mineralized mass, acidic wastewater.

Information about authors:

Kurambayev Sherzod Raimbergenovich — *Doctor of Technical Sciences, Dean of the Faculty of Chemical Technology, Urgench State University named after Abu Rayhon Biruni, 220100, H. Olimjon Street 14, Urgench, Uzbekistan. Email: sherzod.k@urdu.uz; ORCID ID: https://orcid.org/0009-0003-3986-5079*

Qodirova Soxiba Ravshanbek qizi — *Teacher, doctoral student of the Faculty of Natural and Agricultural Sciences of the Urganch State University named after Abu Rayhan Beruni, 14 H. Olimjon Street, 220100, Urganch, Uzbekistan. Email: sohibaazamat2015@gmail.com; ORCID ID: https://orcid.org/0009-0008-4762-0262*

Achilova Sanobar Sobirovna — *Doctor of Philosophy in Technical Sciences, Associate Professor at the Faculty of Chemical Technology, Urgench State University named after Abu Rayhon Beruni, 220100, H. Olimjon Street 14, Urgench, Uzbekistan. Email: sanobar.a@urdu.uz; ORCID ID: https://orcid.org/0000-0003-4691-0248*

Ollaberganova Aziza Matyokubovna — *Doctor of Philosophy in Technical Sciences, Associate Professor at the Faculty of Chemical Technology, Urgench State University named after Abu Rayhon Beruni, 220100, H. Olimjon Street 14, Urgench, Uzbekistan. Email: shamuratovsx@gmail.com*

Abdullayeva Feruza Bayjon qizi — *Doctor of Philosophy in Technical Sciences, Associate Professor at the Faculty of Chemical Technology, Urgench State University named after Abu Rayhon Beruni, 220100, H. Olimjon Street 14, Urgench, Uzbekistan. Email: abdullayevafeya1996@gmail.com; ORCID ID: https://orcid.org/0000-0003-1490-4900*

Matmuratov Azizbek Abdikarimovich — *Doctor of Philosophy in Pedagogical Sciences, Associate Professor at the Department of Pedagogical Sciences, Mamun university, 220900, Bol-Khovuz Street 2, Qibla Tozabog MCG, Khiva, Uzbekistan. Email: my_darling90@mail.ru; ORCID ID: https://orcid.org/0009-0007-4177-3738*

Introduction

Extensive mining and processing of phosphorite rock produce a substantial amount of waste. This waste material also has strong biological capacity and does not convert into a passive substance for a rather extended period of time. Acid wastewater from the fat and oil industry is highly ionized, creating a real danger of pollution of soils and water sources. If the wastewater and mineral waste are separated, the interaction of the combined chemical properties of the two is not understood. This

approach to waste utilization is presently changing in the direction of processing individual wastes together in order to be able to treat the interaction of the two. It is important to investigate the amount of fluoride fixed and liberated into the combined waste products. The physicochemical properties of fluoride are highly sensitive to the components of ionic agents and pH conditions [[1], [2], [3], [4], [5]].

The Central Kyzylkum phosphorite ores have been generating significant low-grade phosphorite waste over the years. Although these wastes appear to be physically stable, they still contain reactive substances such as fluoride, sulfates, and carbonates that can potentially vary through natural weathering. Reaction to rainwater, wind, and solar exposure alters the topological geochemistry of the waste, and geochemical analysis has shown that the concentration of fluoride is high around the waste storage areas [[6], [7], [8], [9]]. Moreover, the presence of finer dust particles in dry environments leads to aerial suspension of the dust particles that is potentially inhalable by the nearby population. These waste substances should therefore not be classified as non-reactive but as potentially reactive technogenic waste that warrants regulation and follow-up treatment strategies [[10], [11], [12]].

In the processes of neutralization and saponification, the fat and oil industry produces a strongly acidic soapstock wastewater (AWW), which always has a pH level below 4 [[13], [14], [15]] The resulting wastewater is rich in anions (SO_4^{2-}, Cl^-, NO_3^-) and cations (Na^+, Mg^{2+}, NH_4^+, Ca^{2+}), a fact that makes it a complex electroactive solution [[16], [17], [18]]. Due to its acidity and higher ions concentration, AWW strongly reacts with other wastes rich in phosphates: Ion exchange, dissolution, and surface-related adsorption phenomena can release fluoride ions, which were unavailable prior to the interaction [[19], [20], [21]]. Generally, the soapstock wastewater can be seen as a reactive effluent rather than a passive one, and it can alter the physicochemical conditions of other wastewaters produced by the industry. In fact, a comprehensive understanding of the soapstock wastewater chemistry is very important for the precise modeling of the behavior of the complex samples of industrial wastes [[22], [23]].

When mineralized mass (MM) and AWW are combined, an intensely reactive dispersion is formed, wherein chemical transformations proceed rapidly. The high acidity of AWW—driven by ions such as H^+, SO_4^{2-}, and Cl^-—can disrupt the ionic balance of structurally bound inorganic fluoride compounds in MM. Fluoride in MM typically exists in relatively stable crystalline phases, such as fluorapatite and cryolite, but their stability decreases sharply at low pH. Under protonation conditions, fluoride minerals undergo partial decomposition, thereby facilitating the conversion of fluoride into ionic or gaseous forms such as *HF* [[6], [12]] (Figure 1).

This process is kinetically governed by acidity level, temperature, and the ionic strength of the reactive medium. Notably, the ion-exchange capacity and complexation potential of sulfate and chloride anions significantly enhance the system's reactivity. The mineralized structure of the MM (mineralized mass) undergoes transformation in acidic environments, particularly in terms of porosity and surface activity. Under such conditions, fluoride components dissociate from the crystalline lattice and transition into mobile forms. The phase recrystallization and surface ion migration induced by interaction with AWW directly influence the residual fluoride content in the final product. In such

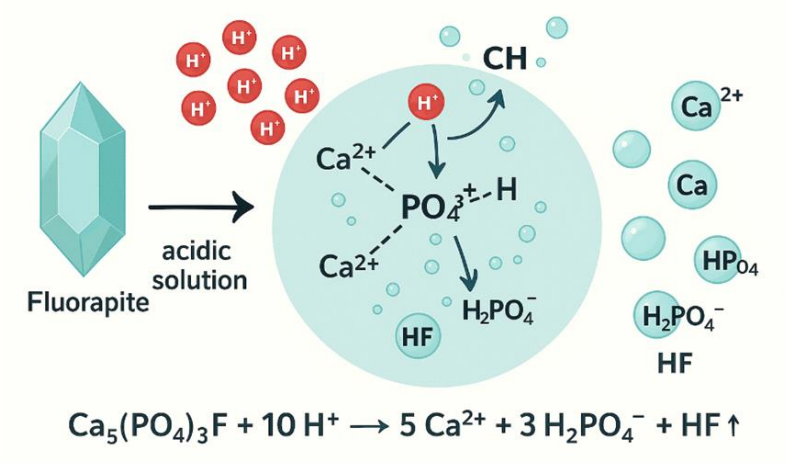

Figure 1 - The decomposition process of fluorapatite ($Ca_5(PO_4)_3F$) in acidic solution

mixed systems, the retention or mobilization of fluoride depends functionally on ionic strength, pH of the medium, and reaction duration. Mathematical modeling enables theoretical interpretation of these conditions and introduces a predictive approach to managing the transformation process. Furthermore, the reactions occurring in AWW-MM mixtures should not be viewed as simple physical interactions, but rather as complex, thermodynamically and kinetically controlled phase transformations. The portion of fluoride retained in the product—without volatilizing into the gaseous phase—can be determined based on mass changes, pH gradients, and the kinetics of dissociation. Such combined systems transition waste into an activated reactive structure, thus enabling controlled environmental risk management. The reactive integration of MM and AWW represents a scientifically grounded direction for the development of alternative waste neutralization technologies [[24], [25], [26], [27]].

The primary objective of this study was to experimentally determine the amount of fluoride retained in the final product derived from MM and AWW mixtures, and to evaluate its loss by comparing experimental results with theoretical calculations. The theoretical amount of fluoride was calculated from the original chemical composition of the waste, and the gap between this value and the measured content in the final product indicated the degree of fluoride release or transfer. In the experiments, mixtures of mineralized mass (MM) and acidic wastewater (AWW) were exposed to controlled conditions of temperature, duration, and mass ratio to reproduce a reactive environment. After processing, the fluoride concentration in the material was determined through analytical techniques and used as a key parameter in modeling. This approach made it possible to identify the main chemical factors influencing whether fluoride was retained or lost in the system. Within the modeling framework, variations in fluoride levels were mathematically related to pH, ionic strength, and mixing proportions. The findings offered a clearer understanding of how fluoride-containing waste undergoes reactive transformations under environmentally relevant conditions.

This research systematically examined ion exchange, phase structure alteration, and component mobility within a reactive medium generated through combined treatment of industrial waste streams. The methodology was grounded in a concept of transforming dual-source waste into an environmentally safe form via chemically activated transformation. This approach redefined the waste materials not as passive inert residues but as chemically reactive substrates. The behavior of fluoride-containing compounds—particularly the dynamic changes arising from pH gradients and ionic strength—was mathematically described through modeling. The methods of conversion of stable fluoride forms into free ions and further retention or release of the ions within the system have been examined using analytical methods. Thus, it has become possible to develop a model based on the physicochemical properties of the substance in relation to ecological risk levels to make technological waste management even more sustainable.

Experimental part

The main focus of this study was on industrial wastes characterized by varied chemical compositions and a high tendency to react.

The first object was MM obtained from the phosphorite deposits of the Central Kyzylkum region. Its composition includes 15.09% P_2O_5, 43.17% CaO, 1.22% Al_2O_3, 1.34% Fe_2O_3, and 1.21% MgO. Additionally, the material contains 1.7% fluoride, 14.01% carbonate compounds, and 2.17% sulfates. The fluoride is primarily bound in the form of fluorapatite, which is highly reactive in acidic environments [[15], [16], [17], [18], [19]].

The second object was AWW generated from technological processes at the “Urganch yog-moy” JSC. The AWW contained 100 mg/L H^+, 43,158 mg/L Na^+, 38,116 mg/L Cl^-, 48,145 mg/L SO_4^{2-}, 1,824 mg/L Mg^{2+}, and 300 mg/L Ca^{2+}. In addition, it included 20.01 mg/L NO_2^-, 840 mg/L NO_3^-, 3,446 mg/L HCO_3^-, 100 mg/L NH_4^+, 30 mg/L Fe^{2+}, and 0.3 mg/L Fe^{3+}. This solution formed a strongly acidic medium with a total ionic strength of 2,148.08 mg-equiv/L and a pH range of 2.1–2.5. The ionic composition of AWW triggers stepwise ion-exchange reactions with the structurally bound fluoride in MM [[15], [16], [17], [18], [19]].

Mixtures of AWW and MM were prepared in mass ratios ranging from 100:10 to 100:40, mixed under a reaction medium at 333 K for 30 minutes. Each mixture was subsequently dried at 353 K to form a solid phase, crushed into powder, and analyzed for residual fluoride content. The interaction of acidic ions with fluoride components in MM promotes fluoride migration and

decomposition in the reactive medium. Furthermore, the increase in pH from 4.10 to 7.30 following the reaction indicates the occurrence of partial neutralization. Owing to their chemical complexity and high reactivity, these two waste streams serve as an excellent laboratory model system for studies on waste recycling, environmental safety, and mathematical modeling. Within such systems, fluoride transformation behavior, decomposition kinetics, and ion equilibrium parameters can be thoroughly investigated.

After drying, the residual fluoride content in powder samples of AWW–MM mixtures was measured using an ion-selective electrode method with a portable ionometer device, calibrated in accordance with the manufacturer's instructions (produced in the Russian Federation).

To enable solubilization of fluoride ions, each powder sample was extracted in a 1:10 ratio with distilled water. The prepared solutions were kept at 20–25 °C for a minimum of 30 minutes to allow the ion balance to reach stability. Subsequent measurements were performed in a buffered medium with a pH of about 5.0–5.5, ensuring that only free and reactive forms of fluoride were detected. The ionometer was calibrated prior to each measurement using standard fluoride solutions of 0.1, 1.0, and 10 mg/L concentrations.

During analysis, the actual fluoride concentration in mg/L was displayed directly on the device screen. Each sample was measured in triplicate, and the arithmetic mean was calculated along with standard deviation to assess analytical precision.

To complete the fluorine material balance and experimentally confirm the transition of fluoride into the gas phase, an additional set of experiments was conducted using a gas absorption method. The experimental setup was supplemented with a fluoride gas trapping system designed to capture hydrogen fluoride (HF) released during the interaction between acidic wastewater (AWW) and mineralized mass (MM).

The reaction was carried out in a sealed glass reactor equipped with a gas outlet. The outlet was connected to a two-stage absorption unit. The first absorber contained 0.1 M NaOH solution, intended for quantitative absorption of HF according to the reaction:

$$HF + NaOH \rightarrow NaF + H_2O$$

The second absorber contained distilled water to capture residual fluoride species and possible aerosol-bound fluorine. All connections were made using chemically resistant tubing to prevent fluoride losses.

Blends of AWW and MM were also synthesized at mass ratios of 100:10 to 100:40. These mixtures were then allowed to react for 30 minutes at 333 K, the same as those in the main experiment. During the reaction process, the gas produced was channeled through the absorption system under natural gas pressure without forced gas flow. Once the experiment was completed, the absorber solution was allowed to stabilize for 30 minutes under room temperature.

The concentration of fluoride in the absorption solutions was analyzed using an ion-selective electrode analysis technique. Before carrying out the test, the NaOH absorber solution was first made to have a pH of 5.0 to 5.5 using a diluted hydrochloric acid. The calibration was carried out using a standard fluoride solution with a concentration of 0.1, 1.0, and 10.0 mg/L. The experiment was done in triple replication.

The amount of fluorine transferred to the gas phase, F_{gas}, was calculated using the measured fluorine concentration, as well as the volume of the absorption solution. This amount was then employed to calculate a complete fluorine material balance via the equation:

$$F_{total} = F_{solid} + F_{liquid} + F_{gas}$$

Where: F_{solid} = residual fluoride in dried solid product, F_{liquid} = fluoride in liquid phase, F_{gas} = fluoride captured in absorption system.

This allowed an experimental distinction to be made between loss of fluoride due to volatilization of HF gas and losses retained within the solid phase or carrier liquid. In addition, gas absorption, as a quantitative gas capture process, ensured that gas phase fluoride was quantified accurately, and this had an impact on improving calculations related to fluorine balance.

This method is distinguished by its rapidity, sensitivity, and low measurement error. The ion-selective electrode approach offers a reliable means of quantifying reactive fluoride, evaluating its retention, and assessing ecological risk levels.

The theoretical fluoride content in MM was calculated based on the mass fraction of structurally bound fluoride. In this study, calculations were performed assuming complete presence of fluoride in the form of fluorapatite ($Ca_5(PO_4)_3F$). For each mixture with a defined mass of MM (m_{MM}), the

theoretical mass of fluoride (m_F) was determined using the following equation:

$$m_F = m_{MM} \cdot \frac{\omega_F}{100}$$

Where:

m_F — theoretical fluoride mass (g),

m_{MM} — mass of mineralized mass used in the mixture (g),

ω_F — mass fraction of fluoride in the mineralized mass (%).

The amount of substance (n_F) of fluoride corresponding to the theoretical mass was then calculated using the molar mass of fluoride:

$$n_F = \frac{m_F}{M_F}$$

Where:

n_F — amount of substance of fluoride (mol),

M_F— molar mass of fluoride (19.00 g/mol).

In all experimental combinations (i.e., varying AWW:MM mass ratios), the theoretical fluoride content was calculated individually based on the above formulas. For each calculation, a reaction efficiency of 100% was assumed, representing an ideal condition. Subsequently, to compare with the experimentally determined values, the mass of fluoride loss was estimated using the following relationship:

$$\Delta m_F = m_F^{theoretical} - m_F^{practical}$$

The above model serves as a basis for theoretically assessing the probability of fluoride decomposition, the reactivity level of acidic components in the environment, and the kinetics of structural breakdown. This mathematical approach, developed based on formulas, is used to model the degree of retention or loss of fluoride in waste materials.

The degree of fluoride loss is expressed through a mathematical model based on the difference between theoretical and practical quantities after the reaction with the waste mixture. In this case, the mass of lost fluoride (*ΔF*) is determined by the following equation:

$$\Delta F = F_{theoretical} - F_{practical}$$

Here,

ΔF — amount of fluoride loss (g or mg),

$F_{theoretical}$ — theoretically calculated fluoride content,

$F_{practical}$— experimentally determined fluoride content.

To evaluate the loss in percentage terms, the following expression is used:

$$P_{loss} = \left(\frac{\Delta F}{F_{theoretical}}\right) \cdot 100 =$$

$$= \left(\frac{F_{theoretical} - F_{practical}}{F_{theoretical}}\right) \cdot 100$$

Using these formulas, the degree of fluoride loss for each AWW:MM mass ratio is quantitatively assessed. Thus, the impact of the acidic medium on fluoride breakdown, the ionic balance of the reactive system, and the overall mechanism of fluoride release can be represented through mathematical modeling. Thanks to its high sensitivity, this model provides predictive insights into the process and serves as a reliable tool for assessing the environmental risks associated with the waste system.

To further assess the scale of fluoride release and the ion balance in AWW:MM mixtures, a modeling approach incorporating differential analysis, empirical coefficients, and regression methods was applied. The decline in fluoride concentration within the mixtures was described as a function of the AWW:MM mass ratios.This relationship was further clarified using an exponential regression model. The general mathematical expression adopted for the modeling is as follows [[28], [29], [30]]:

$$C_F = C_o \cdot e^{-kx}$$

Here,

C_F — final fluoride concentration in the dried powder sample (% or mg/g),

C_o — initial (theoretical) fluoride concentration,

k — exponential decay coefficient of the reaction (experimentally determined),

x — mass of mineralized mass (MM) in the AWW:MM ratio (g or %).

In this model, the value of kkk is determined from actual experimental results, and its fit is statistically evaluated using the coefficient of determination R^2. Additionally, changes in equilibrium caused by ionic interactions in the reactive medium are assessed using the Le Chatelier principle. The dynamic equilibrium shift *ΔQ* is modeled according to the following equation:

$$\Delta Q = f\,(C_{H^+}, C_{F^-}, pH, t)$$

Here,

C_{H^+}, C_{F^-} — concentrations of key ions (hydrogen and fluoride) in the reaction medium,

pH — the acidity level of the reaction environment,

t — temperature in Kelvin (K).

Furthermore, an Excel-based graphical analysis was performed to illustrate the differences between the theoretical and experimental values of fluoride content at each test point. From these results, a correlation model with high accuracy was constructed. This mathematical framework makes it possible to explore the reaction mechanisms in the AWW:MM system in detail, supports predictive modeling of fluoride loss, and provides a quantitative basis for evaluating the ecological impact of the resulting waste mixtures.

Results and Discussion

In this study, the efforts were directed towards investigating the release and loss of fluoride in the mixture of mineralized mass (MM with 1.7% of fluoride content), mined at the Central Kyzylkum phosphorite deposits and the acidic wastewater (AWW of the fat and oil industry), as well as discussing environmental issues associated with them. Experimental tests were conducted at AWW:MM mass ratios of 100:10 to 100:40 at 333 K for 30 minutes. Tests of the solid residues obtained were conducted through the ionometric method.

** In addition, gaseous fluoride released during the interaction was experimentally captured using an absorption system, allowing the completion of a full fluorine material balance across solid, liquid, and gas phases.*

In this chapter, results are presented with supporting tables and figures, together with statistical analysis and a discussion of the involved aspects of the loss of fluoride and relevant scientific observations and recommendations for further studies [[31], [32], [33], [34]].

The results provided data about the theoretical and experimental values of fluoride content in grams, as well as the amount of fluoride loss. Table 1 summarizes the values obtained for each AWW:MM mass ratio (100:10–100:40), showing that the theoretical fluoride content ranged from 1.23 g to 4.90 g, while the experimental values ranged from 0.88 g to 3.68 g. The lowest fluoride loss (0.34 g) was recorded at the 100:20 ratio, whereas the highest loss (1.22 g) occurred at the 100:40 ratio.

Table 2 presents pH values (4.10-7.30) and practical fluoride amounts (0.88 g-3.68 g). The highest amount was observed at pH 5.90 (2.66 g), while at pH 6.33-7.30, it stabilized in the range of 3.08-3.68 g. The standard deviation varied from ±0.002 g to ±0.008 g.

Table 1 - Theoretical and practical fluoride quantities and fluoride losses in AWW:MM mixtures

AWW:MM mass ratio	Theoretical fluoride amount (g)	Practical fluoride amount (g)	Fluoride loss (g)	Standard deviation (g)
100:10	1.23	0.88	0.35	±0.002
100:15	1.84	1.42	0.42	±0.003
100:20	2.45	2.11	0.34	±0.004
100:25	3.06	2.66	0.40	±0.005
100:30	3.68	3.08	0.60	±0.006
100:35	4.29	3.39	0.90	±0.007
100:40	4.90	3.68	1.22	±0.008

Table 2 - pH and fluoride content in AWW:MM mixtures

AWW:MM mass ratio	pH	Practical fluoride amount (g)	Standard deviation (g)
100:10	4.10	0.88	±0.002
100:15	4.81	1.42	±0.003
100:20	5.62	2.11	±0.004
100:25	5.90	2.66	±0.005
100:30	6.33	3.08	±0.006
100:35	6.74	3.39	±0.007
100:40	7.30	3.68	±0.008

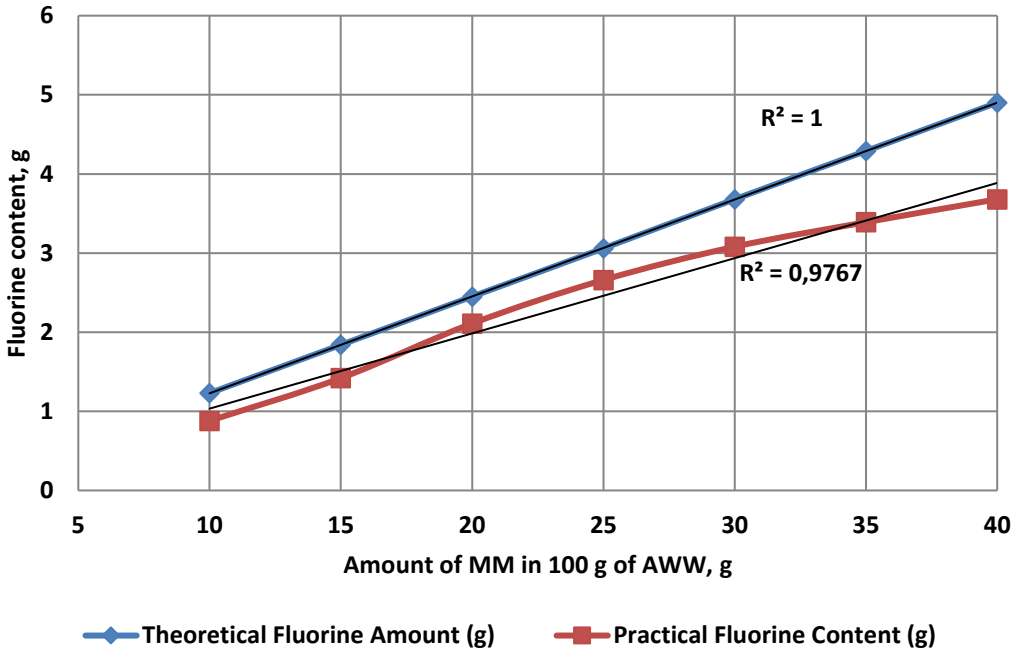

Figure 2 - Theoretical and practical comparison of fluoride quantity

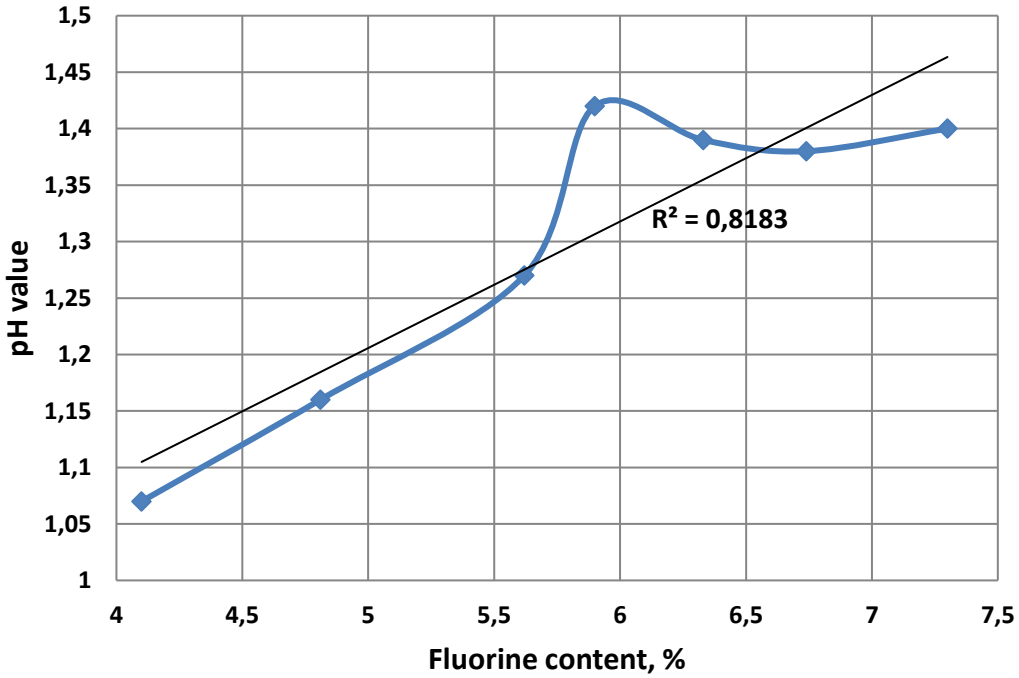

Figure 3 - The relationship between pH and fluoride content

Figure 2 (line graph), comparing the theoretical and practical amounts of fluoride, showed the highest practical amount (2.66 g) at a ratio of 100:25.

Figure 3 (scatter graph) illustrates the relationship between pH and the practical amount of fluoride, showing the highest amount (2.66 g) at pH 5.90 and stabilization in the pH range of 6.33-7.30.

In this study, Figure 2 compares the theoretical (1.23 g–4.90 g) and experimental (0.88 g–3.68 g) amounts of fluoride at various AWW:MM mass ratios (100:10–100:40) using a line graph. The highest experimental fluoride content was observed at the 100:25 ratio with a value of 2.66 g, while the lowest was recorded at the 100:10 ratio with 0.88 g. Fluoride loss ranged from 0.34 g (100:20) to 1.22 g (100:40). Figure 3 presents a scatter plot of pH values (4.10–7.30) versus experimental fluoride content (0.88 g–3.68 g). The peak fluoride retention occurred at pH 5.90, corresponding to 2.66 g. In the

pH range of 6.33 to 7.30, fluoride levels stabilized between 3.08 g and 3.68 g. In both graphs, the standard deviation of ionometric analysis ranged from ±0.002 g to ±0.008 g. These graphs clearly demonstrate the dependence of fluoride content on both mass ratio and pH, confirming the reliability of the experimental conditions.

The fluoride loss (0.34–1.22 g) was evaluated based on a complete fluorine material balance, including experimentally determined fluoride contents in the solid and liquid phases as well as gaseous fluoride captured using an absorption system, and subsequently analyzed using an exponential regression model (R^2 = 0.9767).

Each ionometric measurement was repeated three times, with standard deviations ranging from ±0.002 g to ±0.008 g. The minimum fluoride loss was recorded at the 100:20 ratio (0.34 g), and the maximum at 100:40 (1.22 g). The 100:25 ratio (0.40 g loss and 2.66 g retained fluoride) was identified as the most balanced condition. The correlation between pH (4.10–7.30) and experimental fluoride content (0.88 g–3.68 g) showed a strong relationship. Statistical results confirmed the reliability of data obtained at 333 K and a reaction time of 30 minutes. This analysis allowed accurate evaluation of fluoride behavior in response to varying mass ratios and pH values. The low standard deviation highlighted the high reproducibility of results. The exponential model effectively explained the variability in fluoride loss and provided a robust foundation for subsequent chemical and environmental discussions.

From a chemical standpoint, fluoride loss (0.34 g–1.22 g) was evaluated as a function of pH. At the 100:10 ratio (pH 4.10), the highest loss (0.35 g) was attributed to the formation of hydrogen fluoride (HF) gas. The 100:25 ratio (pH 5.90) provided optimal conditions with the lowest fluoride loss (0.40 g) and highest experimental fluoride retention (2.66 g). In the pH range 6.33–7.30 (ratios 100:30–100:40), fluoride content stabilized between 3.08 g and 3.68 g, attributed to the decreased acidity of the medium. The high ionic strength of AWW, particularly SO_4^{2-} (48,145 mg/L) and Cl^- (38,116 mg/L), accelerated fluoride release under low pH conditions. Environmentally, the release of HF gas (notably at 100:10) contributed to air pollution and posed health risks. Ratios of 100:20 (0.34 g loss) and 100:25 (0.40 g loss) minimized soil and water contamination. The treatment of MM and AWW mixtures promoted stable fluoride retention, making the process an effective waste neutralization strategy. The findings demonstrated the significance of this method in reducing environmental impact and provided a scientific basis for managing fluoride behavior and associated ecological risks [[35], [36], [37]].

Conclusion

This study investigated fluoride loss in a mixture of MM obtained from the Central Kyzylkum phosphorite deposits and AWW from the fat-and-oil industry, yielding several significant findings. The theoretical fluoride content across AWW:MM ratios (100:10–100:40) ranged from 1.23 g to 4.90 g, while the experimental content varied from 0.88 g to 3.68 g. The minimum fluoride loss was observed at the 100:20 ratio (0.34 g), whereas the maximum was recorded at 100:40 (1.22 g). The 100:25 ratio (pH 5.90) demonstrated optimal conditions with only 0.40 g of loss and 2.66 g of retained fluoride. At pH values between 6.33 and 7.30, fluoride content stabilized within the range of 3.08 g to 3.68 g. Ionometric analysis showed high reproducibility, with a standard deviation between ±0.002 g and ±0.008 g.

An exponential regression model (R^2 = 0.9767) confirmed the reliability of fluoride loss predictions. High concentrations of ions in AWW (SO_4^{2-}: 48,145 mg/L; Cl^-: 38,116 mg/L) accelerated fluoride release. At a 100:10 ratio (pH 4.10), the emission of hydrogen fluoride (*HF*) gas contributed to air pollution. In contrast, the 100:20 and 100:25 ratios effectively minimized soil and water contamination. The co-treatment of MM and AWW ensured stable fluoride retention, supporting its application as a waste-neutralization strategy. Statistical findings aligned with literature data indicating fluoride losses in the range of 0.3–1.5 g. A key limitation of the study was the inability to directly measure *HF* gas emissions. Nevertheless, the results support the strategy's effectiveness in mitigating environmental risks. Reducing fluoride loss significantly contributes to lowering ecological impact and provides a foundation for developing advanced waste treatment technologies. These findings offer practical implications for industrial waste management and play a critical role in enhancing environmental safety. Moreover, the study contributes to the advancement of innovative approaches in fluoride control.

Conflicts of interest. On behalf of all authors, the corresponding author states that there is no conflict of interest.

CRediT author statement: **S. Achilova, Sh. Kurambaev**: Conceptualization, Methodology, Software, Visualization, Investigation, Supervision, Software, Validation **A. Matmuratov, S. Qodirova**: Data curation, Writing draft preparation; **A. Ollaberganova, F. Abdullayeva**: Reviewing and Editing.

Formatting of funding sources. This research did not receive any specific grant from funding agencies in the public, commercial, or not-for-profit sectors.

Cite this article as: Kurambayev ShR, Qodirova SR, Achilova SS, Ollaberganova AM, Abdullayeva FB, Matmuratov AA. Mathematical modeling and ecological assessment of fluoride release in a mixture of mineralized phosphorite waste and wastewater from the fat and oil industry. Kompleksnoe Ispolzovanie Mineralnogo Syra = Complex Use of Mineral Resources. 2028; 345(2):95-106. https://doi.org/10.31643/2028/6445.19

Минералданған фосфорит қалдықтары мен май-май өнеркәсібінің ақаба сулары қоспасындағы фтордың бөлінуін математикалық модельдеу және экологиялық бағалау

[1] Құрамбаев Ш.Р., [1] Қодирова С.Р., [1] Ачилова С.С., [1] Оллаберганова А.М., [1] Абдуллаева Ф.Б., [2] Матмуратов А.А.

[1]Әбу Райхон Беруни атындағы Үргеніш мемлекеттік университеті, Өзбекстан
[2]Мамун университеті, Хиуа, Өзбекстан

Мақала келді: *25 желтоқсан 2025*
Сараптамадан өтті: *27 қаңтар 2026*
Қабыданды: *11 маусым 2026*

АННОТАЦИЯ

Бұл зерттеу Орталық Қызылқұм фосфорит кен орындарынан алынған минералданған масса (ММ) мен май-және май өнеркәсібінде түзілетін қышқыл ағынды сулардың (ҚАС) қоспасындағы фтордың жоғалуын зерттеуге бағытталған. Жұмыстың мақсаты фтордың бөлінуін және оның тұрақты сақталуын әртүрлі жағдайларда бағалау. Эксперименттер ҚАС:ММ масса арақатынасы 100:10-нан 100:40-қа дейінгі аралықта, 333 К температурада, 30 минут бойы ионометриялық талдау әдісімен жүргізілді. Теориялық фтор мөлшері 1.23 г-дан 4.90 г-ға дейін, ал тәжірибелік нәтижелер 0.88 г-дан 3.68 г-ға дейін өзгерді. Ең аз фтор жоғалуы 100:20 қатынасында — 0.34 г, ал ең жоғары жоғалту — 1.22 г — 100:40 қатынасында анықталды. Оптималды жағдай 100:25 қатынасында (pH 5.90) байқалып, фтордың жоғалуы 0.40 г, ал қалдық мөлшері 2.66 г болды. pH 6.33–7.30 аралығында фтор мөлшері 3.08 г–3.68 г деңгейінде тұрақтанды. Экспоненциалды регрессия моделі жоғары корреляцияны көрсетті (R^2 = 0.9767). Стандартты ауытқу ±0.002 г–дан ±0.008 г–ға дейін болды. ҚАС құрамындағы иондар (SO_4^{2-}: 48145 мг/л, Cl^-: 38116 мг/л) фтордың ұшуын едәуір жеделдетті. HF газының бөлінуі атмосфераның ластануына әкелді, алайда 100:25 қатынасы экологиялық әсерді барынша азайтты. Алынған нәтижелер әдеби деректердегі фтор жоғалу ауқымына (0.3–1.5 г) сәйкес келеді. Бұл зерттеу өнеркәсіптік қалдықтарды тиімді әрі экологиялық қауіпсіз қайта өңдеуге арналған жаңа тәсілдердің дамуына үлес қосады.

Түйін сөздер: фторидтің жоғалуы, pH көрсеткіші, ионометриялық талдау, экспоненциалды регрессия, минералданған масса, қышқылды ағынды сулар.

Авторлар туралы ақпарат:

Құрамбаев Шерзод Райымбергенұлы — *Техника ғылымдарының докторы, Әбу Райхон Беруни атындағы Үргенч мемлекеттік университетінің Химиялық технология факультетінің деканы, 220100, Ҳ. Олимжон көш., 14, Үргенч, Өзбекстан. Email: sherzod.k@urdu.uz; ORCID ID: https://orcid.org/0009-0003-3986-5079*

Қодирова Сохиба Равшанбеккызы — *Әбу Райхон Беруни атындағы Үргеніш мемлекеттік университетінің Жаратылыстану және ауыл шаруашылығы ғылымдары факультетінің оқытушысы, докторанты. Мекенжайы: Өзбекстан, 220100, Үргеніш қаласы, Х. Олимжон көшесі, 14-үй. Email: sohibaazamat2015@gmail.com; ORCID ID: https://orcid.org/0009-0008-4762-0262*

Ачилова Санобар Собир қызы — *Техника ғылымдарының философия докторы (PhD), Әбу Райхон Беруни атындағы Үргеніш мемлекеттік университетінің Химиялық технология факультетінің доценті. Мекенжайы: 220100, Өзбекстан, Үргеніш қ., Х. Олимжон көшесі, 14. Email: sanobar.a@urdu.uz; ORCID ID: https://orcid.org/0000-0003-4691-0248*

Оллаберганова Азиза Матякубқызы — *Техникалық ғылымдар бойынша философия докторы (PhD), Абу Райхон Беруни атындағы Үргенч мемлекеттік университетінің Химиялық технология факультетінің доценті, 220100, Х. Алимжон көшесі 14, Үргенч, Өзбекстан. Email: shamuratovsx@gmail.com*

Абдуллаева Феруза Байжонқызы	*Техника ғылымдарының философия докторы (PhD), Әбу Райхон Беруни атындағы Үргеніш мемлекеттік университеті, Химиялық технология факультетінің доценті. Өзбекстан, 220100, Үргеніш қаласы, Х. Олимжон көшесі, 14. Email: abdullayevafeya1996@gmail.com; ORCID ID: https://orcid.org/0000-0003-1490-4900*
Матмуратов Азизбек Абдикаримович	*Педагогика ғылымдарының философия докторы (PhD), Педагогикалық ғылымдар кафедрасының доценті, 220900, Мамун университеті, Бол-Ховуз көшесі, 2-үй, Қыбла Тозабоғ МКӘ, Хива, Өзбекстан. Email: my_darling90@mail.ru; ORCID ID: https://orcid.org/0009-0007-4177-3738*

Математическое моделирование и экологическая оценка высвобождения фтора в смеси минерализованных фосфоритных отходов и сточных вод масложировой промышленности

[1] Курамбаев Ш.Р., [1] Кодирова С.Р., [1] Ачилова С.С., [1] Оллаберганова А.М., [1] Абдуллаева Ф.Б., [2] Матмуратов А.А.

[1]Ургенчский государственный университет имени Абу Райхона Беруни, Узбекистан
[2] Университет Мамуня, Хива, Узбекистан

Поступила: *25 декабря 2026*
Рецензирование: *27 января 2026*
Принята в печать: *11 июня 2026*

АННОТАЦИЯ

В настоящем исследовании рассматриваются потери фтора в смеси минерализованной массы (ММ), извлечённой из фосфоритных месторождений Центрального Кызылкума, и кислых сточных вод (КСВ), образующихся в жировой и масложировой промышленности. Целью работы являлась оценка высвобождения фтора и устойчивости его удержания при различных условиях. Эксперименты проводились при массовых соотношениях КСВ:ММ от 100:10 до 100:40 при температуре 333 К в течение 30 минут с использованием ионометрического анализа. Теоретическое содержание фтора варьировало от 1,23 г до 4,90 г, тогда как экспериментальные значения находились в пределах от 0,88 г до 3,68 г. Минимальные потери фтора (0,34 г) наблюдались при соотношении 100:20, максимальные потери (1,22 г) — при 100:40. Оптимальным признано соотношение 100:25 (pH 5,90), при котором потери составили 0,40 г, а остаточное содержание — 2,66 г. При значениях pH от 6,33 до 7,30 концентрация фтора стабилизировалась в пределах 3,08–3,68 г. Модель экспоненциальной регрессии показала высокую степень корреляции (R^2 = 0,9767). Стандартное отклонение варьировало от ±0,002 г до ±0,008 г. Ионы в составе КСВ (SO_4^{2-}: 48145 мг/л и Cl^-: 38116 мг/л) значительно ускоряли испарение фтора. Выделение HF-газа способствовало загрязнению атмосферы, однако при соотношении 100:25 экологическое воздействие было минимальным. Полученные результаты согласуются с литературными данными, указывающими на диапазон потерь фтора от 0,3 до 1,5 г. Исследование вносит вклад в разработку эффективных и экологически безопасных подходов к утилизации промышленных отходов.

Ключевые слова: потеря фтора, значение pH, ионометрический анализ, экспоненциальная регрессия, минерализованная масса, кислые сточные воды.

Информация об авторах:

Курамбаев Шерзод Раймбергенович	*Доктор технических наук, декан факультета химической технологии Ургенчского государственного университета имени Абу Райхона Беруни, 220100, ул. Х. Олимжона, 14, Ургенч, Узбекистан. Email: sherzod.k@urdu.uz; ORCID ID: https://orcid.org/0009-0003-3986-5079*
Кодирова Сохиба Равшанбек кизи	*Преподаватель, докторант факультета естественных и сельскохозяйственных наук Ургенчского государственного университета имени Абу Райхона Беруни, ул. Х. Алимджана, 14, 220100, Ургенч, Узбекистан. Email: sohibaazamat2015@gmail.com; ORCID ID: https://orcid.org/0009-0008-4762-0262*
Ачилова Санобар Собировна	*Доктор философии (PhD) по техническим наукам, доцент факультета химической технологии Ургенчского государственного университета имени Абу Райхона Беруни, 220100, ул. Х. Олимжона, 14, Ургенч, Узбекистан. Email: sanobar.a@urdu.uz; ORCID ID: https://orcid.org/0000-0003-4691-0248*
Оллаберганова Азиза Матёкубовна	*Доктор философии по техническим наукам (PhD), доцент факультета химической технологии Ургенчского государственного университета имени Абу Райхона Беруни, 220100, ул. Х. Алимджана 14, Ургенч, Узбекистан. Email: shamuratovsx@gmail.com*
Абдуллаева Феруза Байжон кизи	*Доктор философии по техническим наукам, доцент факультета химической технологии Ургенчского государственного университета имени Абу Райхона Беруни, 220100, ул. Х. Олимжона 14, Ургенч, Узбекистан. Email: abdullayevafeya1996@gmail.com; ORCID ID: https://orcid.org/0000-0003-1490-4900*
Матмуратов Азизбек Абдикаримович	*Доктор философии (PhD) педагогических наук, доцент кафедры педагогических наук, Университет Мамуня, 220900, ул. Бол-Ховуз, д. 2, МСГ Кибла Тозабог, Хива, Узбекистан. Email: my_darling90@mail.ru; ORCID ID: https://orcid.org/0009-0007-4177-3738*

References

[1] Kurbaniiazov R K, Reimov A M, Namazov Sh S, & Beglov B M. Nitrogen-phosphoric fertilizers obtained by interaction of the concentrated solutions of ammonium nitrate with the mineralized mass of the phosphorites of Central Kyzylkum. Russian Journal of Applied Chemistry. Pleiades Publishing Ltd. 2009. https://doi.org/10.1134/s107042720906038x

[2] Sultonov B E, Nozimov E S, & Kholmatov D S. Recycling of Local Phosphate Waste - mineralized Mass into Activated Phosphorus Fertilizers. Chemical Science International Journal. Sciencedomain International. 2023. https://doi.org/10.9734/csji/2023/v32i6875

[3] Shamuratov S, Baltaev U, Achilova S, Alimov U, Namazov S, & Usanbaev N. Enhancement of availability of high calcareous phosphorite by neutralization of acid effluent and composting of cattle manure. (O. Tursunov, Ed.), E3S Web of Conferences. EDP Sciences. 2023. https://doi.org/10.1051/e3sconf/202337703004

[4] Shamuratov S, Alimov U, Rifky M, Baltaev U, Ibragimova M, Kurambaev S, & Radjabov M. Investigation of the Kinetics of Cotton Soapstock Saponification under Ultrasonic Illumination. Eurasian Chemico-Technological Journal. 2025; 27(4):323–335. https://doi.org/10.18321/ectj1679

[5] Hmidi K, Ksentini I, and Mansour L B. Treatment of Olive-Pomace Oil Refinery Wastewater Using Combined Coagulation-Electroflotation Process. Journal of Water Chemistry and Technology. Allerton Press. 2017. https://doi.org/10.3103/s1063455x17050046

[6] Halstead W D. The thermodynamics of fluoride loss during the chemical analysis of welding fluxes. Journal of Applied Chemistry and Biotechnology. Wiley. 1973. https://doi.org/10.1002/jctb.5020230308

[7] Doniyarov N A, & Tagayev I A. Obtaining a new kind of organic fertilizer on the basis of low-grade phosphorite of Central Kyzylkum. Materials and Geoenvironment. Walter de Gruyter GmbH. 2018. https://doi.org/10.2478/rmzmag-2018-0016

[8] Tagayev I, Doniyarov N, Asrorov A, & Murodov I. The Role of Medium Condition for Uranium Separation from Central Kyzylkum's Low-grade Phosphorite after Sulfuric Acid Treatment. International Journal on Advanced Science, Engineering and Information Technology. Insight Society. 2022. https://doi.org/10.18517/ijaseit.12.2.14060

[9] Juneja A, Kurambhatti C, Kumar D, & Singh V. Techno-Economic Evaluation of Phosphorous Recovery in Soybean Biodiesel Process. Processes. MDPI AG. 2022. https://doi.org/10.3390/pr10081512

[10] Sultonov BE, Kholmatov DS, Rasulov AA, and Temirov USh. Treatment of Phosphate Waste Generated during Thermal Processing of Phosphorites of the Central Kyzylkum. Obogashchenie Rud. Ore and Metals Publishing House. 2024. https://doi.org/10.17580/or.2024.04.06

[11] Shaymardanova Mokhichekhra, Kholtura Mirzakulov, Gavkhar Melikulova, Sakhomiddin Khodjamkulov, Abror Nomozov, and Oybek Toshmamatov. Studying of The Process of Obtaining Monocalcium Phosphate Based on Extraction Phosphoric Acid from Phosphorites of Central Kyzylkum. Baghdad Science Journal. College of Science for Women, University of Baghdad. 2024. https://doi.org/10.21123/bsj.2024.9836

[12] Sidorina E, Isagulov A, Rabatuly M, & Yang Y. Technology of production of aluminosilicate refractories for units processing fluorinated waste. Kompleksnoe Ispolzovanie Mineralnogo Syra = Complex Use of Mineral Resources. 2024; 335(4):89–95. https://doi.org/10.31643/2025/6445.43

[13] Borowski S, & Cieciura-Włoch W. Enzymatic Pretreatment of Byproducts from Soapstock Splitting and Glycerol Processing for Improvement of Biogas Production. Molecules. MDPI AG. 2021. https://doi.org/10.3390/molecules26226782

[14] de Pablos-Martín A, Contreras Jaimes AT, Wahl S, Meyer S, & Brauer DS. Fluoride loss determination in bioactive glasses by laser-induced breakdown spectroscopy (LIBS). International Journal of Applied Glass Science. Wiley. 2021. https://doi.org/10.1111/ijag.15867

[15] Shamuratov Sanzharbek, Umid Baltaev, Umarbek Alimov, Namazov Shafoat, Sherzod Kurambaev, and Bazar Ibadullaev. Utilization Process Research of the Soap Industry Acid Waste Water with High Carbonate Phosphorite of Central Kyzylkum. E3S Web of Conferences. EDP Sciences. 2021. https://doi.org/10.1051/e3sconf/202126404079

[16] Shamuratov Sanjarbek, Umid Baltaev, Olga Myachina, Umarbek Alimov, Elyor Atashev, and Tokhir Kuramboev. Agrochemical Efficiency of Slow Release Phosphate Fertilizers Derived on the Base of Phosphorite Activation. E3S Web of Conferences. EDP Sciences. 2023. https://doi.org/10.1051/e3sconf/202343403014

[17] Sotimboev Ilgizarbek, Umidbek Baltaev, Sanjarbek Shamuratov, Ruzimov Shamsiddin, Umarbek Alimov, and Mirzabek Saporboyev. Technical and Economic Efficiency of Processing Acidic Wastewater from the Oil and Fat Industry into Necessary Agricultural Products. E3S Web of Conferences. EDP Sciences. 2024. https://doi.org/10.1051/e3sconf/202456303072

[18] Turatbekova Aidai, Malokhat Abdukadirova, Sanjarbek Shamuratov, Bakhodir Latipov, Mirzabek Saporboyev, Jafar Shamshiyev, and Yusuf Makhmudov. Investigation of the Effect of Fertilizers on the Biochemical and Physical Characteristics of Carrots (Daucus Carota L.). E3S Web of Conferences. EDP Sciences. 2024. https://doi.org/10.1051/e3sconf/202456303074

[19] Yuldasheva A, Shamuratov S, Kurambayev S, & Radjabov M. Mathematical Analysis of CaO Content Variation in Acidic Wastewater and Mineralized Mass Mixture from Central Kyzylkum Phosphorite Based on Exponential Decay Model. Kompleksnoe Ispolzovanie Mineralnogo Syra = Complex Use of Mineral Resources. 2025; 339(4):79–86. https://doi.org/10.31643/2026/6445.42

[20] Shamuratov S, Baltayev U, Alimov U, Jabbarov M, & Madaminov A. Sigmoid Neutralization Response of Acidic Soapstock Waste by Mineralized Phosphorite Residues: A 4-Parameter Logistic Approach. Kompleksnoe Ispolzovanie Mineralnogo Syra = Complex Use of Mineral Resources. 2026; 342(3):80–89. https://doi.org/10.31643/2027/6445.32

[21] Pintor Ariana MA, Andreia G Martins, Renata S Souza, Vítor JP Vilar, Cidália MS Botelho, and Rui AR Boaventura. Treatment of Vegetable Oil Refinery Wastewater by Sorption of Oil and Grease onto Regranulated Cork – A Study in Batch and Continuous Mode. Chemical Engineering Journal. Elsevier BV. 2015. https://doi.org/10.1016/j.cej.2015.01.025

[22] Mirshafiee Amir, Abbas Rezaee, and Rasol Sarraf Mamoory. A Clean Production Process for Edible Oil Removal from Wastewater Using an Electroflotation with Horizontal Arrangement of Mesh Electrodes. Journal of Cleaner Production. Elsevier BV. 2018. https://doi.org/10.1016/j.jclepro.2018.06.201

[23] Ahmad Talha, Rana Muhammad Aadil, Haassan Ahmed, Ubaid ur Rahman, Bruna CV Soares, Simone LQ Souza, Tatiana C Pimentel, et al. Treatment and Utilization of Dairy Industrial Waste: A Review. Trends in Food Science & Technology. Elsevier BV. 2019. https://doi.org/10.1016/j.tifs.2019.04.003

[24] Tadjiev SM, Atashev EA. Obtaining azosuperphosphate from low-grade phosphates of the central Kyzylkum. Journal of Critical Reviews. 2020; 7(5):472-477.

[25] Tadjiev SM, Atashev EA. Production of azosuperphosphate in the participation of Central Kyzylkum phospharites and ammonium sulphate. Journal of Critical Reviews. 2020; 7(7):358-362.

[26] De Leonardis A, Macciola V, Iftikhar A. Present and Future Perspectives on the Use of Olive-Oil Mill Wastewater in Food Applications. In: Souabi, S., Anouzla, A. (eds) Wastewater from Olive Oil Production. Springer Water. Springer, Cham. 2023. https://doi.org/10.1007/978-3-031-23449-1_4

[27] Jeba RH, Hemada HM, Nadir AA, et al. Improving stability of frying oils and food quality with addition of dried olive mill wastewater. npj Sci Food. 2025; 9:75. https://doi.org/10.1038/s41538-025-00430-x

[28] Fritz Matthew S. An Exponential Decay Model for Mediation. Prevention Science. Springer Science and Business Media LLC. 2013. https://doi.org/10.1007/s11121-013-0390-x

[29] Atashev E. Decomposition of Magnesite-Sparing Waste in Sulfuric Acid with a High Concentration: Empirical Modeling and Determination of Optimal Conditions. Kompleksnoe Ispolzovanie Mineralnogo Syra = Complex Use of Mineral Resources. 2025; 339(4):71–78. https://doi.org/10.31643/2026/6445.41

[30] Baltayev U, Shamuratov S, Alimov U, Madaminov A, & Jabbarov M. Extraction of P_2O_5 from the mineralized mass of the Central Kyzylkum using acidic wastewater generated from cotton soapstock processing: scientific analysis based on equilibrium principles. Kompleksnoe Ispolzovanie Mineralnogo Syra = Complex Use of Mineral Resources. 2025; 341(2):83–96. https://doi.org/10.31643/2027/6445.20

[31] Boyjanov N, Radjabov M, Serkayev Q, Boyjanov I, & Yaxshimuradov N. Activation and comparison of indicators of bentonite clay of the Navbakhor deposit. E3S Web of Conferences. 2024; 563:02018. https://doi.org/10.1051/e3sconf/202456302018

[32] Boyjanov NI, Rakhimov UB, Ataullaev ZM, Boltayev MA, Serkayev QP, Khamidova MO. Mathematical analysis of the linear increase in SIO2 content during the activation of Navbakhor alkaline bentonite with hydrochloric acid. Kompleksnoe Ispolzovanie Mineralnogo Syra = Complex Use of Mineral Resources. 2027; 342(3):90-99. https://doi.org/10.31643/2027/6445.33

[33] Boyjanov NI, Otajonova GM, Kendjayev BB, Matyakubova MX, Sabirova NK, Masharipov AT, Boyjanov IR, Serkayev QP. Exponential modeling of Al_2O_3 reduction during activation of Navbahor alkaline-earth bentonite Kompleksnoe Ispolzovanie Mineralnogo Syra = Complex Use of Mineral Resources. 2027; 343(4):106-115. https://doi.org/10.31643/2027/6445.44

[34] Haidar Abbas, Sarmad Jaafar Mohammed Alrubaye, Ali Fawzi Al-Hussainy, Basim Mohammed Saadi, Mohannad Abdulrazzaq Gati, Talib Kh. Hussein, Boyjanov Nodirbek Ilxomovich, Nafaa Farhan Muften. Role of Carrageenan and Health Approach for Adsorption of Safranin-T Dye from Aqueous Solution by Using Polymer/CNT Surface. Journal Nanostruct. 2025; 15(4): 1798-1807. https://doi.org/10.22052/JNS.2025.04.027

[35] Hussein U A-R, Alalwan D H K, Qabel H A, Abid F M, Hamza H H, Ilxomovich B N, Aljeboree A M, & Alkaim A F. Green synthesis and characterization of guar gum/polyacrylamide/activated carbon hydrogel for efficient methylene blue removal. Journal of Nanostructures. 2025; 15(4):1849-1860. https://doi.org/10.22052/JNS.2025.04.028

[36] Kurayazov, Z., Ollaberganova, A., Jabbarov, M., Matnazarov, U., & Babajanova, R. (2026). Reduction of Fluoride in Central Kyzylkum Phosphate Waste in an Acidic Environment: Experimental and Mathematical Study Based on the Langmuir Model. Kompleksnoe Ispolzovanie Mineralnogo Syra = Complex Use of Mineral Resources, 343(4), 65–76. https://doi.org/10.31643/2027/6445.41

[37] Achilova, S., Saparbaeva, N., Matmuratov, A., Rustamova, N., & Karimboyev, O. (2026). Activation of the mineralized mass of Central Kyzylkum using acidic wastewater from the oil and fat industry: Freundlich-based adsorption kinetics for fluorine release. Kompleksnoe Ispolzovanie Mineralnogo Syra = Complex Use of Mineral Resources, 342(3), 65–79. https://doi.org/10.31643/2027/6445.31

Crossref
DOI: 10.31643/2028/6445.20
Mining & Mineral Processing

Study of the mechanism and efficiency of using mineral-organic bleaching-filtering agents in polishing refining

[1*]Boyjanov N.I., [1]Kurayazov Z.R., [2]Annazarova B.R., [3]Jollibekov S.M., [3]Tajetdinov N.D., [4]Khamidova M.O., [5]Akhmedov A.N.

[1]Urgench State University named after Abu Rayhon Beruni, Urgench, Uzbekistan
[2]Non-government Educational Institution Mamun University, Khiva, Uzbekistan
[3]Karakalpakstan Institute of Agriculture and Agrotechnology, Nukus, Uzbekistan
[4]Tashkent Chemical-Technological Institute, Tashkent, Uzbekistan
[5]Karshi State Technical University, Uzbekistan

**Corresponding author email: b.nodirbek@urdu.uz*

Received: *January 20, 2026*
Peer-reviewed: *May 23, 2026*
Accepted: *June 11, 2026*

ABSTRACT

In this scientific study, the main objective is to purify vegetable oils stored in the state reserve for an extended period to reach consumable quality based on their physicochemical parameters. In the experiments, polishing refining of cottonseed oils stored for 6 months or longer was carried out. By analyzing the physicochemical parameters of polishing-refined vegetable oils, selective bleaching-filtering agents (BFAs) with various pore structures were obtained for use in the bleaching-filtration stage. The BFAs were obtained through acid activation of bentonitic and opoka-type clays, as well as pyrolysis of sunflower husk. The filtration capacities of each activated BFA toward polishing-refined oils were investigated. The findings show that the highest efficiency was achieved when a composite BFA of the BK grade-prepared at a 1:1 mass ratio of acid-activated Navbahor alkali bentonite (ANAB) and pyrolyzed sunflower husk (P-SH) was added at 1.5-2.0% relative to the oil mass. The research results demonstrate that a composition consisting of polar organic and non-polar inorganic components was successfully obtained, capable of filtering fine soapstock particles while not resisting pressure buildup during the filtration process.

Keywords: bentonite clay, opoka-type clay, sunflower husk, BET analysis, activation, pyrolysis, composition, polishing refining, bleaching-filtering agent.

Information about authors:

Boyjanov Nodirbek Ilxomovich — *Doctor of Philosophy in Technical Sciences, Associate Professor at the Faculty of Chemical Technology, Urgench State University named after Abu Rayhon Beruni, 220100, H. Olimjon Street 14, Urgench, Uzbekistan. Email: b.nodirbek@urdu.uz; ORCID ID: https://orcid.org/0009-0002-1454-9478*

Qurayazov Zaripbay Ramatovich — *Doctor of Philosophy in Technical Sciences, Associate Professor at the Faculty of Chemical Technology, Urgench State University named after Abu Rayhon Beruni, 220100, H. Olimjon Street 14, Urgench, Uzbekistan. Email: kurayazovzarifboy@gmail.com; ORCID ID: https://orcid.org/0000-0002-9217-0669*

Annazarova Barno Rustamovna — *Non-government Educational Institution Mamun University, Khiva, Uzbekistan. Email: barno220517@gmail.com; ORCID ID: https://orcid.org/0009-0007-1821-9886*

Jollibekov Spandiyar Makhamadiyarovich — *Karakalpakstan Institute of Agriculture and Agrotechnologies, Nukus, Узбекистан. Email: s.jollibekov@tdaunukus.uz; ORCID ID: https://orcid.org/0009-0001-0390-3892*

Tajetdinov Nauruzbay Daribayevich — *Associate Professor of the Karakalpakstan Institute of Agriculture and Agrotechnology, Nukus, Узбекистан. Email: nauriztajetdinov@gmail.com; ORCID ID: https://orcid.org/0009-0007-0516-3772*

Khamidova Madina Olimjonovna — *Associate Professor at the Tashkent Institute of Chemical Technology, Navoi Street, 32, Tashkent, Uzbekistan. Email: m.khamidova@mail.ru; ORCID ID: https://orcid.org/0000-0002-7299-0395*

Akmedov Azimjon Normominovich — *Doctor of Technical Sciences, Professor of the Shahrisabz Faculty of Food Engineering, Karshi State Technical University, Khanabad Avenue, 19, Uzbekistan. Email: a.ahmedov80@mail.ru; ORCID ID: https://orcid.org/0000-0002-8072-7458*

Introduction

Scientific research is being conducted to improve the technologies for producing natural and synthetic sorbents in various fields of the chemical and food industries. In this regard, special attention is given to improving and testing technologies that utilize modified sorbents possessing micro, meso, and macroporous structures and capable of forming ionic bonds for the removal of coloring

substances from food products and the purification of industrial wastewater in the chemical sector [[1], [2], [3], [4], [5]].

In 2019-2020, global cotton production reached 43 million tons [6], of which Uzbekistan accounted for about 3 million tons. Cottonseed oil belongs to the group of vegetable oils that require full refining.

Refining methods are selected based on the type of oil-bearing raw material and the extraction process used. Oils obtained from low-grade seeds require multi-stage refining procedures [[7], [8], [9]].

Chlorophyll, xanthophylls, carotenoids, gossypol, and soapstock formed during the processing of vegetable oils-along with other soap-like substances, free fatty acids, and peroxides-possess diverse physicochemical properties and vary in their chemical nature. Depending on the nature and concentration of these substances, vegetable oils are refined either through a complete or partial refining cycle [[10], [11], [12], [13]].

Depending on the type of oily raw material and the method of oil extraction, vegetable oils contain various accompanying substances. These properties include the content of phosphatides, moisture and volatile substances, iodine value, color index, refractive index, and saponification value, among others [6].

Cottonseed oil contains biologically active compounds such as antioxidants-including tocopherols, sterols, and flavonoids-as well as a yellow-colored pigment known as gossypol.

The bleaching stage of the vegetable oil refining cycle requires the use of selective sorbents that act through targeted adsorption.

Various mineral-and organic-based adsorbents are used during the bleaching stage [[14], [15]].

Scientific sources have examined the physicochemical mechanisms of the pyrolysis process of sunflower and peanut shells at temperatures of 280 and 350 °C, as well as the effects of the resulting solid carbon-based mass on soil formation and seed germination [16].

Natural mineral sorbents are mineralized clays with high adsorption or ion-exchange capacities, which include natural bentonite, siliceous (opoka) clay, and other similar materials [[4], [14], [17]].

Natural clays are activated through mechanical, physical, and chemical methods. Such treatments modify the physicochemical properties of the clay and enhance its adsorption capacity [[18], [19]].

During the storage of vegetable oils, primary and secondary oxidation products are formed, which can have adverse effects on the human body [20].

In the first stage of the oxidation process, homolytic cleavage of the covalent bonds within the C-H hydrocarbon chains occurs, resulting in the formation of free hydrogen radicals and free fatty acid radicals. Hydroperoxides, which are primary oxidation products found in vegetable oils, enter the oil as a result of enzymatic processes [[21], [22]].

During the storage of vegetable oils, factors such as temperature and ultraviolet radiation contribute to the degradation of fatty acid molecules. At subsequent stages, oxidation proceeds in a chain mechanism, and the first organoleptic changes in the oil become noticeable. [[23], [24]].

All types of vegetable oils undergo oxidation due to the presence of accompanying substances. Oxidation products, in turn, lead to changes in the standard physicochemical parameters of the oil and a decrease in its nutritional value. Under the influence of internal and external factors, the hydrogen atom adjacent to the double bond of unsaturated fatty acids is removed, resulting in the formation of highly reactive free radicals possessing unpaired electrons. These radicals interact with fatty acid molecules and initiate a new chain oxidation process [25].

The increase in acid value and peroxide value in vegetable oils is attributed to the formation of primary oxidation products. However, secondary oxidation products may also form simultaneously with the primary ones, which ultimately leads to the deterioration and unsuitability of the oil for use [26].

The authors extracted oil from flax and hemp seeds using the cold-pressing method, determined changes in parameters such as acid value, peroxide value, and anisidine value in oils stored at room temperature for 6 months, and analyzed their oxidation kinetics using differential scanning calorimetry (DSC). They emphasized that vegetable oils obtained through cold pressing are highly prone to oxidative degradation [27].

The studies also examined the extraction of oil from non-traditional oilseeds and the physicochemical changes occurring during their storage. In particular, an increase in peroxide and acid values was observed during long-term storage of peanut oil. The rise in these compounds imparts a bitter taste to the oil and leads to the formation

of further oxidation products, which may even contribute to the development of certain diseases [28].

Physicochemical methods are used to remove accompanying substances from all types of vegetable oils. The principles of physical and chemical refining methods, as well as their adverse effects on oils, have been extensively described by numerous authors [[29], [30]].

Vegetable oils stored for long periods typically exhibit elevated acid values, and the micro-sized soapstock particles formed during the polishing-refining stage tend to clog the pores of the filter cloth, thereby hindering oil flow. In this study, to eliminate this problem, the possibilities of obtaining and applying BFAs capable of retaining soap-like substances were investigated.

During the filtration process, the pores of the filter cloth are capable of allowing particles up to a certain size to pass through. Various types of filtration equipment are used for this purpose, including both vacuum and non-vacuum systems, operating in either batch or continuous modes.

The filtration process is carried out using fabric, non-fabric, and metal mesh filters, as well as filtration aids-also known as filtering agents-that facilitate the process. The filtration surface determines the primary geometric characteristics of the filter. The filtration surface consists of a filtering barrier whose porosity directly influences the permeability and overall performance of the filter. The following section presents the results of our studies on the use of bleaching-filtering agents with varying adsorption activities in the filtration of vegetable oils and the removal of soap-like substances after the polishing refining process.

Materials and Methods

Materials

The raw materials used in this study included bentonite clay obtained from the Navbakhor deposit and opoka-type clay collected from the Karmana deposit, both located in Uzbekistan. Sunflower husk was utilized as a pore-forming organic additive. Distilled water was used for sample preparation and processing. A 15 wt.% sulfuric acid (H_2SO_4) solution was employed for the acid activation and modification of the clay materials. All chemicals and reagents were of analytical grade and were used without further purification.

Our experiments were conducted using 10 liters of cottonseed oil obtained from the state reserve, which had been stored for more than six months. The physicochemical characteristics of the oil used in the experiments are presented in Table 1 below.

To bring the oil samples with the above quality characteristics to the level required for polishing refining, the free fatty acids were first neutralized with a 250 g/l caustic soda solution, using an excess alkali dosage of 0.5%. During the neutralization process, the temperature was maintained at 55 °C. The resulting soapstock was precipitated and separated using a saline (water-salt) solution. The physicochemical characteristics of the polished refined oil are presented in Table 2 below.

Table 1 - Physicochemical characteristics of long-term stored cottonseed oil

Sample	Acid value, mg KOH/g	Red units	Transparency	Peroxide value, mmol ½O/kg	Qualitative test for soap content	Content of moisture and volatile substances, %
Cottonseed oil	0.6	8	Clear	14	Not available	0.21

Table 2 - Physicochemical characteristics of polished refined cottonseed oil

Sample	Acid valu, mg KOH/g	Red units	Transparency	Peroxide value, mmol ½O/kg	Qualitative test for soap content	Content of moisture and volatile substance, %
Cotton seed oil	0.15	8	Turbid	4.2	Available	0.11

As seen from the table data, both the acid value and peroxide value of the oil decrease several times during the polishing refining process. Although these values are close to standard parameters, they are still considered relatively high for oils undergoing secondary refining. In addition, the turbidity of the oil and the results of the qualitative test for soap content indicate difficulties in removing micro-sized impurities from the oil using primary processing methods such as sedimentation or simple filtration. Based on the above findings, it is necessary to explore the potential for developing specialized bleaching-filtering agents to remove micro-sized impurities from polished refined oils.

Obtaining whitening-filtering agents

Our subsequent experiments focused on the activation of bentonite and opoka-type clays, which served as the primary research objects for obtaining bleaching-filtering agents (BFAs). During the sulfuric acid activation of bentonite and opoka-type clays, optimal results were achieved using a 15% acid solution. A hydromodule ratio of 1:2.5 (clay to acid solution) was selected, and activation was carried out with an acid consumption of 40%. The resulting suspension was washed with distilled water until the pH value reached 4. The resulting clay mass was first air-dried under ambient conditions and then further dried in a drying oven at a temperature of 110-120 °C for 2 hours. Considering the effect of particle size on sorption properties, the dried samples were sieved until 90% of the material passed through a 56 µm mesh (10,000 openings per/sm²).

To produce a microporous, carbon-based organic sorbent, sunflower husks were ground to a particle size of up to 1 mm and subjected to thermal treatment (pyrolysis) at 600 °C in an oxygen-free environment. Based on the study of the sorption properties of the obtained solid carbon-based samples, a composite bleaching-filtering agent (BFA) was developed using activated bentonite and pyrolyzed sunflower husk.

During the filtration of polished refined oils using BFAs, the reagent was added at a dosage of 0.5-2.0% relative to the oil mass and stirred for 15-30 minutes at 60 °C. Filtration was carried out in frame filters at a pressure of 0.1-0.5 MPa using a filter cloth compliant with State Standard 332-91. During the process, changes in flow rate with increasing filtration pressure were monitored, and the operation was stopped when the pressure exceeded 0.5 MPa and the flow rate dropped below 0.02 kg s/m². Under these controlled parameters, after 10 hours of filtration, the thickness of the sediment layer on the filter surface reached 10 mm.

The moisture content of cottonseed oil was determined by the gravimetric method according to ISO 662:2016. The color of the oil was measured in red units at a constant 35 yellow units using a Lovibond Tintometer (Model E) with a 13.5 sm cuvette.

The acid value was determined by the titration method in accordance with ISO 660:2020.

The peroxide value was determined by the iodometric titration method in accordance with ISO 3960:2020.

Sorption pores were determined in accordance with IUPAC requirements.

Analysis of specific surface area and porosity was carried out using the method of low-temperature nitrogen adsorption on a Micromerelies Gemini VII 2390t analyzer (USA).

Results and Discussion

The main objective of our study is to remove micro-sized soapstock particles remaining in the oil after polishing refining and to reduce the acid and peroxide values to standard levels, which requires the preparation of effective bleaching-filtering agents (BFAs).

To obtain BFAs for filtering polished refined oils, the sorption properties of Navbahor alkaline bentonite and opoka-type clay from the Karmana deposit were investigated. Their sorption indicators are presented in Table 3 below.

Table 3 - Sorption characteristics of natural bentonite and opoka-type clays

Parameters	NAB	OG
Specific surface area (BET), m²/g	43.52	153.25
Specific surface area of micropores, m²/g	2.07	-
Specific surface area of meso- and macropores, m²/g	41.45	153.25
Pore volume, cm³/g	0.014	0.262
Average pore diameter, Å	12.94	98

NAB – Navbahor alkaline bentonite; NOA – natural opoka-type clay.

Analyzing the data presented in the table, it can be observed that the natural bentonite clay exhibits a relatively small specific surface area of 43.52 m²/g, a specific surface area of micropores of 2.07 m²/g, and an average pore diameter of 12.94 Å. Although the opoka-type clay has a relatively high specific surface area of 153.25 m²/g, it lacks significant microporosity, with an average pore diameter of 98 Å. Given that alkali-treated, polished refined oils contain colloidal and micro-sized soapstock particles, the sorption characteristics of these two clays alone are insufficient to yield the desired performance when used as bleaching-filtering agents. Our experiments revealed that acid activation of these clays not only increases their specific surface area but also promotes the formation of micropores within the macro and mesoporous structure under the influence of acid treatment, thereby enhancing the characteristics required for our intended application.

Taking the above considerations into account, the bentonite and opoka-type clays were activated

using a 15% sulfuric acid solution. The obtained results are presented in Table 4.

Table 4 - Sorption characteristics of BFAs obtained through acid activation

Parameters	ANAB	AOC
Specific surface area (BET), m^2/g	176.38	164.36
Specific surface area of micropores, m^2/g	15.25	4.70
Specific surface area of meso- and macropores, m^2/g	161.13	159.66
Pore volume, cm^3/g	0.108	0.384
Average pore diameter, Å	35.062	74

Acid-activated Navbahor alkaline bentonite, AOC-acid-activated opoka-type clay

The data presented in Table 4 show that although sulfuric acid treatment of bentonite clay resulted in a significant increase in its specific surface area, the majority of the pore structure consists of macro and mesopores (161.13 m^2/g), while the surface area of micropores remains comparatively low at 15.25 m^2/g. In the acid-activated opoka-type clay, these values were found to be 159.66 m^2/g for macro-and mesopores, and 4.70 m^2/g for micropores. Although an increase in acid concentration leads to the formation of additional micropores, it simultaneously causes a reduction in the overall specific surface area.

It can be concluded that although acid activation of various clay samples increases their specific surface area, the resulting materials are still insufficient for effectively filtering soapstock and colloidal-sized particles from the studied oils. According to the literature review, plants and plant-derived organic sorbents possess microporous structures.

Based on this information, it was concluded that it is necessary to obtain an organic-based sorbent. Therefore, sunflower husks were subjected to pyrolysis at 200 °C for 120 minutes in an oxygen-free environment. This process consists of several stages, including dehydration, decomposition, carbonization, and the formation of active (oxide) sites. During pyrolysis, the main structural components of the husk-cellulose, hemicellulose, and lignin-gradually decompose, resulting in a carbon-rich solid mass with a ring-shaped carbon structure.

Table 5 below presents the sorption characteristics of sunflower seed husks obtained through the pyrolysis method.

Table 5 - Sorption characteristics of pyrolyzed sunflower husk

Parameters	P-SH
Specific surface area (BET), m^2/g	132.14
Specific surface area of micropores, m^2/g	58.72
Specific surface area of meso and macropores, m^2/g	73.42
Pore volume, cm^3/g	0.162
Average pore diameter, Å	33.1

P-SH-pyrolyzed sunflower husk

As shown in the table, the obtained organic-based sorbent possesses micropores with a specific surface area of 58.72 m^2/g. At this stage, it becomes necessary to study the potential of the obtained organic-based sorbent with microporous structure for filtering long-term stored vegetable oils.

Experiments were conducted to determine the filtration efficiency of polished refined cottonseed oil using the sorbent obtained through the pyrolysis process. Table 6 below presents the results of filtering polished refined cottonseed oil using the sorbent described in Table 5, which possesses the specified sorption characteristics.

Table 6 - Results of filtering polished refined cottonseed oil using P-SH grade BFA

Parameters	P-SH dosage 1,0%	P-SH dosage 1,5%	P-SH dosage 2,0%	P-SH dosage 2,5%
Acid value, mg KOH/g	0.15	0.14	0.14	0.14
Red units	8	8	8	8
Transparency	turbid	turbid	turbid	turbid
Peroxide value, mmol ½O/kg	4.1	4.1	3.8	3.8
Qualitative test for soap content	Available	Available	not available	not available
Content of moisture and volatile substances, %	0.09	0.09	0.09	0.09

As seen from the table, when the P-SH grade BFA was added to the oil at dosages of 1%, 1.5%, 2%, and even 2.5% relative to the oil mass, the filtered oil did not show significant improvement in terms of acid value or peroxide value. At the initial stage of the filtration process, the filtration rate was relatively high; however, over time, a noticeable increase in filtration pressure and a sharp decrease in the filtration rate were observed.

This occurred because the P-SH grade organic-based BFA formed a compressible sediment layer on the surface of the filter cloth. All organic-based sediments belong to the category of compressible deposits.

If the particles in the filtration process possess non-deformable characteristics, they belong to the category of incompressible sediments, and an increase in pressure does not alter their resistance [31].

During the filtration process, an increase in pressure leads to deformation and compaction of particles. Such sediment is compressible, and over time this causes an increase in resistance and a decrease in filtration rate (Figure 1). These factors were taken into account in the present study.

On the one hand, despite the presence of micro-sized particles in the P-SH grade BFA, the soapstock particles tended to clog the pores of the filter cloth, which led to an increase in filtration pressure. On the other hand, the accumulation of soapstock particles on the surface of the filter cloth caused them to swell even under slight moisture, resulting in an increase in their volume. In both cases, the formation of a deformable sediment layer on the filter cloth surface reduced the filtration rate.

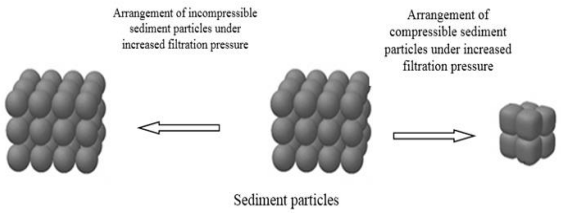

Figure 1 - Change in the void space between particles under the influence of pressure in the filter

It is well known that the permeability of the filter plays a crucial role in the filtration of vegetable oils. The filtration process can be described using the Strouhal criterion as follows (1).

$$S_t = \frac{f \cdot L}{V} \quad (1)$$

Where:

f - frequency of pressure fluctuations (Hz)

L - diameter of the filter cloth pores (μm)

V - flow velocity (m/s)

Based on this, considering that the filtration process consists of the filtrate volume dV_f separated over a time interval dt, the filtration rate S_f can be expressed as follows (2).

$$S_f = \frac{dV_f}{F_f + d_t} \quad (2)$$

Where:

S_f - filtration rate

F_f - filtration surface area

dV_f - filtrate volume

The filtration rate is directly proportional to the driving force acting on the suspension and inversely proportional to the resistance of the filtration surface. The resistance on the filtration surface depends on the properties of the filter medium itself and the thickness of the sediment layer formed during the process. Accordingly, the filtration rate can be expressed as follows (3).

$$S_f = \frac{\Delta P}{\mu \cdot R_{fp} + r_o \cdot l} \quad (3)$$

Where:

ΔP - pressure difference across the filter (driving force), Pa;

R_{fp} - resistance of the filter medium, m^{-1}

r_o - specific resistance of the sediment, m^{-2}

l - thickness of the sediment layer, m

Naturally, both R_{fp} and r_o are variable parameters. The resistance of the filter medium may increase due to partial clogging of the pores or swelling of the fabric fibers under the influence of moisture. The parameter r_o represents a specific resistance value corresponding to a unit thickness of the sediment layer.

P (Pa) represents the driving force in the filter, defined as the difference between the pressure before the filter barrier (P_1) and the pressure at the barrier (P_2) (4).

$$\Delta P = P_1 - P_2 \quad (4)$$

The optimal value of ΔP is achieved by maintaining a sufficiently high filtration pressure (P_1) while ensuring that the resistance of the filter barrier does not lead to an excessive increase in P_2.

Experimental results show that the filtration process proceeds much more easily when the particles form a non-deformable sediment. Such sediments accumulate on the upper surface of the filter barrier, and the interparticle voids help retain finer particles. In this case, the internal pores of the filter cloth remain unblocked, and the filtration resistance R_{fp} does not change. This extends the effective operating life of the filter. The variable resistance depends solely on r_o, which is determined by the increasing thickness of the

sediment layer. R_{fp} - the resistance of the filter medium - in our case corresponds to the clogging of the internal pores of the filter cloth. Once clogged, these pores are difficult to clean and sometimes require separate treatment, which reduces the overall efficiency of the filtration process.

Considering the above theoretical considerations and the sharp increase in pressure observed during filtration with the P-SH grade BFA, a decision was made to develop a composite material based on ANAB and P-SH, whose sorption characteristics were presented in Table 3. The composite obtained in this manner is composed of polar organic and nonpolar inorganic components.

Experimental research was carried out to develop composite BFA based on ANAB and P-SH for the treatment of long-term stored vegetable oils.

By varying the ratio of the obtained components, it is possible to achieve selective sorption of molecules of different sizes and, when necessary, to form an ion-exchanging, micro and mesoporous structure with adjustable properties across a wide range of pore sizes.

To enable control over the porous structure of the resulting BFA, composites were prepared using various ratios of ANAB and P-SH.

Using the following general mathematical formula (5), it is possible to predict in advance the sorption characteristics of composite BFAs obtained at different component ratios.

$$W_{comp} = \frac{W_1 \cdot m_1 + W_2 \cdot m_2}{m_1 + m_2} \quad (5)$$

Where:

W_1, W_2 - specific surface areas of the components, g/m²;

m_1, m_2 - mass ratios, %.

In our subsequent experiments, the effects of the obtained composites on the bleaching-filtration process of long-term stored cottonseed oil were investigated. It was found that the highest efficiency was achieved when using a composite BFA composed of bentonite clay and pyrolyzed sunflower husk in an equal (1:1) mass ratio.

The composite BFAs obtained are expected to possess polarity that enables the coagulation of fine soapstock particles within the oil, facilitating their aggregation and sedimentation. At the same time, due to their macroporous structure, these agents should prevent clogging of the filter cloth during the filtration process.

The BFA we are developing should not only mechanically retain particles but also be capable of reducing the chemical impurities present in the oil-specifically, the acid and peroxide values as well as the secondary oxidation products-to standard levels. The inclusion of acid-activated bentonite clay with a pH of 4 in the composite provides the ability to form ionic bonds. The sorption characteristics of the obtained composite BFA of the BK grade are presented in Table 7.

Table 7 - Sorption characteristics of the composite BFA

Parameters	BK
Specific surface area (BET), m²/g	154.24
Specific surface area of micropores, m²/g	36.36
Specific surface area of meso and macropores, m²/g	117.27
Pore volume, cm³/g	0.135
Average pore diameter, Å	34.08

In the course of our research, the filtration capabilities of acid-activated clays, as well as organic, inorganic, and composite materials, were studied for use in filtering polished refined vegetable oils after long-term storage.

Table 8 presents the changes in the acid value of polished refined cottonseed oil after filtration using various BFAs.

Table 8 - Effect of the amount of BFA obtained by different methods on the acid value

BFA dosage, %	ANAB	AOC	BK
	Acid value, mg KOH/g		
0.5	0.13	0.14	0.11
1	0.13	0.14	0.1
1.5	0.12	0.13	0.09
2	0.11	0.12	0.07
2.5	0.11	0.12	0.07
Standard Deviation	0.01	0.01	0.017888544
Standard Error	0.004472136	0.004472136	0.008
Upper Cl (95%)	0.13241664	0.14241664	0.110211561
Lower Cl (95%)	-0.10758336	0.11758336	0.065788439

As shown in the table, the addition of all BFA samples at a dosage of 2% relative to the oil mass resulted in the greatest reduction of the acid value. Specifically, this parameter was 0.11 mg KOH/g for ANAB, 0.12 mg KOH/g for AOC, and 0.07 mg KOH/g for the BK composite.

Figure 2 illustrates the variation of the acid value of cottonseed oil with respect to reagent consumption during the filtration process using different BFAs.

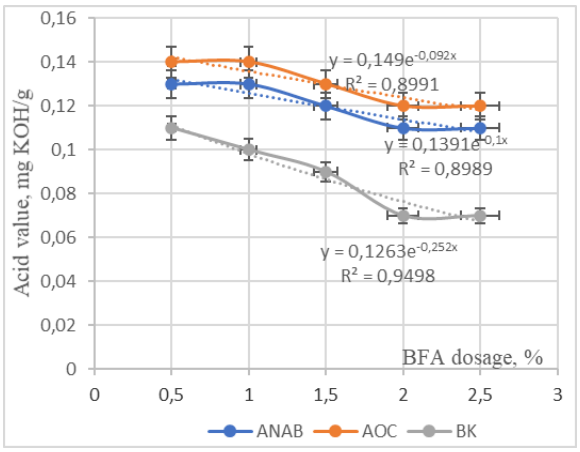

Figure 2 - Change in acid value relative to BFA dosage

As seen from the graph, the acid value consistently decreases for all samples as the reagent dosage increases.

This process is associated with the adsorption of free fatty acids onto the active sites present on the surface of the BFAs. The regression equations for the indicators obtained in the experiments were expressed as follows:

$$ANAB: y=0{,}149e^{-0{,}092x},\ R^2=0.8997$$
$$AOC: y=0{,}1391e^{-0{,}1x},\ R^2=0.8997$$
$$BK: y=0{,}1263e^{-0{,}252x},\ R^2=0.9351$$

For the BK-grade BFA, the value of $R^2 = 0.9351$ indicates that, within this system, the acid value follows an exponential decay pattern with respect to reagent consumption.

Filtration using the BK-grade O-FA resulted in the greatest reduction of acid value and peroxide content in the oil compared with ANAB and AOC. This can be attributed to the fact that both clay samples were activated using an acid-based method, resulting in a final product with an acidic pH environment. Although the acidity of the medium is an important factor for the adsorption of certain substances, temperature and time can also contribute to an increase in the acid value. In the graphs shown in Figure 1, the reduction in the acid value of the oil sample filtered using the BK-grade BFA is attributed to the presence of the P-SH component within its composition.

The capability of the obtained BFAs to remove oxidation products during the filtration of oil samples was also investigated, and the results are presented in Table 9.

Table 9 - Effect of the amount of BFA obtained by different methods on the peroxide value

BFA dosage, %	ANAB	AOC	BK
	Peroxide value, mmol ½O/kg		
0.5	3.8	4	3.7
1	3.6	3.8	3.3
1.5	2.9	3.5	2.1
2	2.6	3.2	1.9
2.5	2.5	3	1.9
Standard Deviation	0.59	0.41	0.855569985
Standard Error	0.124096736	0.08	0.397492138
Upper CI (95%)	4.024547777	4.002115608	3.703615102
Lower CI (95%)	3.335452223	3.557884392	1.496384898

According to the table data, filtration using BFA samples at a dosage of 2% relative to the oil mass had the greatest effect in reducing the peroxide value. At this dosage, the peroxide value of the oil filtered with ANAB decreased from 4.2 mmol ½O/kg to 2.5 mmol ½O/kg, while filtration with AOC reduced it to 4.2 mmol ½O/kg. In contrast, filtration using the BK composite resulted in a further decrease of the peroxide value to 1.9 mmol ½O/kg.

Figure 3 illustrates the variation of the peroxide value of cottonseed oil with respect to reagent consumption during the filtration process using different BFAs.

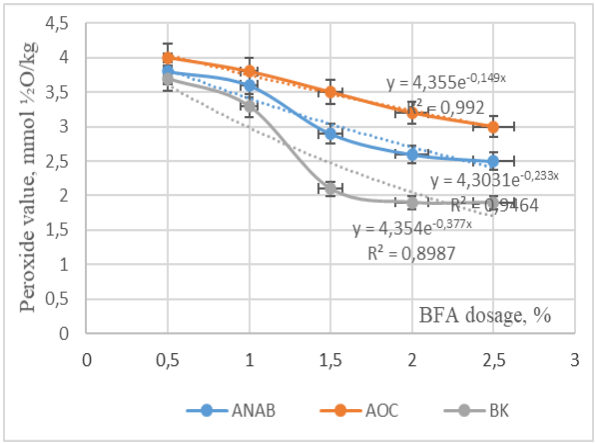

Figure 3 - Change in peroxide value relative to BFA dosage

As observed from the graph, the peroxide value consistently decreases for all samples as the reagent dosage increases. The regression equations describing the relationship between reagent consumption and peroxide value for ANAB, AOC, and BK samples are expressed as follows:

$$\text{ANAB: } y = 4.355e^{-0.149x},\ R^2 = 0.9929$$
$$\text{AOC: } y = 4.3031e^{-0.233x},\ R^2 = 0.9437$$
$$\text{BK: } y = 4.354e^{-0.377x},\ R^2 = 0.8641$$

The results indicate that the R^2 values range from 0.86 to 0.99 which demonstrates that the model shows excellent agreement with the experimental data. In particular, the R^2 value of 0.9929 for the ANAB sample indicates a nearly perfect exponential relationship between the peroxide value and reagent consumption within this system.

Since the pH of the ANAB and AOC samples was higher compared to that of the BK sample, better results in terms of peroxide value reduction were achieved in the oil filtered using the mineral-organic composite BFA. Under the influence of temperature, secondary oxidation products are formed alongside the primary ones. The adsorption of these compounds onto the active sites of the BFAs significantly affects the overall kinetics of the process.

In the BK grade composite, the P-SH component provides sufficient porosity to retain micro-sized impurities from the oil, while the ANAB component prevents clogging of the filter cloth pores under pressure. In other words, it inhibits deformation of the sediment particles and functions as a drainage layer. As a result, both the filtration pressure and the filtration time are reduced. In addition, the presence of ANAB within the BK composition ensures that, during filtration, the acidic environment of the clay promotes both the ionic binding of the oil's coloring substances within the microporous active sites and their adsorption within the meso and macroporous structures.

In this process, the filtration performance of AOC was limited because its adsorption pore structure had a relatively large average pore diameter (74 Å) and a comparatively small specific surface area of micropores (4.70 m^2/g). The adsorption pores present in AOC are primarily composed of macro and mesopores. Since the pore size is larger than that of the particles being filtered, this indicates that AOC functions mainly as a transmission channel rather than as an effective adsorbent medium.

Conclusions

The conducted studies revealed that the mineral-organic BFA obtained by combining bentonite and pyrolyzed sunflower husk in a 1:1 mass ratio demonstrated high efficiency in the filtration process of cottonseed oil. A composite BFA of the BK grade was developed based on the synergistic interaction between the mesoporous, mechanically stable structure of ANAB (with a specific surface area of 176.38 m^2/g) and the microporous, carbon-based structure of P-SH. This combination resulted in a material with enhanced pressure resistance and high filtration efficiency. The simultaneous processes of filtration and adsorption purification significantly improve the color and clarity of the oil, removing oxidized and suspended impurities. ANAB in the composition reduces the compressibility of the filtered precipitate and increases its permeability, while P-SH effectively sorbs micro-sized molecules and oxidation products. This ensures a stable filtration process speed and prevents pressure increase.

At the same time, the proposed BFA oils with organic and mineral composition act as a drainage layer during the filtration stage, forming an incompressible layer under pressure.

The use of BFAs in the filtration process increases the filtration surface area and filtration rate due to the resistance of the formed precipitate. However, from a structural perspective, preventing this issue is considered quite challenging.

Through the use of BFAs, coagulated soapstock particles in polishing refined vegetable oils are effectively retained. As a result, during a continuous one-shift operation, issues such as the need for additional filter cleaning or filter cloth replacement do not arise.

Conflicts of interest. On behalf of all authors, the corresponding author states that there is no conflict of interest.

CRediT author statement: **N. Boyjanov**: Conceptualization, Methodology, Software, Data curation, Writing draft preparation; **Z. Kurayazov and A. Akhmedov**: Visualization, Investigation; **S. Jollibekov** and **N. Tajetdinov:** Supervision; **B. Annazarova:** Software, Validation; **N. Boyjanov** and **M. Khamidova**: Reviewing and Editing.

Formatting of funding sources. This research did not receive any specific grant from funding agencies in the public, commercial, or not-for-profit sectors.

Cite this article as: Boyjanov NI, Kurayazov ZR, Annazarova BR, Jollibekov SM, Tajetdinov ND, Khamidova M.O, Akhmedov AN. Study of the mechanism and efficiency of using mineral-organic bleaching-filtering agents in polishing refining. Kompleksnoe Ispolzovanie Mineralnogo Syra = Complex Use of Mineral Resources. 2028; 345(2):107-119. https://doi.org/10.31643/2028/6445.20

Минералды-органикалық ағартқыш-сүзгілеуіш агенттерді жылтырату рафинациясында қолдану механизмі мен тиімділігін зерттеу

[1]Бойжанов Н.И., [1]Кураязов З.Р, [2] Анназарова Б.Р., [3]Жоллибеков С.М, [3]Таджетдинов Н.Д., [4] Хамидова М.О., [5]Ахмедов А.Н.

[1]Әбу Райхон Беруни атындағы Үргеніш мемлекеттік университеті, Үргеніш, Өзбекстан
[2]Мамун университеті мемлекеттік емес оқу орны, Хиуа, Өзбекстан
[3]Қарақалпақстан ауыл шаруашылығы және агротехнологиялар институты, Нөкіс, Өзбекстан
[4] Ташкент химиялық технология институты, Ташкент, Өзбекстан
[5]Қаршы мемлекеттік техникалық университеті, Өзбекстан

Мақала келді: *20 қаңтар 2026*
Сараптамадан өтті: *23 мамыр 2026*
Қабылданды: *11 маусым 2026*

ТҮЙІНДЕМЕ

Осы ғылыми зерттеудің негізгі мақсаты - мемлекеттік қорда ұзақ уақыт сақталған өсімдік майларын олардың физика-химиялық көрсеткіштері бойынша тұтынушылық сапаға дейін тазарту болып табылады. Тәжірибелерде алты ай немесе одан да ұзақ уақыт сақталған мақта майларын жылтырату рафинациясы жүргізілді. Жылтыратылып рафинацияланған өсімдік майларының физика-химиялық көрсеткіштерін талдау негізінде ағартушы-сүзгілеуші агенттер (АСА) ретінде қолдануға арналған, әртүрлі кеуек құрылымына ие селективті материалдар алынды. АСА-лар бентонитті және опока типті саздарды қышқылмен белсендіру, сондай-ақ күнбағыс қауызын пиролиздеу арқылы алынды. Әрбір белсендірілген АСА-ның жылтыратылып рафинацияланған майларды сүзу қабілеті зерттелді. Зерттеу нәтижелері бойынша ең жоғары тиімділік қышқылмен белсендірілген Навбахор сілтілі бентониті (KNCB) мен пиролизденген күнбағыс қауызының (П-КК) 1:1 массалық қатынаста дайындалған ВК маркалы композициялық АСА-сы қолданылған кезде байқалды. Бұл қоспа май массасына қатысты 1,5–2,0% мөлшерде енгізілгенде ең жоғары нәтиже көрсетті. Зерттеу нәтижелері полярлы органикалық және полярсыз бейорганикалық компоненттерден тұратын композицияның сәтті жасалғанын дәлелдейді. Бұл композиция сүзу процесі кезінде қысымның артуына кедергі келтірмей, ұсақ сабын тұнбасының бөлшектерін тиімді сүзуге қабілетті.

Түйін сөздер: бентонит сазы, опока типті саз, күнбағыс қауызы, БЕТ талдауы, белсендіру, пиролиз, помпозиция, жылтырату арқылы рафинациялау, ағартушы-сүзгілеуші агент.

Авторлар туралы ақпарат:

Бойжанов Нодирбек Илхомович — *Техника ғылымдары бойынша философия докторы, Әбу Райхон Беруни атындағы Үргеніш мемлекеттік университетінің химиялық технология факультетінің қауымдастырылған профессоры, 220100, Х. Әлімжан көшесі, 14, Үргеніш, Өзбекстан. Email: b.nodirbek@urdu.uz; ORCID ID: https://orcid.org/0009-0002-1454-9478*

Кураязов Зарипбай Раматович — *Техника ғылымдары бойынша философия докторы, Әбу Райхон Беруни атындағы Үргеніш мемлекеттік университетінің химиялық технология факультетінің қауымдастырылған профессоры, 220100, Х. Әлімжан көшесі, 14, Үргеніш, Өзбекстан. Email: kurayazovzarifboy@gmail.com; ORCID ID: https://orcid.org/0000-0002-9217-0669*

Анназарова Барно Рустамовна — *Мамун университеті мемлекеттік емес оқу орны, Хиуа, Өзбекстан. Email: barno220517@gmail.com; ORCID ID: https://orcid.org/0009-0007-1821-9886*

Жоллыбеков Спандияр Мамадиярович — *Қарақалпақстан ауыл шаруашылығы және агротехнологиялар институты, Нөкіс, Өзбекстан. Email: s.jollibekov@tdaunukus.uz; ORCID ID: https://orcid.org/0009-0001-0390-3892*

Тажетдинов Наурызбай Дарибаевич — *Қарақалпақстан ауыл шаруашылығы және агротехнологиялар институтының доценті, Нөкіс, Өзбекстан. Email: nauriztajetdinov@gmail.com; ORCID ID: https://orcid.org/0009-0007-0516-3772*

Хамидова Мадина Олимжоновна — *Ташкент химиялық технология институтының доценті, Навои көшесі, 32, Ташкент, Өзбекстан. Email: m.khamidova@mail.ru; ORCID ID: https://orcid.org/0000-0002-7299-0395*

Ахмедов Азимжон Нормуминович — *Техника ғылымдарының докторы, Шахрисабз тамақ инженериясы факультетінің профессоры, Қаршы мемлекеттік техникалық университеті, Ханабад даңғылы, 19, Өзбекстан. Email: a.ahmedov80@mail.ru; ORCID ID: https://orcid.org/0000-0002-8072-7458*

Исследование механизма и эффективности применения минерально-органических отбеливающе-фильтрующих агентов при полировочной рафинации

[1]Бойжанов Н.И., [1]Кураязов З.Р, [2] Анназарова Б.Р., [3]Жоллибеков С.М, [3]Таджетдинов Н.Д., [4] Хамидова М.О., [5]Ахмедов А.Н.

[1]Ургенчский государственный университет имени Абу Райхона Беруни, Ургенч, Узбекистан
[2]Негосударственное образовательное учреждение Мамунский университет, Хива, Узбекистан
[3]Каракалпакский институт сельского хозяйства и агротехнологий, Нукус, Узбекистан
[4]Ташкентский химико-технологический институт, Ташкент, Узбекистан
[5]Каршинский государственный технический университет, Узбекистан

Поступила: *20 января 2026*
Рецензирование: *23 мая 2026*
Принята в печать: *11 июня 2026*

АННОТАЦИЯ

В данном научном исследовании основной целью является очистка растительных масел, длительное время хранившихся в государственном резерве, до потребительского качества на основе их физико-химических показателей. В экспериментах была проведена полировочная рафинация хлопковых масел, хранившихся в течение 6 месяцев и более. Путём анализа физико-химических показателей полировочно рафинированных растительных масел были получены селективные отбеливающе-фильтрующие агенты (ОФА) с различной пористой структурой для использования на стадии отбеливания и фильтрации. ОФА были получены путём кислотной активации бентонитовых и опоковидных глин, а также пиролиза подсолнечной шелухи. Были исследованы фильтрационные способности каждого активированного ОФА по отношению к полировочно рафинированным маслам. Полученные результаты показали, что наивысшая эффективность была достигнута при добавлении композиционного ОФА марки ВК, приготовленного в массовом соотношении 1:1 из кислотно-активированного Навбахорского щелочноземельного бентонита (KANB) и пиролизованной подсолнечной шелухи (П-ПШ), в количестве 1,5–2,0 % по отношению к массе масла. Результаты исследования показали, что была успешно получена композиция, состоящая из полярных органических и неполярных неорганических компонентов, способная фильтровать мелкие частицы соапстока и при этом не препятствовать росту давления в процессе фильтрации.

Ключевые слова: бентонитовая глина, глина опокового типа, шелуха подсолнечника, БЭТ-анализ, активация, пиролиз, қомпозиция, полировальная рафинация, отбеливающе-фильтрующий агент.

Информация об авторах:

Бойжанов Нодирбек Илхомович — *Доктор технических наук, доцент факультета химической технологии Ургенчского государственного университета имени Абу Райхона Бируни, 220100, ул. Х. Олимжон, 14, Ургенч, Узбекистан. Email: b.nodirbek@urdu.uz; ORCID ID: https://orcid.org/0009-0002-1454-9478*

Кураязов Зарипбай Раматович — *Доктор философии по техническим наукам, доцент химико-технологического факультета Ургенчского государственного университета имени Абу Райхона Беруни, 220100, улица Х. Олимджона, 14, Ургенч, Узбекистан. Email: kurayazovzarifboy@gmail.com; ORCID ID: https://orcid.org/0000-0002-9217-0669*

Анназарова Барно Рустамовна — *Неправительственное образовательное учреждение Мамунский университет, Хива, Узбекистан. Email: barno220517@gmail.com; ORCID ID: https://orcid.org/0009-0007-1821-9886*

Жоллибеков Спандияр Махамадиярович — *Каракалпакский институт сельского хозяйства и агротехнологий, Нукус, Узбекистан. Email: s.jollibekov@tdaunukus.uz; ORCID ID: https://orcid.org/0009-0001-0390-3892*

Таджетдинов Наурузбай Дарибаевич — *Доцент Каракалпакского института сельского хозяйства и агротехнологий, Нукус, Узбекистан. Email: nauriztajetdinov@gmail.com; ORCID ID: https://orcid.org/0009-0007-0516-3772*

Хамидова Мадина Олимжоновна — *Доцент Ташкентского института химической технологии, ул. Навои, 32, Ташкент, Узбекистан. Email: m.khamidova@mail.ru; ORCID ID: https://orcid.org/0000-0002-7299-0395*

Ахмедов Азимжон Нормуминович — *Доктор технических наук, профессор, факультет пищевой инженерии, Шахрисабзский государственный технический университет, проспект Ханабад, 19, Узбекистан. Email: a.ahmedov80@mail.ru; ORCID ID: https://orcid.org/0000-0002-8072-7458*

References

[1] Candido I C M, Pires I C B, & de Oliveira H P. Natural and synthetic fiber-based adsorbents for water remediation. CLEAN - Soil, Air, Water. 2021; 49(6):2000189. https://doi.org/10.1002/clen.202000189

[2] Abbas H, Alrubaye S J, Al-Hussainy A F, Saadi B M, Gati M A, Hussein T Kh, Ilxomovich B N, & Muften N F. Role of carrageenan and health approach for adsorption of Safranin-T dye from aqueous solution by using polymer/CNT surface. Journal of Nanostructures. 2025; 15(4):1839-1848. https://doi.org/10.22052/JNS.2025.04.027

[3] Hussein U A-R, Alalwan D H K, Qabel H A, Abid F M, Hamza H H, Ilxomovich B N, Aljeboree A M, & Alkaim A F. Green synthesis and characterization of guar gum/polyacrylamide/activated carbon hydrogel for efficient methylene blue removal. Journal of Nanostructures. 2025; 15(4):1849-1860. https://doi.org/10.22052/JNS.2025.04.028

[4] Boyjanov N, Radjabov M, Serkayev Q, Boyjanov I, & Yaxshimuradov N. Activation and comparison of indicators of bentonite clay of the Navbakhor deposit. E3S Web of Conferences. 2024; 563:02018. https://doi.org/10.1051/e3sconf/202456302018

[5] Boyjanov NI, Rakhimov UB, Ataullaev ZM, Boltayev MA, Serkayev QP, Khamidova MO. Mathematical analysis of the linear increase in SiO_2 content during the activation of Navbakhor alkaline bentonite with hydrochloric acid. Kompleksnoe Ispolzovanie Mineralnogo Syra = Complex Use of Mineral Resources. 2027; 342(3):90-99. https://doi.org/10.31643/2027/6445.33

[6] Kumar M, Zhang B, Potkule J, Sharma K, Radha C H, Sheri V, Chandran D, Dhumal S, Dey A, Rais N, Senapathy M, Natta S, Viswanathan S, Mohankumar P, & Lorenzo J M. Cottonseed oil: Extraction, characterization, health benefits, safety profile, and application. Food Analytical Methods. 2022; 16(2):266-280. https://doi.org/10.1007/s12161-022-02410-3

[7] Soylu TM, Özel C, Karakuzu Ikizler B, et al. Mesoporous silica aerogels for sunflower oil refining and investigation of their adsorption performance. J Sol-Gel Sci Technol. 2025; 115:327–348 https://doi.org/10.1007/s10971-024-06395-9

[8] Karim NAA, Othman NH, Yusoff MM. Vegetable Oil Refining. In: Lee Y, Tang TK, Phuah ET, Lai OM (eds). Recent Advances in Edible Fats and Oils Technology. Springer, Singapore. 2022. https://doi.org/10.1007/978-981-16-5113-7_4

[9] Setyawardhani DA, Satiawardana TH. Innovative approach to vegetable oil production and refining technology in Indonesia: a review. Discov Chem Eng. 2025; 5:27. https://doi.org/10.1007/s43938-025-00099-4

[10] Shamuratov Sanjarbek, Umid Baltaev, Umarbek Alimov, Namazov Shafoat, Sherzod Kurambaev, and Bazar Ibadullaev. Utilization Process Research of the Soap Industry Acid Waste Water with High Carbonate Phosphorite of Central Kyzylkum. E3S Web of Conferences. EDP Sciences. 2021. https://doi.org/10.1051/e3sconf/202126404079

[11] Shamuratov Sanjarbek, Umid Baltaev, Sanobar Achilova, Umarbek Alimov, Shafoat Namazov, and Najimuddin Usanbaev. Enhancement of Availability of High Calcareous Phosphorite by Neutralization of Acid Effluent and Composting of Cattle Manure. E3S Web of Conferences. EDP Sciences. 2023. https://doi.org/10.1051/e3sconf/202337703004

[12] Shamuratov Sanjarbek, Umid Baltaev, Olga Myachina, Umarbek Alimov, Elyor Atashev, and Tokhir Kuramboev. Agrochemical Efficiency of Slow Release Phosphate Fertilizers Derived on the Base of Phosphorite Activation. E3S Web of Conferences. EDP Sciences. 2023. https://doi.org/10.1051/e3sconf/202343403014

[13] Kurayazov Z, Ollaberganova A,Jabbarov M, MatnazarovU, Babajanova R. Reduction of Fluoride in Central Kyzylkum Phosphate Waste in an Acidic Environment: Experimental and Mathematical Study Based on the Langmuir Model. Kompleksnoe Ispolzovanie Mineralnogo Syra = Complex Use of Mineral Resources. 2027; 343(4):65-76. https://doi.org/10.31643/2027/6445.41

[14] Salikhanova D, Sagdullaeva D, Ismoilova M, Ruzmetova D, Sadullaeva M, Karabayeva M, & Kadirov N. Activation of bentonite and palygorskite adsorbents by acid under microwave radiation. E3S Web of Conferences. 2023; 458:02017. https://doi.org/10.1051/e3sconf/202345802017

[15] Boyjanov NI, Otajonova GM, Kendjayev BB, Matyakubova MX, Sabirova NK, Masharipov AT, Boyjanov IR, Serkayev QP. Exponential modeling of Al_2O_3 reduction during activation of Navbahor alkaline-earth bentonite. Kompleksnoe Ispolzovanie Mineralnogo Syra = Complex Use of Mineral Resources. 2027; 343(4):106-115. https://doi.org/10.31643/2027/6445.44

[16] Silva MP, Nieva Lobos ML, Piloni RV, et al. Pyrolytic biochars from sunflower seed shells, peanut shells and Spirulina algae: their potential as soil amendment and natural growth regulators. SN Appl. Sci. 2020; 2:1926. https://doi.org/10.1007/s42452-020-03730-x

[17] Ogbu A I, Ovuoraye P E, Ajemba R O, & Dehghani M H. Functionality and mechanistic parametric study of the potential of waste plantain peels and commercial bentonite for soybean oil refining. Scientific Reports. 2023; 13:19569. https://doi.org/10.1038/s41598-023-46842-1

[18] Sverguzova S V, Gafarov R R, Zubkova O S, Sapronova J A, & Shaikhiev I G. Changes in the physicochemical and sorption properties of bleaching clay in the course of thermal treatment. Colloid Journal. 2024; 86(4):571-579. https://doi.org/10.1134/S1061933X24600490

[19] Vlasova EA, Valueva KA, Solomkina YS, et al. Application of Natural Clays for Purification of Rapeseed Oil from Colorant. Russ J Appl Chem. 2020; 93:1710–1714. https://doi.org/10.1134/S1070427220110129

[20] Salikhanova D, Sadullaeva M, Ruzmetova D, Sagdullayeva D, Mamajanova M, & Karabayeva M. The effect of acid activation on the physicochemical properties of bentonite. AIP Conference Proceedings. 2025; 3304:040019. https://doi.org/10.1063/5.0269999

[21] Sagdullaeva D S, Salikhanova D S, Ismailova M A, Abdurakhimov A A, Khaytmetova S B, Sagdullaeva M Sh, & Mamajonova MA. Improvement of the process of hydrotation of soybean oil. AIP Conference Proceedings. 2025; 3304:040038. https://doi.org/10.1063/5.0269243

[22] Shamuratov S, Alimov U, Rifky M, Baltaev U, Ibragimova M, Kurambaev S, & Radjabov M. Investigation of the Kinetics of Cotton Soapstock Saponification under Ultrasonic Illumination. Eurasian Chemico-Technological Journal. 2025; 27(4):323–335. https://doi.org/10.18321/ectj1679

[23] Pandiselvam R, Rajbongshi B, Deepali D, et al. Advances in non-invasive techniques for enhancing cottonseed oil quality and shelf life: a sustainable approach. Food Measure. 2025. https://doi.org/10.1007/s11694-025-03653-4

[24] Machado M, Rodríguez-Alcalá L M, Gomes A M, & Pintado M. Vegetable oils oxidation: Mechanisms, consequences and protective strategies. Food Reviews International. 2023; 39(7):4180-4197. https://doi.org/10.1080/87559129.2022.2026378

[25] Yaragalla S, Rajendran R, & Bhavitha K B. A review on bioactive compounds and their anti-oxidative properties for the enrichment of vegetable oils. European Food Research and Technology. 2025; 251:2537-2551. https://doi.org/10.1007/s00217-025-04805-y

[26] Khaled B M, Biswas M, Sina A A, Alam A, Alim M A, Hossain M E, Saqib M N, Rana M S, & Rahman Sweet S. Detection of the changes in fatty acid composition and physicochemical properties in selected edible oils heated at different degrees of time. Food Chemistry Advances. 2024; 4:100716. https://doi.org/10.1016/j.focha.2024.100716

[27] Islam M, Kaczmarek A, & Tomaszewska-Gras J. Differential scanning calorimetry as a tool to assess the oxidation state of cold-pressed oils during shelf-life. Journal of Food Measurement and Characterization. 2023; 17:6639-6651. https://doi.org/10.1007/s11694-023-02152-8

[28] Wang Y, Guo N, He X, Shen F, & Liang Y. Disentangling fluorescence of endogenous fluorescent substances from absorption and scattering effects for quantitative prediction for oxidation degree of peanut oils. Food Analytical Methods. 2024; 18(4):532-541. https://doi.org/10.1007/s12161-024-02743-1

[29] Gharby S. Refining vegetable oils: Chemical and physical refining. The Scientific World Journal. 2022, 6627013. https://doi.org/10.1155/2022/6627013

[30] Sonawane A, & Waghmode S. A review on vegetable oil refining: Process, advances and value addition to refining by-products. In Bioremediation for Global Environmental Conservation (Working Title). IntechOpen. 2023. https://doi.org/10.5772/intechopen.108752

[31] Wang Z, Wang W, & Li J. Study of a cake model during stirred dead-end microfiltration. Desalination. 2007; 202(1-3):226-234. https://doi.org/10.1016/j.desal.2007.02.010

Crossref
DOI: 10.31643/2028/6445.21
Mining & Mineral Processing

Optimal evaporation regime of alkaline solution obtained from cotton stalk ash and chemical analysis of precipitation process

[1*]Boltayev M.A., [2]Otajonova G.M., [3]Khakimova B.B., [1]Khamidova M. O., [1]Akramova R.R., [4]Boltayev M.A., [1]Serkayev Q.P.

[1]Tashkent Chemical-Technological Institute, Tashkent, Uzbekistan
[2]Mamun University, Khiva, Uzbekistan
[3]Urgench State University named after Abu Rayhon Beruni, Urgench, Uzbekistan
[4]Tashkent State Agrarian University, Tashkent, Uzbekistan

**Corresponding author email: mirjalolboltayev@mail.ru*

Received: *April 21, 2026*
Peer-reviewed: *April 27, 2026*
Accepted: *July 1, 2026*

ABSTRACT

This article describes a comprehensive analysis of the optimal evaporation method for an alkaline solution that is prepared using the aqueous extract of cotton stalk ash, along with the investigation of the chemical composition of the precipitation that appears during evaporation of the solution. Cotton stalk ash is regarded as a secondary product from burning biomass in household appliances, specifically in tandir ovens used to bake bread and somsa, and is currently being discarded into the environment. In the presented research, the procedure for preparation of the alkaline solution was conducted under optimal conditions, when the mixture of ash and water with the weight ratio of 1:5 was boiled. Then, filtration and evaporation of the obtained suspension were performed. From the results obtained, the optimal evaporation regime was identified as 75%, as during this regime no precipitation occurs. Nevertheless, at an evaporation level of 80%, precipitation was observed in the solution due to the disturbance of the solubility equilibrium. The content of the precipitated components in relation to cations was estimated using flame photometry, and the phase composition was evaluated with FTIR spectroscopy. Thus, the precipitate was found to contain mainly carbonate-like compounds. It was proved that potassium ions prevailed in the solution, and their molar concentration is much greater than that of other cations. Moreover, when the concentration is high, a certain share of potassium ions is transferred from the solution into the precipitate phase. As calculated, the total alkalinity of the prepared solution equals 3.41 N and constitutes about half of the alkalinity of the 6 N NaOH solution employed in the vegetable oils purification process.

Keywords: cotton stalk ash, extraction, evaporation, potassium ions, carbonates, precipitate, flame photometry, FTIR, co-precipitation, alkaline solution.

Information about authors:

Boltayev Mirjalol Allayarovich — *Doctoral candidate at the Tashkent Chemical-Technological Institute, Navoi Street, 32, Tashkent, Uzbekistan. Email: mirjalolboltayev@mail.ru; ORCID ID: https://orcid.org/0000-0002-3172-658X*

Otajonova Gulkhayo Maqsud kizi — *Lecturer, Mamun University, Khiva, Khorezm, Uzbekistan. Email: otajonovagulhayo1508@gmail.com; ORCID ID: https://orcid.org/0009-0008-7529-9656*

Khakimova Bahor Baxtiyarovna — *Doctor of Philosophy in Technical Sciences, Associate Professor at the Faculty of Chemical Technology, Urgench State University named after Abu Rayhon Beruni, 220100, H. Olimjon Street 14, Urgench, Uzbekistan. Email: oot.baxor44@gmail.com; ORCID ID: https://orcid.org/0000-0001-5312-1963*

Khamidova Madina Olimjonovna — *Associate Professor at the Tashkent Chemical-Technological Institute, Navoi Street 32, Tashkent, Uzbekistan. Email: m.khamidova@mail.ru; ORCID ID: https://orcid.org/0000-0002-7299-0395*

Akramova Rano Ramizitdinovna — *Professor at the Tashkent Chemical-Technological Institute, Navoi Street, 32, Tashkent, Uzbekistan. Email: ranoakr123@gmail.com; ORCID ID: https://orcid.org/0000-0002-1417-2044*

Boltayev Murod Allayarovich — *Doctor of Philosophy in Technical Sciences, Tashkent State Agrarian University, 100140 Tashkent, Uzbekistan. Email: murodbek.boltaev.78@mail.ru; ORCID ID: https://orcid.org/0009-0008-7001-2855*

Serkayev Qamar Pardayevich — *Professor at the Tashkent Chemical-Technological Institute, Navoi Street, 32, Tashkent, Uzbekistan. Email: serkayev@mail.ru; ORCID ID: https://orcid.org/0009-0009-8316-4994*

Introduction

Rational and effective use of waste from plant biomass has become one of the priority trends in scientific research. The resulting ash from burning plant biomass consists of a complex mineral composition, where potassium, calcium, and silicon compounds play an important role as predominant elements. There is a considerable difference in the proportion of these elements, depending on the

type of raw materials used and the conditions of the burning process [[1], [2], [3], [4], [5]].

Based on existing scientific publications, it is possible to state that potassium-containing compounds in biomass ash have good solubility in water and transfer to the solution phase during extraction and play the role of active agents. Calcium compounds, in turn, are found mainly in the insoluble carbonate form and do not dissolve in aqueous solutions [[6], [7]].

Extraction of alkaline components from the ash involves a series of complex physicochemical processes, including ion exchange, solubility of substances, and phase equilibrium processes. Due to the high solubility of potassium and sodium salts in water, they selectively dissolve in an aqueous phase, thus forming a high concentration of alkali solution [[8], [9]].

The physicochemical properties of the obtained solution are determined by several main technological parameters: temperature, duration of the extraction process, and the ratio between the liquid and solid phases. The aforementioned technological parameters have a significant impact on the formation and stabilization of the composition of the solution [8].

Technologically, it is important to control the evaporation process and obtain an aqueous solution with high concentration. It should be noted that the higher the concentration of the solution, the higher its degree of alkalinity; but beyond a critical point, the solubility equilibrium is disturbed, leading to precipitation of poorly soluble products of ion reactions [[10], [11].

In conditions of high concentration, the interaction between the ions increases, causing co-precipitation reactions. It contributes to the creation of poorly soluble complexes and alloys, reducing the compositional stability of the solution and causing the loss of a part of the required substances. Thus, setting the required level of evaporation and its effective regulation become essential aspects when striving to improve the performance characteristics of the technological complex [[11], [12]].

The alkaline solution produced based on biomass ash is expected to be a prospective compound applicable in many industrial procedures. For example, in processing vegetable oil, it has a significant function of neutralizing free fatty acids [[13], [14], [15]].

The success rate of the procedure in question largely depends on the concentration and chemical composition of the alkaline solution, and both parameters play a critical role in the effectiveness of neutralization and the quality of the end-product [16]. In addition, the feasibility of utilizing such solutions as an alternative agent instead of traditional sodium hydroxide is justified in the literature as well [3].

From research findings, it can be concluded that biomass-based ash materials, especially plantain (heat-treated edible banana) peel ash, and in the mixture with traditional adsorbents, can efficiently reduce the concentration of free fatty acids (FFA) in vegetable oil. Under optimized conditions, the maximum efficiency of removing FFA through using these materials may range from 70% to 97% [3].

The high efficiency of the method can be attributed to the strong reaction of active substances in the ash with FFA and excellent adsorption properties of the material.

The process of obtaining potassium carbonate from cocoa pod ash has also been studied, where the major impurity element has been revealed to be calcium ions. It was additionally noted that the efficient removal of such impurities from the solution is crucial [1].

Thus, the above data prove the feasibility of the use of alkaline compounds isolated from the biomass ash as an alternative or complementary substance for conventional alkaline reagents in the vegetable oil refining process, especially in neutralizing them. At the same time, this approach is advantageous not only due to its high efficiency but also because it lowers production expenses.

The technology of processing vegetable oils involves several consecutive steps, each one aimed at removing specific impurities from vegetable oils and concluding according to further processing needs. The allowed content of accompanying components of vegetable oils is defined by special standards and requirements, depending on the nature, quality, and application of vegetable oils.

Free fatty acid content in vegetable oils negatively influences the sensory qualities and increases oxidation rate. In addition, there have been proven dependencies between accompanying substance content and composition and ripeness of vegetable seeds used for oil production as well as processing conditions [[17], [18], [19]].

In processing vegetable oils with caustic soda, some part of carotenoids is absorbed by particles within the soap stock phase, which appears due to intensive interaction of oil with highly concentrated alkaline solution. Nevertheless, most of them are eliminated by solid adsorbents, which have an

elaborate structure [[20], [21], [22], [23], [24], [25], [26]].

Thus, the data presented above show that alkaline solutions derived from biomass ash are distinguished by their pronounced alkalinity and have significant prospects for the use of these solutions in industrial processes, including refining vegetable oils [[1], [3]]. Nevertheless, while the process of extraction of ash solutions is described thoroughly in previous scientific research, the further technological step-the process of evaporation and its impact on the composition of the solution and precipitation-is insufficiently studied. Specifically, the issues of ions' redistribution and their transformation in the solid state during the process of high concentration of the solution demand further scientific research.

As recent scientific research has revealed, the alkaline solutions derived from biomass ash may serve as an alternative source of sodium hydroxide in the industry. Such a method provides effective recycling of production wastes, allows decreasing the amount of imported chemicals, and helps use resources rationally [[3], [27], [28], [29]].

Consequently, in the current study, the most effective regimes for the evaporation of the alkaline solution prepared from cotton stalk ash were found, and a detailed analysis of ions' distribution in the solution and precipitate and their chemical properties were carried out using the flame photometry and infrared spectroscopy approaches. However, since the composition and concentrations of the alkaline solutions have a huge impact on the total effectiveness of the purification process, there should be some research conducted in this field. Indeed, it can be noted that such factors as the influence of evaporation on the solution's composition and the content of the active substance have not been considered thoroughly enough yet.

Materials and Methods

As the subject for investigation, the solution derived through the aqueous extraction of cotton stalk ash, along with the precipitates derived through the evaporation of said solution, were chosen. As the first step of the experiment, cotton stalk ash was combined with water in different mass ratios and heated up to dissolve the soluble compounds in the liquid phase. According to the results of the experiments conducted, the highest concentration of compounds in the solution was achieved using an ash-to-water mass ratio of 1:5.

This solution was filtered to separate the solid mass from the solution, and then the filtrate was kept separately and was evaporated to different degrees. In terms of filtrate evaporation, the conclusion is that evaporation up to 75% of the solution can be considered an optimal stage. In the case of such evaporation, the alkaline level of the solution is high, and there is no precipitation. When the evaporation of the solution was increased to 80%, precipitation occurred in the solution, and the precipitate was later examined. The solution with an evaporation rate of 75% was regarded as the optimal solution.

The determination of cations in the solution and precipitate and their precipitation was done by using flame photometry. Flame photometric analyses were performed using a BWB XP flame photometer produced by BWB Technologies Company (United Kingdom).

The determination of potassium ion concentration in the solution was done by taking 1.0 ml of the solution and placing it in a 1000 ml volumetric flask. Distilled water was added up to the mark, after which the solution was thoroughly mixed. Fifteen milliliters were withdrawn from the flask and analyzed using flame photometry.

Flame photometric analysis was done according to a calibration curve, and the concentration of the ions was determined in ppm.

The chemical composition of the precipitate was studied by the method of salt analysis. During the research work, a sample of the precipitate weighing 1 g was weighed exactly, placed in a volumetric flask of 1000 ml capacity, and then dissolved in distilled water. Then the mixture was well stirred, and the concentration of the main cations (potassium K^+, sodium Na^+, calcium Ca^{2+}, and barium Ba^{2+}) in the solution was determined using the flame photometry method.

The structural composition of the precipitate was established by infrared spectroscopy (FTIR). The measurements were carried out on an IRAffinity-1S FTIR spectrometer (Shimadzu, Japan). The spectra obtained allowed the identification of the functional groups present in the sample and an assessment of the mineralogical composition and chemical nature of the precipitate.

Results and Discussion

The research involved an analysis of the main stages of obtaining the alkali solution from cotton stalk ash, which is classified as agricultural waste, and the alkali concentration process. In order to

provide for complete dissolution of the alkaline components from the ash, the dissolution was carried out in water at a ratio of 1:5, providing for the creation of the primary alkali solution. The obtained solution was concentrated through gradual evaporation, thus creating solutions with varying degrees of concentration. In the present research, evaporation degrees of 25%, 50%, 75%, and 80% were tested, with the 75% degree being identified as the most technological one. The alkalinity was estimated by the titrimetric method, and the dependence on the evaporation degree was estimated. Additionally, the solutions with the 75% and 80% evaporation degrees, and the precipitate sample created under conditions of high concentration, were studied from the perspective of their physicochemical characteristics.

It was established that with an increase in the evaporation level, the balance of ions in the solution is disturbed, and individual substances pass into the phase of the precipitate in the form of insoluble compounds. In this regard, the impact on the selectivity of the composition of the solution, as well as the possibility of retaining the main alkaline components in the solution, is quite tangible.

According to the results of flame photometry of the optimal solution, potassium ions prevail in its composition. For a detailed evaluation of these data, the experimental results obtained during repeated tests are shown in Table 1.

Table 1 - Analytical results of the optimally evaporated solution

Experimental samples	Ion concentration (ppm)				
	K	Na	Ca	Ba	Li
Sample 1	114.9	10.1	9.3	8.5	0.35
Sample 2	115.3	10.3	9.5	8.7	0.38
Sample 3	116.1	10.6	9.8	9	0.42
Sample 4	116.5	10.8	10	9.2	0.45
Sample 5	115.7	10.2	9.4	8.6	0.4
SD	0.63	0.29	0.29	0.29	0.038

It is clear from the table above that the potassium ion had the highest concentration among all ions analyzed, and the low standard deviations suggest that the test results were highly reliable.

For instance, in the solution reduced to 75%, the mean concentration of potassium ions was 115.7 ppm, indicating that potassium is indeed the primary alkali element in the sample. However, apart from potassium ions, other ions such as Na^+, Ca^{2+}, and Ba^{2+} ions were also observed, albeit in low concentrations (Figure 1).

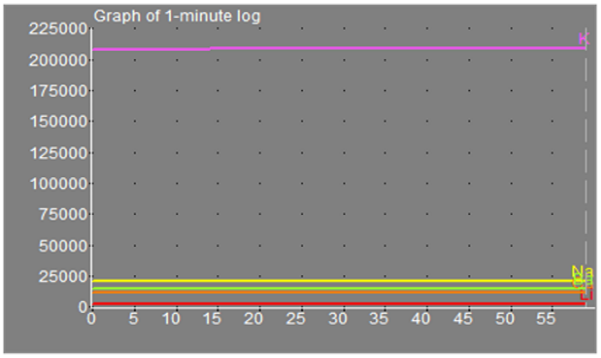

Figure 1 - Flame photometric spectrogram of the optimal solution

Based on the average values of the results from flame photometry, the presence of the following ions was detected in the solution: Na – 10.4 ppm; K – 115.7 ppm; Li – 0.4 ppm; Ca – 9.6 ppm; Ba – 8.8 ppm.

To express the values in terms of molar concentration, it was assumed that ppm is equal to mg/L, and then the calculations were carried out using the molecular mass of each ion.

Moreover, taking into account the fact that the solution sample was diluted 1000 times, the obtained values were recalculated using the appropriate coefficient, which allowed determining the concentration of ions in the initial solution (Figure 2).

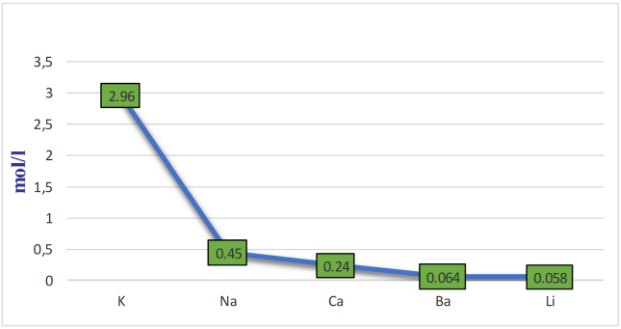

Figure 2 - Ion concentration in the optimal solution

Furthermore, considering that the solution was diluted up to 1000 times (from 1 to 1000 ml) during the test, it was taken into consideration that the resulting data referred to the sample diluted 1000 times, and accordingly, the resulting concentrations were recalculated by multiplying by 1000.

However, with the increasing evaporation degree, which means that the evaporation of the solution proceeded to more than 75%, the

precipitation took place. As shown in Table 2, based on the analysis of the precipitate carried out with the help of the BWB XP flame photometric technique, the precipitation includes not only Ca2+ ions but also considerable amounts of potassium ions.

Table 2 - Results of the analysis of the precipitate composition

Experimental samples	Ion concentration (ppm)				
	K	Na	Ca	Ba	Li
Sample 1	31.8	0.5	3.6	10.4	0.15
Sample 2	32.2	0.55	3.8	10.7	0.18
Sample 3	33	0.65	4.1	11.1	0.22
Sample 4	33.4	0.7	4.2	11.3	0.25
Sample 5	32.1	0.6	3.8	11	0.2
SD	0.67	0.07	0.24	0.35	0.038

From the table, it can be clearly seen that although different types of cations are found in the precipitate, the sum of all these fractions comprises a small proportion of the precipitate. The existence of potassium ions in the precipitate implies that evaporation of the solution should be stopped before the formation of the precipitate (up to 75% evaporation).

In addition, the existence of potassium ions in the precipitate suggests that potassium salts also partially precipitate from the solution at high concentrations.

The reason behind this behavior is the disturbance of the solubility equilibrium of the solution and the process of co-precipitation due to ion interactions. Meanwhile, the relatively large percentage of barium ions in the precipitate suggests the precipitation of carbonates, which means that carbonate ions are also present in the system and readily react with divalent cations to form poorly soluble compounds (Fig. 3).

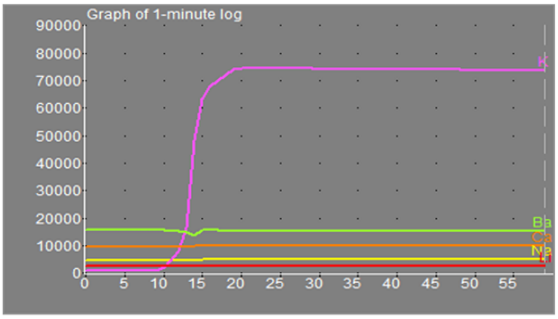

Figure 3 - Flame photometric spectrogram of the precipitate

Based on the average results of flame photometric analysis, it is possible to claim that the precipitate contains Na – 0.6 ppm, K – 32.5 ppm, Li – 0.2 ppm, Ca – 3.9 ppm, Ba – 10.9 ppm.

The analysis was performed according to the methodology, whereby 1 g of precipitate was used as a sample and was placed into a 1000 mL volumetric flask and filled up with distilled water. Then, a portion of this solution was analyzed with the help of a flame photometer. Consequently, the obtained ppm values indicate the content of ions in 1 g of precipitate in 1 L of solution.

The molar concentration of each ion was calculated, and the content of ions in the composition of the precipitate was estimated (Fig. 4).

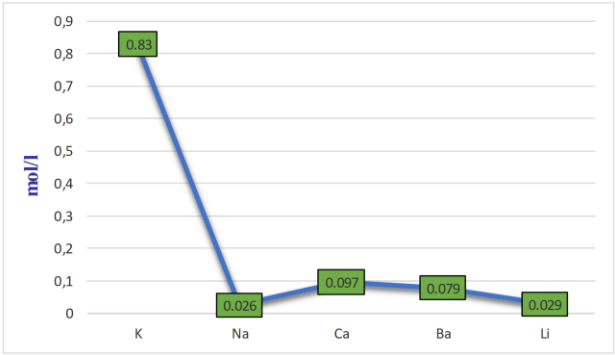

Figure 4 - Ion concentration in the precipitate

Based on the obtained data, it can be said that the content of potassium ions in the precipitate exceeds the content of other alkali metal ions. Thus, along with calcium, the precipitate contains potassium salts. It can also be noted that due to the higher content of barium ions, sodium, and lithium ions, the composition of the precipitate is a heterogeneous mineral mixture. In general, based on the obtained data, the precipitate after evaporation of up to 80% belongs to the complex multicomponent mixture containing a large amount of potassium and carbonate components.

Data on the chemical nature of the precipitate obtained by means of infrared spectroscopy (IRAffinity-1S FTIR) were additionally important. The analysis of the received spectrum (Fig. 5) confirms that the precipitate is predominantly carbonate.

The very strong absorptions appearing at 1477.68 and 1400.32 cm^{-1} represent the ν_3 vibrational transitions of the CO_3^{2-} ion. This high level of intensity and broadness implies that the carbonate species predominate. Furthermore, the absorption band appearing at 837.11 cm^{-1}

represents the v_2 transitions of the CO_3^{2-} ion; additionally, the absorption bands at 696.30 and 638.44 cm^{-1} correspond to the v_4 transitions. Notably, the absorption bands in the ~700 cm^{-1} region reveal the carbonate phases and could imply the existence of $CaCO_3$ or other carbonate forms.

In this context, the very intense absorption appearing at 1238.30 cm^{-1} indicates the existence of ion-ion interactions within the carbonate system or mixed carbonate phases. Additionally, the absorption band appearing at 1555.55 cm^{-1} might signify some other types of bonding interactions in the carbonate system or possibly the presence of organics.

The band located at 988.70 cm^{-1} signifies the presence of silicate compounds (Si-O bonds) within the precipitate sample; hence, the material does not appear to be an entirely carbonate compound but a mineral mixture. This may be attributed to the existence of silicates in the form of biomass ash contaminants. Weak peaks appearing in the high-frequency range (2081, 2144, 2206, and 2264 cm^{-1}) could be due to atmospheric CO_2 or gaseous compounds. The weak peaks found in the low-frequency range (605.65 and 449.41 cm^{-1}) represent metal-oxygen (M-O) bonds.

Generally, based on the FTIR analysis results, one may conclude that the predominant content of the precipitation is represented by carbonate compounds, primarily calcium carbonate. Nevertheless, due to the presence of certain additional peaks, it can be stated that the composition of the precipitate is not pure $CaCO_3$ but is a complex mixture of carbonates containing potassium, sodium, and other elements.

In this regard, based on the data obtained using infrared spectroscopy and flame photometry methods, one can conclude that the principal component of the precipitate is $CaCO_3$, but its composition is complex.

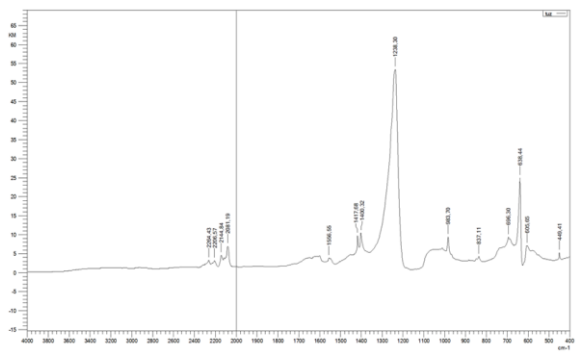

Figure 5 - FTIR spectrogram of the precipitate obtained using the IRAffinity-1S spectrometer

The obtained results indicated the distribution of ions between the solution and precipitate phases. At optimal parameters, potassium ions remained in the solution, while calcium ions migrated to the precipitate phase in the form of insoluble carbonates. Nonetheless, increasing the concentration of the solution resulted in disturbance of solubility equilibrium, thereby causing potassium compounds to migrate to the precipitate. The mechanism involved in this migration is called co-precipitation due to the ion interaction effect, which decreases the selectivity of the system.

It should be noted that the comparison of the results with literature data shows considerable discrepancies. Previously, it was found that potassium compounds remained in the solution phase, while in the current investigation, the migration of potassium ions occurred at a high degree of evaporation.

In this way, even though the evaporation procedure used for the concentration of the solution has positive effects up to a certain point, going past this point causes imbalance in the system and results in negative outcomes. According to the results of this experiment, it was concluded that the best technology in this situation is to stop the evaporation procedure before the appearance of precipitate. With such an approach, the largest amount of potassium ions will remain in the solution.

Conclusion

Based on the findings of this research, it became possible to define the basic physicochemical processes of extract solution evaporation from cotton stalk ash. It was established that the concentration of the solution up to 75% entails an increase in alkalinity, whereby potassium ions are present in a concentration of 2.96 mol/L, and precipitation does not take place. If the degree of evaporation exceeded 75%, then the solubility equilibrium would be disrupted, and precipitation would occur.

According to the analysis results, it is possible to conclude that the nature of the precipitation is predominantly carbonate, containing, besides other compounds, potassium ions and calcium. Thus, co-precipitation takes place owing to the interplay of ions when the concentration is high. Based on the analysis of ion distribution, it was revealed that potassium ions stay in the solution during ideal evaporation conditions, but excessive

concentration leads to their partial transition into the solid phase. This fact is accompanied by a decrease in selectivity and loss of useful substances. On this basis, it can be argued that from the technological perspective, the best regime implies the termination of the evaporation process prior to the appearance of precipitation, that is, at 75%.

According to the calculations, the total alkalinity of the obtained solution is 3.41 N due to K^+ and Na^+ ions. It is known that in conventional vegetable oil refining technology, sodium hydroxide (NaOH) is usually used as a 20% solution with a density of approximately 1.2 g/mL, which corresponds to about 6 N alkalinity for oil with an acid value of 5 mg KOH/g. The comparison results showed that the alkalinity of the ash extract solution is approximately 1.8 times lower than that of the same volume of NaOH solution used in conventional technology, meaning that its alkaline effect is about 56.8%.

However, from a technological point of view, the total amount of alkali introduced can be compensated by appropriately increasing the volume of the solution. On this basis, the use of ash extract solution may significantly reduce the consumption of imported NaOH and, under certain conditions, partially or almost completely replace it. The effectiveness of this approach in vegetable oil refining will be studied in detail in future research.

Conflicts of interest. On behalf of all authors, the corresponding author states that there is no conflict of interest.

CRediT author statement: **M. Boltayev and Q. Serkayev:** Conceptualization, Methodology, Software, Data curation, Writing draft preparation; **M. Boltayev, M. Khamidova and B. Khakimova:** Visualization, Investigation; **B. Khakimova:** Supervision; **G. Otajanova**: Software, Validation; **Akramova**: Reviewing and Editing.

Formatting of funding sources. This research did not receive any specific grant from funding agencies in the public, commercial, or not-for-profit sectors.

Cite this article as: Boltayev MA, Otajonova GM, Khakimova BB, Khamidova M.O, Akramova R.R, Boltayev MA, Serkayev QP. Optimal evaporation regime of alkaline solution obtained from cotton stalk ash and chemical analysis of precipitation process. Kompleksnoe Ispolzovanie Mineralnogo Syra = Complex Use of Mineral Resources. 2028; 345(2):120-129. https://doi.org/10.31643/2028/6445.21

Мақта сабағы күлінен алынған сілтілі ерітіндінің оңтайлы буландыру режимі және тұнба түзілу процесінің химиялық талдауы

[1]Болтаев М.А., [2]Отажонова Г.М., [3] Хакимова Б.Б., [1]Хамидова М.О., [1]Акрамова Р.Р., [4]Болтаев М.А., [1]Серкаев К.П.

[1]Ташкент химия-технология институты, Ташкент, Өзбекстан
[2]Мамун университеті, Хива, Өзбекстан
[3]Әбу Райхан Беруни атындағы Үргенч мемлекеттік университеті, Үргенч, Өзбекстан
[4]Ташкент мемлекеттік аграрлық университеті, Ташкент, Өзбекстан

Мақала келді: *21 сәуір 2026*
Сараптамадан өтті: *27 сәуір 2026*
Қабылданды: *1 шілде 2026*

ТҮЙІНДЕМЕ

Бұл мақалада мақта сабағы күлінің судағы экстракты негізінде алынған сілтілі ерітіндінің оңтайлы буландыру режимі, сондай-ақ ерітіндіні буландыру барысында пайда болатын тұнбаның химиялық құрамына кешенді талдау жүргізілген. Мақта сабағының күлі тұрмыстық мақсаттарда, атап айтқанда нан мен самса пісіруге арналған тандыр пештерінде биомассаны жағу нәтижесінде түзілетін, қазіргі уақытқа дейін іс жүзінде пайдаланылмай, қоршаған ортаға шығарылып жатқан екінші реттік өнім ретінде қарастырылады. Ұсынылған зерттеуде сілтілі ерітіндіні алу үдерісі оңтайлы жағдайда жүргізілді, яғни күл мен судың 1:5 масса қатынасындағы қоспасы қайнатылды. Кейін алынған суспензия сүзгіден өткізіліп, буландыру жүргізілді. Алынған нәтижелер бойынша буландырудың оңтайлы режимі 75% деп анықталды, өйткені осы деңгейде тұнба түзілуі байқалмайды. Алайда буландыру дәрежесі 80%-ға жеткенде, ерігіштік тепе-теңдігінің бұзылуына байланысты ерітіндіде тұнба түзілуі анықталды. Тұнбаның катиондық құрамы жалынды фотометрия әдісімен анықталып, фазалық құрамы FTIR Фурье спектроскопиясы арқылы зерттелді. Нәтижесінде тұнбаның негізінен карбонат текті қосылыстардан тұратыны анықталды. Ерітіндіде калий иондарының басым екендігі және олардың молярлық концентрациясы басқа катиондарға қарағанда едәуір жоғары екендігі дәлелденді. Сонымен қатар, жоғары концентрация жағдайында калий иондарының белгілі бір бөлігі ерітіндіден тұнба фазасына өткендігі байқалды. Есептеулер бойынша алынған ерітіндінің жалпы сілтілігі 3,41 N- құрайды, бұл өсімдік майларын тазарту үдерісінде қолданылатын 6 N натрий гидроксиді (NaOH) ерітіндісінің сілтілігінің шамамен жартысына сәйкес келеді.

Түйін сөздер: мақта сабағының күлі, экстракция, буландыру, калий иондары, карбонаттар, тұнба, жалынды фотометрия, FTIR, бірлесіп тұнбалану, сілтілі ерітінді.

Болтаев Миржалол Аллаярович — ***Авторлар туралы ақпарат:*** *Докторант, Ташкент химия-технология институты, Навои көшесі, 32, Ташкент, Өзбекстан. Email: mirjalolboltayev@mail.ru; ORCID ID: https://orcid.org/0000-0002-3172-658X*

Отажонова Гүлхайо Мақсудтың қызы — *Мамун университеті, Хива, Хорезм, Өзбекстан. Email: otajonovagulhayo1508@gmail.com; ORCID ID: https://orcid.org/0009-0008-7529-9656*

Хакимова Бахор Бахтияровна — *Техника ғылымдарының философия докторы, Әбу Райхан Беруни атындағы Үргеніш мемлекеттік университеті Химия-технология факультетінің доценті, 220100, Х.Олимжон көшесі 14, Үргеніш, Өзбекстан. Email: oot.baxor44@gmail.com; ORCID ID: https://orcid.org/0000-0001-5312-1963*

Хамидова Мадина Олимжоновна — *Ташкент химия-технология институтының доценті, Навои көшесі, 32, Ташкент, Өзбекстан. Email: m.khamidova@mail.ru; ORCID ID: https://orcid.org/0000-0002-7299-0395*

Акрамова Рано Рамизитдиновна — *Ташкент химия-технология институтының профессоры, Навои көшесі, 32, Ташкент, Өзбекстан. Email: ranoakr123@gmail.com; ORCID ID: https://orcid.org/0000-0002-1417-2044*

Болтаев Мурод Аллаярович — *Техника ғылымдары бойынша философия докторы, Ташкент мемлекеттік аграрлық университеті, 100140, Ташкент, Өзбекстан. Email: murodbek.boltaev.78@mail.ru; ORCID ID: https://orcid.org/0009-0008-7001-2855*

Серкаев Камар Пардаевич — *Ташкент химия-технология институтының профессоры, Навои көшесі, 32, Ташкент, Өзбекстан. Email: serkayev@mail.ru; ORCID ID: https://orcid.org/0009-0009-8316-4994*

Оптимальный режим выпаривания щелочного раствора, полученного из золы стеблей хлопчатника, и химический анализ процесса образования осадка

[1]Болтаев М.А., [2]Отажонова Г.М., [3] Хакимова Б.Б., [1]Хамидова М.О., [1]Акрамова Р.Р., [4]Болтаев М.А., [1]Серкаев К.П.

[1]Ташкентский химико-технологический институт, Ташкент, Узбекистан
[2]Университет Мамуна, Хива, Узбекистан
[3]Ургенчский государственный университет имени Абу Райхона Беруни, Ургенч, Узбекистан
[4]Ташкентский государственный аграрный университет, Ташкент, Узбекистан

Поступила: 21 апреля 2026
Рецензирование: 27 апреля 2026
Принята в печать: *1 июля 2026*

АННОТАЦИЯ

В данной статье представлено комплексное исследование оптимального режима выпаривания щелочного раствора, полученного из водного экстракта золы стеблей хлопчатника, а также изучен химический состав осадка, образующегося в процессе выпаривания. Зола стеблей хлопчатника рассматривается как побочный продукт, образующийся при сжигании биомассы в бытовых устройствах, в частности в тандырах, используемых для выпечки хлеба и самсы, который в настоящее время практически не используется и выбрасывается в окружающую среду. В представленном исследовании процесс получения щелочного раствора осуществлялся в оптимальных условиях — путем кипячения смеси золы и воды при массовом соотношении 1:5. Затем полученная суспензия подвергалась фильтрации и выпариванию. По результатам установлено, что оптимальным режимом выпаривания является уровень 75%, поскольку при таком значении образование осадка не наблюдается. Однако при степени выпаривания 80% в растворе было зафиксировано образование осадка, что обусловлено нарушением равновесия растворимости. Состав осадка по катионам определялся методом пламенной фотометрии, а фазовый состав — методом ИК-Фурье спектроскопии (FTIR). Установлено, что осадок преимущественно состоит из соединений карбонатной природы. Показано, что в растворе преобладают ионы калия, при этом их молярная концентрация значительно превышает концентрации других катионов. Кроме того, при высокой степени концентрации часть ионов калия переходит из раствора в осадочную фазу. Согласно расчетам, общая щелочность полученного раствора составляет 3,41 N, что примерно соответствует половине щелочности 6 N раствора гидроксида натрия (NaOH), используемого в процессе рафинирования растительных масел.

Ключевые слова: зола стеблей хлопчатника, экстракция, выпаривание, ионы калия, карбонаты, осадок, пламенная фотометрия, FTIR, совместное осаждение, щелочной раствор.

Болтаев Миржалол Аллаярович — ***Информация об авторах:*** *Докторант, Ташкентский химико-технологический институт, улица Навои, 32, Ташкент, Узбекистан. Email: mirjalolboltayev@mail.ru; ORCID ID: https://orcid.org/0000-0002-3172-658X*

Отажонова Гульхайо Максуд кызы — *Преподаватель, Университет Мамуна, Хива, Хорезм, Узбекистан. Email: otajonovagulhayo1508@gmail.com; ORCID ID: https://orcid.org/0009-0008-7529-9656*

Хакимов Бахор Бахтияровна	*Доктор философии по техническим наукам (PhD), доцент факультета химической технологии Ургенчского государственного университета имени Абу Райхона Беруни, 220100, ул. Х. Алимджана 14, Ургенч, Узбекистан. Email: oot.baxor44@gmail.com; ORCID ID: https://orcid.org/0000-0001-5312-1963*
Хамидова Мадина Олимжоновна	*Доцент, Ташкентский химико-технологический институт, улица Навои, 32, Ташкент, Узбекистан. Email: m.khamidova@mail.ru; ORCID ID: https://orcid.org/0000-0002-7299-0395*
Акрамова Рано Рамизитдиновна	*Профессор, Ташкентский химико-технологический институт, улица Навои, 32, Ташкент, Узбекистан. Email: ranoakr123@gmail.com; ORCID ID: https://orcid.org/0000-0002-1417-2044*
Болтаев Мурод Аллаярович	*Доктор философии в области технических наук, Ташкентский государственный аграрный университет, 100140, Ташкент, Узбекистан. Email: murodbek.boltaev.78@mail.ru; ORCID ID: https://orcid.org/0009-0008-7001-2855*
Серкаев Камар Пардаевич	*Профессор, Ташкентский химико-технологический институт, улица Навои, 32, Ташкент, Узбекистан. Email: serkayev@mail.ru; ORCID ID: https://orcid.org/0009-0009-8316-4994*

References

[1] Afrane G. Leaching of Caustic Potash from Cocoa Husk Ash. Bioresource Technology. 1992; 40:101–104. https://doi.org/10.1016/0960-8524(92)90177-Y

[2] Steenari BM, Lindqvist O. Stabilisation of biofuel ashes. Waste Management. 1997. https://doi.org/10.1016/S0961-9534(97)00024-X

[3] Ogbu AI, Ovuoraye PE, Ajemba RO, Dehghani MH. Functionality of plantain peels for soybean oil refining. Scientific Reports. 2023; 13. https://doi.org/10.1038/s41598-023-46842-1

[4] Haidar Abbas, Sarmad Jaafar Mohammed Alrubaye, Ali Fawzi Al-Hussainy, Basim Mohammed Saadi, Mohannad Abdulrazzaq Gati, Talib Kh. Hussein, Boyjanov Nodirbek Ilxomovich, Nafaa Farhan Muften. Role of Carrageenan and Health Approach for Adsorption of Safranin-T Dye from Aqueous Solution by Using Polymer/CNT Surface. Journal Nanostruct. 2025; 15(4): 1798-1807. https://doi.org/10.22052/JNS.2025.04.027

[5] Hussein U A-R, Alalwan D H K, Qabel H A, Abid F M, Hamza H H, Ilxomovich B N, Aljeboree A M, & Alkaim A F. Green synthesis and characterization of guar gum/polyacrylamide/activated carbon hydrogel for efficient methylene blue removal. Journal of Nanostructures. 2025; 15(4):1849-1860. https://doi.org/10.22052/JNS.2025.04.028

[6] Demirbas A. Combustion characteristics of different biomass fuels. Progress in Energy and Combustion Science. 2004. https://doi.org/10.1016/j.pecs.2003.10.004

[7] Vassilev SV. An overview of biomass combustion ash. Fuel. 2013. https://doi.org/10.1016/j.fuel.2012.10.001

[8] Onyegbado C O, Iyagba E T, & Offor O J. Solid soap production using plantain peel ash as source of alkali. Journal of Applied Sciences and Environmental Management. 2002; 6(1). https://doi.org/10.4314/jasem.v6i1.17200

[9] Jenkins B M. Combustion properties of biomass. Fuel Processing Technology. 1998. https://doi.org/10.1016/S0378-3820(97)00059-3

[10] Wang S, Baxter L. Comprehensive study of biomass ash. Fuel. 2007. https://doi.org/10.1016/j.fuel.2006.01.006

[11] Ghouti M A. Adsorption isotherms. Journal of Hazardous Materials. 2020. https://doi.org/10.1016/j.jhazmat.2019.121621

[12] Ho Y S. Adsorption kinetics models. Process Biochemistry. 1999. https://doi.org/10.1016/S0032-9592(98)00112-5

[13] Salikhanova, D., Sagdullaeva, D., Ismoilova, M., Ruzmetova, D., Sadullaeva, M., Karabayeva, M., & Kadirova, N. (2023). Activation of bentonite and palygorskite adsorbents by acid under microwave radiation. E3S Web of Conferences, 458, 02017. https://doi.org/10.1051/e3sconf/202345802017

[14] Anorov, R., Rakhmonov, O., Salikhanova, D., Khomidov, F., & Abdurakhimov, A. (2023). Justification of the opportunities of obtaining silicate materials based on clay waste adsorbents. E3S Web of Conferences, 376, 01076. https://doi.org/10.1051/e3sconf/202337601076

[15] Zufarov, O., & Serkayev, K. (2024). Phospholipids in cottonseed oil and degumming methods. Bulletin of the Transilvania University of Brasov, Series II: Forestry, Wood Industry, Agricultural Food Engineering, 17(66), 2, 11–22. https://doi.org/10.31926/but.fwiafe.2024.17.66.2.11

[16] Ubaydullayeva, N. N., Salikhanova, D. S., & Karabayeva, M. I. (2023). Studying the sorption properties of adsorbents obtained on the basis of plant waste. E3S Web of Conferences, 390, 05022. https://doi.org/10.1051/e3sconf/202339005022

[17] Shamuratov, S., Baltaev, U., Alimov, U., Khoshimov, A., Matmuratov, A., & Kurambaev, S. (2026). Formation and agronomic efficiency of phosphorus-based fertilizer produced from cotton soapstock acidic wastewater and high-carbonate phosphorite. *Journal of Ecological Engineering*, *27*(6), 312–325. https://doi.org/10.12911/22998993/217637

[18] Yuldasheva, A. P. K., Shamuratov, S. K. U., Kurambayev, S. R., & Radjabov, M. F. (2026). Mathematical Analysis of CaO Content Variation in Acidic Wastewater and Mineralized Mass Mixture from Central Kyzylkum Phosphorite Based on Exponential Decay Model. Kompleksnoe Ispolzovanie Mineralnogo Syra, 339(4), 79–86. https://doi.org/10.31643/2026/6445.42

[19] Shamuratov, S. X., Baltayev, U. S., Alimov, U. K., Jabbarov, M. E., & Madaminov, A. E. (2026). Sigmoid Neutralization Response of Acidic Soapstock Waste by Mineralized Phosphorite Residues: A 4-Parameter Logistic Approach. Kompleksnoe Ispolzovanie Mineralnogo Syra = Complex Use of Mineral Resources, 342(3), 80–89. https://doi.org/10.31643/2027/6445.32

[20] Baltayev, U. S., Shamuratov, S. X., Alimov, U. K., Madaminov, A. E., & Jabbarov, M. E. (2026). Extraction of P_2O_5 from the mineralized mass of the Central Kyzylkum using acidic wastewater generated from cotton soapstock processing: scientific analysis based on equilibrium principles. Kompleksnoe Ispolzovanie Mineralnogo Syra = Complex Use of Mineral Resources, 341(2), 83–96. https://doi.org/10.31643/2027/6445.20

[21] Shamuratov, S., Alimov, U., Rifky, M., Baltaev, U., Ibragimova, M., Kurambaev, S., & Radjabov, M. (2025). Investigation of the Kinetics of Cotton Soapstock Saponification under Ultrasonic Illumination. Eurasian Chemico-Technological Journal, 27(4), 323–335. https://doi.org/10.18321/ectj1679

[22] Salikhanova D, et al. Activation of bentonite and palygorskite adsorbents by acid under microwave radiation. E3S Web of Conferences. 2023; 458:02017. https://doi.org/10.1051/e3sconf/202345802017

[23] Boyjanov, N., Kurayazov, Z., Annazarova, B., Jollibekov, S., Tajetdinov, N., Khamidova, M., & Akhmedov, A. (2026). Study of the mechanism and efficiency of using mineral-organic bleaching-filtering agents in polishing refining. Kompleksnoe Ispolzovanie Mineralnogo Syra = Complex Use of Mineral Resources, 345(2), 107–119. https://doi.org/10.31643/2028/6445.20

[24] Boyjanov N, Radjabov M, Serkayev Q, Boyjanov I, & Yaxshimuradov N. Activation and comparison of indicators of bentonite clay of the Navbakhor deposit. E3S Web of Conferences. 2024; 563:02018. https://doi.org/10.1051/e3sconf/202456302018

[25] Boyjanov NI, Rakhimov UB, Ataullaev ZM, Boltayev MA, Serkayev QP, Khamidova MO. Mathematical analysis of the linear increase in SIO_2 content during the activation of Navbakhor alkaline bentonite with hydrochloric acid. Kompleksnoe Ispolzovanie Mineralnogo Syra = Complex Use of Mineral Resources. 2026; 342(3):90-99. https://doi.org/10.31643/2027/6445.33

[26] Boyjanov NI, Otajonova GM, Kendjayev BB, Matyakubova MX, Sabirova NK, Masharipov AT, Boyjanov IR, Serkayev QP. Exponential modeling of Al_2O_3 reduction during activation of Navbahor alkaline-earth bentonite. Kompleksnoe Ispolzovanie Mineralnogo Syra = Complex Use of Mineral Resources. 2026; 343(4):106-115. https://doi.org/10.31643/2027/6445.44

[27] Salikhanova, D. S., Savrieva, D. D., Karabaeva, M. I., Sagdullaeva, D. S., Ubaydullayeva, N. N., & Ismoilova, M. (2023). Charcoal adsorbents for glycerin purification. IOP Conference Series: Earth and Environmental Science, 1231(1), 012067. https://doi.org/10.1088/1755-1315/1231/1/012067

[28] Palvan K, et al. Information and Measuring System for Monitoring the Moisture Content of Grain and Grain Materials, 2025 IEEE 26th International Conference of Young Professionals in Electron Devices and Materials (EDM), Altai, Russian Federation. 2025, 2260-2265. https://doi.org/10.1109/EDM65517.2025.11096667

[29] Riya Chatterjee, Baharak Sajjadi, Wei-Yin Chen, Daniell L. Mattern, Nathan Hammer, Vijayasankar Raman, & Austin Dorris. Effect of pyrolysis temperature on physicochemical properties and acoustic-based amination of biochar for efficient CO_2 adsorption. Frontiers in Energy Research. 2020; 8:85. https://doi.org/10.3389/fenrg.2020.00085

Crossref
DOI: 10.31643/2028/6445.22
Mining & Mineral Processing

Synergistic Effect of Dual Ionic Liquid PVDF-HFP Polymer Inclusion Membranes: Linking Mechanical, Chemical, Microstructural and Gold Recovery Performance

[1] Lim C.K., [1*]Shoparwe N.F., [2]Lim K.C., [3]Ahmad A.L.

[1]Universiti Malaysia Kelantan (UMK), Malaysia
[2]Universiti Malaysia Perlis (UniMAP), Malaysia
[3]Universiti Sains Malaysia (USM), Malaysia

** Corresponding author email: fazliani.s@umk.edu.my*

Received: *May 8, 2026*
Peer-reviewed: *June 22, 2026*
Accepted: *July 7, 2026*

ABSTRACT

Poly (vinylidene fluoride-co-hexafluoropropylene) (PVDF-HFP) polymer inclusion membranes (PIMs) are widely used across separation industries because of their ability to selectively separate ions or molecules, their chemical stability, and their mechanical flexibility. Still, improving how the membrane performs without making the membrane material properties deteriorate remains a challenge. In this study, Aliquat 336 and Cyphos IL 104 were blended with PVDF-HFP and fabricated through the solvent casting method. The main objective of this study is to understand how the ionic liquids can affect the membrane's chemical properties, physical properties, mechanical stability, and its ability to recover gold through an H-cell setup. FTIR analysis confirmed the presence of Aliquat 336, showing bands associated with quaternary ammonium groups, while Cyphos IL 104 displayed vibrations related to phosphonium-related P–C. SEM images further revealed clear differences in how the membrane morphology looked. Pure PVDF-HFP alone had compact surfaces; Aliquat 336 membranes appeared to have smoother features, and Cyphos IL 104 membranes developed rougher surfaces with micro-voids. The addition of ionic liquids also increased membrane porosity from 25 % in the pure membrane to 45 % with the addition of ionic liquids. At the same time, the contact angle dropped from 90° to 58°, indicating improved hydrophilicity. Mechanical testing showed that pure PVDF-HFP had the highest tensile strength (30 MPa), modulus (450 MPa), and tear resistance (2.5 N/mm). Membranes with higher Aliquat 336 content retained better tear resistance, close to 2.0 N/mm, while maintaining smoother membrane surfaces. In comparison, the addition of Cyphos IL 104 adversely impacts the mechanical properties. Gold extraction experiments showed promising performance. The PVDF-HFP/A15C20 membrane achieved 76 % recovery within 12 h. The combination of both Aliquat 336 and Cyphos IL 104 improved ion transport while maintaining acceptable membrane stability properties. Overall, the results showed that the ionic liquid composition has a strong influence on both the membrane's durability properties and separation performance. These findings provide a useful approach for developing membranes in precious metal recovery applications.

Keywords: Gold Recovery, Polymer Inclusion Membranes (PIMs), Cyphos IL 104, Ionic Liquids, Mechanical Properties, Membrane Science.

Information about authors:

C. K. Lim — *PhD candidate at the Centre for Gold, Rare Earths and Materials Technopreneurship (GREAT), Faculty of Bioengineering and Technology, Universiti Malaysia Kelantan, Jeli 17600 Kelantan, Malaysia. Email: getcheeked@gmail.com; ORCID ID: https://orcid.org/0009-0000-2148-8023*

Shoparwe N.F. — *Associate Professor at Gold, Rare Earth and Material Technopreneurship Centre (GREAT), Faculty of Bioengineering and Technology, Universiti Malaysia Kelantan, Jeli 17600 Kelantan, Malaysia. Email: fazliani.s@umk.edu.my; ORCID ID: https://orcid.org/0000-0002-4329-2459*

K. C. Lim — *Graduate from the Faculty of Chemical Engineering and Technology, Universiti Malaysia Perlis (UniMAP), Arau, Perlis 02600, Malaysia and researcher at Centre for Gold, Rare Earths and Materials Technopreneurship (GREAT), Faculty of Bioengineering and Technology, Universiti Malaysia Kelantan, Jeli 17600 Kelantan, Malaysia. Email: keanchong97@gmail.com; ORCID ID: https://orcid.org/0000-0002-6461-6467*

Ahmad A.L. — *Professor at School of Chemical Engineering, Engineering Campus, Universiti Sains Malaysia (USM), 14300 Nibong Tebal Pulau Pinang, Malaysia. Email: chlatif@usm.my; ORCID ID: https://orcid.org/0000-0003-1612-3032*

Introduction

The demand for advanced separation technologies continues to grow as industries look for sustainable approaches to metal recovery, wastewater treatment, and resource recycling. Researchers suggested Polymer inclusion membranes (PIMs) as a substitution for conventional solvent extraction and precipitation techniques. Their advantages include reduced

chemical consumption, enhanced selectivity, and improved environmental compatibility. When we look among all the polymers used for PIMs, PVDF-HFP stands out because of its chemical stability, mechanical strength, and ability to interact with different ionic liquids and plasticizers [[1], [2]].

PVDF-HFP on its own is like a tough plastic film, strong and stable but chemically silent. To make it innovative and diversify its usage, scientists started to mix in different ionic liquids that supply the missing chemical groups, which allow it to interact or bind ions to facilitate ion transport [[1], [3], [4]]. Scientists often go for Aliquat 336 because it can keep the membrane stable and gives strong anion-exchange ability [[1], [2]]. One of the least favourable ionic liquids is Cyphos IL 104, a phosphonium ionic liquid that is well known for porosity and ability to bind strongly with metal ions even in harsh acidic conditions [[5], [6]].

Tons of studies have looked at how A336 and Cyphos IL 104 can recover metals [[7], [8]], but most of the time researchers focus on how fast or how well the rate of recovery happens. What often gets overlooked are the really important factors, which are the chemical properties, physical microstructure properties, and mechanical properties of the PIMs. Also, the carrier composition on membrane structure-property dynamics is poorly understood. These factors are essential for ensuring durability in real industrial applications.

In this study, we focus on the systematic investigation of carrier-ratio engineering of both ionic liquids, A336 and Cyphos IL 104, into PVDF-HFP. Next, we investigated the chemical groups and physical structures through SEM images, contact angle, porosity test, and destructive testing for mechanical properties, and finally carried out gold recovery experiments. By integrating the optimization of membrane properties and how well the recovery performance, a clearer picture of how the recovery system works. It's not just about how fast the metals can be recovered, but also whether the membrane can stay strong, durable, and stable over time. This allows us to optimize PIMs with dual carriers that may be used in real-world applications.

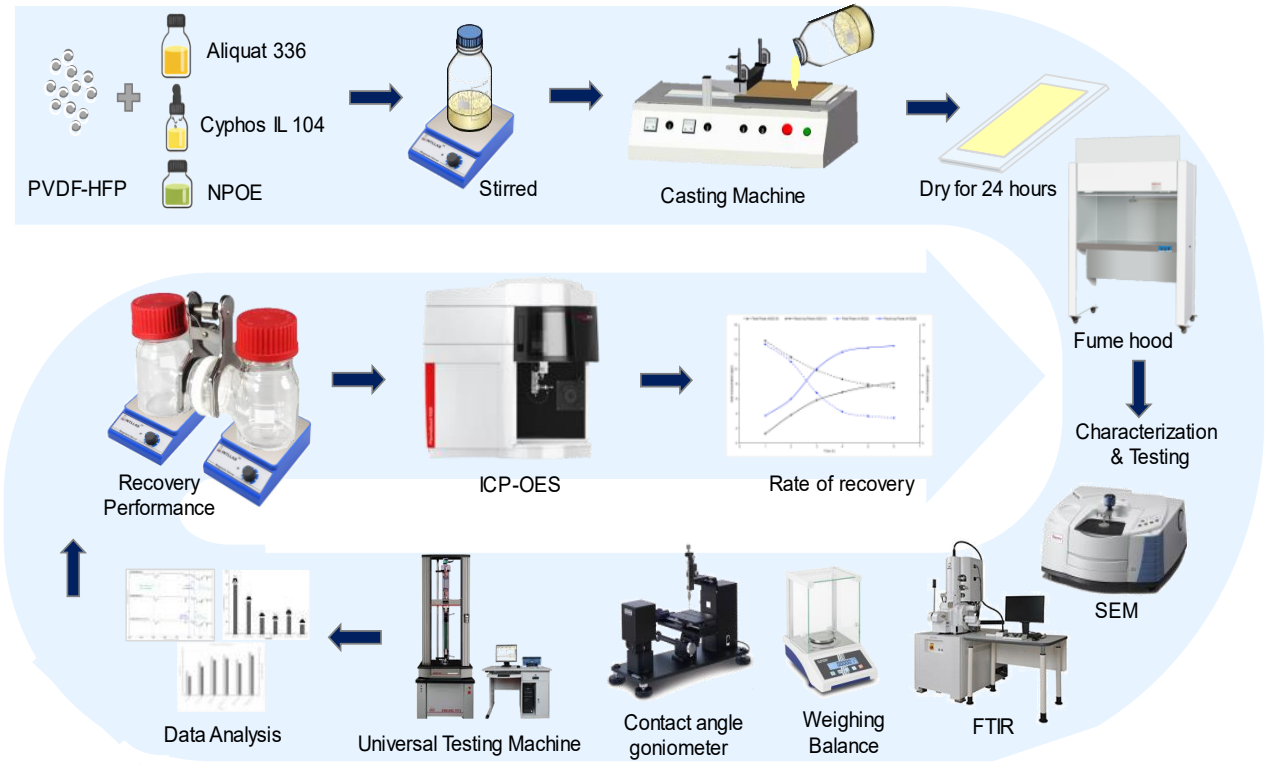

Figure 1 - Graphical Abstract: Linking Mechanical, Chemical, Microstructural and Gold Recovery Performance

Experimental part

Poly(vinylidenefluoride-co-hexafluoropropylene) (PVDF-HFP) pellets were used as the base polymer material. Aliquat 336 (A336) and Cyphos IL 104 were used as the ammonium and phosphonium carriers, respectively. Nitrophenyl octyl ether (NPOE) was added as a plasticizer to improve membrane flexibility. All resins and chemicals were obtained from Sigma-Aldrich only.

Membrane Fabrication

Following Gunasegaran et al. [9], 1.25 g of PVDF-HFP pellets was dissolved in 25 ml of tetrahydrofuran (THF) and kept the mixture under constant stirring until fully dissolved. Once dissolved, 1 ml of A336 and 0.36 ml of NPOE were added, then stirred for another four hours to ensure everything was mixed well. The casting solution was prepared by incorporating the specific amounts of carrier according to the membrane compositions listed in Table 1 below. For single-carrier membranes, only one ionic liquid (either Aliquat 336 or Cyphos IL 104) was added, whereas for dual-carrier membranes, both ionic liquids were introduced simultaneously while maintaining the total carrier listed in Table 1. Next, 25 ml of casting solution was poured onto a glass and spread using a doctor blade. Then, it was left to dry at ambient temperature (25 ± 2 °C) for a day in the fume hood. After peeling the membrane off the glass, the membranes were rinsed with distilled water to remove any residual solvents. Before characterization, the fabricated membranes were dried under vacuum at 40 °C until a constant weight was achieved indicated the residual moisture was eliminated. Lastly, the thickness of the fabricated membrane was measured with a digital micrometer, yielding an average of about 125 ± 25 µm (n=5). Table 1 summarizes the membrane acronyms with different weight % of carrier contents.

Characterization

The fabricated PVDF-HFP PIMs were characterized through spectroscopic, microscopic, and mechanical methods. Fourier transform infrared (FTIR) spectroscopy was carried out on a Thermo Fisher Scientific iZ10 instrument in transmission mode, with spectra collected between 400 and 4000 cm^{-1} at a resolution of 4 cm^{-1} over 16 scans for each sample. All the fabricated membranes were analysed under identical conditions. These spectra were then compared with reference peaks to identify functional groups linked to alkane (–CH, –CH_2), alkyl halide (–C–F, –CF_2, –CF_3), aromatic, ester and alcohol (–P–OH) bonds [[10], [11], [12], [13]].

Surface morphologies of PIMs were examined by scanning electron microscopy (SEM). The membrane samples (5 × 5 mm) were gold-coated and imaged at 4000× magnification under an accelerating voltage of 10 kV [14]. Porosity was determined using the dry–wet weight method, starting with immersing the membranes in water for 24 h, weighing after blotting, drying under vacuum at 40 °C until achieving constant weight, before measuring the dry weight with porosity calculated from the difference in wet and dry weights relative to water and polymer densities. The porosity was calculated using the following equation [15]:

$$\varepsilon(\%) = \frac{(ww-wd)/\rho w}{(ww-wd)/\rho w+wd/\rho p} \times 100 \quad (1)$$

where ε is the membrane porosity, ww is the wet membrane weight (g), wd is the dry membrane weight (g), ρw is the pure water density, while ρp is the polymer density.

Hydrophobicity was assessed using a contact angle goniometer [16] (Model: OCA15plus, DataPhysics). A 1 µL droplet of distilled water was placed on the membrane surface, and the angle was recorded 10 s after deposition. Five measurements (n =5) were performed at different locations for each sample, and the mean was calculated.

Table 1 - Membrane formulation with different carrier content

PVDF-HFP (wt%)	Aliquat 336 (wt%)	Cyphos IL 104 (wt%)	NPOE (wt%)	Acronyms
100	–	–	–	PVDF-HFP
50	35	–	15	PVDF-HFP/A35
50	–	35	15	PVDF-HFP/C35
50	17.5	17.5	15	PVDF-HFP/A17.5C17.5
50	20	15	15	PVDF-HFP/A20C15
50	15	20	15	PVDF-HFP/A15C20

Mechanical properties were evaluated according to ASTM standards. Tensile strength was measured following ASTM D882-91 using an Instron 5569 machine (100 N load cell) and a Shimadzu AG-XD plus tester, with samples of 60 × 20 mm held at a grip distance of 40 mm and tested at 22 ± 3 °C with a crosshead speed of 10 mm/min.

Tear resistance was determined following ASTM D1938-06 using the same machines with a 10 N load cell, employing samples of 80 × 50 mm with a grip separation of 25 mm and a crosshead speed of 250 mm/min at 22 ± 3 °C.

All mechanical, porosity, and contact angle measurements were performed in triplicate unless otherwise stated, and the results are reported as the mean.

Rate of Performance

The membrane that showed the best overall properties was selected for gold extraction experiments. A stock gold solution (1000 ppm Au^{3+}, Brand: Merck) was diluted with deionized water to a working concentration of 15 ppm. The feed phase was prepared by adding analytical-grade nitric acid (HNO_3, Brand: Merck) to stabilize Au^{3+} ions and prevent hydrolysis. For the receiving phase, thiourea (≥ 99 % purity, Brand: Sigma-Aldrich) was dissolved in deionized water. Thiourea served as a complexing agent to promote transport across the PIMs. The PIMs were cut and mounted between the feed and receiving compartments of a H-cell, with equal volumes on both sides. The system was kept under constant stirring at 150 rpm at ambient temperature. Samples were collected at 2 h, 4 h, 6 h, 8 h, 10 h, and 12 h, and the gold concentration was analyzed using inductively coupled plasma optical emission spectrometry (ICP-OES, Optima 8300, PerkinElmer, Yokohama, Japan). Gold recovery (%) was calculated based on the decrease in feed concentration and confirmed by the concentration measured in the receiving phase.

Results and Discussion

The FTIR spectra confirmed the presence of both ionic liquids within the PVDF-HFP PIMs. The base polymer exhibited strong C–H stretching around 2850–3020 cm^{-1} and –CH_2 bends at around 1400–1470 cm^{-1}, in agreement with previously reported PVDF-HFP's characteristics [[17], [18]]. Adding A336 din't introduce new peaks, but it increased the intensity and slightly shifted the C–H and –CH_2 peaks, which is a sign that the long hydrocarbon chain mix into the matrix [[19], [20]]. PIMs containing Cyphos IL 104, showed clear bands around 1040 cm^{-1} and 1250 cm^{-1}, which correspond to the phosphonium parts, specifically P=O and P–O–C stretching. This also confirms the successful incorporation into the membrane that helps it to bind metal ions and improves the transport efficiency in the PIMs system [[21], [22]].

In the dual-carrier system, vibrational signals from both the hydrocarbon backbone and the phosphonium component were detected. Notably, the –CH_2 bending region shifted toward 1470 cm^{-1} and showed slight broadening between 1000 and 1300 cm^{-1}. The shifts indicate that the PVDF-HFP remains structurally intact and interacting with the ionic carriers through weak forces. In other words, the dual-carrier allows the membrane to stay flexible while still able to adjust the efficiency properties.

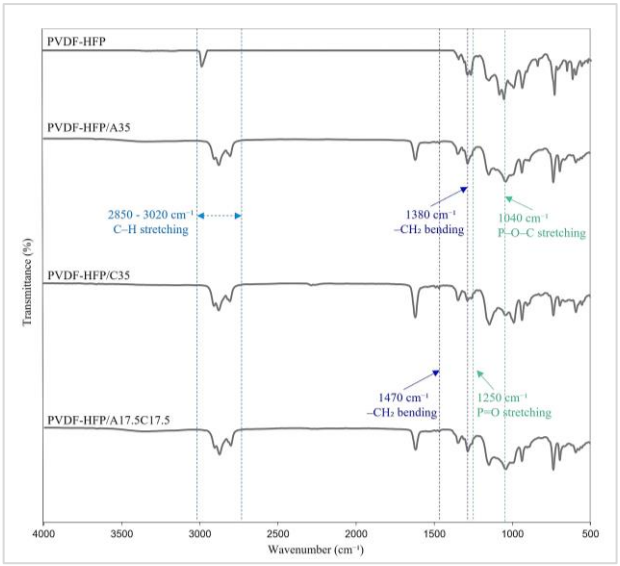

Figure 2 - FTIR spectra of PVDF-HFP, PVDF-HFP/A35, PVDF-HFP/C35 and PVDF-HFP/A17.5C17.5

Figure 3 shows SEM images of PVDF-HFP-based membranes with and without ionic liquid incorporation. This analysis helps to understand how the membrane's microstructure and pore formation affect the performance in separation applications. PVDF-HFP appeared dense and smooth with minimal defects, consistent with its crystalline nature [23]. When A336 was added in higher amounts, the surface showed smoother and more uniform features with occasional small pores compared to PVDF-HFP. The surface felt softer, which is consistent with A336 migrating toward the surface, reducing roughness and improving flexibility [24].

In contrast, Cyphos-rich membranes show rough, irregular surfaces with micro-voids and crack-like features, indicating poor compatibility

between Cyphos IL 104 and PVDF-HFP. Similar gel-like morphologies have been reported previously for Cyphos-modified membranes [25]. When both ionic liquids were present in equal amounts, the SEM images showed mixed features suggesting only partial compatibility. However, when A336 was present in higher proportion than Cyphos IL 104, the SEM images revealed smoother and more uniform features, with fewer cracks and more stable domains. Literature confirms that Aliquat-rich membranes tend to maintain better surface stability and mechanical toughness [26].

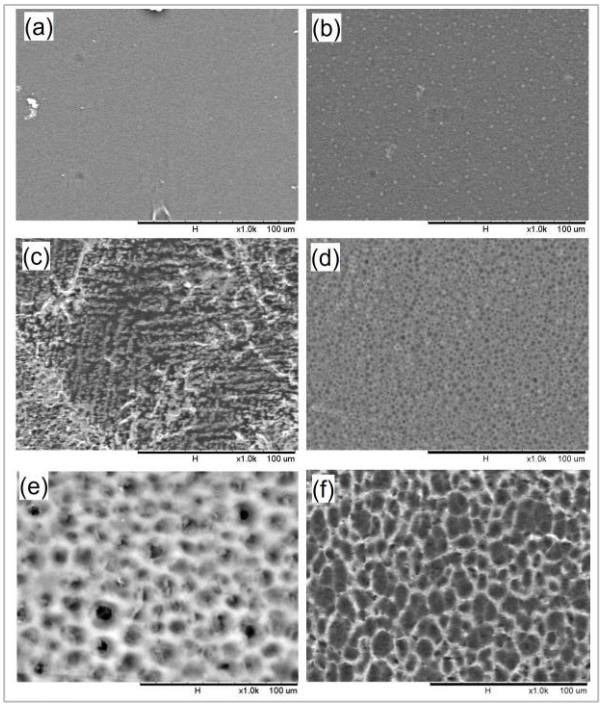

Figure 3 - SEM micrographs of (a) PVDF-HFP, (b) PVDF-HFP/A35, (c) PVDF-HFP/C35, (d) PVDF-HFP/ A17.5C17.5, (e) PVDF-HFP/A20C15, and (f) PVDF-HFP/A15C20

Porosity values are shown in Figure 4. An increasing trend in porosity is observed, especially the PVDF-HFP membrane had the lowest porosity at about 25 %, while the Cyphos-rich (PVDF HFP/A15C20) reached the highest value at 45 %. The porosity increases gradually, highlighting the effect of ionic liquids, where it reshaped the membrane's morphology and enhanced the hydrophilicity [27]. Pure PVDF-HFP membrane alone has limited porosity because of its dense crystalline structure, as per Figure 3 (a) SEM images. The $–CF_2$ groups in PVDF-HFP are hydrophobic, causing the polymer chains to be pulled tightly together. As a result, the available space inside the membrane is reduced, which limits the formation of voids. When 35 wt % A336 was introduced, porosity increased to 35 %, and the membrane became less tightly packed. A336 behaved similarly to a plasticizer by disturbing the crystalline arrangement of the polymer chains and creating more free volume within the membrane. Thus, the formation of pores is facilitated with this change, corresponding to the moderate increment of porosity. Velikova et al. [28] reported similar findings, observing that Aliquat-modified PVDF-HFP membranes increased porosity due to the plasticizing effect of the ionic liquid migration and improved chain flexibility.

An increase to 40 % porosity was attained using 35 wt% of Cyphos IL 104. The introduction of the bulky phosphonium groups did not allow them to mix well homogeneously with PVDF-HFP, resulting in aggregation that gave a gel-like texture. Bahrami et al. [25] reported that Cyphos-modified membranes also developed higher porosity and more irregular structures, which were attributed to phase separation. Use of a combination of A336 and Cyphos IL 104 in equal parts for the optimized blend provided the optimum results with porosity as high as 42 %. In addition to stopping the packing, a simultaneous introduction of ammonium and phosphonium groups also caused additional disruption in packing due to large separation between polymer chains, resulting in increased pore formation. Porosity was also somewhat lower, at 38% in Aliquat-rich blends, indicating that the capacity of A336 to stabilize dimorphic organic phases reduced irregularity. In contrast, the porosity of the PVDF-HFP/Cyphos membranes continued to increase until 45%, with clear evidence for phase separation that fragmented the PVDF-HFP matrix.

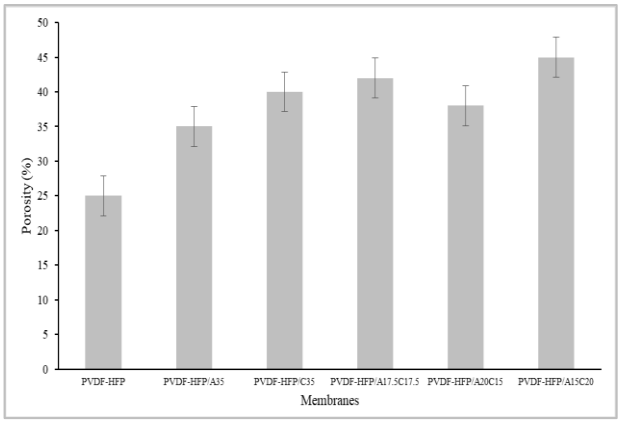

Figure 4 - Porosity values of PVDF HFP based polymer inclusion membranes (PIMs) with varying ionic liquid compositions

Contact angle measurements are illustrated in Fig. 5. A contact angle of approximately 90° was

obtained for the PVDF-HFP membrane, which is in agreement with its water-resistant property that originated from the presence of fluorinated $–CF_2$ groups [29]. Inclusion of 35 wt% A336 reduces this value to below 76°, indicating that surface compositions are starting to change so that the end of ammonium moieties near the surface are moving outward and that there is a trend toward water affinity. At higher concentrations of Aliquat (in PVDF-HFP/A20C15), angles approached 65°. It is clear that A336 somewhat screens the interface and partly offsets the strong polar effects of Cyphos IL 104.

Quite remarkably, once 35wt% of Cyphos IL104 is included (PVDF HFP/C35), the contact angle drops to only 63°. That transition signals deeper-rooted attraction to water. Due to phosphonium ionic liquids disrupting the conformation of polymer chains, surfaces become uneven, exposing more polar sites. To this end, Bahrami et al. [25] described similar findings where the angles of Cyphos IL 104 membranes were lower than those obtained with A336. That is mainly due to the polar regions on the surface that are boosted because of Cyphos IL 104 clusters. In fact, the most potent effect was observed in PVDF-HFP/A15C20, as it was noted to bring the angle down to just 58°. A 50/50 mixture of both gave a result of 61°, which was in the middle, showing an average influence. However, Cyphos IL 104 pushes the surface to a higher polarity more than A336. A336, on the other hand, does soften the membrane, but the contact angle decreases. The dual-binding nature of these carriers makes membranes constructed solely from them absorb water better than those formed solely with one type. However, the most robust results are found when these two interact rather than act alone.

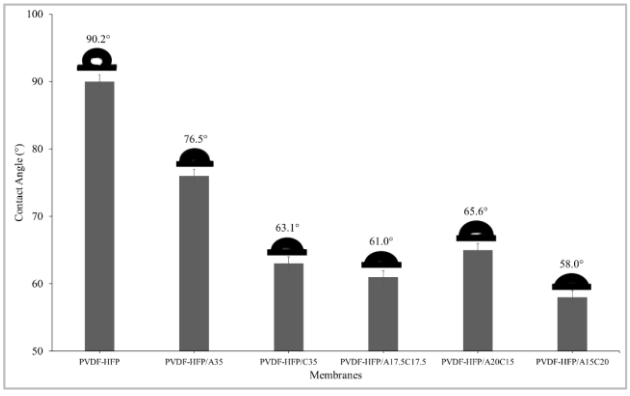

Figure 5 - Contact Angle of PIMs

The tensile strength and tensile modulus are displayed in Figure 6. The intrinsic PVDF–HFP membrane demonstrates leading performance of tensile strength of 30 MPa and modulus of 450 MPa. This makes sense as the chains are so closely packed together [30]. When 35 wt% Cyphos IL 104 was added, the tensile strength dropped to 20 MPa and the modulus to 280 MPa. SEM image above revealed roughness with micro-voids, reflecting poor compatibility between Cyphos IL 104 and PVDF-HFP.

Blends of A336 and Cyphos IL 104 showed intermediate mechanical properties. The equal blend gave 22 MPa strength and 300 MPa modulus, while Aliquat-rich membranes reached 23 MPa and 310 MPa. These results match the above SEM morphologies and highlight A336's stabilizing effect. In contrast, Cyphos-rich membranes showed lower values of 21 MPa strength and 290 MPa modulus, confirming that Cyphos IL 104 has a stronger influence on weakening the polymer matrix. Overall, the findings revealed a clear structure-property relationship. A336 acts as the plasticizer, softening the polymer, reducing crystallinity, and moderating the mechanical loss. On the other hand, Cyphos IL 104 tends to cause phase separation, leading to weaker mechanical properties. Therefore, it is possible to balance the mechanical properties by adjusting the ratio of the ionic liquids within the PIMs.

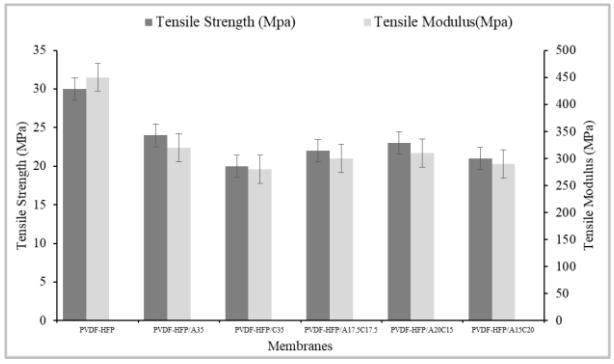

Figure 6 - Tensile strength and tensile modulus of PIMs

Figure 7 shows the tear resistance of PVDF-HFP membranes modified with Aliquat 336 and Cyphos IL 104. PVDF-HFP membrane had the highest tear resistance of 2.5 N/mm, which can be attributed to its crystalline packing and strong intermolecular interactions [[31], [32], [33]]. When A336 was added, tear resistance dropped slightly to 1.9 N/mm. This drop comes from the polymer chains moving more freely, yet the smoother surface feature helped slow down the crack spreading [26]. Previous studies by Bahrami et al. [[25], [33]] reported that membranes modified with A336 maintained a stronger mechanical integrity and

were less prone to cracking compared to those Cyphos-modified ones. Less stress builds up in Aliquat-based membranes, which explains the enhancement.

Less durability marked the membranes with Cyphos IL 104, their tear resistance dipping to just 1.6 N/mm. Bulky phosphonium units lie behind this loss, failing to disperse uniformly through the PVDF-HFP structure. Uneven distribution triggers phase separation - voids form in jagged patterns. Stress gathers where these gaps sit, opening paths for tearing. Reports from Guo et al. [20], Bahrami et al. [25], and Sellami et al. [34] echoed that aggregated ionic liquids weaken mechanical performance. At roughly 1.8 N/mm, the hybrid version held moderate resistance. Equal mixtures of ionic liquids showed evenly distributed tear strength, whereas formulations rich in Aliquat demonstrated marginally higher durability, reinforcing the role of A336 in stabilization. Blends dominated by Cyphos, however, exhibited reduced tear resistance, pointing again to the weakening impact of Cyphos IL 104.

So, these findings suggest that the type of ionic liquid used plays an important role in determining the membrane's tearing resistance. Tear strength is affected by the overall mechanical properties and how uniform the surface structure is. A336 contributed to a smoother and even surface that helped minimize the mechanical loss, while Cyphos IL 104 tends to form phase separation, thus creating a few weak spots that may make the cracks grow.

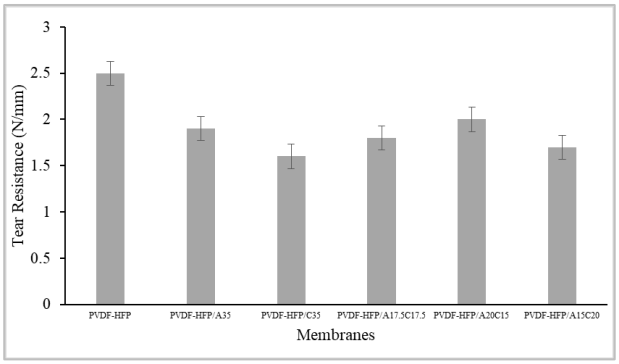

Figure 7 - Tear resistance of PIMs

Rate of Performance

Gold extraction performance was evaluated in a H-cell over 12 h. The feed solution contained 15 ppm Au^{3+} stabilized in nitric acid, while the receiving phase contained thiourea to promote complexation. Figure 8 shows that the dual-carrier membranes enabled steady transport, with gold concentration in the feed gradually decreasing and the receiving phase increasing over time. After 12 h, PVDF-HFP/A35 showed 69 % efficiency, PVDF-HFP/C35 achieved 61 % efficiency, PVDF-HFP/A20C15 reached 53 % efficiency, while PVDF-HFP/A15C20 achieved 76 % efficiency. The presence of both ionic liquids clearly improved the extraction rate. A336 contributed to mechanical stability and minimized adsorption, while Cyphos IL 104 improved the porosity and ion mobility. A small discrepancy between feed and receiving concentrations indicated minor adsorption of Au^{3+} onto the membrane, consistent with the strong affinity of phosphonium groups for gold ions [[35, [36], [37], [38]]. Smoothness of A336's membrane surface limited adsorption more effectively than seen with Cyphos-rich membranes.

While texture played a role, differences emerged clearly under similar test conditions. One notable contrast came from how molecules interacted near the interface. Where Cyphos IL 104 showed higher binding tendencies, A336 maintained lower attachment rates. Surface properties thus influenced performance without altering bulk composition.

These findings indicate that using a dual-carrier membrane of A336 alongside Cyphos IL 104 serves as an effective alternative that helps strike a useful middle ground for lasting longer without slowing down ion movement in the performance. While A336 adds strength and smoothness to the material, it is the addition of Cyphos IL 104 that opens up the internal network, increasing pore formation and speeding ions through. Success hinges on tuning both carrier ratio and the performance traits to get strong materials that still move gold well matters most when systems run efficiently over time.

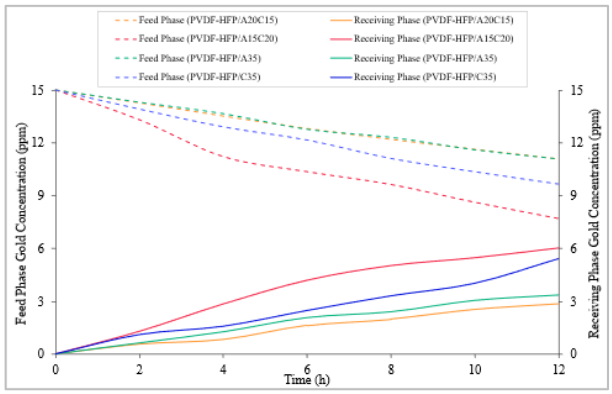

Figure 8 – Feed Phase and receiving phase gold concentrations over time of PVDF-HFP/A35, PVDF-HFP/C35, PVDFHFP/ A20C15, and PVDFHFP/ A15C20

Conclusions

Poly(vinylidene fluoride-co-hexafluoropropylene), when combined with Aliquat 336 and Cyphos IL 104, formed hybrid polymer inclusion membranes via solvent casting. Though preparation followed standard procedures, outcomes depended on the composition details. With FTIR analysis, evidence emerged that both ionic liquids remained present, with subtle shifts in absorption peaks pointing toward molecular-level contact between components. Instead of sharp confirmation, data hinted at bonding tendencies without defining exact mechanisms. Moving to structural features, SEM images exposed visible differences across samples. While pure PVDF-HFP stayed smooth and tightly packed throughout, others diverged dramatically once Cyphos IL 104 levels increased. Roughness appeared alongside tiny voids, suggesting phase separation during drying took place unevenly. These surface variations did not occur uniformly but clustered within specific regions. Smoothness and uniformity rose when A336 concentration increased within the membranes. With ionic liquid included, pore volume expanded, shifting from 25 % up to 45 %. A shift downward in contact angle, dropping from 90° to 58°, revealed a stronger attraction to water. Improved wetting behavior emerged alongside these structural changes.

It turned out that stronger membranes often moved substances less efficiently. The pure PVDF-HFP version stood out with top numbers in stretch resistance, stiffness, and tearing force due to how closely its polymer chain sat. Adding ionic liquids softened the material overall. That softening hit harder in blends rich in Cyphos IL 104, whereas those loaded with more A336 kept their shape better under stress. When comparing all versions made, PVDF-HFP/A15C20 ended up offering a middle ground, strong enough, yet also showing higher porosity and hydrophilicity.

Twelve hours into the test, gold recovery stood at 76 % with the Cyphos-rich membrane. That number dropped to 53 % for the Aliquat-rich membrane setup. What made the difference was how both ionic liquids worked together across the PVDF-HFP/A15C20 barrier. Ion movement got a boost not from one compound alone, but their joint effect. Stability in the membrane came mostly because A336 limited surface stickiness. Meanwhile, pathways inside widened thanks to Cyphos IL 104, letting ions move more freely. Efficiency climbed where structure and flow balanced out.

Surprisingly, results revealed shifting ionic liquid proportions altered how membranes resisted stress while managing flow. With a certain ratio, the strength increased noticeably and boosted transfer rates more distinctly. Some ratios managed to hold firmness steady without sacrificing movement efficiency. Each membrane responded differently based on the exact ratio of ionic liquid involved. This is a useful approach for designing polymer inclusion membranes aimed at precious metal recovery, making sure durability and performance are consistently strong over long-term industrial use.

Conflicts of interest. If you agree, you should not delete this statement: On behalf of all authors, the corresponding author states that there is no conflict of interest.

CRediT author statement: **C. K. Lim**: Conceptualization, Methodology, Validation, Formal analysis, Investigation, Writing – original draft, Writing – review & editing Visualization, Investigation; **N. F. Shoparwe**: Supervision, Writing – Review & Editing; **K. C. Lim**: Methodology, Validation, Formal analysis, Investigation, Writing – original draft, Writing – review & editing Visualization, Investigation; **A. L. Ahmad**: Supervision, Writing – Review & Editing.

Acknowledgements. This work was supported by the Fundamental Research Grant Scheme (FRGS) under the grant number FRGS/1/2023/TK05/UMK/02 from the Ministry of Higher Education Malaysia.

Cite this article as: Lim CK, Shoparwe NF, Lim KC, Ahmad AL. Synergistic Effect of Dual Ionic Liquid PVDF-HFP Polymer Inclusion Membranes: Linking Mechanical, Chemical, Microstructural and Gold Recovery Performance. Kompleksnoe Ispolzovanie Mineralnogo Syra = Complex Use of Mineral Resources. 2028; 345(2):130-141. https://doi.org/10.31643/2028/6445.22

PVDF-HFP полимеріне екі иондық сұйықтықты қосу арқылы мембраналардың синергетикалық әсері: механикалық, химиялық, микроқұрылымдық қасиеттер мен алтынды алу тиімділігі арасындағы байланыс

[1] Lim C.K., [1]Shoparwe N.F., [1,2]Lim K.C., [3]Ahmad A.L.

[1] Малайзия Келантан университеті, Малайзия
[2] Перлис Малайзия университеті, Малайзия
[3] Малайзия ғылым университеті, Малайзия

Мақала келді: *8 мамыр 2026*
Сараптамадан өтті: *22 маусым 2026*
Қабылданды: *7 шілде 2026*

ТҮЙІНДЕМЕ

Поливинилиденфторид-когексафторпропилен (PVDF-HFP) негізіндегі полимерлі мембраналар химиялық тұрақтылығы мен реттелетін микроқұрылымына байланысты бөлу қолданбалары саласында назарға ілікті. Дегенмен, функционалдық қасиеттер мен механикалық беріктік арасындағы тепе-теңдік үнемі қиындық тудырады, себебі дәстүрлі модификациялар көбінесе ұзақ мерзімді сенімділіктің төмендеуі сияқты кемшіліктерге әкеледі. Бұл мәселені шешу үшін бұл зерттеу олардың жұмысын анықтайтын механикалық, химиялық және микроқұрылымдық факторларды анықтау үшін ерітінді құю арқылы PVDF-HFP мембраналарына Aliquat336 және Cyphos IL104 иондық сұйықтықтарының қосылуын зерттейді. ИҚ спектроскопиясы иондық сұйықтықтардың сәтті енгізілгенін растады: Aliquat336 төрттік аммонийдің сипаттамалық созылу тербелістері арқылы, ал Cyphos IL104 фосфониймен байланысты P-C созылу жолақтары арқылы анықтады. Сканерлеуші электронды микроскопия (СЭМ) Cyphosпен байытылған материалдың микроқуыстары бар кедір-бұдыр, дұрыс емес құрылымы бар екенін, ал Aliquatпен байытылған материалдың морфологиясы тегіс екенін көрсетті. PVDF HFP мембраналарында кеуектілік 25%-дан Aliquat-Cyphos мембраналарында 45%-ға дейін өсті, ал жанасу бұрышы 90°-тан 58°-қа дейін төмендеді, бұл гидрофильділіктің артуын растайды. Механикалық сынақтар ымыраға келуді анықтады: PVDF-HFP ең жоғары созылу беріктігіне 30 МПа, созылу модулі 450 МПа және жыртылуға төзімділігі 2,5 Н/мм болды, ал Cyphos-пен байытылған материал ең төмен механикалық беріктікті көрсетті. Aliquat-пен байытылған материал 2,0 Н/мм орташа созылу беріктігі мен тегіс морфологиясын сақтап, ең перспективалы компромисске айналды. Aliquat-пен байытылған материал 2,0 Н/мм орташа созылу беріктігі мен тегіс морфологиясын сақтап, ең перспективалы компромисске айналды. Құрылымдық бағалаудан басқа, алтын өндіру PVDF HFP/A15C20 үшін 12 сағат ішінде 76 % қалпына келтіру тиімділігін көрсетті. Aliquat пен Cyphos қос қосылуы синергетикалық әсерге әкелді, бұл беріктік пен беріліс тиімділігі арасындағы тепе-теңдікті қамтамасыз етті. Бұл зерттеу иондық сұйықтық химиясын тиімділік, механикалық беріктік және экстракция өнімділігі арасындағы тепе-теңдікті қамтамасыз ететін мембраналар жасау үшін стратегиялық тұрғыдан реттеуге болатынын көрсету арқылы жаңа үлес қосады, бұл берік, жоғары өнімді бөлу материалдарын жасауға жол ашады.

Түйін сөздер: алтынды бөліп алу, полимерді қосу мембраналары (PIMs), Cyphos IL 104, иондық сұйықтықтар, механикалық қасиеттер, мембрандық ғылым.

Авторлар туралы ақпарат:

C. K. Lim — *Алтын, сирек жер және материалдар технологиясы орталығында (GREAT) PhD кандидаты, биоинженерия және технология факультеті, Малайзия Келантан университеті, Jeli 17600 Kelantan, Малайзия. Email: getcheeked@gmail.com; ORCID ID: https://orcid.org/0009-0000-2148-8023*

Shoparwe N.F. — *Алтын, сирек жер және материалдық технологиялар орталығының (GREAT) доценті, биоинженерия және технология факультеті, Малайзия Келантан университеті, Джели 17600 Келантан, Малайзия. Email: fazliani.s@umk.edu.my; ORCID ID: https://orcid.org/0000-0002-4329-2459*

K. C. Lim — *Химия инженериясы және технологиялар факультетінің түлегі, Перлис Малайзия университеті, Перлис 02600, Малайзия; ғылыми қызметкер, Алтын, сирек жер және материалдар технопренерациясы орталығы (GREAT), биоинженерия және технология факультеті, Малайзия Келантан университеті, Джели 17600 Келантан, Малайзия. Email: keanchong97@gmail.com; ORCID ID: https://orcid.org/0000-0002-6461-6467*

Ahmad A.L. — *Химиялық инженерия мектебінің профессоры, инженерлік кампусы, Малайзия ғылым университеті, 14300 Нибонг Тебал Пулау Пинанг, Малайзия. Email: chlatif@usm.my; ORCID ID: https://orcid.org/0000-0003-1612-3032*

Синергетический эффект мембран с включением двух ионных жидкостей в полимер PVDF-HFP: связь между механическими, химическими, микроструктурными свойствами и эффективностью извлечения золота

[1] Lim C.K., [1]Shoparwe N.F., [2]Lim K.C., [3]Ahmad A.L.

[1]Университет Малайзии Келантан, Малайзия
[2] Университет Малайзии Перлис, Малайзия
[3] Университет науки Малайзии, Малайзия

Поступила: *8 мая 2026*
Рецензирование: *22 июня 2026*
Принята в печать: *7 июля 2026*

АННОТАЦИЯ

Полимерные мембраны на основе поливинилиденфторида-со-гексафторпропилена (ПВДФ-ГФП) привлекли внимание в области разделительных применений благодаря своей химической стабильности и регулируемой микроструктуре. Однако постоянной проблемой остается баланс между функциональными свойствами и механической прочностью, поскольку традиционные модификации часто приводят к таким недостаткам, как снижение надежности в долгосрочной перспективе. Для решения этой проблемы в данном исследовании изучается включение ионных жидкостей Aliquat336 и Cyphos IL104 в мембраны ПВДФ-ГФП методом литья из раствора с целью выявления механических, химических и микроструктурных факторов, определяющих их характеристики. ИК-спектроскопия подтвердила успешное включение ионных жидкостей: Aliquat336 был идентифицирован по характерным колебаниям растяжения четвертичных аммониевых групп, а Cyphos IL104 — по полосам растяжения P–C, связанным с фосфонием. Сканирующая электронная микроскопия (СЭМ) показала, что обогащенный Cyphos материал имеет шероховатую, нерегулярную структуру с микропустотами, а обогащенный Aliquat – более гладкую морфологию. Пористость увеличилась с 25 % в PVDF HFP до 45 % в мембранах Aliquat-Cyphos, а угол смачивания уменьшился с 90° до 58°, что подтверждает повышенную гидрофильность. Механические испытания выявили компромисс: PVDF-HFP достиг наивысшей прочности на разрыв 30 МПа, модуля упругости при растяжении 450 МПа и сопротивления разрыву 2,5 Н/мм, в то время как обогащенный Cyphos материал продемонстрировал наименьшую механическую прочность. Обогащенный Aliquat материал сохранил умеренное сопротивление разрыву 2,0 Н/мм и более гладкую морфологию, став наиболее перспективным компромиссом. Помимо структурной оценки, экстракция золота продемонстрировала эффективность извлечения 76 % для PVDF HFP/A15C20 за 12 часов. Двойное включение Aliquat и Cyphos привело к синергетическому эффекту, обеспечив баланс между прочностью и эффективностью переноса. Данное исследование вносит новый вклад, демонстрируя, что химию ионных жидкостей можно стратегически настраивать для создания мембран, которые обеспечивают баланс между эффективностью, механической прочностью и производительностью извлечения, открывая путь к созданию долговечных высокоэффективных разделительных материалов.

Ключевые слова: извлечение золота, полимерные мембраны с включениями (PIM), Cyphos IL 104, ионные жидкости, механические свойства, мембранная наука.

Информация об авторах:

C. K. Lim — *Аспирант Центра технологического предпринимательства в области золота, редкоземельных элементов и материалов (GREAT), факультет биоинженерии и технологий, Университет Малайзии Келантан, Джели 17600 Келантан, Малайзия. Email: getcheeked@gmail.com; ORCID ID: https://orcid.org/0009-0000-2148-8023*

Shoparwe N.F. — *Доцент Центра технологического предпринимательства в области золота, редких земель и материалов (GREAT), факультет биоинженерии и технологий, Университет Малайзии Келантан, Джели 17600 Келантан, Малайзия. Email: fazliani.s@umk.edu.my; ORCID ID: https://orcid.org/0000-0002-4329-2459*

K. C. Lim — *Выпускник факультета химической инженерии и технологии Университета Малайзии Перлис (UniMAP), Арау, Перлис 02600, Малайзия; научный сотрудник Центра технологического предпринимательства в области золота, редких земель и материалов (GREAT), факультет биоинженерии и технологий Университета Малайзии Келантан, Джели 17600 Келантан, Малайзия. Email: keanchong97@gmail.com; ORCID ID: https://orcid.org/0000-0002-6461-6467*

Ahmad A.L. — *Профессор Школы химического машиностроения инженерного кампуса, Университет науки Малайзии (USM), 14300 Нибонг Тебал Пулау Пинанг, Малайзия. Email: chlatif@usm.my; ORCID ID: https://orcid.org/0000-0003-1612-3032*

References

[1] Rani I, Arwish S, Shah A, Hussain H. Graphene Oxide-Tailored PVDF-HFP Nanocomposite Electrolytes: A Study of Structural, Thermal, Ionic Conductivity, and Dielectric Properties. Macromolecular Chemistry and Physics. 2026; 227(4):e00358. https://doi.org/10.1002/macp.202500358

[2] Lim CK, Shoparwe NF, Lim KC, Nor'azmi NZ, Abdullah MA, Anbalagan V. Synergistic role of functionalized chitosan nanoparticles in poly (vinylidene fluoride-co-hexafluoropropylene)(PVDF-HFP) polymer inclusion membranes for high-efficiency gold (III) adsorption. Journal of Polymer Research. 2026; 33(4):148. https://doi.org/10.1007/s10965-026-04841-6

[3] Lee DW, Lee RH, Lee SH. Enhancing interfacial stability of hybrid polymer electrolytes via functional additives for solid-state batteries. Journal of Energy Storage. 2026; 141:119455. https://doi.org/10.1016/j.est.2025.119455

[4] Sahu AK, Das D, Pattanayak R, Varadwaj KS, Mohanty S, Nayak SK. MnO2-Embedded PVDF-HFP/PEG Composite Membrane: A Multifunctional Approach for Electrochemical and Biomedical Systems. ACS Applied Electronic Materials. 2026; 8(8):3409–3422. https://doi.org/10.1021/acsaelm.5c02654

[5] Ewa R. Separation Strategies for Indium Recovery: Exploring Solvent Extraction, Ion-Exchange, and Membrane Methods. Metals. 2026; 16(2):156. https://doi.org/10.3390/met16020156

[6] Ait Khaldoun I, Mitiche L, Fontàs C, Sahmoune A. Exploring the Extraction Capability of the Task-Specific Ionic Liquid Trioctylmethylammonium Thiosalicylate (TOMATS) for Cadmium (II): from Solvent Extraction to Polymer Inclusion Membranes. International Journal of Environmental Research. 2026; 20(1):70. https://doi.org/10.1007/s41742-025-01031-y

[7] Kazemi D, Yaftian MR. Kinetic and isotherm modeling of Bi (III) adsorption by D2EHPA-functionalized PVC-and PVDF-HFP-based polymer inclusion membranes. Iranian Polymer Journal. 2026, 1-4. https://doi.org/10.1007/s13726-026-01614-2

[8] Ben-Elijah AT, Lutz-Rechtin TM, Wickramasinghe SR, Wang X. Membrane Separation for Rare Earth Elements (A Review). Membranes. 2026; 16(2):69. https://doi.org/10.3390/membranes16020069

[9] Gunasegaran M, Ravi S, Shoparwe NF. Kinetic studies of reactive orange 16 (RO16) dye removal from aqueous solution using PIMs. InJournal of Physics: Conference Series 2020; 1529(5):052003. https://doi:10.1088/1742-6596/1529/5/052003

[10] Guo W, Chen S, Feng Y, Yang C. Investigations of triphenyl phosphate and bis-(2-ethylhexyl) phosphate self-assembled films on iron surface using electrochemical methods, Fourier transform infrared spectroscopy, and molecular simulations. The Journal of Physical Chemistry C. 2007; 111(7):3109-3115. https://doi.org/10.1021/jp067216t

[11] Jakriya SP, Syed AM, Pillai SK, Rahim DB. High-performance poly (vinylidene fluoride-co-hexafluoropropylene) based electrospun polyelectrolyte mat for lithium-ion battery. Materials Express. 2018; 8(1):77-84. https://doi.org/10.1166/mex.2018.1405

[12] Singh VK, Singh RK. Development of ion conducting polymer gel electrolyte membranes based on polymer PVdF-HFP, BMIMTFSI ionic liquid and the Li-salt with improved electrical, thermal and structural properties. Journal of Materials Chemistry C. 2015; 3(28):7305-7318. https://doi.org/10.1039/C5TC00940E

[13] Zamri SN, Masri MN. Fourier transform infrared spectroscopy of porous zinc with different concentration of potassium hydroxidein agar binder. Int. J. Curr. Res. Sci. Eng. Technol. 2018; 1:361-366. https://doi.org/10.30967/ijcrset.1.S1.2018.361-366

[14] Ling YY, Suah FB. Extraction of malachite green from wastewater by using polymer inclusion membrane. Journal of Environmental Chemical Engineering. 2017; 5(1):785-794. https://doi.org/10.1016/j.jece.2017.01.001

[15] Feng C, Shi B, Li G, Wu Y. Preparation and properties of microporous membrane from poly (vinylidene fluoride-co-tetrafluoroethylene)(F2. 4) for membrane distillation. Journal of Membrane Science. 2004; 237(1-2):15-24. https://doi.org/10.1016/j.memsci.2004.02.007

[16] Ferry JD. Ultrafilter Membranes and Ultrafiltration. Chemical reviews. 1936; 18(3):373-455. https://doi.org/10.1021/cr60061a001

[17] Liu F, Hashim NA, Liu Y, Abed MM, Li K. Progress in the production and modification of PVDF membranes. Journal of membrane science. 2011; 375(1-2):1-27. https://doi.org/10.1016/j.memsci.2011.03.014

[18] Saxena P, Shukla P. A comprehensive review on fundamental properties and applications of poly (vinylidene fluoride)(PVDF). Advanced Composites and Hybrid Materials. 2021; 4(1):8-26. https://doi.org/10.1007/s42114-021-00217-0

[19] Kislik VS, editor. Liquid membranes: principles and applications in chemical separations and wastewater treatment. Elsevier; 2009, 103-122. https://doi.org/10.1016/B978-0-444-53218-3.00001-5

[20] Nghiem LD, Mornane P, Potter ID, Perera JM, Cattrall RW, Kolev SD. Extraction and transport of metal ions and small organic compounds using polymer inclusion membranes (PIMs). Journal of Membrane Science. 2006; 281(1-2):7-41. https://doi.org/10.1016/j.memsci.2006.03.035

[21] Guo L, Liu Y, Zhang C, Chen J. Preparation of PVDF-based polymer inclusion membrane using ionic liquid plasticizer and Cyphos IL 104 carrier for Cr (VI) transport. Journal of Membrane Science. 2011; 372(1-2):314-321. https://doi.org/10.1016/j.memsci.2011.02.014

[22] Wieszczycka K, Staszak K. 8. Polymers in separation processes. Polymer engineering. 2017, 235-76. https://doi.org/10.1515/9783110733822-008

[23] Shukla AK, Alhoshan M, Alam J, Imran A. Mechanical and physical properties of polyvinylidene fluoride and poly (vinylidene fluoride-co-hexafluoro-propylene) membranes. Journal of Materials Science. 2026; 61(5):3536-3555. https://doi.org/10.1007/s10853-025-12013-y

[24] Nowik-Zając A, Sabadash V. Recent Developments in Polymer Inclusion Membranes: Advances in Selectivity, Structural Integrity, Environmental Applications and Sustainable Fabrication. Membranes. 2025; 15(8):249. https://doi.org/10.3390/membranes15080249

[25] Bahrami S, Yaftian MR, Najvak P, Dolatyari L, Shayani-Jam H, Kolev SD. PVDF-HFP based polymer inclusion membranes containing Cyphos IL 101 and Aliquat 336 for the removal of Cr (VI) from sulfate solutions. Separation and Purification Technology. 2020; 250:117251. https://doi.org/10.1016/j.seppur.2020.117251

[26] Kukoc L, Velikova K, Perinovic-Jozic S, Biocic M, Gateshki M, Kolev SD, Spassov TG. Effect of Glass Fibers on the Mechanical and Transport Properties of Polymer Inclusion Membranes Composed of Aliquat 336 and PVDF-HFP. Membranes. 2026; 16(4):141. https://doi.org/10.3390/membranes16040141

[27] Shamsuri AA, Daik R, Md. Jamil SN. A succinct review on the PVDF/imidazolium-based ionic liquid blends and composites: preparations, properties, and applications. Processes. 2021; 9(5):761. https://doi.org/10.3390/pr9050761

[28] Velikova, Kalina, Todor Dudev, Tsveta Sarafska, Lea Kukoc-Modun, Spas D. Kolev, and Tony Spassov. Assessing the Stability of Polymer Inclusion Membranes: The Case of Aliquat 336-Based Membranes. Membranes. 2025; 15(10):309. https://doi.org/10.3390/membranes15100309

[29] Tournis I, Tsiourvas D, Sideratou Z, Boutsika LG, Papavasiliou A, Boukos NK, Sapalidis AA. Superhydrophobic nanoparticle-coated PVDF–HFP membranes with enhanced flux, anti-fouling and anti-wetting performance for direct contact membrane distillation-based desalination. Environmental Science: Water Research & Technology. 2022; 8(10):2373-2380. https://doi.org/10.1039/D2EW00407K

[30] Yu Y, Sun N, Wu A, Lu F, Zheng L. Zwitterion-containing electrolytes with semi–crystalline PVDF-Co-HFP as a matrix for safer lithium-ion batteries. Journal of Molecular Liquids. 2019; 282:340-346. https://doi.org/10.1016/j.molliq.2019.03.027

[31] Domalanta MR, Ali MR, Maalihan RD, Caldona EB. Mechanistic effects of HFP content on the surface structure and protective action of PVDF-HFP coatings. Progress in Organic Coatings. 2025; 198:108879. https://doi.org/10.1016/j.porgcoat.2024.108879

[32] Correia DM, Costa CM, Rodriguez Hernandez JC, Tort-Ausina I, Biosca LT, Torregrosa Cabanilles C, Meseguer-Duenas J, Krakovsky I, Lanceros-Méndez S, Gomez Ribelles JL. Crystallization monitoring of semicrystalline poly (vinylidene fluoride)/1-ethyl-3-methylimidazolium hexafluorophosphate [Emim][PF6] ionic liquid blends. Crystal Growth & Design. 2021; 21(8):4406-4416. https://doi.org/10.1021/acs.cgd.1c00333

[33] Bahrami S, Dolatyari L, Shayani-Jam H, Yaftian MR, Kolev SD. On the potential of a poly (vinylidenefluoride-co-hexafluoropropylene) polymer inclusion membrane containing Aliquat® 336 and dibutyl phthalate for V (V) extraction from sulfate solutions. Membranes. 2022; 12(1):90. https://doi.org/10.3390/membranes12010090

[34] Sellami F, Kebiche-Senhadji O, Marais S, Lanel C, Fatyeyeva K. Novel poly (vinylidene fluoride)/montmorillonite polymer inclusion membrane: application to Cr (VI) extraction from polluted water. Membranes. 2021; 11(9):682. https://doi.org/10.3390/membranes11090682

[35] Wong L, Shen W, Truong YB. Investigation of electrospun and film-cast PVC membranes incorporated with aliquat 336 for efficient Cd extraction: A comparative study. Journal of Applied Polymer Science. 2011; 121(1):327-335. https://doi.org/10.1002/app.33586

[36] Nguyen VT, Lee JC, Jeong J, Kim BS, Cote G, Chagnes A. Extraction of gold (III) from acidic chloride media using phosphonium-based ionic liquid as an anion exchanger. Industrial & Engineering Chemistry Research. 2015; 54(4):1350-1358. https://doi.org/10.1021/ie5045742

[37] Shalu, Chaurasia SK, Singh RK, Chandra S. Thermal stability, complexing behavior, and ionic transport of polymeric gel membranes based on polymer PVdF-HFP and ionic liquid,[BMIM][BF4]. The Journal of Physical Chemistry B. 2013; 117(3):897-906. https://doi.org/10.1021/jp307694q

[38] Bonggotgetsakul Ya Ya N, Robert W Cattrall, and Spas D Kolev. Recovery of gold from aqua regia digested electronic scrap using a poly (vinylidene fluoride-co-hexafluoropropene)(PVDF-HFP) based polymer inclusion membrane (PIM) containing Cyphos IL 104. Journal of Membrane Science. 2016; 514:274-281. https://doi.org/10.1016/j.memsci.2016.05.002

Crossref
DOI: 10.31643/2028/6445.23
Mining & Mineral Processing

Sulfate-Resistant Portland Cement Clinker Based on the Raw Material Base of Karakalpakstan: Technology, Economics and Ecology

[1*]Begzhanova G.B., [1]Mukhitdinov D.D., [2]Ruzmetova A.Sh., [3]Shengwen T., [4]Tursunov Z.R., [5]Tojiev I.I.

[1] Institute of General and Inorganic Chemistry of the Academy of Sciences of Uzbekistan, Tashkent
[2]Urgench State University named after Abu Rayhon Beruni, Urgench, Uzbekistan
[3] Wuhan University, Wuhan, China
[4] Navoi State University of Mining and Technology, Uzbekistan
[5] Bukhara State Technical University, Bukhara, Uzbekistan

** Corresponding author email: atabaev_farruh@mail.ru*

Received: *April 16, 2026*
Peer-reviewed: *May 21, 2026*
Accepted: *July 8, 2026*

ABSTRACT

This study is devoted to the production of sulfate-resistant Portland cement clinker based on local raw materials found in the Aral Sea region of the Republic of Uzbekistan and the study of its properties. The results obtained highlight technological, economic, and environmental advantages. The raw material mixtures consisted of limestone, barren sand, kaolin, and iron-rich industrial waste, resulting in a clinker with an optimized oxide composition (LSF = 0.82, SR = 2.15, AR = 0.94). X-ray phase analysis shows a high content of alite (C_3S ≈ 38.6%) and belite (C_2S ≈ 41.0%) phases, which provides high mechanical strength. The low content of tricalcium aluminate (tricalcium aluminate < 5%) and the sufficient content of ferrite (C_4AF ≈ 16.2%) increased sulfate resistance and phase dominance. Sulfate resistance tests performed in accordance with ASTM C1012/C1012M showed that sulfate-resistant Portland cement had the lowest swelling index among samples placed in a 5% Na_2SO_4 solution, proving its high resistance compared to ordinary Portland cement and mixed cement types. The results of the experiments prove the feasibility of producing high-quality sulfate-resistant Portland cement clinker based on local raw materials and demonstrate its potential for use in the sulfate-rich conditions of the Aral Sea region. Economically, the use of local raw materials reduces production costs, the need for imports, and increases the competitiveness of the cement industry in our region. Ecologically, the long service life of sulfate-resistant Portland cement and the possibility of using industrial waste are consistent with the principles of the "green economy" and contribute to waste reduction and sustainable growth.

Keywords: sulfate-resistant Portland cement, clinker synthesis, mineral resources, sulfate resistance, green economy, sustainability.

Information about authors:

Begzhanova Gulrukh Bakhtiyarovna — *Doctor of Technical Sciences, Chief Scientific Researcher at the STROM Research Laboratory and Testing Center of the Institute of General and Inorganic Chemistry of the Academy of Sciences of Uzbekistan, 100170, 77 Mirzo Ulugbek Street, Tashkent, Uzbekistan. Email: gulrukh-begzhanova@rambler.ru; ORCID ID: https://orcid.org/0000-0002-0492-3246*

Dilshod Mukhitdinov Davronovich — *Doctor of Technical Sciences, STROM Research Laboratory and Testing Center, Institute of General and Inorganic Chemistry, Academy of Sciences of Uzbekistan, Tashkent, Uzbekistan. Email: mukhitdinov28@gmail.com; ORCID ID: https://orcid.org/0000-0002-4795-6080*

Ruzmetova Aida Shonazarovna — *Doctor of Philosophy in Technical Sciences (PhD), Associate Professor of the Department of Chemical Technologies, Urgench State University, Urgench, Uzbekistan. Email: aida0330@list.ru; ORCID ID: https://orcid.org/0009-0004-1008-4057*

Shengwen Tang — *Wuhan University, China. Email: tangsw@whu.edu.cn; ORCID ID: https://orcid.org/0000-0001-6635-9444*

Tursunov Zarif Ruzimuradovich — *Doctor of Philosophy in Technical Sciences, Associate Professor, Navoi State University of Mining and Technology, 210100, 76v Galaba Avenue, Navoiy, Uzbekistan. Email: tzarif5658@gmail.com; ORCID ID: https://orcid.org/0009-0003-6432-4442*

Tojiev Inomjon Ilhomovich — *Doctor of Technical Sciences, Head of the Department of Civil Engineering, Bukhara State Technical University, Bukhara, Uzbekistan. Email: tojiyevinomjon0@gmail.com; Scopus ID: 57552794300*

Introduction

In recent years, the rapid development of the construction industry, particularly in the expansion of hydraulic structures, industrial facilities, and residential infrastructure, has significantly increased the demand for durable and long-lasting types of cement and concrete. However, specific

natural and geographical conditions in some regions pose unique challenges for construction materials. In the Republic of Karakalpakstan, especially in the Aral Sea region, soils and groundwater are characterized by high salinity, where the presence of sulfate ions (SO_4^{2-}) poses a serious threat to concrete and reinforced concrete structures. Ordinary Portland cement is rapidly corroded in a sulfate environment, since sulfates interacting with the three calcium aluminate phases in the composition form expanding ettringite, resulting in cracking and a decrease in strength. Therefore, the development of sulfate-resistant Portland cement is an urgent task for this region.

According to the standards of UzM St 337:2024 and GOST 22266-2013, the content of tricalcium aluminate (tricalcium aluminate) in the cement composition should not exceed 5%, and in some cases it should be reduced to 3%. This is because tricalcium aluminate reacts with sulfate ions and forms harmful expansion products. Therefore, reducing the content of tricalcium aluminate by reducing the content of Al_2O_3 or increasing Fe_2O_3 increases sulfate resistance. As a result, reducing the C_3A phase — that is, by reducing the Al_2O_3 content in the clinker or increasing the Fe_2O_3 content — is one of the most effective approaches to increasing sulfate resistance.

The Republic of Karakalpakstan has great scientific and practical potential in this area. The region is rich in raw material deposits for cement production, including limestone ($CaCO_3$ ≈ 85–90%), kaolin (Al_2O_3 ≈ 36–38%), basalt, and iron-rich rocks. The rational use of these resources will not only help achieve economic efficiency, but also produce high-quality sulfate-resistant Portland cement SRC clinker that is suitable for the aggressive sulfate environments of the region. Consequently, the production and application of sulfate-resistant cement has become a critical requirement for the construction of buildings, reservoirs, sewage systems, and other engineering structures in the Aral Sea region.

In international and regional standards, specific requirements are imposed on the mineralogical composition of cement clinker in order to ensure sulfate resistance. Among these, one of the most critical parameters is the content of tricalcium aluminate (C_3A). Studies have shown that the higher the proportion of the C_3A phase in cement, the more rapidly it reacts with sulfate ions, forming expansive products in concrete. Therefore, the content of C_3A in sulfate-resistant Portland cement clinker is strictly regulated by the requirements of the established normative documents and should not exceed 5%, and in some cases it is required to reduce it to 3%. In the production of sulfate-resistant cement clinker, it is possible to reduce the C_3A phase by reducing the content of Al_2O_3, which is an important component of the clinker, or by increasing the content of Fe_2O_3. For this, it is necessary to correctly select the composition of the main components and correctly calculate the batch ratios.

The Republic of Karakalpakstan has great potential for rational use of mineral resources on the territory of the Republic of Karakalpakstan and to conduct competent scientific research in this area. The region has sufficient reserves of raw materials such as limestone, clay, porphyry, and iron-rich rocks necessary for cement production. The use of these mineral resources, while ensuring economic efficiency, will help produce high-quality sulfate-resistant Portland cement clinker that can withstand the aggressive sulfate environments of this region.

The main goal of this scientific research is to synthesize sulfate-resistant Portland cement clinker based on mineral raw materials from the Aral Sea region, determine its chemical and mineralogical composition, and study the effect of spatial structure on sulfate resistance.

The issue of producing sulfate-resistant Portland cement is of interest to many researchers around the world, since concrete made from ordinary Portland cement is very quickly corroded and destroyed by sulfate ions, which reduces the service life of engineering and hydraulic structures [1]. Therefore, many other research works are aimed at improving the mineralogical composition of sulfate-resistant Portland cement clinker, namely, reducing the amount of tricalcium aluminate (C_3A) [2]. Research by world scientists shows that reducing the tricalcium aluminate phase in clinker can be achieved by reducing the Al_2O_3 content or increasing the Fe_2O_3 content. The results of the study show that the synthesis of clinker with a high iron/aluminum ratio, dominated by ferrite phases, dramatically reduces the C_3A content and increases the sulfate resistance of cement [[3], [4]].

It has been scientifically proven that by optimizing the batch composition, the content of tricalcium aluminate can be reduced to values below 5 % [5]. The use of iron-rich additives is effective in reducing tricalcium aluminate. Thermodynamic modeling has confirmed the high sulfate resistance of clinkers with a predominance

of ferrite phases [[6], [7], [8]]. As a result of a detailed study of the mechanism of sulfate action, two-stage studies have confirmed that tricalcium aluminate phases react with sulfate ions to form expanding products. By observing the microstructural changes of concrete under the influence of sulfate ions for a long time, it has been shown that cements with a low C_3A content have higher strength. Analysis of cements with the addition of limestone powder has shown that mineral additives have a significant effect on the sulfate-resistant Portland cement system. Long-term tests of cements mixed with blast furnace slag have shown a significant increase in sulfate resistance [[9], [10], [11], [12], [13]].

It has also been reported that sulfate-resistant Portland cements can be degraded in long-term humid environments and under strong sulfate conditions. Scientific approaches to improving sulfate resistance offer several effective methods. The use of iron-rich mineral additives to increase the iron/aluminum ratio and reduce tricalcium aluminate to increase ferrite phases, as well as the use of additional mineral components such as slag and limestone [14].

Studies conducted in Spain have investigated the technical and environmental performance of sulfate-resistant Portland cement clinkers with the addition of new mineral components such as iron-rich sand, slag and “albero” [15].

The results showed that partial replacement of slag up to 30% did not harm the mechanical strength of the cement, but increased its sulfate resistance.

It was found that the optimal use of additional cementing materials in Portland-limestone cements improves sulfate resistance [16]. The interaction between clinker, gypsum, and other sulfate additives has been studied, and the SO_3 content of the cement has been shown to affect its sulfate resistance [17].

However, practice shows that the production of sulfate-resistant Portland cement clinker can be achieved not only by adjusting the raw material composition, but also by using mineral additives and secondary materials appropriately. As a result, the environmental efficiency of the cement industry is increased, as well as the cost of production and carbon dioxide (CO_2) emissions are reduced [[18], [19]].

Studies conducted in the regions adjacent to Uzbekistan have explored in depth the possibilities of producing sulfate-resistant cement based on mineral resources. These studies were mainly aimed at improving the batch composition, studying the phase composition, and increasing the durability of cement in sulfate environments.

Practical results have also been obtained. Trials at the “Karakalpak Cement” LLC enterprise confirmed that siliceous additives improve the physico-mechanical properties of cement and enhance sulfate resistance [[20], [21], [22], [23], [24], [25]]. Buriev et al. reported that a high replacement level with pozzolanic materials (e.g., fly ash) has a positive impact on sulfate durability [26]. In addition, recent research by Iskandarova and collaborators analyzed innovative approaches in the development of composite Portland cements, pointing to promising directions for the future development of the cement industry in the region.

Kazakhstani scientists have carried out studies on the synthesis of ferrite-phase cements using manganese- and iron-rich ores. Results published in the journal Complex Use of Mineral Resources confirmed that the increase in C_4AF content reduces C_3A and improves cement durability under sulfate environments [27]. Moreover, regional studies on feldspar, talc-magnesite, and other useful minerals have shown that their physicochemical characteristics make them suitable for future applications in cement and other silicate material production.

From an economic point of view, the use of limestone, barren sand, kaolin, and iron-rich industrial waste reduces the demand for imported raw materials and reduces production costs. Bu esa ushbu mintaqa uchun sement sanoatining raqobatbardoshligini oshiradi. By using local raw materials properly, it is possible to increase technological efficiency and at the same time reduce production costs. This will contribute to the sustainable development of the industry of the Aral Sea region. In the future, effective cement production will be established based on new innovative projects using local resources, and economic stability will be achieved. In terms of economic significance, such studies also show the advantages of rational use of resources in the national economy [28].

From an ecological point of view, sulfate-resistant Portland cement clinker is more resistant to sulfate ions than ordinary Portland cement, extending the service life of hydraulic and general construction structures. This is especially important for sulfate-rich areas of the Aral Sea region, reducing the need for frequent repairs or reconstruction. As a result, resource consumption is

reduced, and environmental impact is reduced. From the perspective of the "green economy" principles, these processes are fully consistent with the concepts of modern economic approaches - the "green economy" and "circular economy" - while ensuring the long service life of sulfate-resistant Portland cement clinker and the ecological balance through the efficient use of industrial waste [29].

The addition of iron-rich industrial waste to the batch composition increases the efficiency of industrial waste processing and serves to implement the principles of the "green economy" and "circular economy". This process is consistent with modern requirements for production and helps to reduce carbon dioxide (CO_2) emissions in the cement industry.

The production of sulfate-resistant Portland cement clinker has technological advantages, economic efficiency, and environmental sustainability, making it a useful material for the Aral Sea region.

Experimental part

The production of sulfate-resistant Portland cement clinker was carried out using local raw materials from the Lower Aral Sea region. The main composition of the raw material mixture consisted of limestone, barren sand, and kaolin, with gypsum and iron-rich industrial waste used as additional components.

Laboratory-scale samples were prepared on the basis of Karakalpak Cement LLC, and the analyses were carried out at the STROM Research and Testing Center under the Institute of General and Inorganic Chemistry of the Academy of Sciences of Uzbekistan.

Chemical Composition

The chemical composition, determined according to UzM St 337:2024 and GOST 5382-2019 using classical titration and gravimetric methods, was as follows (wt.%): CaO – 61.09, SiO_2 – 22.10, Al_2O_3 – 4.98, Fe_2O_3 – 5.32, MgO – 2.07, SO_3 – 0.80, LOI – 1.14, Free CaO – 0.94.

Calculated module values were: LSF = 0.82, SR = 2.15, AR = 0.94 — all within SULFATE-RESISTANT PORTLAND CEMENT normative limits.

Mineralogical composition (XRD)

X-ray phase analysis (Rigaku MiniFlex, Cu-Kα radiation) and Rietveld recalculation revealed the main phases in the cement clinker: C_3S – 38.6%, C_2S – 38.0%, tricalcium aluminate – 4.2%, C_4AF – 14.8%.

These results are consistent with Bogue calculations and the solid phase composition of sulfate-resistant Portland cement clinker.

Test conditions

All analyses were performed in accordance with the requirements of UzM St 337:2024 and GOST 5382-2019 [[30], [31]]. Sulfate resistance was assessed according to ASTM C1012/C1012M: samples were immersed in a 5% Na_2SO_4 solution for testing, and their expansion was compared with reference samples stored in distilled water [32].

To ensure reliability, two control samples were used in each case, which allowed to accurately determine the effect of sulfate ions on dimensional stability and strength.

Results and Discussion

The selection of raw materials for the production of sulfate-resistant Portland cement clinker is of particular scientific and practical importance. Therefore, the economical use of local raw materials is an urgent issue. In the Republic of Karakalpakstan, dune sands, kaolin, iron-rich industrial waste, and limestone deposits are considered promising sources of raw materials. By analyzing their chemical composition, it is possible to determine the mineralogical composition of sulfate-resistant Portland cement clinker.

The ratio of the main oxides in the raw material mixture is an important factor in the synthesis of sulfate-resistant Portland cement clinker. Calcium oxide (CaO) serves to form alite (C_3S) and belite (C_2S) phases, and silicon dioxide (SiO_2) is the basis for silicate phases; aluminum oxide (Al_2O_3) serves to form tricalcium aluminate (tricalcium aluminate). Also, to ensure sulfate resistance, it is necessary to reduce the content of tricalcium aluminate to ≤5%, preferably to 3%. Iron oxide (Fe_2O_3) is part of the ferrite phase (C_4AF) and is important in reducing the content of tricalcium aluminate.

Also, achieving the correct distribution of oxides is an important factor in ensuring the strength and long-term stability of cement in sulfate environments. The chemical composition of local raw materials in the Republic of Karakalpakstan by main oxides is presented in Table 1.

Table 1 - Chemical composition of local raw materials selected for the synthesis of sulfate-resistant portland cement

Raw Material	Chemical composition by major oxides (wt.%)									
	SiO_2	Al_2O_3	CaO	MgO	Fe_2O_3	Na_2O	K_2O	TiO_2	SO_2	LOI
Limestone	–	0.15	53.14	2.56	0.12	–	–	–	–	42.49
Barxan sand	89.22	3.15	0.68	2.32	0.97	0.94	0.70	0.24	0.20	1.61
Kaolin	54.07	16.47	0.85	2.57	9.93	1.72	–	0.17	–	9.23
Iron-rich by-product	40.40	6.00	2.05	4.00	45.24	–	0.40	–	0.22	3.10
gypsum stone	2.80	0.49	30.98	–	–	–	2.63	2.80	42.80	20.30
	$CaSO_4 \times 2H2O = 42.80x2.15 = 92.02\%$									

The chemical composition of these raw materials is suitable for ensuring the optimal balance required in the synthesis of sulfate-resistant Portland cement clinker. Barkhan sands are characterized by a very high SiO_2 content (89.22%), which provides a primary source for silicate phases (e.g., C_3S and C_2S) and contributes to improved mechanical strength of clinker. However, due to their relatively low Al_2O_3 (3.15%) and Fe_2O_3 (0.97%) contents, these sands are mainly useful for increasing the silica modulus (SM).

The iron-rich by-product contains a high Fe_2O_3content (45.24%), which plays a critical role in forming the ferrite phase (C_4AF) and thus contributes to sulfate resistance by reducing the calcium aluminate content. Meanwhile, its SiO_2 (40.40%) and Al_2O_3 (6.00%) levels are moderate, allowing adjustment of the iron modulus (IM) in the raw mix. Low levels of alkaline oxides such as Na_2O and K_2O ensure that adverse effects do not occur during clinker hydration. Kaolin is high in Al_2O_3 (16.47%) and SiO_2 (54.07%), and acts as the main raw material for the formation of aluminate phases. However, due to the relatively high Al_2O_3 content, kaolin consumption must be carefully controlled; otherwise, the tricalcium aluminate content in the clinker may exceed 5%. Kaolin has moderate Fe_2O_3 (9.93%) and Na_2O (1.72%) levels, and it is suitable for adjusting the aluminum modulus (AM). The low content of SO_2 (0%) and TiO_2 (0.17%) does not adversely affect the quality of sulfate-resistant clinker.

Limestone is the main source of CaO (53.14%), which is essential for the formation of alite and belite phases. The almost complete absence of SiO_2 and Al_2O_3(0% and 0.15%) in it proves that it is a pure calcium source. The low content of MgO (2.56%) and Fe_2O_3 (0.12%) does not cause problems during the clinker hydration process. The loss on heat (LOI, ≈ 42.49%) proves the carbonate nature of the limestone and indicates the release of CO_2 during the calcination process.

In general, the mixture of these raw materials provides the ratio of oxides necessary for the synthesis of sulfate-resistant Portland cement clinker. It is recommended to conduct laboratory tests to determine the main composition. According to preliminary calculations, the optimal batch composition may be as follows: barren sand 15-20%, iron-rich industrial waste 5-10%, kaolin 10-15%, and limestone 60-70%. This approach allows for the maximum use of local raw materials and increases the resistance of cement to sulfate environments by 20-30%. In addition to these raw materials, gypsum plays an important role in the cement production process. It is mainly used as a component that regulates the rate of hardening at the cement setting stage.

Figure 1 - Gypsum stone sourced from the Tashaba deposit, Karakalpakstan

According to the results of chemical analysis, gypsum from the Tashaba deposit in the Republic of Karakalpakstan contains 42.80% SO_3, which is approximately 92.02% $CaSO_4 \cdot 2H_2O$. Such a very high purity and very low content of SiO_2 (2.80%), Al_2O_3 (0.49%), MgO, and Fe_2O_3 indicate that Tashaba gypsum is an ideal raw material for the cement industry. Such a pure chemical composition of Tashaba gypsum ensures the stable formation of ettringite during the hydration process, prevents secondary reactions, and increases the sulfate resistance of cement. The low content of impurities

Table 2 - Chemical and mineralogical composition of sulfate-resistant portland cement clinker

Material name	LOI	SiO_2	Al_2O_3	Fe_2O_3	CaO	MgO	SO_3	Cl^-	CaO (Free CaO)	Σ
Portland cement clinker	1.14	22.1	4.98	5.32	61.09	2.07	0.8	0.0	0.935	100.0
	Mineralogical composition (%) and module indices									
		C_3S=38.64; C_2S=41.03; C_3A=4.17; C_4AF=16.16; CaO/SiO_2=2.76; LSF=0.86; SR=2.15; AR=0.94								

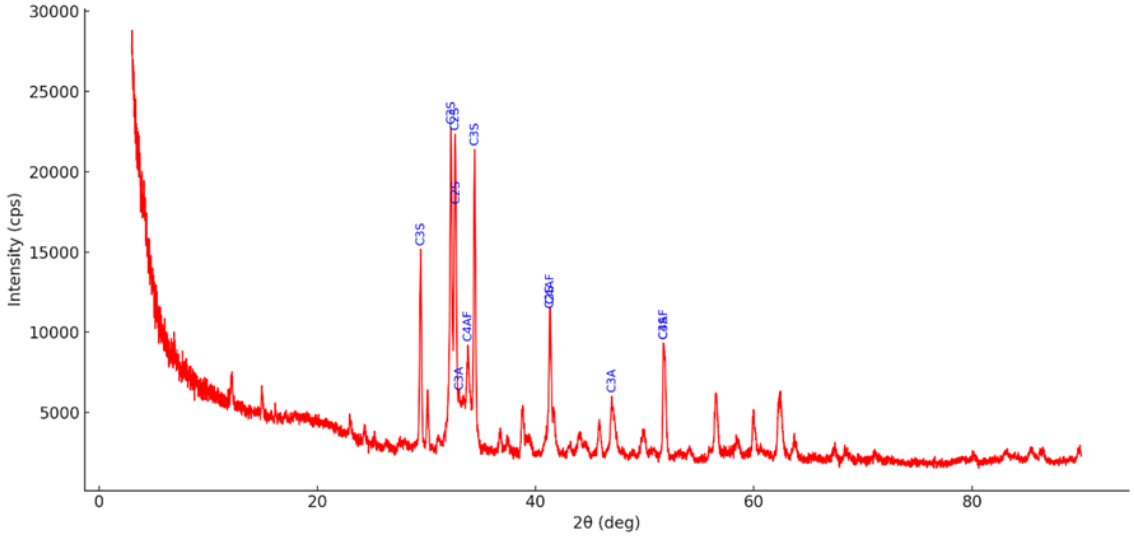

Figure 2 - XRD pattern of SRC clinker showing the main phases (C_3S, C_2S, C_3A, C_4AF)

in the mixture has a positive effect on the friability, color, and stability of the composition of the cement. Therefore, the use of Tashaba gypsum in the production process of sulfate-resistant clinker not only improves the quality of cement, but also serves to effectively use local mineral resources, reduce production costs, and ensure the environmental sustainability of the cement industry (Fig. 1).

The successful balance of the above raw material components is reflected in the mineralogical composition of the synthesized sulfate-resistant Portland cement clinker, since the ratio of oxides directly affects the phases formed (Table 2).

According to the data from the table, the clinker contains CaO (61.09%). It is mainly derived from limestone and is important in the formation of the main part of the alite (C_3S) and belite (C_2S) phases, which determine the strength of the cement and the hydration process. The SiO_2 content (22.1%) is moderate, which plays an important role in the formation of silicate phases in particular. This oxide is mainly derived from barren sands and kaolin. The amounts of Al_2O_3 (4.98%) and Fe_2O_3 (5.32%) serve to form the aluminate and ferrite phases in the clinker due to kaolin and iron-rich industrial waste. Small amounts of oxides such as MgO (2.07%) and SO_3 (0.80%) improve the stability of the clinker in sulfate environments and at the same time prevent undesirable reactions. The absence of Cl^- (0.0%) and the low content of free CaO (0.935%) greatly increase corrosion resistance. The low heat loss (1.14%) confirms the very good quality of the raw materials. The total oxide content of 100.0% indicates that the clinker composition is optimal and fully balanced.

In the mineralogical composition, the clinker is dominated by C_3S (38.64%) and C_2S (41.03%) phases, which primarily determine its mechanical properties. The relatively low content of tricalcium aluminate (4.17%, ≤5%) is the main indicator of sulfate resistance, since it greatly reduces the formation of ettringite. This is directly related to the low content of Al_2O_3 in the raw materials. The presence of the C_4AF (16.16%) phase indicated a high ferrite content in the clinker. This phase is formed due to Fe_2O_3 introduced through iron-rich industrial waste and, replacing part of the tricalcium aluminate, increases the strength of sulfate-resistant cement clinker. The calculated modulus values once again prove that the raw

material mixture is in equilibrium. The CaO/SiO_2 ratio (2.76) — the silicon modulus — provides high mechanical strength of the cement. The lime saturation factor (LSF = 0.86) indicates that the firing process was carried out under optimal conditions. The aluminum modulus n (2.15) and iron modulus p (0.94) confirm that the oxides have a stable ratio. These results prove that it is possible to effectively produce sulfate-resistant Portland cement clinker based on local raw materials such as barren sand, iron-rich industrial waste, kaolin, and limestone.

Reducing the amount of tricalcium aluminate can reduce the expansion and erosion of cement in sulfate environments by 15–25%, resulting in increased long-term durability of structures. However, to maintain optimal modulus values, it is necessary to precisely control the firing temperature in the range of 1350–1450 °C, as well as the time of burning the clinker in the kiln. In future studies, it is proposed to study the mineralogy of the raw material mixture in depth, analyze the hydration kinetics, and conduct mechanical tests in order to improve the efficiency of the synthesized clinker. The chemical composition and phase structure of the clinker were evaluated by X-ray phase analysis along with tabular data. The XRD diffractogram showed clear peaks corresponding to the main crystal phases, the presence of which confirmed the results obtained by the Bogue method (Fig. 2). The strongest diffraction peaks observed between 2θ ≈ 29–34° and 51–52° indicate the dominance of the C_3S and C_2S phases.

The above data are in complete agreement with the X-ray diffraction pattern analysis. The most intense diffraction peaks were recorded in the ranges of 2θ = 28–35° and 50–53°, corresponding to the alite (C_3S) and belite (C_2S) phases. These values confirm the quantitative data obtained from Bogue's calculations. Peaks around 2θ = 32–34° and 48° correspond very well to the tricalcium aluminate phase (C_3A = 4.2%) and indicate that its content in the clinker is very low. The low content of tricalcium aluminate clearly demonstrates that it is an important factor in increasing sulfate resistance. The peaks observed at 2θ = 32–34°, 41–42° and 52° also correspond to the tricalcium aluminoferrite phase (C_4AF = 16.2%), which is completely consistent with the results of chemical and mineralogical analyses. Thus, when the results of the chemical and mineralogical analyses were compared with the X-ray diffractogram, the predominance of alite and belite, the low content of tricalcium aluminate, and the high content of C_4AF were scientifically confirmed. These characteristics allow us to consider the synthesized clinker as a sulfate-resistant Portland cement clinker.

The discrepancy observed between the Rietveld refinement results and the Bogue calculations (C_2S: 41.03% vs. 38.0%; C_4AF: 16.16% vs. 14.8%) is due to methodological differences between the two approaches: the Rietveld method performs a full-profile X-ray diffraction fit taking into account crystal structure parameters, while the Bogue method provides a stoichiometric estimate based only on the oxide composition. Discrepancies of 2–5% between these methods are well documented and are considered acceptable for clinker phase analysis.

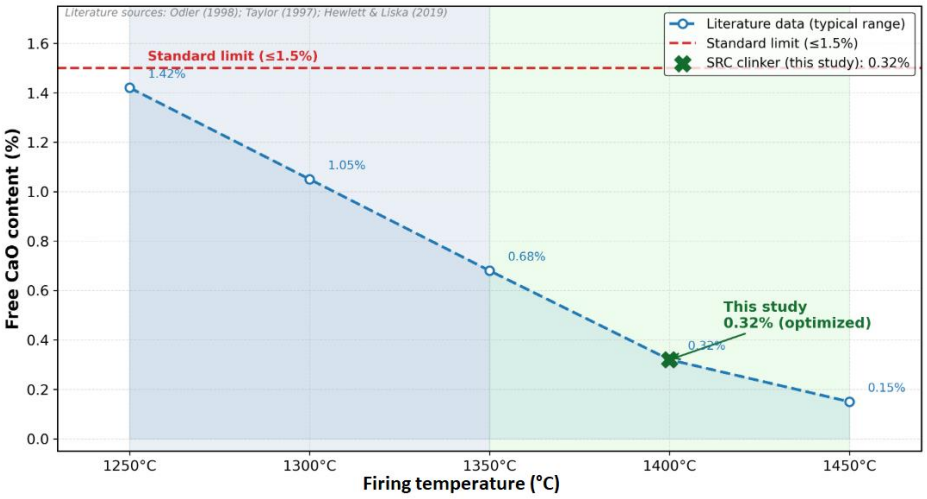

Figure 3 - Free CaO content in sulfate-resistant Portland cement (SRC) clinker

Table 3 — Free CaO content as a function of firing temperature

Firing temp. (°C)	Free CaO (%)	Source
1250	1.42	Odler (1998); Taylor (1997)
1300	1.05	Odler (1998); Taylor (1997)
1350	0.68	Hewlett & Liska (2019)
1400	**0.32**	**This study (experimental)**
1450	0.15	Hewlett & Liska (2019)

Table 4 - ASTM C1012/C1012M sulfate resistance test results (28-day immersion)

Specimen ID	Cement type	L_o (mm)	Immersion medium	L_{28} (mm)	ΔL (mm)	Expansion (%)	ASTM limit (%)
—	—	Initial	28-day immersion	28-day	$L_{28}-L_o$	$\Delta L/L_o \times 100$	≤ 0.10
SRC Clinker — Batch I (L_o = 160.1 mm)							
1.1	SRC clinker	160.1	Distilled water	160.1	0.0	**0.000**	≤ 0.10
1.2	SRC clinker	160.1	Distilled water	160.1	0.0	**0.000**	≤ 0.10
1.3	SRC clinker	160.1	5% Na_2SO_4 solution	160.1	0.0	**0.000**	≤ 0.10
Mean ± SD (Batch I):						**0.000 ± 0.000**	≤ 0.10
SRC Clinker — Batch II (L_o = 160.1 mm)							
2.1	SRC clinker	160.1	Distilled water	160.1	0.0	**0.000**	≤ 0.10
2.2	SRC clinker	160.1	Distilled water	160.1	0.0	**0.000**	≤ 0.10
2.3	SRC clinker	160.1	5% Na_2SO_4 solution	160.1	0.0	**0.000**	≤ 0.10
Mean ± SD (Batch II):						**0.000 ± 0.000**	≤ 0.10
SRC Clinker — Batch III (L_o = 160.0 mm)							
3.1	SRC clinker	160.0	Distilled water	160.0	0.0	**0.000**	≤ 0.10
3.2	SRC clinker	160.0	Distilled water	160.0	0.0	**0.000**	≤ 0.10
3.3	SRC clinker	160.0	5% Na_2SO_4 solution	160.0	0.0	**0.000**	≤ 0.10
Mean ± SD (Batch III):						**0.000 ± 0.000**	≤ 0.10
SRC Clinker — Batch IV (L_o = 160.0 mm)							
4.1	SRC clinker	160.0	Distilled water	160.0	0.0	**0.000**	≤ 0.10
4.2	SRC clinker	160.0	Distilled water	160.0	0.0	**0.000**	≤ 0.10
4.3	SRC clinker	160.0	5% Na_2SO_4 solution	160.0	0.0	**0.000**	≤ 0.10
Mean ± SD (Batch IV):						**0.000 ± 0.000**	≤ 0.10
Overall Mean ± SD (all 12 specimens):						**0.000 ± 0.000**	**≤ 0.10**

Notes: *L_o — initial length measured on 21.05.2025; L_{28} — length measured after 28 days (17.06.2025); $\Delta L = L_{28} - L_o$; Expansion (%) = $\Delta L / L_o \times 100$. Gauge length = 160 mm (ASTM C1012 standard prisms). Immersion solutions: distilled water (control) and 5% Na_2SO_4.No visible cracks, delamination, or surface deterioration were observed in any specimen.*

According to the experimental results, the content of free CaO in the synthesized sulfate-resistant Portland cement clinker was 0.32%. This value is much lower than the regulatory requirements (≤1.5%), indicating complete reaction of lime in the clinker. On the one hand, this ensured the optimal formation of C_3S and C_2S phases, and on the other hand, it led to the minimal formation of the three calcium aluminate phases (Fig. 3).

As can be seen from the graph, the measured value (0.32%) is much lower than the normative limit (1.5%). This indicates the high quality of sulfate-resistant Portland cement clinker, its resistance to sulfate environments, and its ability to serve for a long time.

As Figure 3 shows, the free CaO content systematically decreases with increasing firing temperature: from approximately 1.42% at 1250°C to 0.15% at 1450°C (Table 3). The experimentally obtained value of 0.32% in the optimized firing temperature range of 1350–1450°C is fully consistent with this trend and confirms the

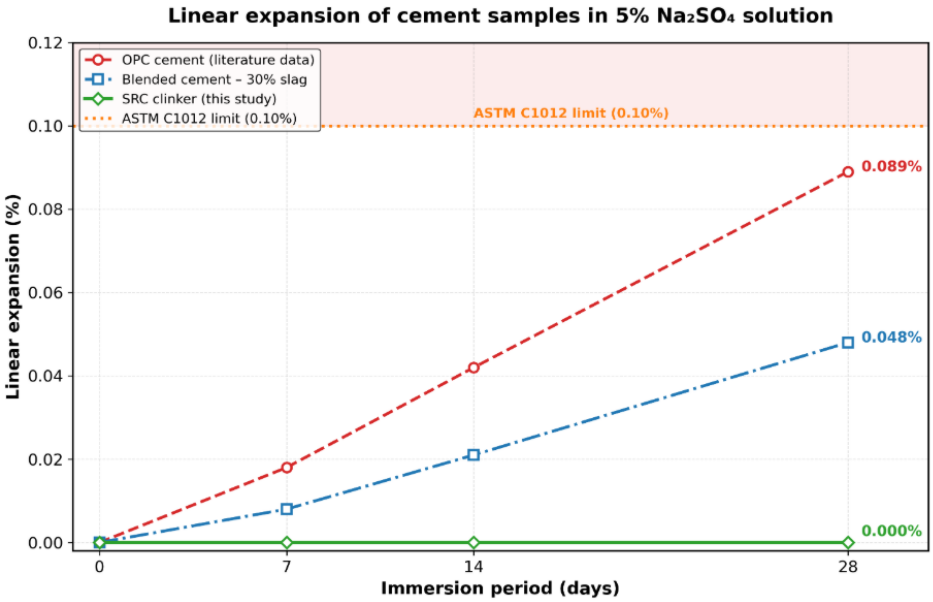

Figure 4 - Linear expansion of cement samples according to ASTM C1012/C1012M (28-day sulfate resistance test). SRC clinker: experimental data (this study)

efficiency of the clinker synthesis process. As the graph shows, the measured value (0.32%) is significantly lower than the regulatory limit (1.5%). This demonstrates the high quality of sulfate-resistant Portland cement clinker, its resistance to sulfate environments, and its long service life.

The fact that free CaO is lower than the required standard indicates the efficiency of the synthesis process. These results scientifically justify the possibility of using the obtained sulfate - resistant Portland cement clinker in the production of sulfate-resistant cement in accordance with the standards of the Republic of Uzbekistan St 337:2024 and GOST 22266-2013.

Sulfate resistance tests conducted according to the ASTM C1012/C1012M standard showed significant differences in cement samples. The degree of expansion observed in a Na_2SO_4 solution for 28 days was directly related to the composition of the mineral phases of the cement (Table 4).

The 28-day exposure results clearly show that the cement based on sulfate-resistant Portland cement clinker showed significantly higher durability than OPC (ordinary Portland cement) and blended cements (Figure 4).

First, the cement based on sulfate-resistant Portland cement clinker had the lowest expansion values. This is explained by the limited content of tricalcium aluminate in the composition (tricalcium aluminate ≤ 5%). Due to the low calcium aluminate, it reduces the reaction with sulfate ions and reduces the formation of excess ettringite or secondary gypsum. As a result, sulfate-resistant Portland cement exhibits long-term durability.

Second, ordinary Portland cement (OPC) showed high expansion. At the end of 28 days, the deformation values approached or exceeded the limit values specified in the ASTM C1012 standard. This is explained by the high content of three calcium aluminates in the OPC composition. Tricalcium aluminate actively reacts with sulfate ions, forming expansive ettringite.

Third, the mixed cements obtained from local raw materials showed lower expansion than OPC, but did not reach the level of sulfate-resistant Portland cement. This indicates that local mineral additives (kaolin, clay derivatives, iron-rich additives) have a partially limiting effect on the reaction with sulfate ions.

In general, experiments have shown that sulfate-resistant Portland cement, which can be produced in Karakalpakstan, has significantly higher resistance to sulfate-rich conditions - in particular, in the conditions of high-sulfate groundwater of the Aral Sea region - than ordinary Portland cement. These scientific results confirm the increased resistance of sulfate-resistant Portland cement to the effects of sulfate ions and its possible use as a promising construction material in aggressive environments.

Conclusions

The conducted studies comprehensively assessed the possibility of obtaining sulfate-

resistant Portland cement clinker from local raw materials of the Karakalpakstan region - limestone, barren sand, kaolin and iron-rich industrial waste.

The analysis of the chemical composition showed that the raw mixture has an optimal balance of oxides CaO, SiO_2, Al_2O_3 and Fe_2O_3. As a result, the modulus values (LSF = 0.82; SR = 2.15; AR = 0.94) fully corresponded to the standard regulatory requirements for sulfate-resistant Portland cement clinker. Mineralogical analyses showed the predominance of alite (C_3S ≈ 38.6%) and belite (C_2S ≈ 41.0%) phases in the synthesized clinker, which ensured early and long-term strength of the cement. The most important indicator — the content of tricalcium aluminate (C_3A ≈ 4.2%) below 5% — ensured the resistance of the cement to sulfate environments. The high content of C_4AF due to the introduction of iron-rich additives further increased the stability of the clinker.

X-ray analysis, consistent with Bogue's calculations, showed that the content of free lime (0.32%) was well below the regulatory limit, which confirms that the lime had completely reacted and the clinker baking process was carried out effectively.

Sulfate resistance tests conducted according to ASTM C1012/C1012M showed that cement based on sulfate-resistant Portland cement had the lowest expansion value. Ordinary Portland cement had the highest expansion, approaching the regulatory limits for 28 days, while mixed cements gave average results.

Finally, it has been scientifically proven that sulfate-resistant Portland cement clinker synthesized from local raw materials has high stability in aggressive sulfate environments. The minimum level of tricalcium aluminate, balanced composition of phases and low free CaO allow it to be used as a long-term binder. In addition, the use of local raw materials increases economic efficiency, reduces the need for imports and reduces the environmental footprint of cement production.

Conflicts of interest. On behalf of all authors, the corresponding author states that there is no conflict of interest.

CRediT author statement: **G. Begzhanova**: Conceptualization, Methodology, Software; **I. Tojiev**: Data curation, Writing draft preparation; **T. Shengwen**: Visualization, Investigation; **A. Ruzmetova**: Supervision; **D. Mukhitdinov**: Software, Validation; **Z. Tursunov**: Reviewing and Editing.

Acknowledgements. We express our deep gratitude to **Atabaev Farrukh Bakhtiyarovich**, Chief Scientific Researcher at the "STROM" Research Laboratory and Testing Center of the Institute of General and Inorganic Chemistry of the Academy of Sciences of Uzbekistan, for his practical assistance in conducting the experiments for this research. We also extend our sincere appreciation to **Khadzhiev Azamat Shamuratovich** for his support in translation and language-related matters, as well as to the co-authors for their contributions to the writing and editing of the article.

Formatting of funding sources. This research did not receive any specific grant from funding agencies in the public, commercial, or not-for-profit sectors.

Cite this article as: Begzhanova GB, Mukhitdinov DD, Ruzmetova ASh, Shengwen T, Tursunov ZR, Tojiev I I. Sulfate-Resistant Portland Cement Clinker Based on the Raw Material Base of Karakalpakstan: Technology, Economics and Ecology. Kompleksnoe Ispolzovanie Mineralnogo Syra = Complex Use of Mineral Resources. 2028; 345(2):142-154. https://doi.org/10.31643/2028/6445.23

Қарақалпақстанның шикізат базасына негізделген сульфатқа төзімді портландцемент клинкері: технологиясы, экономикасы және экология

[1]Бегжанова Г.Б., [1]Мухитдинов Д.Д., [2]Рузметова А.Ш., [3]Shengwen T., [4]Турсунов З.Р., [5]Тоджиев И.И.

[1]Өзбекстан Ғылым академиясының Жалпы және бейорганикалық химия институты, Ташкент
[2]Әбу Райхон Беруни атындағы Үргенч мемлекеттік университеті, Үрген, Өзбекстан
[3]Ухань университеті, Қытай
[4]Навои тау-кен технологиялары мемлекеттік университеті, Өзбекстан
[5]Бухара мемлекеттік техникалық университеті, Бухара, Өзбекстан

Мақала келді: *16 сәуір 2026*
Сараптамадан өтті: *21 мамыр 2026*
Қабылданды: *8 шілде 2026*

Бұл зерттеу Өзбекстан Республикасының Арал өңірінен табылған жергілікті шикізат негізінде сульфатқа төзімді портландцемент клинкерін өндіруге және оның қасиеттерін зерттеуге арналған. Алынған нәтижелер технологиялық, экономикалық және экологиялық артықшылықтарды көрсетеді. Шикізат қоспалары әктас, құнарсыз құм, каолин және темірге бай өндірістік қалдықтардан тұрды, нәтижесінде оңтайландырылған оксидтік құрамы бар клинкер алуға мүмкіндік берді (LSF = 0,82, SR = 2,15, AR = 0,94). Рентгендік фазалық талдау жоғары механикалық беріктікті қамтамасыз ететін алит (C_3S ≈ 38,6%) және белит (C_2S ≈ 41,0%) фазаларының жоғары құрамын көрсетеді. Үшкальций алюминатының төмен мөлшері (үшкальций алюминатының < 5%) және ферриттің жеткілікті мөлшері (C_4AF ≈ 16,2%) сульфатқа төзімділігі мен фазалық басымдылығын арттырды. ASTM C1012/C1012M стандартына сәйкес орындалған сульфатқа төзімділік сынақтары сульфатқа төзімді портландцементтің 5% Na_2SO_4 ерітіндісіне салынған үлгілер арасында ісіну индексінің ең төмен екенін көрсетті, бұл қарапайым портландцемент пен аралас цемент түрлерімен салыстырғанда оның жоғары төзімділігін дәлелдеді. Алынған нәтижелер жергілікті шикізат негізінде сульфатқа төзімді жоғары сапалы портландцемент клинкерін шығаруға және оның Орал өңірінің сульфатқа бай жағдайларына жарамдылығын көрсетуге мүмкіндік береді. Экономикалық тұрғыдан жергілікті шикізатты пайдалану өндіріс шығындарын азайтады, импортқа тәуелділікті азайтады, цемент өнеркәсібінің бәсекеге қабілеттілігін арттырады. Экологиялық тұрғыдан алғанда, сульфатқа төзімді портландцементтің ұзақ қызмет ету мерзімі және өнеркәсіптік қалдықтарды пайдалану жасыл экономикаға сәйкес келеді, қалдықтарды азайтуға көмектеседі және тұрақты дамуға ықпал етеді.

Түйінді сөздер: сульфатқа төзімді портландцемент, клинкер синтезі, минералды ресурстар, сульфатқа төзімділік, жасыл экономика, тұрақтылық.

Авторлар туралы ақпарат:

Бегжанова Гулрух Бахтиярқызы — *Техника ғылымдарының докторы, Өзбекстан Республикасы Ғылым академиясының Жалпы және бейорганикалық химия институтының STROM зерттеу зертханасы мен сынақ орталығының Бас ғылыми қызметкері, 100170, Мирзо Улуғбек к-сі, 77, Ташкент. Email: gulrukh-begzhanova@rambler.ru; ORCID ID: https://orcid.org/0000-0002-0492-3246*

Мухитдинов Дилшод Давронович — *Техника ғылымдарының докторы, STROM зерттеу зертханасы және сынақ орталығы, Жалпы және бейорганикалық химия институты, Өзбекстан Республикасы Ғылым академиясы, Ташкент, Өзбекстан. Email: mukhitdinov28@gmail.com; ORCID ID: https://orcid.org/0000-0002-4795-6080*

Рузметова Айда Шоназарқызы — *Техника ғылымдарының философия докторы (PhD), Ургенч мемлекеттік университетінің химиялық технологиялар кафедрасының доценті, Ургенч, Өзбекстан. Email: aida0330@list.ru; ORCID ID: https://orcid.org/0009-0004-1008-4057*

Shengwen Tang — *Ухань университеті, Қытай. Email: tangsw@whu.edu.cn; ORCID ID: https://orcid.org/0000-0001-6635-9444*

Турсунов Зариф Рузимурадович — *Техника ғылымдарының философия докторы, доцент, Навои тау-кен технологиялар мемлекеттік университеті, 210100, Ғалаба даңғылы, 76, Навои, Өзбекстан. Email: tzarif5658@gmail.com; ORCID ID: https://orcid.org/0009-0003-6432-4442*

Тоджиев Иномжон Ильхомович — *Техника ғылымдарының докторы, «Құрылыс инженериясы» кафедрасының меңгерушісі, Бухара мемлекеттік техникалық университеті, Бухара, Өзбекстан. Email: tojiyevinomjon0@gmail.com; Scopus ID: 57552794300*

Сульфатостойкий портландцементный клинкер на основе сырьевой базы Каракалпакстана: технология, экономика и экология

[1]Бегжанова Г.Б., [1]Мухитдинов Д.Д., [2]Рузметова А.Ш., [3]Shengwen T., [4]Турсунов З.Р., Тоджиев И.И.

[1]Институт общей и неорганической химии Академии наук Узбекистана, Ташкент
[2]Ургенчский государственный университет имени Абу Райхона Беруни, Узбекистан
[3]Уханьский университет, Ухань, Китай
[4]Навоийский государственный горно-технологический университет, Узбекистан
[5]Бухарский государственный технический университет, Бухара, Узбекистан

Поступила: *16 апреля 2026*
Рецензирование: *21 мая 2026*
Принята в печать*: 8 июля 2026*

АННОТАЦИЯ

Данное исследование посвящено получению сульфатостойкого портландцементного клинкера на основе местного сырья, обнаруженного в регионе Аральского моря Республики Узбекистан, и изучению его свойств. Полученные результаты подчеркивают технологические, экономические и экологические преимущества. В качестве сырьевых смесей использовались известняк, пустые пески, каолин и богатые железом промышленные отходы, что позволило получить клинкер с оптимизированным оксидным составом (LSF = 0,82, SR = 2,15, AR = 0,94). Рентгенофазовый анализ показывает высокое содержание фаз алита (C_3S ≈ 38,6%) и белита (C_2S ≈ 41,0%), что обеспечивает высокую механическую прочность. Низкое содержание трикальцийалюмината

	(трикальцийалюминат < 5%) и достаточное содержание феррита (C_4AF ≈ 16,2%) повысили сульфатостойкость и фазовое доминирование. Испытания на сульфатостойкость, проведенные в соответствии со стандартами ASTM C1012/C1012M, показали, что сульфатостойкий портландцемент имел самый низкий индекс набухания среди образцов, помещенных в 5% раствор Na_2SO_4, что подтверждает его высокую стойкость по сравнению с обычным портландцементом и смешанными видами цемента. Полученные результаты открывают возможность производства высококачественного сульфатостойкого портландцементного клинкера на основе местного сырья и демонстрируют его пригодность для условий региона с высоким содержанием сульфатов. С экономической точки зрения использование местного сырья снижает производственные затраты, уменьшает потребность в импорте и повышает конкурентоспособность цементной промышленности. С экологической точки зрения длительный срок службы сульфатостойкого портландцемента и использование промышленных отходов совместимы с «зеленой» экономикой, способствуют сокращению отходов и устойчивому развитию.
	Ключевые слова: сульфатостойкий портландцемент, синтез клинкера, минеральные ресурсы, сульфатостойкость, зелёная экономика, устойчивое развитие.
Бегжанова Гулрух Бахтиярована	***Информация об авторах:*** *Доктор технических наук, Главный научный сотрудник лаборатории и испытательного центра STROM Института общей и неорганической химии Академии наук Республики Узбекистан, 100170, ул. Мирзо Улугбека, 77, Ташкент, Узбекистан. Email: gulrukh-begzhanova@rambler.ru; ORCID ID: https://orcid.org/0000-0002-0492-3246*
Мухитдинов Дилшод Давронович	*Доктор технических наук, лаборатория и испытательный центр STROM, Институт общей и неорганической химии, Академия наук Республики Узбекистан, Ташкент, Узбекистан. Email: mukhitdinov28@gmail.com; ORCID ID: https://orcid.org/0000-0002-4795-6080*
Рузметова Айда Шоназаровна	*Доктор философии по техническим наукам (PhD), доцент кафедры химических технологий, Ургенчский государственный университет, Ургенч, Узбекистан. Email: aida0330@list.ru; ORCID ID: https://orcid.org/0009-0004-1008-4057*
Shengwen Tang	*Уханьский университет, Китай. Email: tangsw@whu.edu.cn; ORCID ID: https://orcid.org/0000-0001-6635-9444*
Турсунов Зариф Рузимурадович	*Доктор философии по техническим наукам, доцент, Навоийский государственный горно-технологический университет, 210100, пр. Галаба, 76, Навои, Узбекистан. Email: tzarif5658@gmail.com; ORCID ID: https://orcid.org/0009-0003-6432-4442*
Тоджиев Иномжон Илхомович	*Доктор технических наук, заведующий кафедрой Строительная инженерия, Бухарский государственный технический университет, Бухара, Узбекистан. Email: tojiyevinomjon0@gmail.com; Scopus ID: 57552794300*

References

[1] Al-Amoudi OSB. Attack on plain and blended cements exposed to aggressive sulfate environments. Cement and Concrete Composites. 2002; 24(3–4):305–316.

[2] Mehta PK, & Monteiro PJM. Concrete: Microstructure, Properties, and Materials (4th ed.). McGraw-Hill, New York. 2014, 704.

[3] Lothenbach B, Matschei T, Möschner G, & Glasser FP. Thermodynamic modelling of the effect of temperature on the hydration and porosity of Portland cement. Cement and Concrete Research. 2008; 38(1):1–18.

[4] Shao Y, Chen X, & Li W. Study on the preparation and sulfate resistance of Portland cement clinker with the high Fe/Al ratio of ferrite phase. Cement and Concrete Composites. 2022; 134:104699. https://doi.org/10.1016/j.cemconcomp.2022.104699

[5] Labidi I. Optimization of sulfate resistant Portland cement raw mixes. Journal of Building Materials and Structures. 2017; 4(1):53–61.

[6] Labidi I, Megriche A, & Benazzouk S. Natural resources exploitation in sulfate-resisting Portland cement manufacturing. Frontiers in Chemistry. 2022; 10:806433. https://doi.org/10.3389/fchem.2022.806433

[7] Khalifa SA, & AlSadig DY. Adjustment of clinker raw mix design to produce sulfate resisting cement. International Journal of Trend in Research and Development. 2017; 4(5):187–193.

[8] Costa ARD, Figueiredo M, & Canda L. Thermodynamic modelling of the clinkering process in sulfate resistant cements. Scientific Reports. 2023; 13:16542. https://doi.org/10.1038/s41598-023-44078-7

[9] Santhanam K, Cohen MD, & Olek J. Mechanism of sulfate attack: Part I. Experimental study. Cement and Concrete Research. 2002; 32(6):915–921. https://doi.org/10.1016/S0008-8846(02)00724-X

[10] Santhanam K, Cohen MD, & Olek J. Mechanism of sulfate attack: Part II. Numerical simulation. Cement and Concrete Research. 2003; 33(3):341–346. https://doi.org/10.1016/S0008-8846(02)00925-6

[11] Whittaker M, Black J, & Jones S. A review of external sulfate attack in concrete. Advances in Cement Research. 2015; 27(9):519–529. https://doi.org/10.1680/adcr.14.00089

[12] González MA, Ros F, & Blanco MT. The effect of limestone filler on the sulfate resistance of low C_3A Portland cements. Cement and Concrete Research. 1998; 28(11):1653–1667. https://doi.org/10.1016/S0008-8846(98)00144-1

[13] Higgins DD. The use of ground granulated blastfurnace slag to improve the sulfate resistance of concrete. Cement and Concrete Composites. 2003; 25(8):913–919. https://doi.org/10.1016/S0958-9465(03)00148-3

[14] Abubaker F. Long-term durability of concrete in sulfate environment: Role of sulfate resisting Portland cement. Construction and Building Materials. 2014; 72:272–278. https://doi.org/10.1016/j.conbuildmat.2014.10.079

[15] Martínez Infante MA, Rosales J, & Morón MA. Sulfate-resistant clinker based cement with new secondary main constituents: Technical, economic and environmental assessment. Buildings. 2025; 15(3):479. https://doi.org/10.3390/buildings15030479

[16] Tiburzi NB, Le Saout P, & Damidot D. Performance of portland-limestone cements with supplementary cementitious materials in sulfate exposure. Construction and Building Materials. 2019; 220:187–197. https://doi.org/10.1016/j.conbuildmat.2019.06.009

[17] Neto R, Cincotto A, & Fernandes L. Influence of sulfates on the hydration and durability of Portland cement systems. Construction and Building Materials. 2021; 302:122188. https://doi.org/10.1016/j.conbuildmat.2021.122188

[18] Tursunova G, Atabaev F, Begzhanova G, Khomidov F, Wang L, Matmuratov A, & Khadzhiev A. Thermal activation of Karakalpakstan margels and pozzolan properties in their low-carbon composite Portland cement. Journal of Ecological Engineering. 2026; 27(7).

[19] Khadzhiev A, Atabaev F, & Tursunova G. Influence of sandstone on physical and chemical processes of interaction of components and genetic formation of cement composite. E3S Web of Conferences. 2024; 563:02027. https://doi.org/10.1051/e3sconf/202456302027

[20] Iskandarova MI, Atabaev FB, Yakubzhanova ZB, Kahhorov U, Hadjiev ASh. Development of Technology for Obtaining Portland Cement with New Types of Composite Additives. AIP Conference Proceedings. 2022; 2432:050063 https://doi.org/10.1063/5.0090576

[21] Iskandarova M, Atabaev F, Tursunova G, Tursunov Z, Khadzhiev A. Composite Portland cements: Innovations and future directions in cement technology. Innovative Infrastructure Solutions. 2025. https://doi.org/10.1007/s41062-025-02067-x

[22] Iskandarova MI, Atabaev FB, Khadzhiev AS. Utilization of natural silicate rocks to reduce the carbon footprint in the cement industry. Kompleksnoe Ispolzovanie Mineralnogo Syra = Complex Use of Mineral Resources. 2026; 338(3):40–50. https://doi.org/10.31643/2026/6445.27

[23] Khadzhiev A, Abdullaev M, Yakubov Y, Jumaniyozov J. The effect of hybrid mineral additives on the genetic formation and physico-chemical processes of cement composites. E3S Web of Conferences. 2025; 633:08003. https://doi.org/10.1051/e3sconf/202563308003

[24] Atabaev FB, Aripova MKh, Khadzhiev ASh, Tursunova GR, Tursunov ZR. Effect of multicomponent mineral additives on the microstructure and strength of composite cement. Kompleksnoe Ispolzovanie Mineralnogo Syra = Complex Use of Mineral Resources. 2025; 1(322):45–57. https://doi.org/10.31643/2027/6445.05

[25] Khadzhiev A, & Atabaev F. Influence of silica-containing additives on physical and mechanical properties of Portland Cement Co. Ltd Karakalpaksement. E3S Web of Conferences. 2023; 401:05051. https://doi.org/10.1051/e3sconf/202340105051

[26] Buriev AI, Iskandarova MI, & Begzhanova GB. Influence of a high degree of filling on the properties of pozzolanic cement. RA Journal of Applied Research. 2023; 9(2):60–65. https://doi.org/10.47191/rajar/v9i2.02

[27] Bagdaulet B, & Aitkulov N. Application of regional mineral resources for the synthesis of sulfate resisting cements. Kompleksnoe Ispolzovanie Mineralnogo Syra = Complex Use of Mineral Resources. 2023; 4:33–42. https://doi.org/10.31643/2023/6445.18

[28] Habert G, et al. Cement production technology improvement compared to factor 4 objectives: can we reach individually based targets? Journal of Cleaner Production. 2011; 17(12):1179–1187.

[29] Lotfi S, et al. Circular economy as a strategy for sustainable development of the cement industry. Construction and Building Materials. 2020; 255:119397.

[30] O‘zM St 337:2024. Sulfatga chidamli portlandsement. Texnik shartlar [Sulfate-resistant Portland cement. Technical conditions]. Uzbekistan National Standard. 2024. (in Uzbek).

[31] GOST 22266-2013. Sulfatstoykiy portlandtsement i shlakoportlandtsement. Tekhnicheskiye usloviya [Sulfate-resistant Portland cement and slag Portland cement. Technical conditions]. Mezhgosudarstvennyy standart. 2013. (in Russ.). https://meganorm.ru/Data/592/59275.pdf

[32] ASTM International. ASTM C1012/C1012M–24: Standard Test Method for Length Change of Hydraulic-Cement Mortars Exposed to a Sulfate Solution. West Conshohocken, PA: ASTM International. 2024. https://www.astm.org/c1012_c1012m-24.html

МАЗМҰНЫ
СОДЕРЖАНИЕ
CONTENTS

Техникалық редакторлар:
Г.К. Қасымова, Н.М.Айтжанова, Т.И. Қожахметов

Компьютердегі макет:
Г.К. Қасымова

Дизайнер:*Г.К. Қасымова, Н.М.Айтжанова*

“Металлургия және кен байыту институты” АҚ
050010, Қазақстан Республикасы, Алматы қаласы, Шевченко к-сі, 29/133

Жариялауға 8.07.2026 жылы қол қойылды

Технические редакторы:
Г.К. Касымова, Н.М. Айтжанова, Т.И. Кожахметов

Верстка на компьютере:
Г.К. Касымова

Дизайнер:
Г.К. Касымова, Н.М.Айтжанова

АО “Институт металлургии и обогащения”
050010, г. Алматы, Республика Казахстан. ул. Шевченко, 29/133

Подписано в печать 8.07.2026 г.

Technical editors:
G.K. Kassymova, N.M. Aitzhanova, T.I. Kozhakhmetov

The layout on a computer:
G.K. Kassymova

Designer:
G.K. Kassymova, N.M. Aitzhanova

“Institute of Metallurgy and Ore Beneficiation” JSC
050010, Almaty city, the Republic of Kazakhstan. Shevchenko str., 29/133

Signed for publication on 8.07.2026